pISSN 2615-5109
eISSN 2621-0541

INTERNATIONAL JOURNAL OF ENGINEERING

E P I

Volume 4 Number 1, February 2021

Publisher:
Center of Technology
Fakultas Teknik, Universitas Hasanuddin
Gowa, Indonesia

Print edition ISSN 2615-5109
Electronic edition ISSN 2621-0541

Publisher:
Center of Technology, Fakultas Teknik, Universitas Hasanuddin

Address:
Engineering Faculty Campus, Hasanuddin University
Jl. Poros Malino km. 6, Bontomarannu
Kabupaten Gowa, Sulawesi Selatan, Indonesia, 92171
Email : epi-ije@unhas.ac.id
Website : cot.unhas.ac.id/journals/index.php/epiije
Telp/Fax : +62-(0)411-58601

EPI International Journal of Engineering
Editorial Board

Foreword

It is with great pleasure that we can present the EPI International Journal of Engineering (EPI-IJE) Volume 4 Number 1 February 2021. All manuscripts published in this edition have been reviewed by peer reviewers who are not only from Hasanuddin University but also from other institutions. The editorial team will invite more participation and collaboration from other universities and institutions either as authors or reviewers so that contributors' diversity, as well as journal popularity, can be increased.

This edition consists of 14 manuscripts which are divided into 5 topic categories. The first topic category is civil and environmental engineering with 2 (two) manuscripts. The first manuscript applied the empirical bathymetry method for measuring the water depth of Maninjau Lake, while the second manuscript studied the environmental impact and scenario treatment using the life cycle assessment approach in the Tofu industry. The second topic category is electrical and informatics engineering with only 1 manuscript. The manuscript studied the development of a low-cost vehicle counting based on the internet of things.

The third topic category which is mechanical and industrial engineering contains 4 (four) manuscripts. The first manuscript designed a contact-free mortuary trolley for covid-19 victims. Other manuscripts are about free vibration of doubly curved shallow shells of rectangular planform, comparison of fractional derivative and classical spring-dashpot model of viscoelastic characteristics of rubber material, and simulation of fluid flow through serial-parallel circular cylinder arranged in tandem using CFD.

The fourth topic which is naval architecture, ocean, and marine engineering contains 2 (two) manuscripts. The first manuscripts in this category investigated the local stress of car deck of ro-ro 5000 GT ship. The second manuscript compared the strength of midship structures with and without margin plate.

The last topic category is architecture and urban & regional development engineering which contains 5 (five) manuscripts. They are about the integration of natural and artificial light of the Mega bank Makassar tower building, air quality of Bosowa tower parking building, the artificial lighting analysis of study rooms in dormitories and classrooms Islamic boarding school of Lil Banat Parepare, the influence of transit area in public open space of Losari beach Makassar pavilion on the activities of group visitors, and accessibility based on user perception of rehabilitation center for people with physical disabilities Wirajaya Makassar.

We are grateful and thank all manuscripts authors of this edition. We also thank all other people and institutions for their supports for the publication of this edition. We hope that the high-quality manuscripts published in this edition would be useful in the development of science and technology.

Warm regards,

Prof. Baharuddin Hamzah
Editor-in-Chief of EPI-IJE

TABLE OF CONTENTS

EPI International Journal of Engineering
Volume 4, Number 1, February 2021, pp. 1-6
DOI: 10.25042/epi-ije.022021.01

*p*ISSN 2615-5109
*e*ISSN 2621-0541

Application of Empirical Bathymetry Method on Sentinel 2A for Measuring Water Depth of Maninjau Lake

Wendri Arifin[a,*], Muhammad Hanif[b,*], Febriandi[a], Triyatno[c], Ernieza Suhana Mokhtar[d], Eka Mutia[e]

[a]Department of Remote Sensing Technology, Faculty Social Science, State University of Padang. Email: wendriarifin970@gmail.com
[b]Department of Geography, Faculty of Social Science, State University of Padang. Email: hanif12mphy@gmail.com
[c]Department of Environmental Science, School of Postgraduate Study, State University of Padang. Email: triyatno@fis.unp.ac.id
[d]Department of Surveying Science and Geomatics, Faculty of Architecture Planning & Surveying, Universiti Teknologi MARA. Email: ernieza@uitm.edu.my
[e]Department of Civil Engineering, Faculty of Engineering, University Samudra, Aceh. Email: ekamutia@unsam.ac.id

Abstract

Lake Maninjau is a lake formed by volcanic activity. Many human activities occur in the catchment area, but also in exploited waters. This study aims to map the depth of the waters in Lake Maninjau and assess the effect of field sample distribution on the quality results of the image transformation. The data used are satellite imagery Sentinel 2A, results of the point survey. The analysis technique uses the normalized difference water index algorithm, sun glint, empirical bathymetry method, and linear regression. The result of the research has found that variations of distribution into the dispersion of the recording process of the depth of the object represented by the cell. The depth of the water from the results of this transformation refers to the measurement sample in the field survey. The maximum depth of the waters is in the range of 107m. Shallow waters are predominantly distributed in the northern region which is the out late of Lake Maninjau. The southern area forms a deep basin. The distribution of this sample is in the form of an empirical bathymetry map and the relationship between the results of field measurements and the transformation with a regression value of 0.769, this indicates the consideration of total and distribution of survey sample is influence on the quality of the results of the transformation.

Keywords: Bathymetry; image transformations; water observation

1. Introduction

Lake is one of the natural landforms that is formed by natural processes and has very complex functions and systems. The lake ecosystem in Indonesia stores a wealth of germplasm, supplies by surface water, and use full for agriculture, community development, water sources, fisheries, agriculture, hydroelectric power, tourism, and others. Currently, many lakes in Indonesia have been degraded which is caused by population growth, land conversion, waste, chemical pollution, and erosion.

Lake Maninjau is the lake in Agam Regency, West Sumatra Province, Indonesia. Lake Maninjau is a volcanic lake located at an altitude of 461.50 meters above sea level. This is a caldera from a large volcanic eruption that scattered approximately 220-250 km^3 of pyroclastic material. The other facts also reveal that the water quality of Lake Maninjau tends to decline in two decades, due to the increasing level of pollution due to domestic and agricultural waste disposal [1]. The environmental dynamics that occur in the catchment area of Lake Maninjau are the degradation of vegetation which largely decreases vegetation density as the impact of land use around the catchment area [2]. Lake Maninjau exploited which is not followed by conservation efforts. The general problem faced is an increase in waste content which results in pollution and silting of these problems which in turn results in degradation of the lake environment and the death of fish in fishpond [3].

Mapping water body and bathymetric measurements were carried out by lowering the rope or cable using a weight to the seabed. This method is less efficient because it only measures the depth point in one point for a long time and has unsatisfactory accuracy. Advance technology of remote sensing has been used quite a lot for studies with the theme of limnology such as water quality monitoring, mapping of resource potentials, etc. Technology for measuring and mapping bathymetry is always evolving [4]. Remote sensing data to study the change of environment dynamic [5]. Furthermore, many remote sensing algorithms have been developed according to the user's need and develop geospatial modeling to assess environmental phenomena[6], [7]. The technology uses an active sensor (LIDAR) is very useful in environmental observation, this technology is able to distinguish the condition of objects in the *x*, *y* point information and height data in the form of *z* points [8].

*Corresponding author. Tel.: +62-852-1050-4212
AddressJl. Hamka. Air Tawar Barat Kota Padang. Padang, Indonesia, 25173

Figure 1. Satellite Sentinel 2 MSI [14]

Nevertheless, In this technology also provide sensitivity for water observation the method for bathymetric measurement [9]. The acoustic methods such as the use of echo-sounders and multi-beam provide accurate results however, both techniques in relatively high costs, large size, and limited coverage area. One solution for measuring and mapping bathymetry at an affordable cost and covering a wide area is to use remote sensing satellite technology [10], [11].

Today using a low-cost digital camera was use full to capture and observe the images of water bodies [12] Advance high-resolution imagery such as Quick-Bird is use full for investigation and study about hydrology process, water dynamic, rivers changes, and deposition [13]. QuickBird is also used to mapping bathymetry with the spatial (~ 2 m) such as QuickBird and WorldView-2 can produce good bathymetry maps with a coefficient of determination above 0.80 and a root mean square error (RMSE) value below 0.6 m [14]. Unfortunately, these satellite images come at a high price. In contrast, the free use of satellite imagery with medium spatial resolution such as Landsat (30 m) can be used to produce medium resolution bathymetry maps with a determination coefficient of 0.6 [14], [15]. Nevertheless, advance remote sensing in the Copernicus project such as sentinel 2a (Fig. 1) imagery and the arrival of new technologies for mapping bathymetry.

Sentinel-2 is a wide-swath, high-resolution, multi-spectral imaging mission, supporting Copernicus Land Monitoring studies, including the monitoring of vegetation, soil, and water cover, as well as observation of inland waterways and coastal areas. The SENTINEL-2 Multispectral Instrument (MSI) samples 13 spectral bands: four bands at 10 meters, six bands at 20 meters, and three bands at 60 meters spatial resolution. The acquired data, mission coverage, and high revisit frequency provide for the generation of geo-information at local, regional, national, and international scales. The data is designed to be modified and adapted by users interested in thematic areas such as spatial planning, agro-environmental monitoring, forest, and vegetation monitoring, land carbon, natural resource monitoring, global crop monitoring, and water monitoring [14]. With the availability of Sentinel satellite data with a higher resolution than medium resolution imagery for earth observation, sentinel satellites can be used for the exploration of water resources because they are supported by spectral sensitivity for water objects.

This research aims is to mapping the water's depth in the Lake Maninjau area of Agam Regency and assess the effect of field sample distribution on the quality of the result of image transformation. The research location is Lake Maninjau, West Sumatra Province. This lake is a volcanic lake or commonly known as the caldera of Tinau Mountain which is the result of ancient mountain eruptions. We decide to choose this location because it has a unique geological and natural landscape, and has complex environmental problems.

2. Materials and Method

2.1. Data

In this research, we use two data which we obtain from a website and ask the government. The data used is Sentinel 2A satellite imagery sourced from http://earthexplorere.usgs.gov this data free access and field sample output of echo-sounder which is obtained from River Basin Institute Indonesian government (BWS V).

2.2. Analysis

a. Normalized Difference Water Index

The index for separating the body of water and land is used to focus the research location on water areas. By applying the NDWI algorithm, it can discriminate between water and land where the band/image waves used are green-swri equation [16] as follows:

$$NDWI = \frac{Green - Swri}{Green + Swri} \tag{1}$$

b. Sun Glint Correction

Sun glint is also commonly known as the Glinting, where sun glen is the sparkle on the surface of the water due to the reflection of the sparkling sunlight, the sparkling conditions of the sun on the surface of the water can cause errors when mapping the depth of the water body, then the equation is applied [17]:

$$R'_i = R_i - bi\left(R_{NIR} - \min_{NIR}\right) \tag{2}$$

c. Ratio Transform Algorithm (RTA)

One of the algorithms that work in the empirical bathymetry method is the ratio transform algorithm, in which this transformation builds the results of the regression equation from the field measurement data with the logarithmic ratio of the two channels. The image used is usually a blue band or coastal band, this algorithm is able to extract it into a body of water up to a depth of 25m, provided that the water is in condition. This method is part of the Empirical Bathymetry method, which is the key in this study using field measurement data, in this study for field validation reference data used measurement data with eco-sounder measurement results by the BWS River Basin Institute equation [18]:

$$Z = m1\frac{\ln\left(nRw(\lambda i)\right)}{\ln\left(nRw(\lambda j)\right)} - m0 \tag{3}$$

where,

Z : water depth,
$m1$: is (gain) to each depth ratio,
$m0$: is (offset)
Rw : reflectance of water in the ʎi or ʎj band
λ : spectral band

n : a constant value per area for the confidence of the positive logarithmic value of each case and the ratio which will refer to the linear regression response to the water depth response.

3. Results and Discussion

The bathymetric mapping process with the empirical bathymetry algorithm method will go through three main data processing stages, in which the sentinel image 2a is used and specifically is bands 2 and 3. The selection of bands 2 and 3 are based on sentinel specifications and wave sensitivity in mapping water depth.

The first stage of the NDWI analysis is carried out in which this analysis aims to separate water and non-marine objects. In this stage, the researcher successfully implemented the NDWI algorithm to highlight marine objects and discriminate non-waters objects to the made focus area in the bathymetric analysis process, then the results of the NDWI image transformation can be seen on the following map. The researchers succeeded in delineation the waters with an area of 9,950 ha. Furthermore, the bathymetry mapping process goes through the sun glint correction stage. In principle, sun glint correction aims to eliminate the reflection bias of sunlight reflected by the surface of the water to the atmosphere so that the original image will show the sparkle of the water surface so that it will cause an error in the analysis. So the application of sun glint correction, the sparkle of the water surface can be muted so that it is able to display the appearance of the actual water depth according to normal reflectance. At this stage, the sun glint correction is implemented to the two bands used. Figure 2 is a sun glint corrected image.

Figure 2 reveals the true color composite of the sentinel satellite image transformed by sunglint. The digital number of sentinel imagery that result of sun glint is at a high value of 4935 and low 0. From the appearance of the image, the results of sunglint correction, the sun's glare bias are not visible to the sun. The comparison of the appearance of the image before sun glint correction and after the correction, which result of sun glint is very clear the difference in the appearance of the water surface. The image corrected by the sunglint which is free from light reflection by the water surface is suitable for the process of estimating the depth of the water because the quality of bias results of recording of objects by satellite has been eliminated in this process.

In this stage before using sentinel imagery, the most important thing to look at is the clean appearance of the object (not covered by clouds), for consideration of the situation when recording objects after or before the rain is not really explained in the principle of the sun glint method because sun glint only tries to eliminate reflection bias sunlight by water objects.

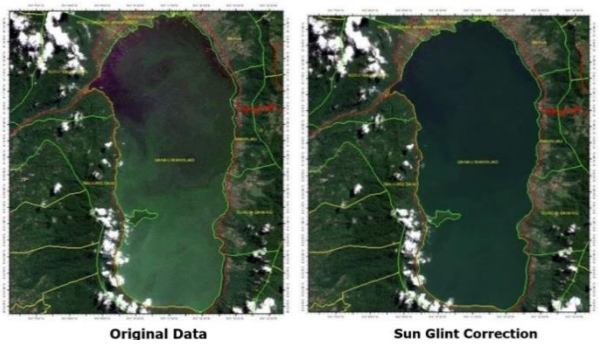

Figure 2. Comparison of images before and after sun glint correction

The next stage is an analysis of empirical bathymetry which is the image that is processed output of sun glint correction. Then the important thing in the process is the transformation empirical bathymetry method which is the use of field data as a reference for transformation in analyzing image pixels. In this research, we used data from field surveys using echo-sounder data obtained from the Sumatra River Basin Institute (BWS V) therefore researchers did not have to re-measure to take primary data. The field survey data we use for the total sample is 1.220 points. This sample point will be a reference in the ratio transform algorithm analysis because in the extraction of sentinel image pixels into water depths, this algorithm must have reference sample data that is a reference for calculating the estimated water depth. To measuring water depth using the Empirical Bathymetry Method algorithm, several researchers also tried to carry out experiments but they did not use field primary data but used water depth points obtained from bathymetry maps, digital elevation mode DEM with coarser resolution as a reference point for water depth.

Figure 3 is the result of empirical bathymetry and interpolation survey data. The original result of empirical bathymetry it presenting depth. To facilitate interpretation of the depth of the waters, which is depth grouping is carried out in the form of interval classes. From Fig. 3, the researcher gives a symbol of dark blue to bright blue, where the dark blue color indicates that the location is deep water, while bright blue is shallow water. In this study, we also present the results of interpolation of waters using it to compare the waters from the survey data and the results of the transformation of satellite images. These two images show the comparison of the depth of the waters measured in the field with the results of the digital image transformation. The map information is not very informative so it is necessary to classify the depth of the waters on an interval scale.

Figure 3 is a map image of the results for the depth waters. From this figure, it can be seen that there is a difference in the depth of the waters between the interpolation of field measurements and the results of bathymetric analysis using the image algorithm. This figure compares contras difference on object shallow water at a depth of 0 - 37 meters, wherein the result of the survey the area around of the edge of the lake shows a faded color which is the appearance of shallow water. However the results of analysis image sentinel 2A, it can be seen that the shallow water area of 0 – 37 meters is only clearly scattered on the left and right of the lake. In the deepwater interpolation model from 91 - 107 meters, it is centered on the spot in the middle of the lake caldera, while in the 2A sentinel analysis model the deep waters of the lake Maninjau are more spread out in the caldera part of the lake.

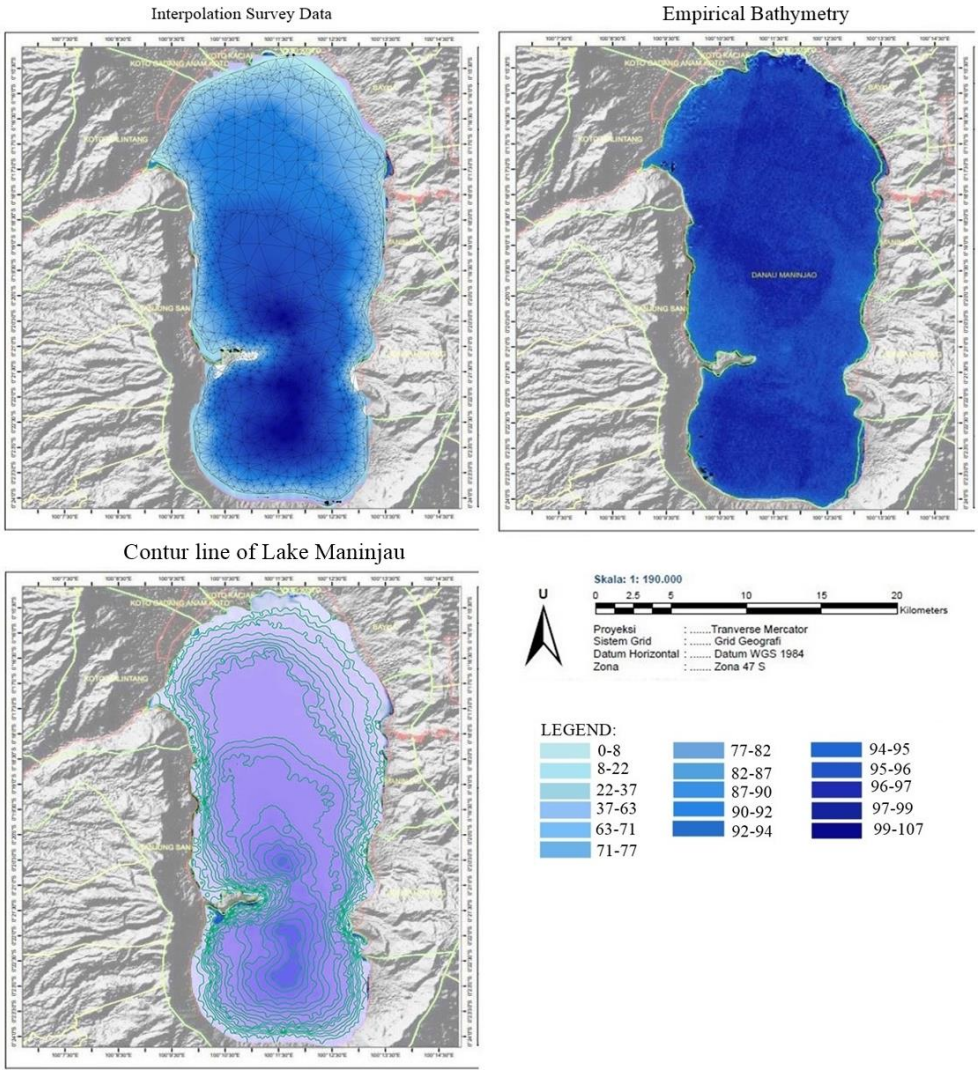

Figure 3. Bathymetry of Lake Maninjau

The difference between the results of field measurements and the results of sentinel image analysis is due to the process of data collection. satellites record objects based on the response of light reflected by objects that reflect the depth of the water, this shows the depth of the water, and this sentinel analysis model is very dependent on field data. This sentinel satellite is not a satellite with active sensors such as LAS LiDAR, the extraction of this water depth can be done without using field data, but it must have water depth information in a location, for example from DEM digital elevation mode data, it is necessary to pay attention to the difference in data that is a reference for calculations in This empirical bathymetry algorithm will affect the quality of the results.

From Fig. 3, the results of this study for the distribution of water depths using Sentinel have differences in the location of deep waters with the results of the Eco sounder measurement. This difference does not only occur in variations in the distribution of deep waters. This difference has been widely discussed by previous researchers because sentinels are very effective for mapping shallow water depths. The limitation of this sentinel is because the sentinel is a passive sensor satellite that only records object information from the reflection of the object with the help of sunlight, the sentinel does not have the technology to emit its own waves, so this limitation makes a difference in the bias of the analysis results.

The process of analyzing the relationship between survey data and the results of the empirical transformation of the bathymetry is important because the results of the literature study state that this algorithm is very efficient for measuring water depths up to a depth of 25 m, whereas from the transformation model carried out, the researchers succeeded in finding the maximum depth waters of the Lake Maninjau at 107 m.

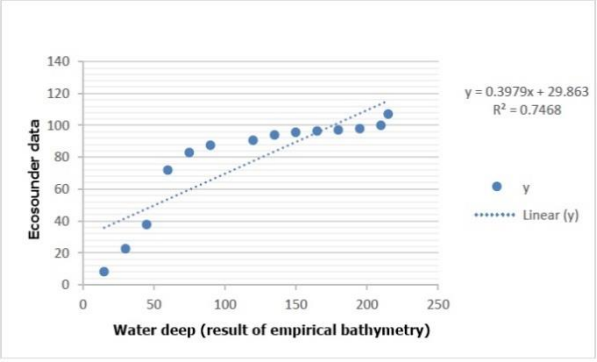

Figure 4. Relationship field data and result of empirical bathymetry

The process of analyzing the relationship between these two data is by making the field data from the eco-sounder measurement as the *x* variable and the result of the transformation of the empirical bathymetry as the *y* variable (Fig. 4). Researchers take the same pixel information as the coordinates of the field measurements. From the analysis of the relationship between the two data, the researcher managed to find the regression coefficient value with a value of 0.7468. Based on the research, it was found the depth waters of Lake Maninjau by going through several stages of data analysis. The use of NDWI transformations is proven to be very efficient in delineating the watershed area because this transformation is very sensitive in discriminating against non-water objects. The results of this study are very relevant to the NDWI transformation concept described by Xu [17] which the use of green and swirling waves in NDWI transformation is able to separate water and non-water objects. Furthermore, the results of this study also reveal the comparison on image information which appearance of the object from the image recording result of sun glint correction and the original image. It was found that sun glint correction was able to eliminate the bias of light on the water. Information on water imagery as research objects looks more normal on the true color image. Based on the statement of Hedley [18] the application of sun glint correction is very effective in removing the glint of sunlight on the surface of the exposure in the recorded image. So the findings in the results of this study are very relevant to the statements made by previous researchers regarding the use of the sun glint correction method in reducing light bias on the water surface.

The depth of the waters was successfully mapped in this case where the maximum depth was obtained in the range of 107 m, the depth of this circulation was from the extraction of data bands 2 and 3 which was further analyzed with field data, the depth distribution of this circulation has two main spots scattered in the northern region. and south. Stumpf [19] who have proposed an empirical transformation model of bathymetry in their journals has also succeeded in discriminating water depth objects. So the results of this study are proven to have successfully implemented the same algorithm at locations with different geographical characteristics.

The linear regression test has succeeded in proving the performance between the field data and the results of the transformation of the empirical bathymetry method with the regression coefficient value obtained that is 0.769. This proves that the two variables have a strong relationship. Nevertheless, a linear regression curve also represents the extent of the relationship between the two variables where the variable x and variable y are not too far away, so we can understand that the empirical transformation of this method can be implemented in the region of the broadcast with different geographical characteristics. Field measurement data and water objects that are mapped are in clear conditions, meaning that the water area does not have a solid sediment suspension which causes errors in the water depth mapping.

4. Conclusion

In the process of mapping bathymetry, the empirical bathymetry algorithm method was used. Results of the shallow waters are at intervals of 0 to 8 meters, moderate waters are 77 to 92 meters, deep waters are 93 to 96 meters and very deep waters are 97 to 107 meters were taken. The linear regression test relationship has succeeded in proving the performance between field data and the results of the transformation of the empirical bathymetry method with the regression coefficient value obtained is 0.769 where the relationship is very strong this indicates the consideration of total and distribution of survey sample is influence on the quality of the results of the transformation.

Acknowledgment

The authors wish to thank the government for support and we also express our gratitude to all those who have helped with the administration process, as well as those who helped us in the field.

References

[1] Asnil, et al., "Policy Analysis of Sustainable Utilization of Lake Resources (Case Study of Lake Maninjau, West Sumatra)," *J. Pengelolaan Sumberd. Alam dan Lingkung.*, vol. 3, no. 1, pp. 1–9, 2013. [in Bahasa]

[2] M. Hanif, "Study of Changes in Vegetation Density in Lake Maninjau Area Catchment with Remote Sensing Technology and Geographic Information Systems," Universitas Negeri Padang, 2016. [in Bahasa]

[3] Lembaga Ilmu Pengetahuan Indonesia, "Hydroclimatological Studies as the Basis for Development of Disaster Early Warning System Mass Death of Fish 01 Maninjau Lake, West Sumatra," 2010. [in Bahasa]

[4] P. I. Wahyuningrum, "Algorithm Development for Estimating Depth of Shallow Waters Using LANDSAT-7 ETM Data," Institut Pertanian Bogor, 2007. [in Bahasa]

[5] M. Hanif, et al., "Multi Spectral Satellite Data to Investigate Land Expansion and Related Micro Climate Change as Threats to the Environment," in *IOP Conf. Series: Earth and Environmental Science*, 2019.

[6] J. B. Cambell and R. H. Wynee, *Introduction to Remote Sensing*, Fifth Ed. New York: Guildford Press, 2011.

[7] R. A. Hidayat, "Spatial Modeling of The Threat of Damage to The Peatland Ecosystem In The Mainland of Bengkalis Regency, Riau Province," *J. Soc. Polites*, vol. 20, no. 2, 2020.

[8] M. Hanif and A. Y. Nofrizal, "Investigation Natural Forest Ecosystem Use High Resolution and Lidar Data," *J. Environ. Earth Sci. IIESTE*, vol. 9, 2017.

[9] H. Joanne and C. Kaitlyn, "Submerged and Emergent Land Cover and Bathymetric Mapping of Estuarine Habitats Using WorldView-2 and LiDAR Imagery," *J. Remote Sens. MDPI*, vol. 8, no. 9, 2016.

[10] M. Arief, "A New Approach to Bathymetric Mapping Using SPOT Remote Data, Case Studies of Parigi Bay and Popoh Bay," *J. Teknol. Dirgant.*, vol. 10, no. 1, pp. 71–72, 2012. [in Bahasa]

[11] H. Joa, et al., "Can recreational Echosounder-Chartplotter systems be used to perform accurate nearshore bathymetric surveys?," *J. Ocean Dyn. Springer*, vol. 64, no. 11, pp. 1555–1567, 2014.

[12] M. S. Ernieza and M. W. N. M. Wan, "Utilizing Low-Cost Digital Cameras And Gis Technique For Mapping Water Quality Of Inland Water Bodies," in *ISG & ISPRS*, 2011, pp. 27–29.

[13] M. Hanif, et al., "The High Resolution Imagery to Mapping the Dynamics of River Flow Patterns, and Deposition on Fluvial Landform of Sianok Canyon," *J. Remote Sens. GIS Technol.*, vol. 6, no. 1, 2020.

[14] M. A. Correa Liceaga and J. I. Avila Euan, "Assessment of coral reef bathymetric mapping using visible Landsat Thematic Mapper data," *Int. J. Remote Sens.*, vol. 23, no. 1, pp. 3–14, 2002.

[15] N. C. Kiat, *The kings of the rivers Mahseer in Malayan and the region*. Selangor: Inter Sea Fishery, 2004.
[16] European Space Agency, *Sentinel 2 User Hand Book*. European Commission, 2015.
[17] H. Xu, "Modofication of Normalized Diffrerence Water Index (NDI) to enchance Open Water Feautures in Remote Sensed Imagery," *Int. J. Remote Sens.*, vol. 27, no. 14, pp. 3025–3033, 2006.
[18] D. Hadley, et al., "Simple and robust removal of sun glint for mapping shallow water benthos," *Int. J. Remote Sens.*, vol. 26, no. 10, pp. 2107–2112, 2005.
[19] R. P. Stumpf, et al., "Determination of Water Depth With high resolution satellite imagery over variable bottom types," *Limnol. Oceanogr.*, vol. 48, no. 1/2, pp. 547–556, 2003.

EPI International Journal of Engineering
Volume 4, Number 1, February 2021, pp. 7-13
DOI: 10.25042/epi-ije.022021.02

*p*ISSN 2615-5109
*e*ISSN 2621-0541

A Study of Environmental Impact and Scenario Treatment using Life Cycle Assessment Approach in Tofu Industry

Intan Rahmalia[a], Syifa Khairun Nisa[b], Vita Palupi[c], Aninda Putri[d], I Wayan Koko Suryawan[e*]

[a]Department of Environmental Engineering, Faculty of Infrastructure Planning, Universitas Pertamina, Jakarta. Email: intanrahmalia11@gmail.com
[b]Department of Environmental Engineering, Faculty of Infrastructure Planning, Universitas Pertamina, Jakarta. Email: syifakh22@gmail.com
[c]Department of Environmental Engineering, Faculty of Infrastructure Planning, Universitas Pertamina, Jakarta. Email: vitapalupi99@yahoo.com
[d]Department of Environmental Engineering, Faculty of Infrastructure Planning, Universitas Pertamina, Jakarta. Email: jsnindi31@gmail.com
[e]Department of Environmental Engineering, Faculty of Infrastructure Planning, Universitas Pertamina, Jakarta.
Email: i.suryawan@universitaspertamina.ac.id

Abstract

One of the types of tofu industries in Indonesia is that the small-scale tofu industry was located in the East Jombor, Ketapang Village, on the Blorong River. This tofu industry, with a 1300 kg/day production capacity, produces liquid waste that is disposed of into the Blorong River with a BOD parameter of 2726 mg/L, COD of 4972 mg/L, and TSS of 388 mg/L. These values greatly exceed the quality standards based on the Regional Regulation of Central Java Province Number 10 of 2004 concerning Tofu Industry. The entry of these pollutants into the Blorong River, over time, can cause water bodies to become toxic and pollute the Blorong River. Therefore, one of the efforts to protect the environmental condition of this river is to increase the efficiency of the Wastewater treatment plant and substitute the determined fuel through alternative scenarios. In the MBBR scenario, substituting diesel fuel into biomass is a type of biodiesel. It has an advantage for the fire tube boiler industry because it can reduce exhaust emissions compared to diesel. Meanwhile, the existing wastewater treatment is substituted for the MBBR unit. The choice of MBBR as a wastewater treatment unit is because it is economical, does not require large land, simple in development design, and accessible in operation and maintenance. In the second scenario (SBR), a transition of diesel fuel to LPG as a fuel input in the cooking process will result in a cleaner emission, especially on the SO_2 parameter, and better because it has a higher heating value than diesel, 47.3 Tj/Gg. Both scenarios are analyzed regarding the magnitude of the impact on the environment using the OpenLCA method. The result of this method from each alternative is evaluated to obtain the best scenario. In the tofu industry, the best design the resulting impact is smaller than the SBR alternative.

Keywords: Environmental impact; OpenLCA; life cycle assessment; tofu production

1. Introduction

The majority of Indonesian businesses have a strong interest in the tofu industry because making tofu is relatively easy, simple, and inexpensive [1]. Besides, making tofu uses simple technology with relatively low levels of resource use, such as water and raw materials. The tofu industry is dominated by small to medium-scale businesses with limited capital. However, behind the advantages of the cheap and straightforward, Tofu industry could harm the environment. In the process of making tofu, from the raw materials to tofu products, each stage of making tofu produces relatively high solid waste and liquid waste, as well as emissions released into the air. The resulting waste and air emissions are disposed of in the environment without any treatment. The environmental impact that can be felt from the absence of wastewater treatment is the damage to environmental aesthetics [2].

One of the tofu industries is the Industri X, located in the East Jombor, Ketapang Village, to be precise on the Blorong River. These values greatly exceed the quality standard based on Regional Regulation of the Province of Central Java Number 10 of 2004 concerning Industry Tofu. High levels of Biological Oxygen Demand (BOD) in water bodies can reduce dissolved oxygen (DO) concentrations needed for aquatic life to survive. Over time, dissolved oxygen levels can make living aquatic organisms die, and then decay occurs so that the condition of the water body becomes toxic. The liquid waste from the tofu industry is a source of water pollutants in the Blorong River.

Therefore, one of the efforts to protect this river's environmental conditions is to increase the efficiency of Waste Water Tteatment Plant (WWTP) and substitute the determined fuel by providing alternative scenarios by Life Cycle Assessment (LCA). LCA has been widely applied in Indonesia to determine industrial activities' environmental impact [3]–[5]. This study aims to determine the environmental impact and update the tofu industry management with LCA.

*Corresponding author. Tel.: +6282227774992
Jl. Teuku Nyak Arief, RT.7/RW.8, Simprug
Kec. Kebayoran Lama, Jakarta Selatan, Jakarta
Indonesia 12220

2. Method

LCA is a method to evaluate the potential environmental impacts of the life cycle by calculating the inputs such as natural resources demand and outputs such as emissions and solid waste that can impact ecological aspects such as climate change, ecotoxicity, etc. [6]. Generally, the LCA method consists of four steps: goal and scope, life cycle inventory analysis, life cycle impact assessment, and interpretation [7].

According to Sala et al. [7], this method aims to define the intended application and determine both spatial and temporal boundaries so the study can focus on environmental assessment's important issues.

The goal and scope ensuring the choices of functional unit, system boundaries, identification of parametric quality requirement, and the intended audience is already made up.

Goals:

- Finding the best scenario by considering aspects of land requirements, economic, aesthetic, environmental health, and technology.
- The effluent can meet the quality standard threshold criteria for the Central Java Provincial Regulation Number 10 of 2004 concerning Tofu Industry.
- Reducing the impact of pollution from industrial activity processes.

Scopes:

- Tofu made from soybean seeds
- The dregs of X Tofu Industry are ± 30 sacks to produce ± 60 barrels of tofu.
- The need for soybeans is ± 840 kg/day with a capacity of 1300 kg/day.
- The need for diesel (for cooking) is ± 5 - 10 L/day.
- The amount of wastewater is 35 m^3/day.
- System Limits: Gate to Gate.
- Allocation and System Expansion: based on mass and volume, and based on other rules (frequency and substance content).
- Data Quality Requirements: Water requirements, the number of soybeans, acid and $CaSO_4$ needs, and fuel requirements (diesel).

As stated in Life Cycle Inventory (LCI) is one of the steps in the LCA method that gave a result in a flow model by collecting and calculating all the input and output data for each process. By the limitation of collection data, the calculation of industrial tofu can be made by using parametric quality from journal literature.

3. Result and Discussion

3.1. The existing treatment method

The existing WWTP that has been applied to processing the wastewater from the tofu process uses anaerobic-aerobic technology. The resulting wastewater will be flowed into the bar screen to filter the coarse fractions and continue to the equalization basin through trenches in the factory. The residence time of water in the equalization tank is 37.8 hours or 1.5 days, with the volume capacity of the storage tank is 63 m^3. Through this stage, 11% of Total Suspended Solid (TSS) is removed. Then, after going through the process at the equalization stage, the wastewater is flowed into an anaerobic tank to remove the organic content in the wastewater. With anaerobic tanks' capacity is 300 m3, it can accommodate wastewater with a residence time of 7,5 days. Several organic materials were removed in this process, namely 65% TSS, 95.2% BOD, 92% COD. The type of anaerobic tank is the Anaerobic Baffled Reactor (ABR). In the anaerobic removal process, the activated sludge has been formed through anaerobic fermentation process of anaerobic bacteria [8], [9].

This activated sludge plays an essential role in removing the organic material that takes place in the reactor. The activated sludge that settles in the bottom of the reactor will be recirculated in the reactor so that the organic removal process can achieve maximum efficiency. The by-product of the anaerobic process that occurs in the reactor is methane gas (CH_4). Then, the methane gas is flowed into the flare pipe to be burned so that it doesn't smell. Also, methane gas (CH_4) has the potential to be used as an alternative fuel or biogas, which can be distributed to local residents' homes or to the production process in the tofu factory itself or lighting the area around the factory location. Due to the lack of facilities to distribute the gas flow, it isn't yet been implemented. The effluent from ABR will flow into the aeration tank. In this reactor, dissolved oxygen in the wastewater will encourage the degradation of organic material in the wastewater by aerobic bacteria, which will continue to produce activated sludge. The residence time of wastewater in the reactor is 3.6 hours with a tank capacity of 6 m^3. The organic material content was removed at this processing stage, namely BOD of 56%, TSS of 51.5%, COD of 48.9%. After going through the aeration treatment process, the wastewater will then be flowed into the outlet tank or final tank and continue to the water body or the Blorong river.

The maximum processing results and the uncomplex unit operation in the anaerobic-aerobic treatment method make the treatment a standard method for most industries to treat their wastewater, even though the processing time is longer than other processing methods. The existing WWTP has been operating for 14 years since 1996. This WWTP was not built when the factory was built for the first time. Previously, the community had protested to the factory because of the pollution from the discharge wastewater production that polluted the water river. However, for the past 14 years, the company has started to be concerned about their behaviour to damage the environment. A WWTP was built along with the employment of human resources which could operate it.

Based on the processing flow, the overall processing unit performance is obtained for each pollutant parameter obtained through Fibria research [10], described in Table 1 and Table 2.

Table 1. The removal characteristic in existing WWTP

No	Parameter	Influent WWTP (Output Industry)	Effluent WWTP	Load (kg/day)	Quality Standard		Removal Efficiency (%)
					Maximum Content	Maximum Pollution Load (kg/ton)	
			PHYSIC				
1.	Temperature	43.1 oC	36.9 oC	-	38	-	-
2.	TSS	388 mg/L	62 mg/L	2.170	100	2	87%
			CHEMICAL				
3.	BOD	2726 mg/L	57.6 mg/L	2.016	150	3	97.80%
4.	COD	4972 mg/L	203.2 mg/L	7.112	275	5.5	95%
5.	pH	5.51	7.06	-	6.0-9.0	-	-

Table 2. The removal result from each unit at the existing treatment

Parameter	Influent	Bar Screen		Equalization Tank		Anaerobic Tank		Aerobic Tank		Outlet	Quality Standard
		Efficiency	Effluent	Efficiency	Effluent	Efficiency	Effluent	Efficiency	Effluent		
	(mg/L)	(%)	(mg/L)	(%)	(mg/L)	(%)	(mg/L)	(%)	(mg/L)	(mg/L)	(mg/L)
TSS	388	0	388	11	345.32	65	120.86	51.5	62.24	62	100
BOD	2726	0	2726	0	2726	95.2	130.85	56	57.57	57.6	150
COD	4972	0	4972	0	4972	92	397.76	48.9	203.24	203	275
pH	5.51	5.92	5.51	-	6.42	-	6.92	-	7.06	7.06	6.0-9.0

3.2. Moving Bed Biofilm Reactor (MBBR) treatment method – Scenario 1

The principle of the Moving Bed Biofilm Reactor (MBBR) is the activated sludge process with the addition of media and the presence of an aeration process in the reactor [11]. The MBBR method is included in the attached growth reactor type because of the media's addition into the reactor. It will encourage the biological growth process of microbes with suspended and attached cultures. The MBBR has the advantages: easy to maintain and requires less land area. The results of the calculation of the removal efficiency scenario with the MBBR unit can be seen in Table 3.

3.3. Sequencing Batch Reactor (SBR) treatment method – Scenario 2

SBR has the advantage of the need for the area. The SBR unit does not require a large area because it is compact while still providing high efficiency in treating liquid waste and making unit costs cheaper than the standard activated sludge technology. SBR consists of five processing phases and is carried out sequentially as follows:

a. Fill in the phase when the volume of wastewater enters the reactor and mixes with the sedimented biomass. After the tank reaches its maximum capacity, the process will proceed to the next stage. The time given for each stage depends on the purpose of wastewater treatment. The typical time for the fill stage is two to four hours. In a two-tank system, the time required to fill is the same as the amount of reacting, settle, decant, and idle time so that when one tank is in the fill stage, the other tank can complete the cycle. Anoxic conditions at the fill stage are recommended to achieve a good condition for settling organisms [12].
b. React is a phase where the process occurs is the same as in the aeration of the activated sludge process. Under suitable environmental conditions, biomass will eat the substrate. During the reaction stage, the mixing unit and the aeration unit are actively used, and no more wastewater enters this stage, and there is a removal of the carbonaceous BOD. Besides, it is necessary to determine the duration of aeration removal so that nitrification removal can occur.
c. Settle is a phase where the process is the same as the sedimentation unit or clarification unit in the activated sludge process. This process causes the solid to sink and separate from the water.
d. The draw is the phase where water that has been cleaned is disposed of as effluent.
e. Idle is the phase that occurs between the draw-and-fill phases, and it is used to provide time before the switching process. This stage can be on short-period or long-period depending on the amount of discharge of treated wastewater. This phase can be eliminated if the wastewater has a high release. Conversely, if the wastewater has a low release, this stage will take a long time so that the sludge turns anaerobic.

The results of the calculation of the removal efficiency scenario with the SBR unit can be seen in Table 4.

Table 3. The removal result from each unit at MBBR treatment

Parameter	Influent WWTP	Bar Screen		Equalization Tank		MBBR		Effluent WWTP	Quality Standard (mg/L)
	(mg/L)	Efficiency	Effluent (mg/L)	Efficiency	Effluent (mg/L)	Efficiency	Effluent (mg/L)	(mg/L)	
TSS	388	0	388	11%	345.32	73%	93.24	93.24	100
BOD	2726	0	2726	0	2726	80%	545.2	545.2	150
COD	4972	0	4972	0	4972	82%	895	894.96	275

Table 4. The removal result from each unit at SBR treatment

Parameter	Influent WWTP	Bar Screen		Equalization Tank		SBR		Effluent WWTP	Quality Standard (mg/L)
	(mg/L)	Efficiency	Effluent (mg/L)	Efficiency	Effluent (mg/L)	Efficiency	Effluent (mg/L)	(mg/L)	
TSS	388	0	388	11%	345.3	98%	6.906	6.91	100
BOD	2726	0	2726	0	2726	98%	54.52	54.52	150
COD	4972	0	4972	0	4972	99%	49.72	49.72	275

3.4. Life Cycle Impact Assessment (LCIA) of existing condition

The LCIA is a step of classifying the emission from product production into impact categories, and then these categories will be compared by characterizing it into common units [7]. The comparison of common units of all categories can be done by converting the data using some of the assumptions from the literature that can be seen in Table 3 and Table 4.

The inventory analysis results were reviewed further using an impact assessment of the product or activity according to specific indicators. This assessment using the 2013 Environmental Product Declaration (EPD) assessment method available on the OpenLCA application. The following is a table of the resulting environmental impact categories in Table 5.

a. Acetic Acid (CH_3COOH). The need for acetic acid used during production is influenced by the amount of soybean raw material used in the production of tofu. The X tofu industry needs 840 kg of soybeans to produce 1300 kg of tofu per day [13] showed that using 144 kg of soybean raw materials and supporting materials in the form of 1 L of vinegar acid water could produce 260 kg of tofu per day.

Table 5. Input and output value of existing scenario

Material	Unit	Quantity
Input Material		
Acetic acid	kg/day	6.125
Energy, unspecified	MJ/day	373
Transformation, to agriculture, mosaic	ha/day	1.292
Water, well, in ground	m^3/day	3,024,000
Output Material		
BOD5, Biological Oxygen Demand	kg/day	174182.4
Carbon dioxide, fossil	kg/day	27.628
COD, Chemical Oxygen Demand	kg/day	614476.8
NO_2, Nitrogen dioxide	kg/day	0.00768
Sulfur dioxide	kg/day	0.0479
Tofu	kg/day	1300
Waste, unspecified	kg/day	390

The need for acetic acid to make tofu from 840 kg of soybean raw materials is 6.125 Liters.

b. Solar (Unspecified energy). Solar is the fuel used in the cooking and maturation process of soybeans before being processed into tofu. Then diesel is used to cook and ripen 840 kg of soybeans is 10 litres per day [14]. The amount of diesel emission released was obtained by multiplying between the amount of diesel used and the diesel emission factor of 37.3 MJ/Litre.
c. Soybean (transformation, to agriculture, mosaic). Soybean is an input material used in the tofu production process. The soybean mass value needs to be transformed into a unit area to be input into the LCA application. Based on the results of a study on the distribution pattern of soybean productivity in Central Java Province by district/city, X Regency has soybean productivity 14-11 quintals per hectare [15]. The data on average soybean productivity will be used as an indicator to estimate the acreage of soybean gardens that can produce 1300 kg of soybeans. So, the area of the soybean plantation obtained 1.292 ha.
d. Water Discharge (water, well, in the ground). The water discharge used in processing soybeans into tofu is 3,024,000 m^3/day.
e. BOD) and COD parameters are parameters used in determining the quality of wastewater because they both have characteristics in knowing the presence of pollution induction from a decrease in the amount of dissolved oxygen.
f. Sulfur dioxide (SO_2) and Nitrogen dioxide (NO_2) are exhaust gases from the combustion of diesel fuel in a soybean grinding machine in the X Industrial tofu production. The amount of emission $SO2$ that it produces is determined by calculating the fuel requirement and the default emission factor for diesel fuel. In the study of the analysis of emission load estimation SO_2 and NO_X from industrial activities in Karang Pilang Surabaya, it was stated that the SO emission factor from the use of diesel fuel was 4.79 kg/1000L and the emission factor NO_2 was 0.768 kg/1000L [16]. The literature data are used to estimate the total emissions resulting from the use of diesel in tofu production is 0.0479kg SO_2 and 0.00768kg NO_2.

Table 6. Result of impact analysis of existing scenario

Environmental Impact	Score	Unit
Abiotic Depletion	373	MJ
Global Warming	27.628	kg CO_2
Eutrophication	135,185	kg PO_4
Acidification	0.05328	kg SO_2
Photochemical Oxidation	0.00251	kg C_2H_4

After inputting data into the OpenLCA application based on the calculation of the input and output values above, the resulting impact will be automatically calculated. The overall results of the impact assessment of the input and output data that have been carried out can be seen in Table 6.

Based on the impact assessment using the OpenLCA application with the 2013 EPD method, the existing conditions have several impacts, while the most impacting is global warming of 27.628 kg CO_2. Based on Table 6, the existing conditions' impact is classified as significant, so a scenario is created to reduce the negative impact of the environment. This scenario substitutes the use of diesel fuel in the existing conditions to the use of biomass. Also, this scenario uses the MBBR unit to treat wastewater generated from tofu production.

In this scenario, the choice to substitute diesel fuel is because diesel has a high enough contribution to global warming. In one of the efforts to minimize global warming, the Indonesian government is committed to using renewable energy resources as a substitute for conventional fuels. The potential for renewable energy that can be utilized is biomass. The type of biomass used in this scenario is biodiesel. The use of biodiesel has an advantage for the fire tube boiler industry because it can reduce exhaust emissions compared to diesel/diesel oil. Pollutant gas emissions decrease with the increase in the biodiesel content in the mixture [17]. However, the amount of use of biodiesel is more than the amount of use of diesel. Biodiesel has a calorific value of 5-13% lower than diesel oil. When applied to the fuel system, more fuel is injected to achieve combustion stoichiometry to increase fuel consumption [17]. The amount of biomass used is 1-2% more than the use of diesel as fuel [18]. Emissions resulting from burning biodiesel include CO_2, CH_4, N_2O.. CO_2 emissions produced if biodiesel is burned are not included in total emissions or are considered excluding emissions, while CH_4 and N_2O emissions are calculated as emissions [19]. The following is the number of emissions released by the biodiesel type biomass:

Input

$$\begin{aligned} Biodiesel &= The\ amount\ of\ diesel,\ used \times 2\% \\ &= 373\ MJ \times 2\% \\ &= 380.5\ MJ \end{aligned}$$

Output

$$\begin{aligned} N_2O\ Emission &= \sum FC \times CEF \times NCV \\ &= 380.5\ MJ \times 4\ {}^{kg}\!/_{TJ} \times 1000000\ {}^{MJ}\!/_{TJ} \\ &= 0.001522\ kg \end{aligned}$$

$$\begin{aligned} CH_4\ Emission &= \sum FC \times CEF \times NCV \\ &= 380.5\ MJ \times 30\ {}^{kg}\!/_{TJ} \times 1000000\ {}^{MJ}\!/_{TJ} \\ &= 0.011415\ kg \end{aligned}$$

where

$\sum$ FC is the amount of fossil fuel used (mass /volume)
NCV is Net Calorific Volume (energy content) value per unit mass or volume of fuel
CEF is the carbon emission factor

3.5. Life Cycle Impact Assessment (LCIA) of MBBR scenario

This scenario also uses the MBBR unit to treat wastewater generated from tofu production. The choice of MBBR as a wastewater treatment unit is because it is economical, does not require large land, simple in development design, and easy to operate and maintain. In general, tofu industry players lack knowledge about the tofu wastewater treatment process, so that tofu industry players tend to choose simple tofu wastewater treatment. However, the allowance for MBBR units still exceeds the quality standard of the Central Java Provincial Regulation Number 10 of 2004 concerning the Tofu Industry. The following is the number of COD and BOD generated through the MBBR processing unit:

$$\begin{aligned} BOD &= \text{effluent BOD processing unit MBBR} \times \text{discharge} \\ &= 545.2\ {}^{mg}\!/_{liter} \times 3,024,000\ {}^{m^3}\!/_{day} \times 10^{-3} \\ &= 1,648,684.8\ kg \end{aligned}$$

$$\begin{aligned} COD &= \text{effluent COD processing unit MBBR} \times \text{discharge} \\ &= 894.96 \times 3,024,000\ {}^{m^3}\!/_{day} \times 10^{-3} \\ &= 2,706,359.04\ kg \end{aligned}$$

Table 7 are the inputs and outputs of MBRR scenario.

Table 7. Input and output value MBBR scenario

Material	Unit	Quantity
Technical Input		
Acetic acid	kg/day	6.125
Energy, unspecified	Mj/day	380.5
Transformation, to agriculture, mosaic	ha/day	1.292
Water, well, in ground	m^3/day	3,024,000
Technical Output		
BOD5, Biological Oxygen Demand	kg/day	1,648,684.8
Carbon dioxide, fossil	kg/day	0
COD, Chemical Oxygen Demand	kg/day	2706359.04
Nitrogen dioxide	kg/day	0.001522
Methane	kg/day	0.011415
Tofu	kg/day	1.3
Waste, unspecified	kg/day	390

Table 8. Result of impact analysis of MBBR scenario

Environmental Impact	Score	Unit
Abiotic Depletion	0	MJ
Global Warming	0.722	kg CO_2
Eutrophication	59539	kg PO_4
Acidification	0	kg SO_2
Photochemical Oxidation	0.594	kg C_2H_4

Based on the input and output of the tofu-making process, an impact analysis (impact assessment) using the EPD 2013 method was obtained. This scenario succeeded in reducing global warming, but there was an increase in the eutrophication impact of 59,539 kg PO_4. Table 8 is the impact on the environment in the scenario MBBR:

3.6. Life Cycle Impact Assessment (LCIA) SBR scenario

The conversion of diesel fuel to LPG as a source of heat energy in the boiling process of soybeans is part of the environmental recovery scenario for emissions produced in the tofu production process. This scenario was chosen to consider environmental aspects. Reducing greenhouse gas (GHG) emissions from burning diesel fuel is the main scope of scenario studies for environmental aspects. The proportion of CO_2 exhaust emissions is the largest emission resulting from diesel use in the X industrial tofu production process and partly by SOx and NOx gases. The GHG emission reduction target is based on Presidential Regulation Number 71 of 2011, which is 26% in 2020 in the CO_2 exhaust element.

The use of LPG fuel is a processed product from fossil energy. The combustion process carried out on the fuel will contribute to atmospheric pollutants with different types and amounts of content. LPG and Solar are the two fuels that have additional combustion capabilities according to their calorific value. Still, the combustion capability is not always in line with exhaust gas as a byproduct produced. Solar has a 43.3 TJ/Gg and LPG heating value of 47.3 TJ/Gg [20]. However, this does not instantly mean that CO2, SOx, and NOx exhaust gases are in small amounts compared to LPG. According to Suarma [21], using LPG as a fuel input in the cooking process will result in cleaner emissions, especially in the SO_2 parameter.

Besides using alternative fuels in making tofu, it is necessary to treat wastewater generated from the X industrial tofu processing activity. The second scenario using the Sequencing Batch Reactor (SBR) as a wastewater treatment unit by considering the small area requirement. Even in a single basin, there are already several processing stages of wastewater treatment in general. The emission from the wastewater produced can be reduced, and it is known based on the efficiency of the unit used. Furthermore, inputting parameter data Liquid waste in the openLCA application is carried out by converting mg/L to kg, then calculations will be outlined in Table 9.

Table 9. Input and output value SBR scenario

Material	Unit	Quantity
Technical Input		
Acetic acid	kg/day	6.125
Energy, unspecified	L/day	14.647
Transformation, to agriculture, mosaic	ha/day	1.292
Water, well, in ground	m^3/day	3,024,000
Technical Output		
BOD5, Biological Oxygen Demand	kg/day	164868.48
Carbon dioxide, fossil	kg/day	5.678
COD, Chemical Oxygen Demand	kg/day	150353.28
Nitrogen dioxide	kg/day	0.00033
Sulfur dioxide	kg/day	0.0016
Tofu	kg/day	1.3
Waste, unspecified	kg/day	390

Table 10. Result of impact analysis of MBBR scenario

Environmental Impact	Score	Unit
Abiotic Depletion	0.50532	MJ
Global Warming	5.67890	kg CO_2
Eutrophication	3307.772	kg PO_4
Acidification	0.00183	kg SO_2
Photochemical Oxidation	0.0000861639	kg C_2H_4

After inputting all the data into the openLCA application, the impact analysis will load automatically by determining a specific impact assessment method. In this case, the method used is the 2013 EPD method as shown in Table 10.

4. Conclusion

The tofu production in industrial tofu X produces 373 MJ abiotic depletion, 27.628 kg-CO_2 that contributes to global warming, 135,185 kg-PO_4 that contributes to eutrophication, 0.053 kg-SO_2 that contribute to acidification, and 0.002 kg-C_2H_4 that contribute to photochemical oxidation. Based on mass balance calculation, the second scenario can meet the standard quality of Central Java Provincial Regulation Number 10 of 2004 concerning the Tofu Industry. The best scenario chosen can be determined by normalizing, weighting the result by identifying the significant issue. The best recommendation of waste treatment for the industry is using the first scenario, which is by adding MBBR for the wastewater treatment and substitute the diesel fuel with the alternate biomass. This scenario has more advantages than the second scenario in reducing the environmental aspect's impact, and the reduction can be high up to 373 MJ for abiotic depletion, 26.906 kg-CO_2 that contribute to global warming and 0.591 kg-C_2H_4 that contribute to photochemical oxidation.

References

[1] N. A. M. B. Simanjuntak, N. L. Zahra, and I. W. K. Suryawan, "Tofu Wastewater Treatment Planning with Anaerobic Baffled Reactor (ABR) and Activated Sludge Application," *J. Ilmu Alam dan Lingkung.*, vol. 12, no. 1, pp. 21–27, 2021.

[2] E. S. Sofiyah and I. W. K. Suryawan, "Cultivation of Spirulina Platensis and Nannochloropsis Oculata for Nutrient Removal from Municipal Wastewater," *Rekayasa*, vol. 14, no. 1, pp. 93–97, 2021.

[3] A. M. Fauzi, M. S. Rusli, and E. Rustiadi, "A Study of the Smallholder Coffee Agroindustry Sustainability Condition Using the Life Cycle Assessment Approach in Bengkulu Province, Indonesia," *J. Ecol. Eng.*, vol. 20, no. 6, 2019.

[4] R. Masayu, A. Masruri, and R. A. Putra, "Analysis Of Environmental Impact With The Life Cycle Assessment (LCA) Method On Tofu Production," *Int. J. Sci. Technol. Manag.*, vol. 1, no. 4, pp. 428–443, 2020.

[5] S. D. Kurniawati, W. Supartono, and A. Suyantohadi, "Life Cycle Assessment on a Small Scale Tofu Industry in Baturetno Village–Bantu District-Yogyakarta," in *IOP Conference Series: Earth and Environmental Science*, 2019.

[6] I. W. K. Suryawan, A. Rahman, I. Y. Septiariva, S. Suhardono, and I. M. W. Wijaya, "Life Cycle Assessment Of Solid Waste Generation During And Before Pandemic Of Covid-19 In Bali Province," *J. Sustain. Sci. Manag.*, vol. 16, no. 1, pp. 11–21, 2021.

[7] S. Sala, F. Reale, J. Cristobal-Garcia, and Marelli, "Pant R Life Cycle Assessment for The Impact Assessment of Policies," 2016.

[8] I. W. K. Suryawan, G. Prajati, A. S. Afifah, M. R. Apritama, and Y. Adicita, "Continuous Piggery Wastewater Treatment with Anaerobic Baffled Reactor (ABR) by Bio-activator Effective Microorganisms (EM4)," *Indones. J. Urban Environ. Technol.*, vol. 3, no. 1, pp. 1–12, 2019.

[9] A. S. Afifah, M. R. Apritama, Y. Adicita, and I. Y. Septiariva, "Enhanced Effluent Quality of Anaerobic Baffled Reactor (ABR) With Ozone and Aerobic Activated Sludge for Livestock Wastewater Treatment," *EPI Int. J. Eng.*, vol. 3, no. 2, pp. 108–112, 2020.

[10] K. Fibria, "Technical Study of Tofu Industry Solid and Liquid Waste Treatment," Universitas Diponegoro, 2007. [in Bahasa]

[11] N. Alisa and Y. S. Purnomo, "Reduction of Pollutant Content in Tempe Industrial Wastewater Using Moving Bed Biofilm Reactor (MBBR)," *EnviroUS*, vol. 1, no. 1, pp. 42–47, 2020. [in Bahasa]

[12] R. L. Irvine and A. W. Busch, "Sequencing Batch Biological Reactors: An Overview," *Water Pollut. Control Fed.*, pp. 235–243, 1979.

[13] R. Gunanda, "Analysis of Soybean Agroindustry in Seberida District, Indragiri Hulu Regency, Riau Province," *J. Agribisnis*, vol. 18, no. 2, pp. 100–117, 2016. [in Bahasa]

[14] F. Kaswinarni, "Technical Study of Solid and Liquid Waste Treatment in the Tofu Industry: A Case Study of the Semarang, Simple and Crow Sipat Tofu Industry in Semarang, Boyolali," Diponegoro University, 2007. [in Bahasa]

[15] F. Arnanda, Y. Kriswanto, I. Izzatun, D. Nurlita, A. Fajriyani, and T. W. Tami, "Soybean Food Security Modeling (Glysine Soya Max (Lenus&Merril) in Central Java Province Using Spatial Regression Approach," *J. Stat. Univ. Muhammadiyah Semarang*, vol. 3, no. 1, 2015. [in Bahasa]

[16] R. E. Handriyono and M. N. Kusuma, "Estimation of SO2 and NOx Emissions from Industrial Activities in Karang Pilang Surabaya," in *Seminar Nasional Sains dan Teknologi Terapan V*, 2017, pp. A19–A24. [in Bahasa]

[17] L. N. Komariah, "Analysis of the Effects of Using Biodiesel as a Fuel on Fire Tube Boiler Performance," Sriwijaya University, 2015. [in Bahasa]

[18] A. E. Afriyadi, "Want to be used for fuel, biodiesel is a bit wasteful," 2018. [Online]. Available: https://finance.detik.com/energi/d-4191308/mau-dipakai-untuk-bahan-bakar-biodiesel-sedikit-boros. [Accessed: 01-Dec-2020]. [in Bahasa]

[19] Kementerian Industri Republik Indonesia, *Draft of Technical Guidelines for Calculation of Greenhouse Gas (GHG) Emissions in the Industrial Sector*. Jakarta, 2012. [in Bahasa]

[20] Q. Nugrahayu, "Determination of Specific Emission Factors from the Transportation and Industry Sector for Carbon Footprint Estimation and Mapping in Sumenep Regency, East Java," Insititut Teknologi Sepuluh Nopember, 2015. [in Bahasa]

[21] E. Suarna, "The 'Kerosene To LPG Conversion Program' as an Emissions Reduction Technique," *J. Rekayasa Lingkung.*, vol. 6, no. 2, pp. 215–221, 2010. [in Bahasa]

EPI International Journal of Engineering
Volume 4, Number 1, February 2021, pp. 14-20
DOI: 10.25042/epi-ije.022021.03

*p*ISSN 2615-5109
*e*ISSN 2621-0541

A Low-Cost Vehicle Counting System based on the Internet of Things

Lanny Sitanayah[a], Apriandy Angdresey[b,*], Jeri Wahyu Utama[c]

[a]Department of Informatics Engineering, Faculty of Engineering, Universitas Katolik De La Salle, Manado - Indonesia.
Email: lsitanayah@unikadelasalle.ac.id
[b]Department of Informatics Engineering, Faculty of Engineering, Universitas Katolik De La Salle, Manado - Indonesia.
Email: aangdresey@unikadelasalle.ac.id
[c]Department of Informatics Engineering, Faculty of Engineering, Universitas Katolik De La Salle, Manado - Indonesia.
Email: 15013071@unikadelasalle.ac.id

Abstract

In urban areas where land for parking is very limited, drivers often waste time, fuel, and emissions circling around without information if unoccupied parking spaces are available or not. In this paper, we design and implement a low-cost wireless system to count the number of cars and motorcycles in a parking lot. The system consists of two sensor devices, which are installed at an entrance gate and an exit gate of a parking lot. Each device has a NodeMCU ESP8266, an HC-SR04 ultrasonic sensor, and an MPU-92/65 accelerometer. REST API is used as the web service to connect sensor devices and users, that will access the parking information using a web browser. The C4.5 algorithm is utilized to construct a decision tree to classify detected objects like cars, motorcycles, or people. We show by experiment that our sensor devices and the wireless monitoring system work correctly.

Keywords: C4.5 algorithm; data mining; decision tree; sensor device

1. Introduction

Population growth increases the need for land transportation, especially for the four-wheeled vehicles (cars) and the two-wheeled ones (motorcycles). This happens as people have to commute every day. In urban areas where land for parking is very limited, it is difficult to find parking spaces, especially during busy hours. Parking lots owned by shopping centers or business premises are either attended by operators or equipped with vehicle parking systems. However, some parking lots which are dedicated to public places – for example, sports arenas and parks – are usually unattended and do not have parking systems. In this case, drivers often waste time, fuel, and emissions circling around such parking lots without information on whether unoccupied parking spaces are available or not.

To solve this problem, an inexpensive sensor-based solution can be used, thanks to the Internet of Things (IoT) technology. In IoT, a device with one or more sensors, batteryless [1] or with batteries, can be used to sense physical phenomena, such as in [2]–[5] and send data wirelessly for further processing. Some works in the literature that detect the presence of vehicles have been done. In [6], they use the background subtraction method from Open-CV to detect, count and classify objects. To detect moving objects, they use motion detection functions based on video recordings from cameras. In [7], a car detection system for an IoT-based toll payment is built. With an objective to reduce congestion, the government has implemented the Radio Frequency Identification (RFID)-based electronic transaction payments on several tolls as an alternative. In this research, every vehicle is installed with a receiver that is connected to one user data. This is used to detect the position of the vehicle when it enters the toll gate without obstructing other vehicles. Another research to find unoccupied parking spaces in off-street parking lots is presented in [8]. They utilize ultrasonic sensors and IoT technology using ESP-8266 to provide information regarding the position and status of the parking lots.

Different from the previous works, in this paper, we propose a vehicle counting system based on IoT. Our contributions in this paper are summarized as follows.

1) We design and implement a low-cost wireless system to count the number of cars and motorcycles in a parking lot. The system consists of two sensor devices – one device is deployed at an entrance of a parking lot and the other one is deployed at an exit. Each device has a NodeMCU ESP8266, an HC-SR04 ultrasonic sensor, and an MPU-92/65 accelerometer.

*Corresponding author. Tel.: +62-813-9807-8886
Universitas Katolik De La Salle
Manado, Indonesia

2) We use the C4.5 algorithm to construct a decision tree, which is used to classify detected objects as cars, motorcycles, or people.

Part of this work has been published as a poster abstract in [9]. The rest of this paper is organized as follows. Section 2 reviews some works in the literature relevant to ours. Section 3 shows our system design and implementation, including hardware and software. Section 4 describes the object classification method used in this paper. Section 5 shows our performance evaluation, and finally Section 6 concludes the paper.

2. Related Works

A system to count the number of vehicles in an open parking area in real-time using the Open-CV background subtraction method is proposed in [6]. This motion detection function is used to detect moving objects based on video recordings from a camera. It is made using functions available in the Open-CV library through the C++ Application Programming Interface. This study uses several parameters, one of which is *learningRate*. The value of the *learningRate* parameter is based on environmental conditions and determined from the test results of the *learningRate* parameter variation. In this study, they also classify vehicles, *i.e.* cars or motorcycles, using the coordinate data of the height and width to determine the size of the detected vehicles.

In [7], a car detection system for toll payment based on the Internet of Things is proposed. The purpose of this research is to reduce congestion at the toll entrance gate. The Internet of Things technology is utilized since the Radio Frequency Identification (RFID)-based electronic transaction payment system cannot reduce the congestion problem significantly. On the Internet of Things-based system, each vehicle is equipped with a receiver connected to one user data. Hence, the system is able to detect the position of the vehicle when entering the toll gate without obstructing other vehicles. This transaction process can be carried out at a radius of 10 meters from the toll gate without stopping vehicles with an average speed of 10 km/hour. In the implementation, the time required is around 10 seconds for the toll entrance gate and 15 seconds for the toll exit gate.

In [8], an application to track or find empty parking spaces in off-road parking lots by utilizing ultrasonic sensors and the Internet of Things is developed. To track or find an empty parking space, they use an ultrasonic sensor and an ESP-8266 chip, which can provide information about the position and status of a parking space, whether it is filled or empty.

Data mining is a process of dredging or gathering important information from a large amount of data, resulting in several models to identify patterns between attributes that exist in the data set. Classification is a process in data mining that aims to find valuable patterns from a relatively large amount of data, build a model that describes and differentiates the classes or concepts for future prediction. For example, in [10], the authors use large amounts of ad-hoc vehicle's real-time traffic data to predict traffic congestion in a city by using classification and clustering methods. This study shows that traffic congestion can be predicted more accurately and the percentage of accuracy can be increased by increasing the size of the training data.

In [2], the authors created a wireless system based on the Internet of Things to monitor and predict water quality in public swimming pools. They utilize a data mining prediction model, namely the Iterative Dichotomiser 3 decision tree algorithm. In [11], data mining is used to identify the sex of a tarantula by classifying the training data obtained for almost a year.

The C4.5 algorithm is one of the algorithms used for classification or segmentation and is predictive. This algorithm is the development of the Iterative Dichotomiser 3 (ID3) algorithm and hence they have the same basic principles. C4.5 is used in [12] to determine a model for predicting soil quality by using training data on soil composition. The experimental results obtained show that the expression of knowledge using the C4.5 algorithm is easy to understand, improves forecasting accuracy, and provides a reliable theoretical basis for precision fertilization. Another example of C4.5 utilization is to minimize the workload of student admissions in planning school promotions and improving planning strategies by classifying demographics [13]. In addition, the C4.5 algorithm is also used to identify diseases from existing symptoms [14].

In this work, the authors identify the possibility of indications of diabetes insipidus apart from gestational diabetes insipidus at productive age (students). They use the *k*-means algorithm to classify the symptoms, and the C4.5 algorithm to identify the type of diabetes. Furthermore, in [15], C4.5 is used to analyze catfish and carp diseases to determine the history of fish disease relationships, which will be used to identify fish diseases.

3. System Design and Implementation

The wireless vehicle counting system is illustrated in Fig. 1. We attach two sensors – an HC-SR04 ultrasonic sensor and an MPU-92/65 accelerometer – to each sensor device. We use the ultrasonic sensor to measure the physical distance to an object in front of it, while the accelerometer is used to measure any vibration resulted from the moving object. The distance and vibration data from the sensors is sent to a web server wirelessly using the NodeMCU ESP8266's ESP-12E Wi-Fi module. This data is received by REST API and forwarded to the application.

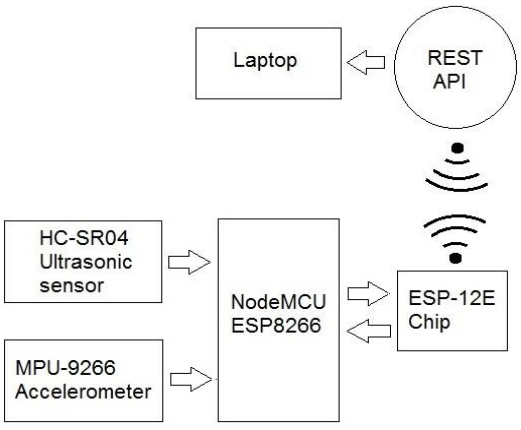

Figure 1. The wireless vehicle counting system

Table 1. Hardware and software

Hardware/Software	Purpose
NodeMCU ESP8266	Gather and send data
HC-SR04	Ultrasonic sensor
MPU-92/65	Accelerometer
Laptop/Mobile Device	Access data from the web server
Arduino Program	Gather and send data
PHP Program	Process data

In this work, we use two sensor devices, where we deploy one device at an entrance of a parking lot and the other one is at an exit. Table 1 lists the hardware and software components used in the system.

The total cost of the main components, i.e. a NodeMCU ESP8266, an HC-SR04 ultrasonic sensor and an MPU-92/65 accelerometer for one sensor device in our system is approximately US$ 8. Compared to [6] that uses a webcam and a Raspberry Pi 3 model B, the total cost is around US$ 43. The system in [7] requires that each vehicle must be equipped with a receiver, while the system in [8] requires that each parking space must be monitored by one sensor device. Even though the total cost for a receiver in [7] that consists of a NodeMCU ESP8266, a buzzer, and an LCD 16x2 is only around US$ 4, they must take into account the number of cars that use the system. Similarly, even though the total cost for a sensor device in [8] that consists of an ESP8266 D1 mini, an HC-SR04 ultrasonic sensor, and an LCD 16x2 is around US$ 4, they must provide as many devices as the number of parking spaces. Our system, on the other hand, only requires two devices and hence its total cost is the lowest. The prices reported in this paper are calculated based on prices from www.tokopedia.com.

3.1. Hardware

We show the hardware design of our sensor device in Fig. 2. Each sensor device has a NodeMCU ESP8266, an HC-SR04 ultrasonic sensor, and an MPU-92/65 accelerometer. NodeMCU and the ultrasonic sensor are attached to a breadboard, while the accelerometer is tied to a rope as a physical medium to carry vibrations. Both NodeMCU and the ultrasonic sensor are powered by external batteries, while the accelerometer gets power from NodeMCU. To connect NodeMCU and the accelerometer, we connect NodeMCU's D5 pin to the accelerometer's SDA pin, D6 pin to SCL pin, GND pin to GND pin, and 3V pin to VCC pin. Then, to connect NodeMCU and the ultrasonic sensor, we connect NodeMCU's D7 pin to the ultrasonic sensor's echo pin, while D8 pin is connected to the trigger pin. The pins configuration is summarized in Table 2 and the hardware implementation is shown in Fig. 3.

Table 2. Pins configuration

NodeMCU	Accelerometer	Ultrasonic Sensor
D5 pin	SDA pin	-
D6 pin	SCL pin	-
D7 pin	-	Echo pin
D8 pin	-	Trigger pin
GND	GND	-
3V	VCC	-

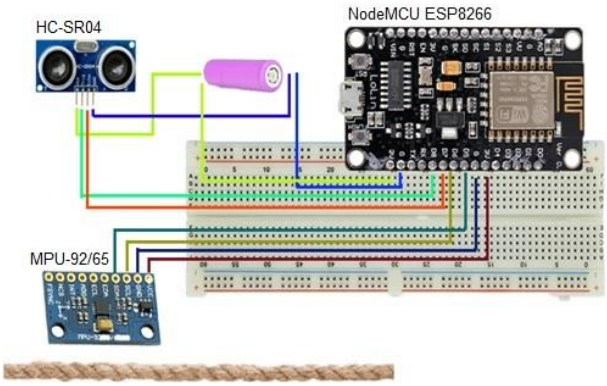

Figure 2. Hardware design

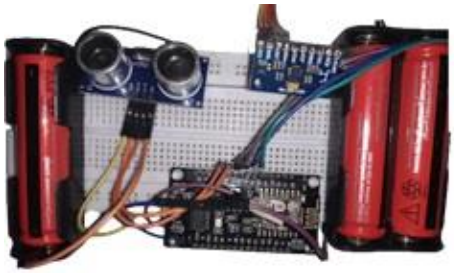

Figure 3. Hardware implementation

3.2. Software

The wireless vehicle counting system is divided into the client-side and the server-side. At the client-side, we have an Arduino program that is uploaded to NodeMCU of both sensor devices. The client flowchart is shown in Fig. 4. First, the Arduino program checks if all sensors are connected to NodeMCU and whether the Internet connection is available. Then, the Arduino program reads the sensors' data and sends it wirelessly to the webserver.

At the server-side, we have REST API as the back end and a PHP (Hypertext Preprocessor) program as the front end. The server flowchart is depicted in Fig. 5.

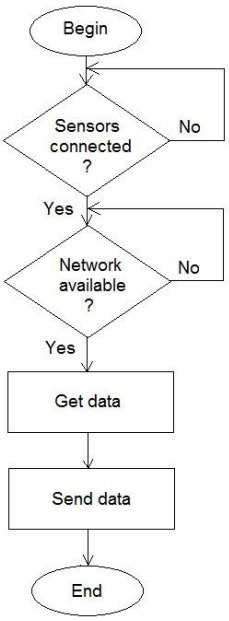

Figure 4. Client flowchart

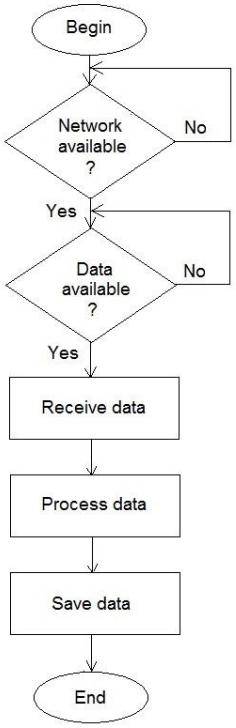

Figure 5. Server flowchart

First, if the Internet connection is available, we check if data is successfully received. If the data is available, it is processed and then stored in the database. To access the parking information from the web server, users can use a web browser. We utilize the C4.5 algorithm to construct a decision tree in order to classify objects as cars, motorcycles, or people. Then, we count how many cars and motorcycles that enter and exit the parking lot. The calculation result is displayed to users as the number of free parking spaces.

4. Object Classification Method

In this section, we present some classified objects based on data obtained from the sensor devices. We utilize the C4.5 algorithm for object classification. C4.5 is a method used for classification problems in machine learning and data mining. Its objective is for grouping and it is predictive for finding patterns with relatively large to very large values. In general, C4.5 has the following steps to build a decision tree: (1) find an attribute to be the root, (2) create a branch for each value and divide cases into branches, and (3) repeat the process for each branch until all cases on the branch have the same class. To choose a variable as the root, we calculate and select the highest gain using the following formula:

$$Gain(S,A) = Entropy(S) - \sum_{i=1}^{n} \frac{|S_i|}{|S|} * Entropy(S_i) \quad (1)$$

$$Entropy(S) = \sum_{i=1}^{n} P_i * Log_2(P_i) \quad (2)$$

where S is a set of cases, A is the attribute, and n is the number of partitions of attribute A. Furthermore, the number of cases in the i-th partition is $|S_i|$ and the number of cases in S is $|S|$. Before we calculate gain, we need to calculate entropy (see Equation 2) to determine how informative an input variable is, where P_i is the proposition of S_i to S.

Table 3 shows some of the raw data taken using the ultrasonic sensor and the accelerometer. Distances acquired by the ultrasonic sensor are measured in centimeters. The three-axis accelerometer data on the X-axis is denoted by A_x, on the Y-axis is denoted by A_y, and on the Z-axis is denoted by A_z. We also record the time when the data is captured and the class of objects to be classified. The class is divided into car, motorcycle, and person. Then, from the raw data that we obtained, we further clean and transform the data into categories in order to simplify the algorithm's calculations.

The following range formula is used to create categories for each variable:

$$Range(S) = \frac{X_{\max} - X_{\min}}{n} \quad (3)$$

Table 3. Raw data

Distance	A_x	A_y	A_z	Time	Class
92	-1.80	3.39	3.11	16:03:36	Person
72	-1.66	3.47	3.13	16:03:37	
88	-1.24	3.42	3.17	16:06:29	Car
77	-1.46	3.31	3.27	16:06:30	
79	-1.58	3.27	3.09	16:06:30	
73	-1.63	3.66	3.15	16:09:29	Car
72	-1.59	3.43	2.97	16:09:30	
72	-1.58	3.31	3.02	16:09:30	
94	-1.40	3.44	3.06	16:11:33	Person
95	-1.79	3.43	3.39	16:13:38	Motorcycle
85	-1.59	3.29	2.89	16:13:38	
74	-1.63	3.54	3.08	16:13:39	
95	-1.62	3.20	3.09	16:14:11	Motorcycle
80	-1.71	3.47	3.02	16:14:11	
90	-1.57	3.71	3.02	16:15:40	Car
80	-1.53	3.23	2.79	16:15:40	
78	-1.53	3.27	3.12	16:15:41	
76	-1.64	3.82	3.25	16:15:41	
76	-1.73	3.31	3.17	16:15:41	
79	-1.65	3.25	3.11	16:17:23	Motorcycle
89	-1.73	3.32	3.06	16:17:24	
95	-1.72	3.19	3.21	16:17:24	
80	-1.69	3.25	3.09	16:18:11	Person
81	-1.73	3.26	2.93	16:18:12	

Table 4. Clean data

Distance	A_x	A_y	A_z	Time	Class
Medium	Low	Medium	Medium	Low	Person
Medium	High	Medium	High	Medium	Car
Near	Medium	High	High	High	Car
Far	Low	Medium	Low	Low	Person
Medium	Low	High	Medium	Medium	Motorcycle
Far	Medium	Medium	Low	Low	Motorcycle
Medium	Medium	High	High	High	Car
Far	Medium	Low	High	Medium	Motorcycle
Near	Medium	Low	Low	Low	Person

Table 5. Entropy and gain

Variable	Category	Total (S)	Person (S_i)	Motorcycle (S_i)	Car (S_i)	Entropy	Gain
Distance	Near	2	1	0	1	0	0.91829
	Medium	4	1	1	2	1.5	
	Far	3	1	2	0	0	
A_x	Low	3	2	1	0	0	0.91829
	Medium	4	1	2	2	1.5	
	High	2	0	0	1	0	
A_y	Low	2	1	1	0	0	0.91829
	Medium	4	2	1	2	1.5	
	High	3	0	1	1	0	
A_z	Low	3	2	1	0	0	1.36274
	Medium	2	1	1	2	1	
	High	4	0	1	1	0	
Time	Low	4	3	1	0	0	1.5849
	Medium	3	0	2	1	0	
	High	2	0	0	2	0	
Total		9	3	3	3	1.584962	

where X_{max} is the highest reading of a variable, X_{min} is the lowest reading of that variable, and n is the number of categories that we want. In this paper, we use n = 3. For example, the categories for the distance variable are near (70.23 cm - 78.153 cm), medium (78.153 cm - 86.076 cm), and far (86.076 cm - 94.00 cm). After that, for each variable, we calculate the average value for each available data to decide in which categories the data belongs. Table 4 shows the data that has been cleaned.

A decision tree is then created after calculating the total entropy, entropy of each variable, the gain, and the highest gain. In this case, the total entropy = 1.5849625 and gain = 0.918295834. The calculation results of the entropy and gain are shown in Table 5.

5. Performance Evaluation

To evaluate our proposed system, including both hardware and software, we conduct a series of experiments, which are described in the following. The parameters used in the evaluation are given in Table 6.

Table 6. Evaluation parameters

Parameter	Value
Time interval between objects	≥ 1 sec
Object's speed	≤ 10 km/hour
Sensor device's height	0.5 m
Sensor device's distance	≤ 4 m

5.1. Experimental setup

In this research, we do not detect the direction of vehicles. Therefore, we assume that cars and motorcycles enter the parking lot through the entrance gate and leave through the exit gate. To count the number of cars and motorcycles, we utilize two sensor devices – one at an entrance to sense them entering the parking lot and one at an exit to sense them leaving. Each sensor device is mounted at a certain height above the ground as shown in Fig. 6. The height is carefully chosen, *i.e.* 0.5 m, so that the ultrasonic sensor can sense moving objects in front of it. As for the sensor device's distance to the moving object, we use the HC-SR04 ultrasonic sensor detection range, *i.e.* from 2 centimeters to 4 meters.

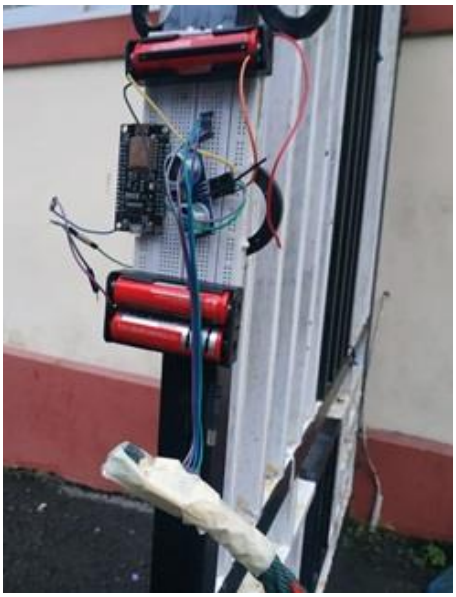

Figure 6. Sensor device installation

The accelerometer is attached to a rope that is put on the ground across the road. Therefore, when vehicles' wheels touch the rope, the accelerometer can sense the vibration.

Furthermore, we also assume that two moving objects are at least one second apart. Otherwise, they are detected as one object. The moving speed of an object is at most 10 km/hour as it is the maximum speed allowed for vehicles in the parking area. An object is detected when the readings of the ultrasonic sensor and the accelerometer change. When this happens, the sensor readings are sent to the webserver. To classify the detected objects, we use a decision tree which is constructed using the C4.5 algorithm. Our system classifies the objects as either cars, or motorcycles, or people. When the system detects a car or a motorcycle, it updates its counter and users can get the parking information using a web browser.

5.2. Experimental Results and Discussion

First of all, we test the hardware that has been built, whether all sensors can function properly and the device can send data to the webserver. We also test if the webserver can receive the data. The results of our experiment show that all sensors work properly, the device can send data and the web server can receive the data as shown in Fig. 7.

```
gx : -4.64, gy : 3.26, gz : 2.67 us : 45
gx : -1.91, gy : 2.09, gz : 2.65 us : 75
gx : -1.36, gy : 2.11, gz : 2.89 us : 76
gx : -1.96, gy : 1.76, gz : 1.96 us : 51
gx : -2.31, gy : 0.73, gz : 3.23 us : 40
gx : -1.69, gy : 3.47, gz : 1.33 us : 74
gx : -0.64, gy : 1.45, gz : 2.76 us : 69
gx : -2.23, gy : 2.97, gz : 1.73 us : 75
gx : -1.13, gy : 2.40, gz : 3.01 us : 68
gx : -0.05, gy : 2.84, gz : 3.45 us : 76
```

Figure 7. Sensor data received at the webserver

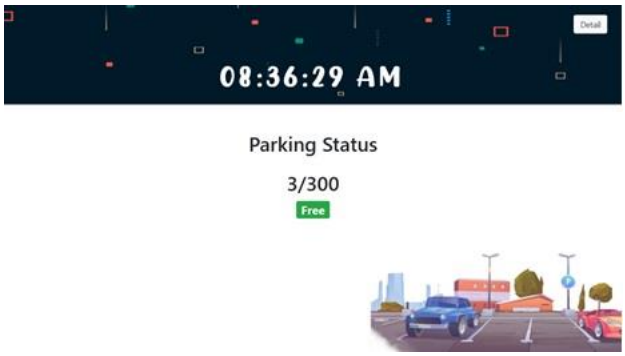

Figure 8. Application's main page in a web browser

Figure 9. Application's parking details in a web browser

To access the parking information from the web server, users can use a web browser. We use three web browsers for testing purposes. They are Google Chrome Version 84.0.4147.89, Mozilla Firefox version 76.0.1, and Microsoft Edges version 84.0.522.40. The application's main page in a web browser is depicted in Fig. 8 and the parking details are shown in Fig. 9. Figure 8 is the main page of the application. On this page, there is a digital clock at the top of the application and the parking information in the middle, which indicates the status of the parking lot. Free means there are unoccupied parking spaces, whereas full means all parking spaces are occupied. Furthermore, Figure 9 shows parking details that contain detailed information from the acquired data. On this page, there is a bar chart that informs us how many vehicles (cars and motorcycles) enter and leave the parking lot.

6. Conclusion and Future Work

This paper proposes a low-cost Internet of Things-based vehicle counting system to count the number of cars and motorcycles in a parking lot. Two sensor devices are required in this system – one at an entrance gate and one at an exit gate of a parking lot. Each sensor device consists of a NodeMCU ESP8266, an HC-SR04 ultrasonic sensor and an MPU-92/65 accelerometer. We use REST API as the web service to connect sensor devices and users. We use C4.5 to build a decision tree to classify detected objects like cars, motorcycles, or people. We show by experiment that the sensor devices and the system work correctly.

Due to the COVID-19 pandemic and social restrictions that has been in place when we carried out the evaluation, we were unable to conduct a thorough experiment. We will continue to acquire more data over a

longer period of time once we are able to do so. We also plan to deploy more sensor devices at more entrance and exit gates.

References

[1] J. Hester *et al.*, "Persistent Clocks for Batteryless Sensing Device," *ACM Trans. Embed. Comput. Syst.*, vol. 15, pp. 1–28, 2016.

[2] A. Angdresey, L. Sitanayah, and V. J. A. Sampul, "Monitoring and Predicting Water Quality in Swimming Pools," *EPI Int. J. Eng.*, vol. 3, no. 2, pp. 119–125, 2020.

[3] L. Sitanayah, A. Angdresey, and E. Kristalino, "Poster Abstract: A Sensor-based Application for Road Conditions Detection," in *The 18th ACM Conference on Embedded Networked Sensor Systems (SenSys)*, 2020, pp. 651–652.

[4] J. B. Sanger, L. Sitanayah, and V. D. Kumenap, "Detection System for Cigarette Smoke," in *The 4th International Conference on Information Technology, Information Systems and Electrical Engineering (ICITISEE)*, 2019, pp. 145–149.

[5] J. B. Sanger, L. Sitanayah, and I. Ahmad, "A Sensor-based Garbage Gas Detection System," in *The 11th Annual Computing and Communication Workshop and Conference (CCWC)*, 2021, pp. 1359–1364.

[6] M. Hariyanto, A. Sofwan, and A. Hidayatno, "Design of a Vehicle Counting System in a Parking Area Using the Internet of Things-Based Background Subtraction Method," *Transient J. Ilm. Tek. Elektro*, vol. 7, no. 3, 2019. [in Bahasa]

[7] A. R. Muzakhir, M. Imroba, and A. G. Putrada, "Car Detection System on Internet of Things-Based Toll Gate Payment Application," *SMARTICS J.*, vol. 5, pp. 97–103, 2019. [in Bahasa]

[8] A. D. Limantara, Y. C. S. Purnomo, and S. W. Mudjanarko, "Modeling of Empty Parking Lot Tracking System Based on Ultrasonic Sensors and Internet of Things (IoT) in Off-Road Parking Lot," in *Prosiding Semnastek*, 2017.

[9] L. Sitanayah, A. Angdresey, and J. W. Utama, "Poster: An Internet of Things-based Vehicle Counting System," in *The International Conference on Embedded Wireless Systems and Networks (EWSN)*, 2021.

[10] A. Angdresey and P. K. Sahoo, "Analysis of VANET Big Data for Predicting Traffic Congestion in a City," in *The 12th Workshop on Wireless Ad Hoc and Sensor Networks (WASN)*, 2016.

[11] A. Angdresey and M. Wongkar, "Identification of The Reproductive Apparatus of Tarantula Genus Brachypelma Using Linear Discriminant Analysis Method," in *International Conference on Electrical Engineering and Computer Science (ICECOS)*, 2018, pp. 409–414.

[12] L. Dongming, L. Yan, Y. Chao, L. Chaoran, L. Huan, and Z. Lijuan, "The Application of Decision Tree C4.5 Algorithm to Soil Quality Grade Forecasting Model," in *The 1st IEEE International Conference on Computer Communication and the Internet (ICCCI)*, 2016, pp. 552–555.

[13] S. A. Abaya and B. D. Gerardo, "An Education Data Mining Tool for Marketing Based on C4.5 Classification Technique," in *The 2nd International Conference on E-Learning and E-Technologies in Education (ICEEE)*, 2013, pp. 289–293.

[14] A. Angdresey and J. Matrutty, "Implementation of k-Means and C4.5 Algorithm in Identifying Diabetes Insipidus in Productive Age. Case Study: Students of Unika De La Salle Manado," in *SeminarNasional Riset dan Teknologi Terapan Ke-8 (RITEKTRA VIII)*, 2018, pp. 515–520. [in Bahasa]

[15] K. Sucipto and E. L. Taufiq, "Classification Method of Multi-Class on C4.5 Algorithm for Fish Diseases," in *The 2nd International Conference on Science in Information Technology (ICSITech)*, 2016, pp. 5–9.

EPI International Journal of Engineering
Volume 4, Number 1, February 2021, pp. 21-28
DOI: 10.25042/epi-ije.022021.04

*p*ISSN 2615-5109
*e*ISSN 2621-0541

Contact-Free Mortuary Trolley Design as a Device for the Mobility of Covid-19 Victims

Vania Katherine Mulia[a], Nanda Indriana[b], Qurriyatus Zahro[c], Farid Triawan[d,*]

[a]Mechanical Engineering Department, Faculty of Engineering and Technology, Sampoerna University.
Email: vania.mulia@my.sampoernauniversity.ac.id
[b]Mechanical Engineering Department, Faculty of Engineering and Technology, Sampoerna University.
Email: nanda.indriana@my.sampoernauniversity.ac.id
[c]Mechanical Engineering Department, Faculty of Engineering and Technology, Sampoerna University.
Email: qurriyatus.zahro@my.sampoernauniversity.ac.id
[d]Mechanical Engineering Department, Faculty of Engineering and Technology, Sampoerna University.
Email: farid.triawan@sampoernauniversity.ac.id

Abstract

The Covid-19 pandemic has caused many issues, especially in the medical field. One of the groups that are affected by the pandemic the worst is the health workers. The surge of demand for health services, especially for Covid-19 patients, overwhelms health workers, forcing them to work extra hard and eventually experience exhaustion. Due to this condition, the health workers may face difficulties in doing heavy-duty work. This paper proposes a design of a mortuary trolley as a device to ease the health workers in handling the dead bodies of Covid-19 victims. Considering the need for a corpse mobility aid that is contact-free, the design utilizes a combination of a scissor lift structure, a power screw mechanism to elevate and lower the table, and a conveyor system to load and unload the table. To ensure that the device can operate without experiencing unwanted failure, strength analyses are done on the most critical components, such as the scissor arm, pin joint, power screw, and scissor arm connector, to determine the safety factor at maximum load in static and fatigue loading condition. Analysis results show that all those components have a safety factor greater than 1 for both static and fatigue loading conditions, indicating the device will not yield and is predicted to have infinite life. The design and analyses of this device can be a reference for manufacturers of medical devices to design a mortuary trolley to ease the work of health workers.

Keywords: Engineering design; fatigue analysis; mortuary trolley; static analysis

1. Introduction

It has been more than a year since the first appearance of Covid-19 in the world and Indonesia, and this pandemic has not yet subsided and continues to make such big changes to our lives. A heavy burden is especially experienced by the health workers who must serve in the emergency room and make decisions about patient priorities. What is meant by health workers according to *Undang-Undang No. 36 of 2014* is "everyone who devotes himself to the health sector and has the knowledge and/or skills through education in the health sector which for certain types requires the authority to make health efforts [1]. This group of health workers includes medical personnel such as doctors and nurses.

Currently, health workers must work harder than usual at the forefront of handling Covid-19 and many of them experience fatigue, burnout, to psychological stress. A study conducted by a research team from the Master of Work Medicine Study Program at the Faculty of Medicine, University of Indonesia (*MKK FKUI*) in 2020 showed 83 percent of health workers had burnout syndrome, which affects their performance in carrying out their duties and their quality of life [2]. In fact, many have died to deal with Covid-19 patients. Statistical data shows that as of April 26th, 2021, 900 health workers have died fighting Covid-19 [3]. The condition of health workers who are starting to become exhausted creates new problems, where various heavy jobs can become difficult.

One problem that can be highlighted is the process of handling the dead bodies of Covid-19 sufferers. In fact, there are still many processes in it that require health workers to move the bodies, for example from the corpse bed into the coffin or to the place where the corpse is bathed. Apart from being a heavy job to move them from one place to another, this has the potential to violate the health protocols proclaimed by the World Health Organization (WHO), in which physical contact must be minimized. In a situation like this, it is necessary to have a device that allows the transfer of the dead bodies

*Corresponding author. Tel.: +62-21-5022-2234, Ext:7849
Jl. Raya Pasar Minggu, Kav 16
Jakarta Selatan, Indonesia, 12780

without making any slightest physical contact. By modifying the shape of the existing mortuary trolley, a plate-shaped base supported by a conveyor feature connected to a slider mechanism can be added to allow for the lifting of the body with minimal force and a contact-free process. Hopefully, this tool can make it easier for exhausted health workers to carry out the process of caring for the corpse more safely and efficiently.

Based on the existing background, the objective of this paper is to find the most possible design of the mortuary trolley that allows the mobility of the dead body without any physical contact. This paper also explores how the mortuary trolley system works, as well as the advantages and constraints of the mortuary trolley design which will allow the mobility of the dead body without any physical contact. This design can be used as a reference for manufacturers of medical devices in producing a mortuary trolley for Covid-19 victim mobility purposes.

2. Methodology

To overcome this, an attempt is made to design a contact-free mortuary trolley. The design process is done according to the flow of mechanical design proposed by Shigley, which consists of the identification of needs, problem definition, synthesis, analysis and optimization, evaluation, and presentation [4]. During the synthesis stage, various sketches are made with different ideas of the mechanism, and design ranking is done to pick the best design based on the desired specifications [5]. The dimensions of the components are determined and optimized from the stress analyses in the analysis and optimization stage.

2.1. Design concept

Figure 1 shows the proposed design of the contact-free mortuary trolley, with the numbered parts corresponding to Table 1. The contact-free mortuary trolley is designed with several specifications. One of its specifications is that it can lift 250 kg in 150 cm of height at maximum. To satisfy the specification, this design is adopting a scissor lift working system to lift the dead bodies in up and down direction. The working system of a scissor lift is considered to be very advantageous in many applications due to its solid structure which can withstand a heavy load and provides smooth movement [6]. The strength of the scissor lift is derived from a pair of scissor arms which are strung together to form the letter 'X,' so the weight of the load placed on the platform is equally distributed on the two scissor arms. Furthermore, by stretching and folding the scissor arm arrangement, this crossing mechanism will increase and decrease the load. Usually, to increase the load, pressure is applied to the lower cross-section, so that the cross structure can extend vertically [7].

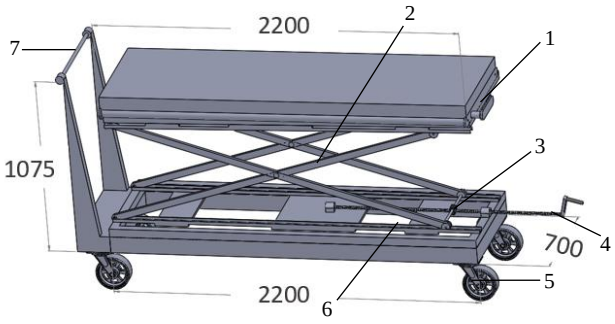

Figure 1. The final design of the mortuary trolley (dimension in mm)

Table 1. List name of the part

No	Name of the Part
1	Conveyor System
2	Scissor Lift
3	Connector between Scissor lift and Power Screw
4	Power Screw
5	Wheel
6	Wheel Rail
7	Handle

Initially, this mortuary trolley was designed with a hydraulic as a source of power so the arm will be able to move up and down. However, this idea will lead to failure in achieving one specification (Price estimation IDR 12-15 million) since hydraulic is considered to be having a high price on the market. Hence, the source of the power of the mortuary trolley is decided to be using a power screw. Furthermore, by turning the power screw with a ratchet handle on one side of the device, the heavy load received by the horizontally positioned power screw can be overcome through minimal effort applied to the power screw [8].

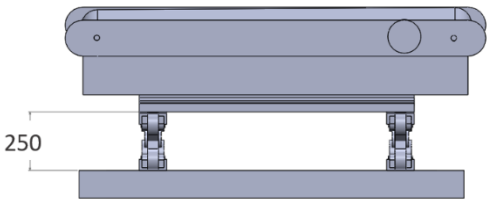

Figure 2. Illustration of the mortuary trolley in the minimum point (dimension in mm)

Figure 2 shows its lowest position. The height of the mortuary trolley is 250 mm. This device is expected to be able to reach low places even in the process of moving corpses from one place to another so that this device can later be maximized its use without limitation in how low the area can be reached by this device.

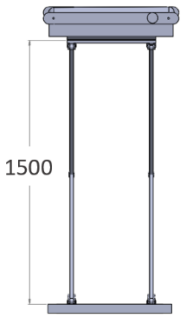

Figure 3. Illustration of the mortuary trolley in the maximum point (dimension in mm)

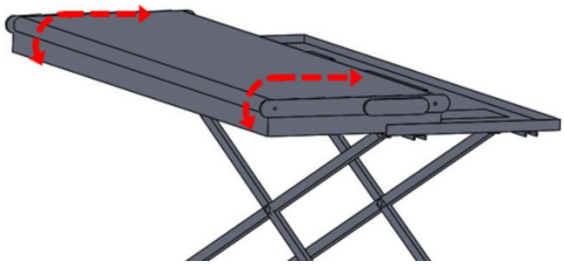

Figure 4. Illustration of the table slider at the furthest position with the conveyor direction

Figure 3 shows the condition of the scissor lift when the table is in its highest position. At the maximum point, the mortuary trolley can reach a height of about 1500 mm. There is a possibility that some high enough areas that may generally require health workers have to lift corpses where we both know that the higher the load is lifted, the greater the energy required. Therefore, it is hoped that this tool can help a crucial part in removing corpses to a high enough area.

This design adopts a conveyor system that will be used to move dead bodies from one place to another with a contactless process. A conveyor mechanism is a mechanical system used to move material from one location to another location [9]. By adopting a conveyor system for the mobility of the movement of dead bodies, this tool can really minimize the physical touch that can cause the virus infection. This conveyor system is connected to a structure resembling a scissor lift which functions to control the height of the table where the bodies are placed. This conveyor will be in the form of a thin board with a cylindrical rod inside it which will move left or right to shift the dead body. The direction of the conveyor movement is indicated by the red arrows in Fig. 4.

The movement of the conveyor can be controlled by a lever that is connected to the end of one of the cylinder rods, and it can be rotated in both directions. In addition, this conveyor system is attached to a slider table that can slide sideways, with its furthest position as seen in Fig. 4. The goal of this slider table is to be positioned underneath the dead body while still on the bed or table, thus reducing the distance that the health worker needs to lift the dead body in order to move it from the bed or table to this mortuary trolley.

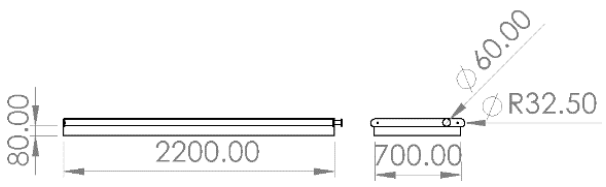

Figure 5. Conveyor part (dimension in mm)

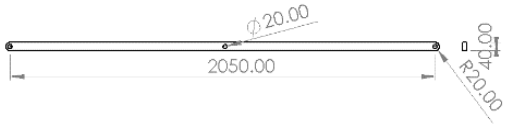

Figure 6. Scissor arm (dimension in mm)

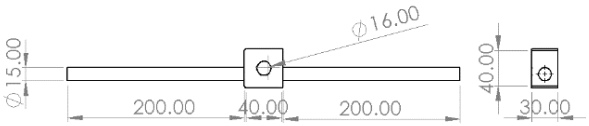

Figure 7. The connector between the scissor lift and power screw (dimension in mm)

Like a trolley, this design is equipped with four wheels and handrails, so it is easy to move. Furthermore, to facilitate the movement of dead bodies, it is necessary to develop further ideas through system modifications that can control the movement of platforms that have been facilitated by conveyors so that the movement of bodies can still be carried out with the appropriate moral values.

The design is divided into three main parts. The first is the conveyor part (Fig. 5), the second is the scissor lift part (Fig. 6), and the last is the power screw part (Fig. 7).

2.2. Material selection

The material for the mortuary trolley should be strong, not heavy, and safe for humans. This can encourage this tool to be operated by one person. Based on this condition, the suitable material is stainless steel. Stainless steel has corrosion-resistant properties and optimum hardness at room temperature, so stainless steel is essential for medical, chemical, cryogenic, and biotechnological applications [10]. Furthermore, stainless steel also has strong strength, good formability, and good weldability [11]. This proposed design, therefore, uses stainless steel material for the frame, power screw, and scissor lift. The dimensions have been optimized to be compact enough for a small weight.

The material that is used is stainless steel 304. Stainless steel 304 has several material properties that are shown in Table 2 [12].

Table 2. Mechanical properties of stainless steel 304

Mechanical Properties	Metric	English
Density	8.00 g/cc	0.289 lb/ln^2
Hardness, Rockwell B	70	70
Tensile Strength, Ultimate	505 MPa	73200 psi
Tensile Strength, Yield	215 MPa	31200 psi
Modulus of Elasticity	193 GPa	28000 ksi

2.3. Strength analysis procedure

Analyses must be done to ensure that the device is functional and that it does not experience unwanted failure, either due to static or fatigue loading. To do this, the load is assumed on the device at the most critical condition, which is when the table is at its highest position. In this position, the scissor arm connected to a pin-sliding joint will be the closest to the midpoint of the table where the load is concentrated. This position will force the scissor arm to withstand the maximum possible load.

To describe the safety of the device, strength analyses are performed for the most critical components, which are the scissor arm, the power screw/thread used to control the table's height, the connecting pins, and the connector between the scissor arms and the thread. A free-body diagram (FBD) is made for each component, and by applying the force and moment equilibrium equations, all the forces exerted on each body can be found. From the FBD, shear force diagrams (SFD) and bending moment diagrams (BMD) can be drawn to find the location at which the body experiences the greatest bending moment and thus the greatest stress [13]. In addition, the torque in the power screw required to raise the table is also calculated, assuming that the thread is an Acme thread. Eventually, the stresses can be calculated and the safety factor under static loading can be found using the distortion-energy failure criterion.

For fatigue analysis, the components are assumed to experience fluctuating load between maximum loaded and unloaded. The maximum stress value is taken from the static force analysis, while the minimum stress value is taken to be zero (unloaded). The fatigue analysis is done by calculating the endurance limit, Marin factors, midrange and alternating stresses, and finally the fatigue safety factor. Soderberg fatigue failure criterion is used as it is the most conservative criterion.

The formula used in the analysis are [4], [14]:

$$\sigma_b = \frac{Mc}{I} \tag{1}$$

$$\sigma_a = \frac{P}{A} \tag{2}$$

$$T_R = \frac{Fd_m}{2}\left(\frac{l + \pi f d_m \sec\alpha}{\pi d_m - fl\sec\alpha}\right) \tag{3}$$

$$\tau = \frac{16T_R}{\pi d_r^3} \text{ (for power screw)} \tag{4}$$

$$\sigma' = \frac{1}{\sqrt{2}}[(\sigma_x - \sigma_y)^2 + (\sigma_y - \sigma_z)^2 + (\sigma_z - \sigma_x)^2 + 6(\tau_{xy}^2 + \tau_{yz}^2 + \tau_{zx}^2)]^{1/2} \tag{5}$$

$$n_s = \frac{S_y}{\sigma'} \tag{6}$$

$$n_f = \left(\frac{\sigma_a}{S_e} + \frac{\sigma_m}{S_{ut}}\right)^{-1} \tag{7}$$

where,

σ_b : normal stress due to bending (MPa)
M : bending moment (N.m)
c : maximum distance from the bending neutral axis (m)
I : area moment of inertia about the neutral axis (m^4)
σ_a : normal stress due to axial load (MPa)
P : axial load (N)
A : cross-section area (m^2)
T_R : torque required to raise the load (N.m)
F : loading force (N)
d_m : power screw mean thread diameter (m)
l : power screw thread lead (m)
f : friction coefficient between the power screw thread and nut element
α : power screw thread angle (degrees)
τ : shearing stress due to torsion (MPa)
d_r : power screw thread minor diameter (m)
σ' : Von Mises stress (MPa)
$\sigma_x, \sigma_y, \sigma_z$: normal stress in the x, y, and z direction (MPa)
$\tau_{xy}, \tau_{yz}, \tau_{zx}$: shear stress in the x-y, y-z, and z-x direction (MPa)
n_s : safety factor under static loading
S_y : yield strength (MPa)
n_f : safety factor under fatigue loading
σ_a : amplitude of the alternating component of stress (MPa)
σ_m : midrange steady component of stress (MPa)
S_e : endurance limit (MPa)
S_{ut} : ultimate tensile strength (MPa)

3. Results and Discussion

3.1. Static analysis

For the scissor lift structure itself, static analysis is performed only for one side of the scissor lift. The maximum load (2500 N) is assumed to be evenly distributed to both sides of the scissor lift. Although there is a conveyor mechanism and a table slider which can shift the load sideways, the table slider is expected to still be supported by the bed or table on which the dead body is initially placed, thus not accounted as the critical condition of this trolley. The weight of the components is neglected in this calculation. The FBD of the scissor lift structure can be seen in Fig. 8. The joints at point B and G are pin-sliding joints, while at point D, E, and H they are pin joints.

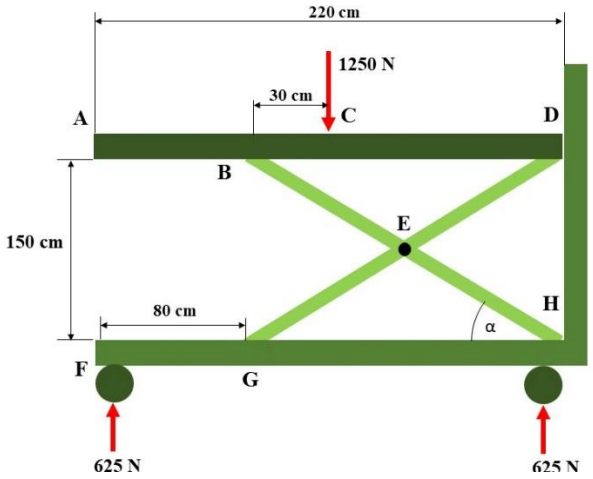

Figure 8. FBD of the scissor lift structure

From the FBD in Fig. 8, the forces at each joint can be found by applying the equation of equilibrium of forces and moments. Then, the FBD of each component can be drawn to find the forces exerted on each component. Figures 9, 10, 11, and 12 show the FBD and the found forces for the scissor lift table, scissor arms, pin joint, and scissor arm connector, respectively. The load is initially transferred from the scissor lift table (Fig. 9) to the scissor arms as reaction forces at points B and D. In the scissor arms (Fig. 10), there are also reaction forces at the pin joint connecting each other at point E. The pin at point E experiences transverse load from both scissor arms (Fig. 11), represented by two distributed loads along the scissor arms' thickness. Finally, the connector between the two sides of the scissor lift structure experiences a three-point bending (Fig. 12) due to the force at point G in the x-direction.

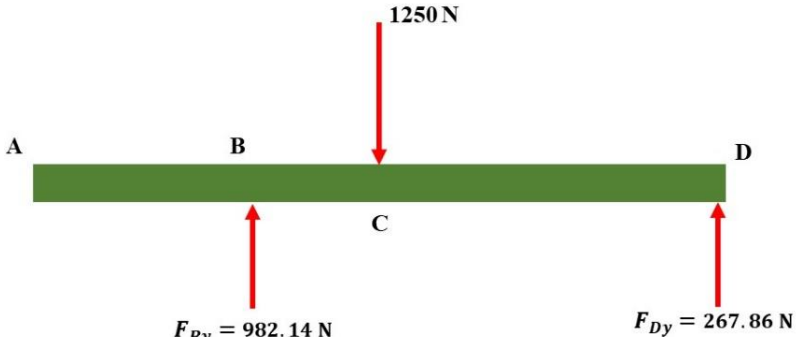

Figure 9. FBD of the scissor lift table

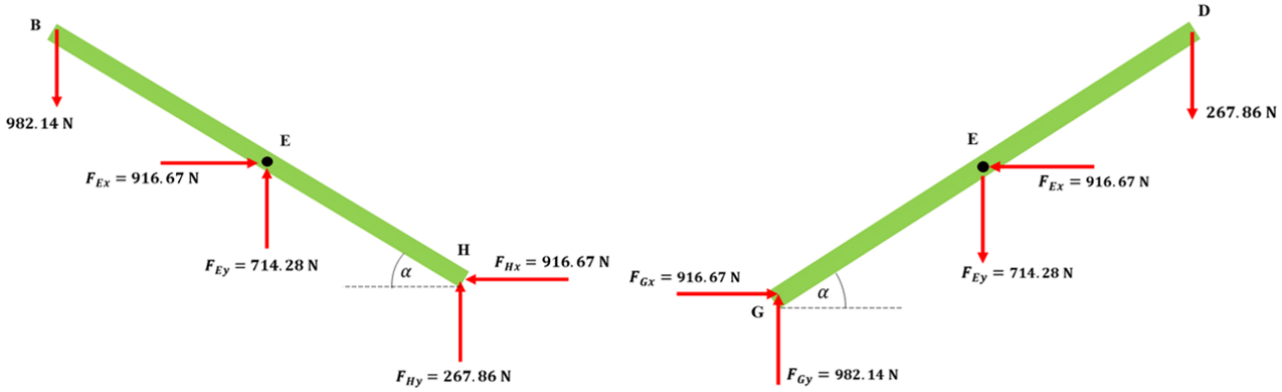

Figure 10. FBD of scissor arms

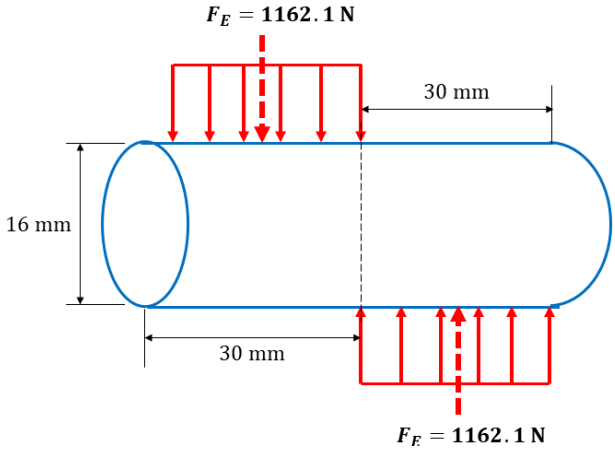

Figure 11. FBD of pin

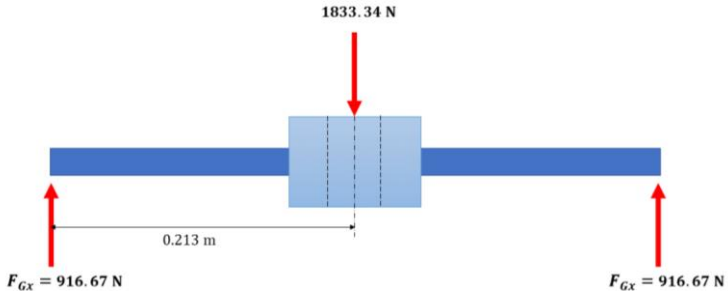

Figure 12. FBD of scissor arm connector

Based on calculations, the most critical component is the scissor arm, specifically the one passing through points B-E-H (Fig. 10, left). For analysis purposes, the scissor arm is rotated so that it is positioned. The forces are projected to the transverse direction to determine the transverse forces and bending moments. This projection can be seen in Fig. 13. The axial components of the forces are ignored in further analyses because the normal stress generated is relatively much smaller than the normal stress due to bending. The SFD and BMD of this scissor arm can be seen in Fig. 14.

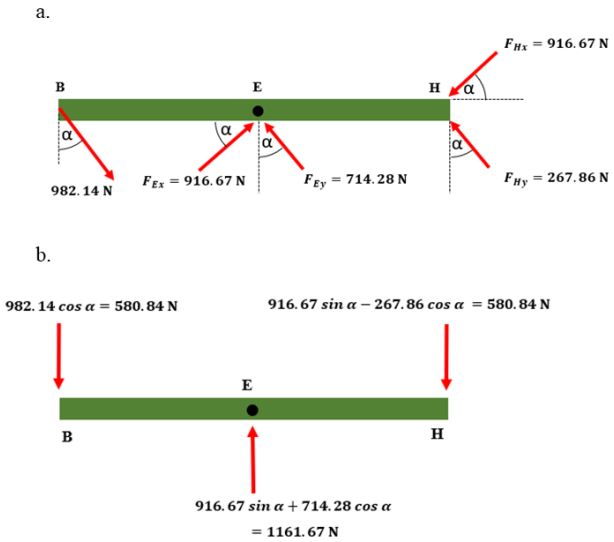

Figure 13. (a) Rotated scissor arm B-E-H and its forces, (b) Projected transverse load on scissor arm B-E-H

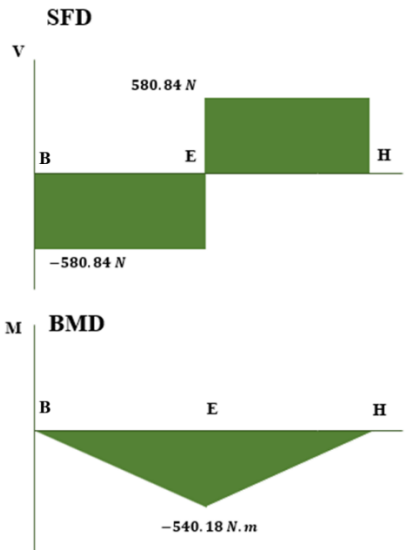

Figure 14. SFD and BMD of scissor arm

Based on the BMD in Fig. 14, the maximum bending moment occurs at point E. The normal stress can be calculated using Eq. 1, where b = 30 mm = 0.03 m, c = 25 mm = 0.025 m, and I can be expressed as

$$I = \frac{1}{12} b(2c)^3$$

Thus, Eq. 1 can be rewritten as

$$\sigma_b = \frac{3M}{2bc^2} = \frac{3(540.18)}{2(0.03)(0.025)^2} = 43.21 \text{ MPa}$$

At point E, stress concentration exists because of the existence of a pinhole. According to the geometry of the scissor arm, the stress concentration factor K_t is found to be 1.9. The Von Mises stress can be found using Eq. 5 where only one component exists which is

$$\sigma_x = 1.9(43.21) = 82.1 \text{ MPa}$$

Thus, the Von Mises stress is $\sigma' = 82.1$ MPa. For the material chosen (stainless steel 304), the yield strength S_y is 215 MPa. Thus, the safety factor under static loading can be calculated using Eq. 6.

$$n_s = \frac{215}{82.1} = 2.62$$

and since the value is greater than 1, thus yielding will not occur. The safety factor for other components are calculated using similar steps, and the result can be seen in Table 3. It can be seen that all safety factors are greater than 1, thus the device is considered safe under static loading.

3.2. Power screw analysis

Parallel to the static stress analysis, additional analysis is done to the power screw to determine the torque required to lift the scissor lift table. This torque will be exerted by a human hand; thus, it has to be made sure that the value is reasonable to allow easy usage of the device.

Table 3. The safety factor of all critical components under static loading

Component	n_s
Scissor arm	2.62
Pin	4.97
Power screw	4.2
Connector	3.61

The torque required to raise the load can be calculated using Eq. 3 [4]. The load F is 1833.33 N according to the static force calculation. In addition, the friction coefficient *f* is assumed to be 0.25, based on experimental data for steel on steel in dry condition. Thus, the torque needed is

$$T_R = \frac{1833.33(0.0135)}{2}\left(\frac{5\times10^{-3}+\pi(0.25)(0.0135)\sec 30°}{\pi(0.0135)-0.25(5\times10^{-3})\sec 30°}\right)$$
$$= 5.21 \text{ N.m}$$

In addition, a self-locking condition is desired. This is necessary to ensure that the table stays in its position when loaded. The condition of self-locking is [4]:

$$\frac{\pi f d_m}{\cos\alpha} > l$$
$$\frac{\pi(0.25)(0.0135)}{\cos 30°} > 5\times10^{-3}$$
$$0.0122 > 5\times10^{-3}$$

Since the inequality is satisfied, thus, the power screw will self-lock.

For the stress analysis, the thread experiences three components of stress. They are normal stress due to compression from the load, shear stress due to torsion, and normal stress due to bending at thread root [4]. These stresses can be calculated using Eq. 1 for bending stress, (2) for axial stress, (4) for shear stress due to torsion. The formulae for normal stresses are modified according to the thread geometry. Thus, the stress components are calculated by

$$\sigma_x = \sigma_b = \frac{6(0.38F)}{\pi d_r n_t p}$$
$$= \frac{6(0.38)(1833.33)}{\pi(0.011)(1)(5\times10^{-3})}$$
$$= 24.19 \text{ MPa}$$
$$\sigma_y = \sigma_a = -\frac{4F}{\pi d_r^2}$$
$$= -\frac{4(1833.33)}{\pi(0.011)^2}$$
$$= -19.3 \text{ MPa}$$
$$\tau_{yz} = \frac{16T_R}{\pi d_r^3} = \frac{16(5.21)}{\pi(0.011)^3}$$
$$= 19.94 \text{ MPa}$$

Calculating the Von Mises stress using Eq. 5, the value is obtained as 51.16 MPa. The safety factor under static loading can be found using Eq. 6, and the value obtained is 4.2 (as can be seen in Table 3) which indicates no yielding.

3.3. Fatigue analysis

Fatigue analyses are done by considering the loaded and unloaded conditions. To determine the life period of the device, the endurance limit is first determined by

$$S_e' = \frac{1}{2}S_{ut} = \frac{1}{2}(505) = 252.5 \text{ MPa}$$

Table 4. Endurance limit of all critical components under fatigue loading

Component	S_e (MPa)
Scissor arm	188.92
Pin	225.17
Power screw	219.675
Connector	186.72

The endurance limit is modified by the Marin factors. There are six Marin factors in total, however, only three are considered in this analysis: surface factor (k_a), size factor (k_b), loading factor (k_c). The other three factors, which are temperature factor (k_d), reliability factor (k_e), and miscellaneous factor (k_f) are assumed unity. Thus, the real endurance limit can be determined by

$$S_e = k_a k_b k_c k_d k_e k_f S_e'$$

The endurance limit of each component can be seen in Table 4.

Based on the calculation, the most critical part is the scissor arm which is the same component as in static analysis. At the most critical point, which is at point E, stress concentration exists due to the existence of a pinhole. The fatigue stress concentration factor (K_f) can be calculated by

$$K_f = 1 + \frac{K_t - 1}{1 + \sqrt{\frac{a}{r}}} \quad (8)$$

where $\sqrt{a}$ is defined as the Neuber constant, and it can be expressed as a curve fit equation of the notch sensitivity chart for steels subjected to reversed bending or reversed axial loads [4].

$$\sqrt{a} = 0.246 - 3.08(10^{-3})S_{ut} + 1.51(10^{-5})S_{ut}^2 - 2.67(10^{-8})S_{ut}^3$$
$$= 0.246 - 3.08(10^{-3})(73.2441) + 1.51(10^{-5})(73.2441)^2$$
$$-2.67(10^{-8})(73.2441)^3$$
$$= 0.091$$

In the above formula, the ultimate tensile strength S_{ut} is in kpsi. Referring back to Eq. 8, the fatigue stress concentration factor is

$$K_f = 1 + \frac{1.9 - 1}{1 + \frac{0.091}{\sqrt{8}}} = 1.872$$

The maximum stress is 43.21 MPa, which is the normal stress due to bending found in the static analysis before amplified by the static stress concentration factor. The minimum stress is taken as zero which indicates the unloaded condition. The midrange and alternating stresses can be found by

$$\sigma_m = K_f \frac{\sigma_{max} + \sigma_{min}}{2}$$
$$= 1.872\left(\frac{43.21 + 0}{2}\right)$$
$$= 40.44 \text{ MPa}$$

$$\sigma_a = K_f \left| \frac{\sigma_{max} - \sigma_{min}}{2} \right|$$
$$= 1.872 \left| \frac{43.21 - 0}{2} \right|$$
$$= 40.44 \text{ MPa}$$

Finally, the safety factor under fatigue loading can be calculated using the Soderberg fatigue failure criterion, expressed as Eq. 7, where a safety factor greater than 1 means infinite life.

$$n_f = \left(\frac{40.44}{188.92} + \frac{40.44}{215} \right)^{-1} = 2.49$$

Since the safety factor due to fatigue is greater than 1, infinite life is predicted for the scissor arm. A similar process is done on other critical components to get the fatigue safety factor. Table 5 shows the safety factor due to fatigue loading of all critical components. It can be seen that all safety factors are greater than 1, thus it is predicted that the device has infinite life.

All of the above analyses are done with the assumption of ideal condition with no other defects. Future studies may include measuring the residual stress from the fabrication process, especially the machining process [15]. In addition, stress analysis using Finite Element Analysis (FEA) may also be done to show the stress condition of the whole system more accurately [16].

4. Conclusion

Health workers, as a group of people who are very vulnerable to the exposure of this Covid-19 virus because of their frequent interactions with the sufferers, need more attention and support so that they can do their duties well. With this condition, a contact-free mortuary trolley is proposed complete along with its design and analysis to help health workers on moving the dead bodies of Covid 19 sufferers without any physical contact. This mortuary trolley is designed with 3 main parts, the first one is the lower section of the frame where the wheels are installed, 4 scissor arms that will function as a mechanism to lift up and down the trolley table, and the last one is the trolley table where the table is equipped with a thin conveyor mechanism. From the analysis of each part at its maximum position, it is found that the most critical part is the scissor arm of the trolley because as the trolley is at its maximum position, the scissor arm will experience the most load and forces from the whole device. However, by calculating the safety factor of the device in either static loading or fatigue loading conditions with a value greater than 1, it is estimated that this tool will be safe in operation to achieve the expected objectives. Therefore, this paper is proposed with great hope so that this trolley can actually be produced and contribute to the medical field.

Table 5. Safety factor of all critical components under fatigue loading

Component	n_f
Scissor arm	2.49
Pin	5.08
Power screw	3.3
Connector	3.41

References

[1] "hukumonline.com." .

[2] Fakultas Kedokteran Universitas Indonesia, "83% of Indonesian Health Workers Experienced Moderate and Severe Burnout Syndrome During the COVID-19 Pandemic," 2020. [in Bahasa]

[3] Lapor Covid-19, "Thank you Indonesian Health Hero," 2021. [Online]. Available: https://nakes.laporcovid19.org/. [Accessed: 04-Mar-2021]. [in Bahasa]

[4] R. G. Budynas and J. K. Nisbett, *Shigley's Mechanical Engineering Design*, 10 Ed. McGraw-Hill Education, 2015.

[5] M. Oktaviandri and D. K. A. V. Paramasivam, "Design and Fabrication of Customized Ais Kacang Vending Machine," *Indones. J. Comput. Eng. Des.*, vol. 2, no. 1, p. 24, 2020.

[6] G. G. Momin, R. Hatti, K. Dalvi, F. Bargi, and R. Devare, "Design, Manufacturing & Analysis of Hydraulic Scissor Lift," *Int. J. Eng. Res. Gen. Sci.*, vol. 3, no. 2, pp. 733–740, 2015.

[7] M. K. Kumar, J. Chandrasheker, M. Manda, and D. V. Kumar, "Design & Analysis of Hydraulic Scissor Lift," pp. 1647–1653, 2016.

[8] M. O. Stanley, "A Project on Scissor Lift Design for Use in The Automotive Industry," August, 2012.

[9] D. Dave, "Study and Performance of Belt Conveyor System with Different Type Parameter," vol. 2, no. 6, pp. 29–31, 2015.

[10] H. M. Hdz-Garcia *et al.*, "304 Stainless Steel Brazing Inxoporating Tungsten Nanoparticles," *J. Mater. Process. Technol.*, vol. 215, pp. 1–5, 2015.

[11] M. Mukherjee and T. Pal, "Microstructure , Texture , and Mechanical Property Analysis of Gas Metal Arc Welded AISI 304 Austenitic Stainless Steel," June 2015, 2014.

[12] MatWeb, "304 Stainless Steel." [Online]. Available: http://matweb.com/search/DataSheet.aspx?MatGUID=abc4415b0f8b490387e3c922237098da&ckck=1.

[13] A. Widjaya, A. N. Rabbani, K. R. A. N. Ningrum, and F. Triawan, "The Design and Analysis of a Child Seat for a Motorcycle," *J. Mech. Eng. Mechatronics*, vol. 5, no. 2, pp. 101–113, 2020.

[14] S. Zulaikah, W. H. Rahmanda, and F. Triawan, "Foldable Front Child-Seat Design for Scooter Motorcycle: Strength Analysis Under Static and Dynamic Loading," *Int. J. Sustain. Transp. Technol.*, vol. 3, no. 2, pp. 37–44, 2020.

[15] K. Saptaji, S. N. Afiqah, and R. D. Ramdan, "A Review on Measurement Methods for Machining Induced Residual Stress," *Indones. J. Comput. Eng. Des*, vol. 1, no. 2, p. 106, 2019.

[16] I. P. Nurprasetio, B. A. Budiman, and F. Triawan, "Failure Investigation of Plastic Shredding Machine's Flange Coupling Based on Mechanical Analysis," *Indones. J. Sci. Technol.*, vol. 2, no. 2, pp. 124–133, 2017.

EPI International Journal of Engineering
Volume 4, Number 1, February 2021, pp. 29-36
DOI: 10.25042/epi-ije.022021.05

*p*ISSN 2615-5109
*e*ISSN 2621-0541

Accurate Results for Free Vibration of Doubly Curved Shallow Shells of Rectangular Planform (Part 1)

Daisuke Narita [a,*], Yoshihiro Narita[b]

[a]Hokkaido University of Science, Teineku, Sapporo, Japan. Email: narita@hus.ac.jp
[b]Yamato University, Katayama, Suita, Osaka. Email: ynarita@eng.hokudai.ac.jp

Abstract

A method is presented for determining the free vibration frequencies of doubly curved, isotropic shallow shells under general edge conditions and is used to obtain accurate natural frequencies for wide range of geometric parameters. Based on the shallow shell theory applicable to thin thickness shells, a method of Ritz is extended to derive a frequency equation wherein the displacement functions are modified to accommodate arbitrary sets of edge conditions for both in-plane and out-of-plane motions. In numerical computation, convergence is tested against series terms and comparison study is made with existing results by other authors. Twenty one sets of frequency parameters are tabulated for a wide range of shell shape and curvature ratio to serve as data for future comparison and practical design purpose.

Keywords: Accuracy; free vibration; natural frequency; Ritz method; shallow shell

1. Introduction

Open shallow shell is one of practical shell shapes, and has been widely used as structural components in many mechanical, aeronautical, building and marine structures. These shallow shell components are often subjected to vibration environment and the vibration analysis of shallow shells constitutes important part of structural engineering.

Development in the field of general shell vibration is summarized in a famous monograph [1] compiled by Leissa, and shallow shell vibration is a part of this monograph. The mechanics of shells is described in textbooks, for example in [2], and a handbook on shell vibration was published [3] in 2003. Use of shallow shell structure in automobiles was introduced [4] in connection with composite material.

First notable work on this topic is one [5] by Leissa and Kadi that formulated the exact solution of shallow shells of rectangular planform supported along four edges by shear diaphrams. The shear diaphragm gives the edge condition similar to simple support in the flat plate theory, except that the in-plane displacement parallel to the edge is constrained but displacement perpendicular to the edge is free. For general boundary conditions other than the shear diaphragm, exact solution is not derivable.

By using approximate methods, vibration of cantilevered cylindrical [6] and doubly curved [7] shallow shells were studied in the first half of 1980's. Leissa and one of the present authors analyzed vibration of completely free [8] and corner point supported shallow shells [9]. In the 1990's, research on this topic became more active. Effects of edge constraints on natural frequencies were studied [10], and one of these authors published a review paper on shallow shell vibration [11]. Yu and his co-workers presented free vibration analysis of circular cylindrical shells [12]. Liew and Lim published analysis of shallow shells of curvilinear planform [13], doubly curved shell [14], and use of so-called pb-2 Ritz method on the topic [15]. They also presented a review paper on shallow shell vibration [16].

In the 2000's, Qatu once again summarized on development on shallow shell vibration [17] to follow up his previous review [11]. Design problem was studied [18] for maximizing natural frequencies of laminated shallow shell where more complicated stress-strain relations are included. Monterrubio [19] introduced penalty parameters in the analysis of shallow shell vibration. Qatu studied effect of in-plane edge constraints on frequencies of simply supported doubly curved shallow shells [20].

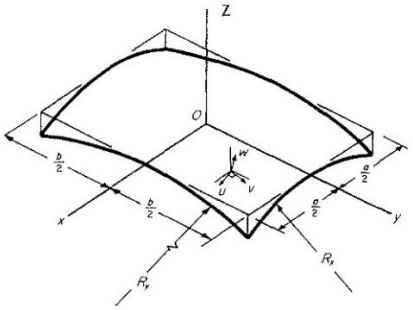

Figure 1. Shallow shell of rectangular planform

*Corresponding author. Tel.: +81-11-681-2161
Maeda Teine, Sapporo
Japan, 006-8585

More recently, Mochida et al. [21] and Qatu and Asadi [22] published lists of frequencies for general boundary conditions. Particularly in [21], they extended a method of superposition method to shallow shell vibration for the first time. In the authors' opinion, their numerical results seem most accurate in the literature published this far, but are limited to the case of very thin shell (edge length/ thickness=100). Considering the situations, it is obvious that thorough list of accurate frequency parameters should be tabulated for wide range of general edge conditions, which is the purpose of the present paper.

2. Analytical Method

2.1. Ritz method for general boundary condition

The quadratic mid-surface of a shallow shell (panel) may be expressed in a rectangular coordinate system as

$$\phi(x,y) = -\frac{1}{2}\left(\frac{x^2}{R_x} + 2\frac{xy}{R_{xy}} + \frac{y^2}{R_y}\right) \qquad (1)$$

where R_x and R_y are the radii of curvature in the x and y directions, respectively, and R_{xy} is the radius of twist but is not included in this study (i.e., $1/R_{xy}=0$). For a doubly curved shell, the orientation of the x-y coordinates may be chosen so that R_x and R_y are principal constant curvature radius as shown in Fig.1. The dimension of its planform is given by $a \times b$ and the thickness is h. The four sides are subjected to uniform in-plane (i.e., stretching) and out-of-plane (bending) boundary conditions. This shell takes geometric form of a cylindrical shell for "$1/R_x$=(finite) and $1/R_y=0$ ($R_y=\infty$)" or "$1/R_y$=(finite) and $1/R_x=0$ ($R_x=\infty$)". Similarly, it takes form of a spherical shell for $1/R_x=1/R_y$=(finite), and does form of a hyper paraboloidal shell for $1/R_x= -1/R_y$=(finite) where positive curvature exists in x direction and negative curvature in y direction.

Using the Kirchhoff hypothesis, the displacements $u^*(x,y,z,t)$, $v^*(x,y,z,t)$ and $w^*(x,y,z,t)$ of an arbitrary point in a shell are written as

$$u^* = u - z\frac{\partial w}{\partial x},\ v^* = v - z\frac{\partial w}{\partial y},\ w^* = w \qquad (2)$$

where z is the coordinate measured from the mid-surface in the direction of outer normal. The $u(x,y,t)$ and $v(x,y,t)$ are displacement components, tangent to the mid-surface and parallel to the xz and yz planes, respectively, and $w(x,y,t)$ is a displacement component normal to the mid-surface at a point on the mid-surface.

In the linear theory, the strain components at an arbitrary point (x,y,z) are

$$\varepsilon_x^* = \varepsilon_x + z\kappa_x,\ \varepsilon_y^* = \varepsilon_y + z\kappa_y,$$

$$\gamma_{xy}^* = \gamma_{xy} + z\kappa_{xy} \qquad (3)$$

assuming that z is negligible in comparison with R, where the membrane strains are given by

$$\varepsilon_x = \frac{\partial u}{\partial x} + \frac{w}{R_x},\ \varepsilon_y = \frac{\partial v}{\partial y} + \frac{w}{R_y},\ \gamma_{xy} = \frac{\partial v}{\partial x} + \frac{\partial u}{\partial y} \qquad (4)$$

and the curvature changes due to the vibratory displacements are

$$\kappa_x = -\frac{\partial^2 w}{\partial x^2},\ \kappa_y = -\frac{\partial^2 w}{\partial y^2},\ \kappa_{xy} = -2\frac{\partial^2 w}{\partial x \partial y} \qquad (5)$$

For an isotropic shallow shell, the stress-strain equation is written as

$$\begin{Bmatrix}\sigma_x\\ \sigma_y\\ \tau_{xy}\end{Bmatrix} = \begin{bmatrix}Q_{11} & Q_{12} & Q_{16}\\ Q_{12} & Q_{22} & Q_{26}\\ Q_{16} & Q_{26} & Q_{66}\end{bmatrix}\begin{Bmatrix}\varepsilon_x\\ \varepsilon_y\\ \gamma_{xy}\end{Bmatrix} \qquad (6)$$

where the coefficients are elastic constants

$$Q_{11} = Q_{22} = \frac{E}{1-\nu^2},\ Q_{12} = \nu Q_{11},\ Q_{66} = G \qquad (7)$$

where E is the moduli of elasticity, $G=E/2(1+\nu)$ is the shear modulus and ν is Poisson's ratios.

The force resultants and the moment resultants are obtained by integrating the stresses and the stresses multiplied by z, respectively, over the shell thickness h, and are written in matrix form as

$$\begin{Bmatrix}N\\ M\end{Bmatrix} = \begin{bmatrix}A & B\\ B & D\end{bmatrix}\begin{Bmatrix}\varepsilon\\ \kappa\end{Bmatrix} \qquad (8)$$

where $\{N\}$, $\{M\}$, $\{\varepsilon\}$ and $\{\kappa\}$ are the vectors of force resultants, moment resultants, mid-surface strains and curvatures, respectively, given by

$$\{N\} = \begin{Bmatrix}N_x\\ N_y\\ N_{xy}\end{Bmatrix},\ \{M\} = \begin{Bmatrix}M_x\\ M_y\\ M_{xy}\end{Bmatrix},$$

$$\{\varepsilon\} = \begin{Bmatrix}\varepsilon_x\\ \varepsilon_y\\ \gamma_{xy}\end{Bmatrix},\ \{\kappa\} = \begin{Bmatrix}\kappa_x\\ \kappa_y\\ \kappa_{xy}\end{Bmatrix} \qquad (9a,b,c,d)$$

and $[A]$,$[B]$ and $[D]$ are the matrices of stiffness coefficients defined by

$$[A] = \begin{bmatrix}A_{11} & A_{12} & A_{16}\\ A_{12} & A_{22} & A_{26}\\ A_{16} & A_{26} & A_{66}\end{bmatrix} \qquad (10a)$$

$$[B] = \begin{bmatrix}B_{11} & B_{12} & B_{16}\\ B_{12} & B_{22} & B_{26}\\ B_{16} & B_{26} & B_{66}\end{bmatrix} \qquad (10b)$$

$$[D] = \begin{bmatrix}D_{11} & D_{12} & D_{16}\\ D_{12} & D_{22} & D_{26}\\ D_{16} & D_{26} & D_{66}\end{bmatrix} \qquad (10c)$$

The stiffness coefficients in Eqs. (10a,b,c) are values determined by

$$A_{ij} = hQ_{ij} \ , \ B_{ij} = 0 \qquad (11a,b)$$

$$D_{ij} = \left(\frac{h}{12}\right) Q_{ij} \qquad (11c)$$

(i,j=1,2,6) for specific case of shallow shells composed of isotropic material. For more complicated shells including laminated composite materials, Eqs. (11) take more complicated form as shown in Ref. [18].

In the present study, the free vibration problem can be solved by means of the Ritz method. This requires the evaluation of energy functionals. The strain energy stored in a shell during elastic deformation is written in the classical (thin) shallow shell theory by

$$V = V_s + V_{bs} + V_b \qquad (12)$$

where V_s , V_{bs} and V_b are the parts of the total strain energy due to stretching, bending- stretching coupling and bending, respectively:

$$V_s = \frac{1}{2}\iint \{\varepsilon\}^T [A]\{\varepsilon\}\, dArea \qquad (13a)$$

$$V_{bs} = \frac{1}{2}\iint \left(\{\kappa\}^T [B]\{\varepsilon\} + \{\varepsilon\}^T [B]\{\kappa\}\right) dArea \qquad (13b)$$

$$V_b = \frac{1}{2}\iint \{\kappa\}^T [D]\{\kappa\}\, dArea \qquad (13c)$$

The kinetic energy of the panel due to translational motion only is given by

$$T = \frac{1}{2}\rho h \iint \left[\left(\frac{\partial u}{\partial t}\right)^2 + \left(\frac{\partial v}{\partial t}\right)^2 + \left(\frac{\partial w}{\partial t}\right)^2\right] dArea \qquad (14)$$

where ρ is the mass density of the shell per unit volume.

For simplicity in the formulation, the following dimensionless quantities are introduced.

$$\xi = \frac{2x}{a}, \ \eta = \frac{2y}{b} \ \text{(dimensionless coordinates)} \qquad (15a)$$

$$\Omega = \omega a^2 \sqrt{\frac{\rho h}{D}} \ \text{(dimensionless frequency parameter)} \qquad (15b)$$

$$D = \frac{Eh^3}{12\left(1-\nu^2\right)} \ \text{(reference plate stiffness)} \qquad (15c)$$

In the Ritz method the displacements may be assumed in the form

$$u(\xi,\eta,t) = \sum_{i=0}^{M-1}\sum_{j=0}^{N-1} P_{ij} X_i(\xi) Y_j(\eta) \sin\omega t \qquad (16a)$$

$$v(\xi,\eta,t) = \sum_{k=0}^{M-1}\sum_{l=0}^{N-1} Q_{kl} X_k(\xi) Y_l(\eta) \sin\omega t \qquad (16b)$$

$$w(\xi,\eta,t) = \sum_{m=0}^{M-1}\sum_{n=0}^{N-1} R_{mn} X_m(\xi) Y_n(\eta) \sin\omega t \qquad (16c)$$

where P_{ij} , Q_{kl} and R_{mn} are unknown coefficients and $X_i(\xi)$, $Y_j(\eta)$, .. and $Y_n(\eta)$ are the functions that satisfy at least the kinematical boundary conditions at the edges. The upper limit in each of the summations (16) is arbitrary but is unified here for simplicity in the convergence test.

After substituting Eqs.(16) into the functional L

$$L = T_{max} - V_{max} \qquad (17)$$

composed of the maximum strain and kinetic energies obtained from Eqs.(12) and (14), the stationary value is obtained by

$$\frac{\partial L}{\partial P_{ij}} = 0, \ \frac{\partial L}{\partial Q_{kl}} = 0, \ \frac{\partial L}{\partial R_{mn}} = 0 \qquad (18a,b,c)$$

$$(i,k,m = 0,1,2,..,(M-1); \ j,l,n = 0,1,2,...,(N-1))$$

The result of the minimization process (18) yields a set of homogeneous, linear simultaneous equations in the unknowns $\{P_{ij}, Q_{kl}, R_{mn}\}$. For non-trivial solutions, the determinant of the coefficient matrix is set to zero. The (M×N)×3 eigenvalues may be extracted and the lowest several eigenvalues (natural frequencies) are important from a practical viewpoint.

The above procedure is a standard routine of the Ritz method, and is modified to incorporate arbitrary edge conditions. This approach introduces the following polynomials

$$X_i(\xi) = \xi^i (1+\xi)^{Bu1} (1-\xi)^{Bu3} \qquad (19a)$$

$$Y_j(\eta) = \eta^j (1+\eta)^{Bu2} (1-\eta)^{Bu4} \qquad (19b)$$

$$X_k(\xi) = \xi^k (1+\xi)^{Bv1} (1-\xi)^{Bv3} \qquad (19c)$$

$$Y_l(\eta) = \eta^l (1+\eta)^{Bv2} (1-\eta)^{Bv4} \qquad (19d)$$

$$X_m(\xi) = \xi^m (1+\xi)^{Bw1} (1-\xi)^{Bw3} \qquad (19e)$$

$$Y_n(\eta) = \eta^n (1+\eta)^{Bw2} (1-\eta)^{Bw4} \qquad (19f)$$

where B_{rs} $(r = u,v,w; \ s = 1,2,3,4)$ is the boundary index [18] which is used to satisfy the kinematic boundary conditions. The capital letter B stands for Boundary. The first subscript letter in B_{rs} indicates which displacement (u,v or w) is dealt with and the second subscript number indicates which edge, Edge (1),.. or Edge (4), is under consideration. The Edge (1),(2),(3) and (4) denote the boundary along x=-a/2, y=-b/2, x=a/2 and y=b/2, respectively (See Fig. 1).

For in-plane displacements u and v, B_{rs} =0 (r=u, v; s=1,2,3,4) denote that the specified displacement along the specified edge is free and B_{rs} =1 denote that the displacement is rigidly fixed. For out-of-plane displacement w, B_{rs} =0, 1 and 2 (r=w; s=1,2,3,4) denote that the specified displacement along the specified edge is free, simply supported and clamped, respectively. With such boundary indices, one can accommodate arbitrary sets of both in-plane and out-of-plane boundary conditions in the vibration analysis and computation.

The introduction of the boundary index makes it possible to deal with a tremendous number of edge conditions in the analysis. The number of combinations in the boundary condition is $(2\times2\times3)^4$ =20736, when one of the two conditions (free or fixed) in u and v and one of the three conditions (free, simply supported or clamped) in w are imposed along each of the four edges. This is significantly larger than the *plate* analysis where only out-of-plane displacement is concerned. The present vibration analysis can calculate natural frequencies for any of these combinations.

In the following numerical examples, however, the boundary conditions are limited to those similar to the standard plate boundary conditions, such as free edge, simply supported edge and clamped edge. For example, at the Edge (1) along x= -a/2

B_{u1}= B_{v1}= B_{w1}=0 for the free edge (no constraint), denoted by F (20a)

B_{u1}=0, B_{v1}=1, B_{w1}=1 for the simply supported edge denoted by S (20b)

B_{u1}= B_{v1}=1, B_{w1}=2 for the clamped edge denoted by C (20c)

The entire set of boundary conditions is denoted by four capital letter, such as CSFF, in the counterclockwise starting from Edge(1).

2.2. Exact solution for specific boundary condition

When a shallow shell of rectangular planform is supported along four edges by shear diaphragms, the exact solution is possible [1], [3], [5] by assuming

$$u(x,y,t) = P_{ij}\cos\frac{i\pi x}{a}\sin\frac{j\pi y}{b}\sin\omega t \qquad (21a)$$

$$v(x,y,t) = Q_{kl}\sin\frac{k\pi x}{a}\cos\frac{l\pi y}{b}\sin\omega t \qquad (21b)$$

$$w(x,y,t) = R_{mn}\sin\frac{m\pi x}{a}\sin\frac{n\pi y}{b}\sin\omega t \qquad (21c)$$

Equations (21) are substituted in the governing equation, and the exact solution is obtained in the form of 3×3 frequency matrix. This solution procedure is given in detail in Refs. [3], [5].

3. Numerical Examples and Accuracy of Solution

3.1. Convergence and comparison of the solution

In numerical examples, square planform (a/b=1) and moderately thin thickness (a/h=20) are used. Poisson's ratio is kept as ν =0.3.

Table 1 Convergence and comparison of frequency parameters Ω of simply supported shallow shells (SSSS), a/b =1, a/h =20, ν =0.3.

	Ω_1	Ω_2	Ω_3	Ω_4	Ω_5	Ω_6
Spherical shell (Rx/Ry=1, a/Rx=0.2)						
8×8	23.715	51.052	51.052	80.021	99.563	99.563
10×10	23.715	51.052	51.052	80.021	99.543	99.543
12×12	23.715	51.052	51.052	80.021	99.542	99.542
Exact	23.715	51.052	51.052	80.021	99.542	99.542
Ref.[22]	23.70	51.04	51.04	80.02	—	—
Spherical shell (Rx/Ry=1, a/Rx=0.5)						
8×8	38.080	59.134	59.134	85.361	103.88	103.88
10×10	38.080	59.134	59.134	85.361	103.85	103.85
12×12	38.080	59.134	59.134	85.361	103.85	103.85
Exact	38.080	59.134	59.134	85.361	103.85	103.85
Ref.[22]	38.01	59.10	59.10	85.32	—	—
Cylindrical shell (Rx/Ry=0, a/Rx=0.2)						
8×8	20.786	49.391	50.451	79.203	98.700	99.420
10×10	20.786	49.391	50.451	79.203	98.680	99.400
12×12	20.786	49.391	50.451	79.203	98.680	99.400
Exact	20.786	49.391	50.451	79.203	98.680	99.400
Ref.[22]	20.78	49.39	50.44	79.19	—	—
Cylindrical shell (Rx/Ry=0, a/Rx=0.5)						
8×8	25.509	49.613	55.861	80.479	98.616	103.03
10×10	25.509	49.613	55.861	80.479	98.616	103.03
12×12	25.509	49.612	55.861	80.479	98.593	103.01
Exact	25.509	49.612	55.861	80.479	98.594	103.01
Ref.[22]	25.48	49.61	55.84	80.46	—	—
Hyperbolic paraboloidal shell (Rx/Ry=−1, a/Rx=0.2)						
8×8	19.659	49.924	49.924	78.873	99.244	99.244
10×10	19.659	49.924	49.924	78.873	99.224	99.224
12×12	19.659	49.924	49.924	78.873	99.224	99.224
Exact	19.659	49.924	49.924	78.873	99.224	99.224
Ref.[22]	19.66	49.92	49.92	78.85	—	—
Hyperbolic paraboloidal shell (Rx/Ry=−1, a/Rx=0.5)						
8×8	19.252	52.806	52.806	78.438	101.96	101.96
10×10	19.252	52.805	52.805	78.438	101.94	101.94
12×12	19.252	52.805	52.805	78.438	101.94	101.94
Exact	19.252	52.805	52.805	78.438	101.94	101.94
Ref.[22]	19.25	52.79	52.79	78.46	—	—

Table 1 presents convergence study of frequency parameters of spherical (R_x/R_y=1), cylindrical (R_x/R_y=0) and hyperbolic paraboloidal (R_x/R_y= -1) shells of square planform. These shells (SSSS) are supported by shear diaphram along four edges. For each shell configuration, two degrees of curvature a/R_x=0.2 and 0.5 are used. The present results are calculated for the number of terms 8×8, 10×10 and 12×12 for each of u, v and w that yield frequency matrix size of 192×192, 300×300 and 432×432, respectively.

The present parameters converge well within five significant figures, and show exact match with the exact results obtained from Eq. (21). They are also compared to the parameters in Ref. [22], and are generally in good agreement with slight differences. In the following tables, the present results are calculated by using the 12×12 solution and presented in five significant figures.

Table 2 Comparison of frequency parameters Ω of shallow shells, a/Rx =0.5, a/b =1, a/h =100, ν =0.3.

	Ω_1	Ω_2	Ω_3	Ω_4	Ω_5	Ω_6
CCSS						
Spherical shell (Rx/Ry=1)						
Present	171.60	180.27	186.99	195.32	204.04	210.09
Ref.[21]	171.6	180.3	187.0	195.3	204.1	210.1
Cylindrical shell (Rx/Ry=0)						
Present	72.375	105.48	127.24	133.02	147.49	168.62
Ref.[21]	72.37	105.5	127.2	133.0	147.5	168.6
Hyperbolic paraboloidal shell (Rx/Ry=−1)						
Present	94.181	122.38	136.98	149.24	173.01	173.62
Ref.[21]	94.18	122.4	137.0	149.2	173.0	173.6
CSCC						
Spherical shell (Rx/Ry=1)						
Present	179.90	187.88	192.50	202.47	208.02	228.73
Ref.[21]	179.9	187.9	192.5	202.5	208.0	228.7
Cylindrical shell (Rx/Ry=0)						
Present	95.798	116.43	145.24	150.67	170.30	187.31
Ref.[21]	95.81	116.4	145.2	150.6	170.3	187.3
Hyperbolic paraboloidal shell (Rx/Ry=−1)						
Present	131.20	139.90	154.35	158.42	186.02	189.83
Ref.[21]	131.2	139.9	154.4	158.4	186.0	189.8
CCCC						
Spherical shell (Rx/Ry=1)						
Present	191.99	191.99	196.93	209.96	216.19	242.22
Ref.[21]	192.0	192.0	169.9	210.0	216.2	242.2
Cylindrical shell (Rx/Ry=0)						
Present	99.263	119.00	151.13	156.35	172.52	192.43
Ref.[21]	99.26	119.0	151.1	156.3	172.5	192.4
Hyperbolic paraboloidal shell (Rx/Ry=−1)						
Present	157.35	157.35	157.41	166.52	204.03	208.69
Ref.[21]	157.3	157.3	157.4	166.5	204.0	208.7

Table 2 is another comparison study with values of Ref. [21] by Mochida and his co-workers. Note that only in Table 2, the thickness ratio is kept as a/h=100 (very thin) due to the need for comparison, while in all other tables, the ratio is a/h=20 (moderately thin) throughout. They [21] extended the method of superposition, commonly used in plate vibration analysis, to shallow shell vibration analysis. Three sets of boundary condition CCSS, CSCC and CCCC are considered. When the present values are rounded with four significant figures, most of the results are exactly identical with the referred values [21] for wide ranges of boundary conditions, shell configuration and degree of curvature. Thus, the accuracy of the present solution is well demonstrated

3.2. Comprehensive results of shallow shells

Table 3(a) presents the lowest six frequency parameters Ω of shallow spherical shells (R_x/R_y=1) of square planform (a/b=1) with moderate thickness (a/h=20) for 21 different sets of boundary conditions. The degree of curvature is taken as a/R=0.2. Table 3(b) is the same format as Table 3(a) except that the curvature is larger in a/R=0.5.

Table 3(a) Frequency parameters Ω of shallow spherical shells, R_x/R_y=1, a/R_x=a/R_y=0.2, a/b =1, a/h =20, ν =0.3.

B.C.	Ω_1	Ω_2	Ω_3	Ω_4	Ω_5	Ω_6
FFFF	13.460	19.563	25.991	34.838	34.838	61.770
SFFF	6.6294	15.343	25.400	27.084	49.196	51.604
CFFF	3.7518	8.4865	21.518	28.262	30.515	44.098
SSFF	3.3668	17.321	20.788	39.706	51.532	54.319
CSFF	5.5638	19.350	25.461	44.633	53.198	54.137
CCFF	7.8923	23.895	27.922	49.256	62.962	66.231
SFSF	10.066	16.105	38.895	39.592	46.867	71.588
CFSF	15.629	21.677	41.802	49.902	56.556	78.415
SSSF	12.221	30.508	41.852	60.149	63.216	64.384
CSSF	17.921	33.738	51.986	65.351	68.576	101.91
CCSF	18.464	38.646	52.338	72.133	75.507	106.00
CFCF	25.385	28.722	45.607	61.561	67.417	80.888
SCSF	12.951	35.762	42.269	64.111	64.384	73.590
CSCF	26.453	38.140	63.338	68.064	78.336	109.64
CCCF	26.907	42.737	63.637	77.905	81.563	117.42
SSSS	23.715	51.052	51.052	80.021	99.542	99.542
CSSS	27.338	53.342	60.177	87.149	101.11	113.97
CCSS	30.659	62.026	62.352	93.819	115.29	115.45
CSCS	32.577	56.377	70.634	95.546	103.05	128.77
CCCS	35.610	64.875	72.385	101.74	117.10	131.04
CCCC	40.422	74.713	74.713	109.14	132.24	133.06

Table3(b) Frequency parameters Ω of shallow spherical shells, R_x/R_y=1, a/R_x=a/R_y=0.5, a/b =1, a/h =20, ν =0.3.

B.C.	Ω_1	Ω_2	Ω_3	Ω_4	Ω_5	Ω_6
FFFF	13.414	19.392	32.522	34.952	34.952	64.993
SFFF	6.5501	16.251	25.460	31.034	52.846	57.290
CFFF	4.7227	8.3836	22.089	28.777	32.298	46.445
SSFF	3.3328	17.287	24.642	48.041	53.468	58.038
CSFF	6.3859	19.708	27.976	52.485	54.138	56.256
CCFF	11.139	23.818	32.726	57.426	63.892	69.438
SFSF	11.118	15.910	42.201	47.454	48.857	76.185
CFSF	17.086	26.233	50.914	52.202	57.953	83.723
SSSF	13.137	42.426	44.253	64.383	66.009	69.874
CSSF	21.832	45.242	54.358	71.892	74.084	105.86
CCSF	22.097	50.022	54.536	77.648	81.379	107.00
CFCF	37.260	38.449	55.161	63.247	68.605	86.273
SCSF	13.672	44.410	47.411	64.384	69.935	79.514
CSCF	37.802	49.827	65.270	74.501	83.417	113.60
CCCF	37.993	55.089	65.419	83.845	86.719	121.32
SSSS	38.080	59.134	59.134	85.361	103.85	103.85
CSSS	41.361	61.292	67.571	92.265	105.39	117.76
CCSS	44.688	69.242	69.928	98.789	119.07	119.22
CSCS	46.965	64.210	77.040	100.41	107.29	128.77
CCCS	50.623	72.403	78.805	106.52	120.86	134.53
CCCC	58.167	81.187	81.187	113.82	135.61	137.50

Table 4(a) Frequency parameters Ω of shallow cylindrical shells, R_x=(infinity), a/R_y=0.2, a/b=1, a/h=20, ν=0.3.

B.C.	Ω_1	Ω_2	Ω_3	Ω_4	Ω_5	Ω_6
FFFF	13.463	20.120	24.765	34.783	34.906	61.080
SFFF	6.6433	15.762	25.444	26.011	48.826	51.057
CFFF	3.8031	8.520	21.967	27.283	31.040	43.507
SSFF	3.3642	17.606	19.790	38.566	51.306	53.876
CSFF	5.6203	19.155	25.344	43.415	52.701	54.069
CCFF	7.2165	24.291	27.072	48.195	62.925	65.837
SFSF	10.293	16.180	36.802	39.703	46.889	70.965
CFSF	15.820	20.652	39.843	50.076	56.427	77.325
SSSF	12.306	28.033	41.887	59.537	61.866	64.383
CSSF	17.374	31.420	51.973	64.044	67.958	101.23
CCSF	18.147	36.578	52.369	71.598	74.409	106.18
CFCF	22.728	26.490	43.729	61.700	67.313	79.829
SCSF	13.345	33.608	42.359	63.602	64.383	72.471
CSCF	23.879	35.887	63.362	66.802	77.744	108.98
CCCF	24.466	40.558	63.695	76.806	81.039	116.81
SSSS	20.786	49.391	50.451	79.203	98.680	99.400
CSSS	24.612	51.746	59.574	86.374	100.26	113.84
CCSS	28.366	60.815	61.677	93.135	114.62	115.26
CSCS	29.790	54.843	70.118	94.807	102.22	128.77
CCCS	32.959	63.515	71.936	101.07	116.37	130.89
CCCC	37.829	73.541	74.364	108.53	131.81	132.63

Table 4(b) Frequency parameters Ω of shallow cylindrical shells, R_x=(infinity), a/R_y=0.5, a/b=1, a/h=20, ν=0.3.

B.C.	Ω_1	Ω_2	Ω_3	Ω_4	Ω_5	Ω_6
FFFF	13.439	21.283	28.119	34.685	35.450	61.010
SFFF	6.6395	19.427	25.800	26.100	49.939	54.147
CFFF	5.1616	8.5893	24.644	28.095	31.467	43.520
SSFF	3.3471	17.926	22.680	40.568	51.774	56.461
CSFF	6.7779	19.523	28.273	45.235	52.659	54.228
CCFF	8.4374	25.562	29.549	51.099	63.347	67.845
SFSF	13.103	16.415	37.219	43.261	47.666	72.235
CFSF	18.606	21.000	40.435	53.085	57.183	77.330
SSSF	14.789	29.570	44.943	61.893	62.205	64.383
CSSF	19.768	33.149	54.601	64.160	70.320	101.83
CCSF	20.504	39.505	54.881	74.396	74.918	108.09
CFCF	25.302	26.920	44.474	64.255	68.018	79.895
SCSF	15.790	36.420	45.243	64.384	66.824	72.867
CSCF	26.034	37.687	65.624	67.010	79.819	109.57
CCCF	26.625	43.567	65.872	77.322	83.608	117.65
SSSS	25.509	49.612	55.861	80.479	98.593	103.01
CSSS	29.072	52.119	64.209	87.612	100.21	116.97
CCSS	34.217	61.768	66.606	94.692	114.64	118.46
CSCS	33.797	55.363	74.117	95.957	102.21	128.77
CCCS	38.182	64.505	76.253	102.52	116.41	133.67
CCCC	46.241	74.300	79.239	110.14	132.35	135.51

Table 5(a) Frequency parameters Ω of shallow cylindrical shells, R_y=(infinity), a/R_x=0.2, a/b=1, a/h=20, ν=0.3.

B.C.	Ω_1	Ω_2	Ω_3	Ω_4	Ω_5	Ω_6
FFFF	13.463	20.120	24.765	34.783	34.906	61.080
SFFF	6.6292	14.925	25.340	26.889	48.649	50.799
CFFF	3.4675	8.4672	21.301	27.977	30.489	44.084
SSFF	3.3642	17.606	19.790	38.566	51.306	53.876
CSFF	5.3411	19.816	24.606	43.658	53.213	54.191
CCFF	7.2160	24.291	27.072	48.195	62.925	65.837
SFSF	9.6216	16.062	38.095	38.927	46.707	70.902
CFSF	15.125	21.586	41.173	49.350	56.387	78.225
SSSF	11.656	29.019	41.175	59.160	62.868	64.384
CSSF	17.291	32.612	51.402	65.052	67.756	101.44
CCSF	18.233	37.348	51.833	71.290	75.213	105.65
CFCF	24.782	28.631	45.173	61.099	67.253	80.746
SCSF	13.046	34.169	41.694	63.122	64.384	73.255
CSCF	25.874	37.417	62.847	67.846	77.615	109.24
CCCF	26.364	41.684	63.207	77.660	80.811	117.00
SSSS	20.786	49.391	50.451	79.203	98.680	99.400
CSSS	25.089	52.840	58.803	86.447	100.98	113.22
CCSS	28.366	60.815	61.677	93.135	114.62	115.26
CSCS	31.159	56.022	69.447	94.935	102.95	128.77
CCCS	33.866	64.448	71.213	101.12	117.01	130.41
CCCC	37.829	73.541	74.364	108.53	131.81	132.63

Addition of curvature causes frequencies to be increased. In Table 3(a), the average increase from flat plates for the fundamental frequencies in Ω_1 is 9 percent, including the highest increase 20 percent of SSSS shell. The deeper curvature a/R=0.5 in Table 3(b) shows the average increase of 39 percent in Ω_1 with the maximum 93 percent of SSSS shell.

Table 4(a) and (b) list up the lowest six frequency parameters of shallow cylindrical shells with R_x=(infinity) and a/R_y=0.2 and a/R_y=0.5, respectively. This represents straight edges of the shell along the *x* axis, and curvature is given only in *y* direction. When the increase of the fundamental frequencies due to the curvature increase is considered, the average percent increases are 4 percent and 20 percent in Table 4(a) and (b), respectively. Roughly speaking, this effect is a half of the spherical shells, and the effect of curvature increase in one direction is a half of curvatures in two directions of spherical shells.

Tables 5(a) and (b) also tabulate the lowest six frequency parameters of shallow cylindrical shells, but with R_y=(infinity) and a/R_x=0.2 and a/R_x=0.5, respectively. Straight edges of the shell exist along the *y* axis, and curvature is only in *x* direction. For cylindrical shells with FFFF, SSSS and CCCC, the results are the identical as in Table 4(a) and (b) due to uniform boundary condition along four edges, and also shells with SSFF, CCFF and CCSS give the identical results as in Table 4(a) and (b) since the 90 degree rotation (or flipping about a diagonal symmetric axis) of the shell gives essentially the same boundary conditions.

Table 5(b) Frequency parameters Ω of shallow cylindrical shells, R_y=(infinity), a/R_x=0.5, a/b=1, a/h=20, ν=0.3.

B.C.	Ω_1	Ω_2	Ω_3	Ω_4	Ω_5	Ω_6
FFFF	13.439	21.284	28.119	34.685	35.450	61.010
SFFF	6.5537	14.962	25.159	30.710	49.135	52.689
CFFF	3.4369	8.2686	21.129	28.647	31.417	46.386
SSFF	3.3474	17.927	22.681	40.569	51.774	56.461
CSFF	5.2853	22.217	24.740	46.690	53.805	56.634
CCFF	8.4374	25.562	29.549	51.099	63.347	67.845
SFSF	9.5542	15.696	38.833	44.561	46.547	71.739
CFSF	14.777	25.870	47.889	48.900	57.008	80.148
SSSF	11.506	34.831	41.059	59.650	64.384	67.893
CSSF	19.550	39.366	51.429	68.895	70.218	103.10
CCSF	21.313	43.499	51.948	72.439	79.696	105.04
CFCF	35.338	38.115	52.645	60.699	67.650	85.438
SCSF	14.725	39.385	41.653	63.678	64.384	77.594
CSCF	36.143	45.846	62.698	73.258	78.852	111.13
CCCF	36.473	49.547	63.134	82.043	82.448	118.79
SSSS	25.509	49.612	55.861	80.479	98.594	103.01
CSSS	31.345	58.522	59.672	88.079	104.65	113.21
CCSS	34.217	61.768	66.606	94.692	114.64	118.46
CSCS	40.744	62.278	70.066	96.739	106.73	128.77
CCCS	42.928	69.997	71.914	102.84	120.35	130.73
CCCC	46.241	74.300	79.239	110.14	132.35	135.51

Their identical results of six cases are underlined. As expected, the increase of the fundamental frequencies due to the curvature increase is basically same as in Table 4(a) and (b).

Finally, Table 6(a) and (b) list up the lowest six parameters of shallow hyperbolic paraboloidal shells with a/R_y=0.2 and a/R_y=0.5, respectively. The negative curvature ratio (R_x/R_y= -1) indicates that the shell geometry is convex in one direction and concave in another direction. This geometric feature gives rise unusual response in frequency. For shells of spherical and cylindrical curvature, addition of curvature causes more stiffness in the structure, and it results in the increase of natural frequencies. But for shell of hyperbolic paraboloidal shell, addition of negative curvature causes the decrease of frequencies, when shell has free edges. For example, the SFFF shell gives Ω_1=6.648 for a/R_x=0 (plate), Ω_1=6.628 for a/R_x=0.2 and Ω_1=6.548 for a/R_x=0.5. As the constrained is increased along the edges, this tendency disappears.

4. Conclusions

The purpose of this paper was to present lists of accurate natural frequencies for free vibration of doubly curved, isotropic shallow shells of rectangular (square) planform under different sets of boundary conditions. For this purpose, mathematical procedure was described and accuracy of the present numerical solutions was well established by convergence and comparison studies. Thus, with strong background in solution accuracy, all the present frequency parameters were given in five

Table 6(a) Frequency parameters Ω of shallow hyperbolic paraboloidal shells, R_x/R_y=-1, a/R_y=0.2, a/b=1, a/h=20, ν=0.3.

B.C.	Ω_1	Ω_2	Ω_3	Ω_4	Ω_5	Ω_6
FFFF	13.458	21.894	24.244	34.929	34.929	61.775
SFFF	6.6281	16.057	25.414	26.762	48.931	50.889
CFFF	3.8095	8.4752	22.356	27.892	30.617	44.083
SSFF	3.3591	18.781	19.323	38.159	51.803	54.022
CSFF	5.6190	20.369	25.086	43.345	53.237	54.290
CCFF	7.0680	25.562	27.018	48.207	63.436	65.918
SFSF	10.406	16.107	37.451	39.768	46.847	70.668
CFSF	15.839	21.623	40.753	50.048	56.513	78.037
SSSF	12.206	28.062	41.865	59.114	62.527	64.384
CSSF	17.735	32.074	51.964	64.796	67.770	101.19
CCSF	19.183	37.091	52.437	71.488	75.079	106.08
CFCF	25.159	28.691	44.999	61.683	67.361	80.627
SCSF	14.387	33.591	42.424	63.306	64.384	73.063
CSCF	26.181	37.301	63.325	67.705	77.629	109.05
CCCF	26.786	41.703	63.724	77.602	80.988	116.90
SSSS	19.659	49.924	49.924	78.873	99.224	99.224
CSSS	24.592	52.471	59.269	86.220	100.84	113.69
CCSS	28.542	61.369	61.547	93.043	115.07	115.19
CSCS	31.282	55.859	69.836	94.764	102.86	128.77
CCCS	34.232	64.379	71.753	101.07	116.93	130.85
CCCC	38.732	74.301	74.301	108.54	132.15	132.74

Table 6(b) Frequency parameters Ω of shallow hyperbolic paraboloidal shells, R_x/R_y=-1, a/R_y=0.5, a/b=1, a/h=20, ν=0.3.

B.C.	Ω_1	Ω_2	Ω_3	Ω_4	Ω_5	Ω_6
FFFF	13.406	24.102	31.229	35.444	35.444	63.315
SFFF	6.5483	19.020	25.562	31.448	49.885	54.027
CFFF	4.8347	8.3111	25.101	29.276	32.576	46.547
SSFF	3.3096	19.414	24.886	37.875	55.594	56.620
CSFF	6.3397	24.220	28.365	44.741	54.552	56.821
CCFF	7.5551	28.612	32.675	51.171	67.028	67.642
SFSF	12.909	15.945	41.288	43.783	47.396	70.296
CFSF	18.435	26.084	45.659	53.025	57.756	79.27
SSSF	14.054	29.794	45.098	59.410	64.383	65.895
CSSF	21.710	36.488	54.729	68.581	69.133	101.62
CCSF	25.820	41.998	55.400	73.706	78.889	107.56
CFCF	36.944	38.401	51.656	64.224	68.305	84.713
SCSF	20.858	36.118	45.769	64.383	64.882	76.477
CSCF	37.483	45.199	65.551	72.410	78.955	110.01
CCCF	38.249	49.610	66.142	82.098	83.171	118.21
SSSS	19.252	52.805	52.805	78.438	101.94	101.94
CSSS	28.811	56.335	62.406	86.712	103.76	116.05
CCSS	35.016	65.275	65.497	94.178	117.69	117.73
CSCS	41.267	61.320	72.397	95.686	106.13	128.77
CCCS	44.601	69.579	75.114	102.50	119.86	133.46
CCCC	50.691	78.836	78.836	110.19	135.10	135.53

significant figures, while other previous literature provide four significant figures.

It is hoped that the present comprehensive sets of frequency parameters will serve as good reference for future comparison. Due to the space limitation, the present results were given only for the case of relatively thick case (a/h=0.05) to complement Ref. [22]. In the next study, computation of frequency parameters will be done for very thin case (a/h=0.01) to match with Ref. [21], and the effect of the shell thickness will be clarified.

Acknowledgement

The second author expresses his gratitude to the Japan Society for the Promotion of Science (JSPS) for the Funding Program MEXT/JSPS KAKENHI Grant Number 21K03957.

References

[1] A. W. Leissa, "Vibration of Shells," 1973.
[2] W. Soedel, *Vibrations of Shells and Plates*. 2004.
[3] The Japan Society of Mechanical Engineers, *Handbook for Vibration and Buckling of Shells, Gihodo Shuppan Co., Ltd.* Tokyo, 2003.
[4] D. Narita and Y. Narita, "Modelling of thin structural polymer composites for use of automobiles -review," *EPI Intl. J. Eng.*, vol. 1, no. 1, pp. 13–20, 2018.
[5] A. W. Leissa and A. S. Kadi, "Curvature effects on shallow shell vibrations," *J. Sound Vibr.*, vol. 16, pp. 173–187, 1971.
[6] A. W. Leissa, J. K. Lee, and A. J. Wang, "Vibrations of cantilevered shallow cylindrical shells of rectangular planform," *J. Sound Vibr.*, vol. 78, pp. 228–311, 1981.
[7] A. W. Leissa, J. K. Lee, and A. J. Wang, "Vibrations of cantilevered doubly curved shallow shells.," *Int. J. Solids Struct.*, vol. 19, pp. 411–424, 1983.
[8] A. W. Leissa and Y. Narita, "Vibrations of completely free shallow shells of rectangular planform," *J. Sound Vibr.*, vol. 96, pp. 207–218, 1984.
[9] Y. Narita and A. W. Leissa, "Vibrations of corner point supported shallow shells of rectangular planform," *Earthq. Eng. Struct. Dynam*, vol. 12, pp. 651–661, 1984.
[10] M. S. Qatu and A. W. Leissa, "Effects of edge constraints upon shallow shell frequencies," *Thin. Wall. Struct.*, vol. 14, pp. 347–379, 1992.
[11] M. S. Qatu, "Review of shallow shell vibration research, Shock and Vibration Digest," vol. 24, pp. 3–15, 1992.
[12] S. D. Yu, W. L. Cleghorn, and R. G. Fenton, "On the accurate analysis of free vibration of open circular cylindrical shells," , *J. Sound Vibr*, vol. 188, pp. 315–336, 1995.
[13] K. M. Liew and C. W. Lim, "Vibratory behavior of doubly curved shallow shells of curvilinear planform," *J. Eng. Mech*, vol. 121, pp. 1277–1284, 1995.
[14] K. M. Liew and C. W. Lim, "Vibration of doubly-curved shallow shells," *Acta Mech*, vol. 114, pp. 95–119, 1996.
[15] C. W. Lim and K. M. Liew, "A pb-2 Ritz formulation for flexural vibration of shallow cylindrical shells of rectangular planform," *J. Sound Vibr*, vol. 173, pp. 343–375, 1994.
[16] K. M. Liew, C. W. Lim, and S. Kitipornchai, "Vibration of shallow shells: a review with bibliography," *Appl. Mech. Rev.*, vol. 50, pp. 431–444, 1997.
[17] M. S. Qatu, "Recent research advances in the dynamic behavior of shells. Part 2: Homogeneous shells," *Appl. Mech. Rev*, vol. 55, pp. 415–434, 2002.
[18] Y. Narita and P. Robinson, "Maximizing the fundamental frequency of laminated cylindrical panels using layerwise optimization," *Intl. J. Mech. Sci.*, vol. 48, pp. 1516–1524, 2006.
[19] L. E. Monterrubio, "Free vibration of shallow shells using the Rayleigh–Ritz method and penalty parameters, Proc. Inst. Mech. Engr., Part C," *J. Mech. Eng. Sci.*, vol. 23, pp. 2263–2272, 2009.
[20] M. S. Qatu, "Effect of inplane edge constraints on natural frequencies of simply supported doubly curved shallow shells," *Thin Walled Struct.*, vol. 49, pp. 797–803, 2011.
[21] Y. Mochida, S. Ilanko, M. Duke, and Y. Narita, "Free vibration analysis of doubly curved shallow shells using the Superposition-Galerkin method," . *Sound Vibr.*, vol. 331, pp. 1413–1425, 2012.
[22] M. S. Qatu and E. Asadi, "Vibration of doubly curved shallow shells with arbitrary boundaries," *Appl. Acous.*, vol. 73, pp. 21–27, 2012.

EPI International Journal of Engineering
Volume 4, Number 1, February 2021, pp. 37-44
DOI: 10.25042/epi-ije.022021.06

*p*ISSN 2615-5109
*e*ISSN 2621-0541

The Comparison of Fractional Derivative Model and Classical Spring-Dashpot Model in the Identification of Viscoelastic Characteristics of a Rubber Material

Daisuke Narita[a,*], Yoshiki Ohta[b]

[a]Hokkaido University of Science. Email: narita@hus.ac.jp
[b]Hokkaido University of Science, Faculty of Engineering. Email: ohta@hus.ac.jp

Abstract

In the design of viscoelastic materials used in rubber products, not theoretical approaches but experimental approaches have been usually employed. This is due to the difficulties in mathematical procedures of the dynamic material characteristics such as the dependencies of strain amplitude, frequency and/or environmental temperature in deformation. In mathematical approach there are two kinds of analytical models for a complex module of the material, which are a fractional derivative model and a spring-dashpot model. However, there are few papers dealing with the study of not only the identifications of parameters for the experimental modulus actually obtained both of by using the fractional derivative model by using the spring-dashpot model and but also the discussion of the comparisons of the two models. In the present paper, the complex elastic modulus for a rubber material is obtained experimentally for a wide range of excitation frequency, and the modulus-frequency relations are derived analytically by using the two models, respectively. Finally, the applicability of the models for parameter identification are discussed from the numerical results.

Keywords: *Complex module; fractional derivative model; parameter identification; spring-dashpot model; viscoelastic material*

1. Introduction

In the design of viscoelastic material used in rubber products such as automobile tires, not theoretical approaches but experimental approaches have been employed usually. This is due to the difficulties in mathematical procedures of the dynamic material characteristics, complex elastic module, which are the dependencies of strain amplitude, excitation frequency and/or environmental temperature in deformation.

In Jones's handbook [1] there are two kinds of the mathematical, analytical models for complex elastic module for the materials. First one is called as a classical spring-dashpot model, and the model consists of the serial and/or parallel combinations of spring elements and dashpot elements, which represents elastic and viscous behaviors, respectively. On the other hand, another one is a fractional derivative model, and the model is assumed to be the mathematical fractional derivative of the displacement with respect to time.

In the past researches by using the fractional derivatives, Shimizu [2] elucidated the fundamental characteristics of the oscillator composed of the silicone gel and a mass, and the fractional time-derivative Voigt model of the silicone gel and the equation of motion of a single degree of freedom oscillator having the fractional derivative term was derived. Shimizu and Iijima [3] also studied the fractional differential approach to model the polymeric viscoelastic material, and the fractional differential equation for a single degree of freedom viscoelastic oscillator was solved, and the characteristics of the oscillatory system with the material were discussed. Nasuno et al. [4] proposed the appropriate models to describe the behavior of the fractional derivative viscoelastic body by considering nonlinear statical and dynamical models in order to understand the behavior of higher damping capacity by pre-stress due to pre-displacement. Fukunaga and Shimizu [5] proposed two type of models for describing nonlinear fractional derivative dynamical behavior of viscoelastic materials subject to impulse forced. Narita et al. [6] studied the identification of parameters of the fractional derivative model for the experimental results of complex elastic modulus of a viscoelastic material, and the applicability of the model for constructing the modulus-frequency relations of the material was discussed. However, there are few papers dealing with

*Corresponding author. Tel.: +81-11-681-2161
Maeda, Teine
Sapporo, Hokkaido, Japan, 006-8585

the comparisons of the fractional derivative model and the classical spring-dashpot model in identification for the complex elastic modulus (Young's modulus and loss factor) of a viscoelastic material such as a rubber material.

This paper studies the applicability of the two models in constructing the curves between the complex elastic modulus and excitation frequency in vibration. For this purpose, the vibration tests for the material are carried out, and the master curve, which indicates the dynamic characteristics of the material for wider range of frequency, is obtained numerically by applying the W.L.F. equation. The fractional derivative model and the classical spring-dashpot model are then assumed for the material, and the parameters of the two models are identified for the master curve. In numerical identification the Solver Procedure of the Microsoft EXCEL is employed in the present study. Finally, the applicability of the fractional derivative models is discussed by comparing the numerical results.

2. Dynamic Characteristics of a Rubber Material

Figure 1 shows the general dynamic characteristics of a viscoelastic material to an environmental temperature, which are Young's modulus and loss factor of a viscoelastic material. As shown in the figure, the property of the characteristics is divided into 4 regions, which are a glass region, a transition region, a rubber-like region and a flow region. There are the similar tendencies in the general dynamic characteristics of the material with respect to the excitation frequency, and time-temperature superposition principles for a viscoelastic material is also well-known.

According to the time-temperature superposition principle for the transition region of the material the superposition parameter α_T is given by the W.L.F. equation:

$$\log\alpha_T(T,T_o) = -\frac{C_1(T-T_o)}{C_2+T-T_o} \quad (1)$$

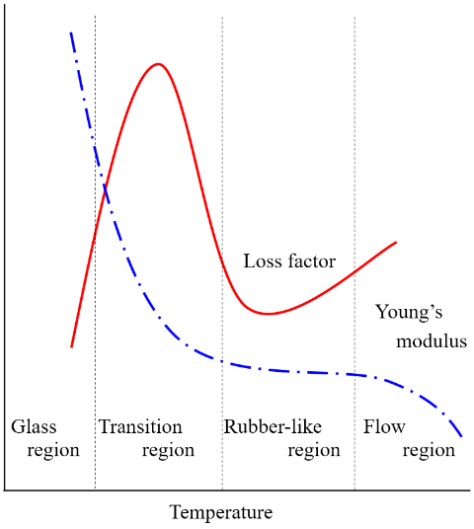

Figure 1. General dynamic characteristics of viscoelastic materials

where T is environmental temperature, T_o is a reference temperature chosen to construct the compliance master curve and C_1, C_2 are empirical constants adjusted to fit the values of the superposition parameter α_T.

By applying the W.L.F. equation to the experimental results for the frequency range where a vibration test can be actually carried out, the dynamic characteristics for the wider frequency range is numerically estimated.

In the present study Young's modulus and loss factor of a natural rubber sheet (NR0505, AS ONE) in stretching vibration are obtained experimentally by using the experimental device shown in Fig. 2 (Dynamic Mechanical Analyzer DMA7100, HITACHI). In experiment the complex module is measured at the environmental temperatures from 183K to 373K by oscillating at frequency of 0.1, 0.2, 0.5, 1, 2, 5, 10, 20 Hz, respectively. The master curve is also construed numerically from the experimental results by using the optional software, DMA Master Curve Analysis Option.

Figure 3 shows storage modulus (real part of complex modulus) (E'), loss modulus (imaginary part of complex modulus) (E'') and loss tangent (tan D) obtained experimentally with strain amplitude 20μm. The complex moduli obtained experimentally are almost same even by oscillating with the strain amplitude of 5, 10 and 20μm, respectively.

Figure 4 shows the master curve obtained by using the optional software from the experimental results in Fig.3, whereas a glass-transition temperature and a reference temperature are set to be -70℃ and 23℃, respectively. The empirical constants are also given by C_1 = 27.0 and C_2 = 52.0.

3. Identification Models for Complex Module

3.1. Fractional derivative model

The simplest fractional derivative formulation for a stress-strain relation can be assumed to be the form:

Figure 2. Experimental equipment used in vibration test (DMA7100, HITACHI)

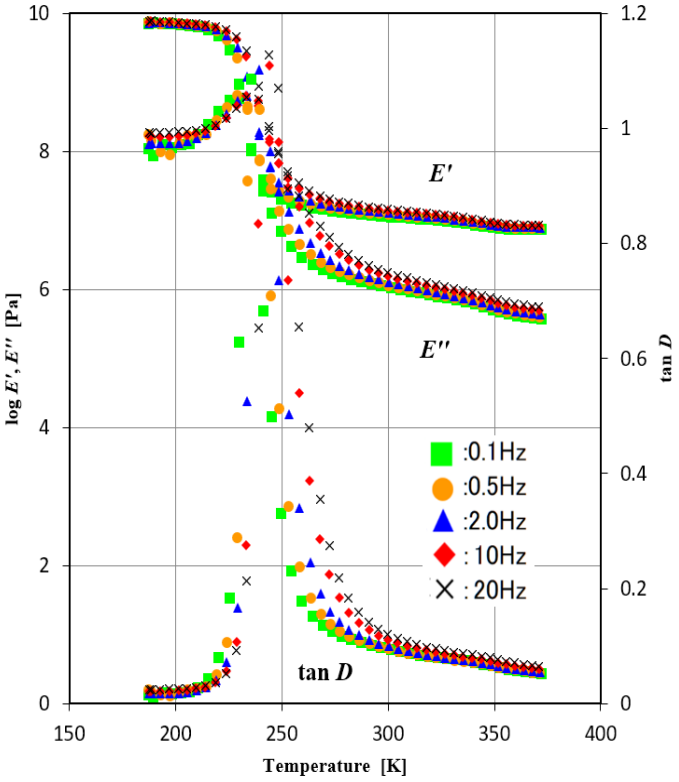

Figure 3. Experimental results of complex module from vibration test

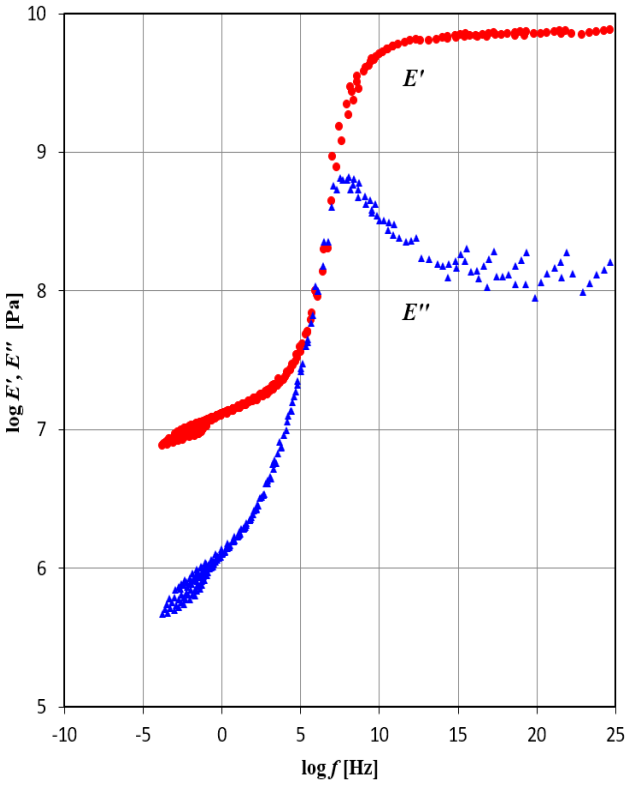

Figure 4. Master curve obtained numerically from experimental result

$$\sigma(t)+c\frac{d^{\beta}\sigma(t)}{dt^{\beta}}=a\,\varepsilon(t)+b\frac{d^{\beta}\varepsilon(t)}{dt^{\beta}} \tag{2}$$

where a, b, c and β are unknown parameters to be chosen by parameter identification to the master curve. The above relation can be reduced for a steady vibration by using a circular frequency ω into the equation:

$$\sigma(t)=\frac{a+b(i\omega)^{\beta}}{1+c(i\omega)^{\beta}}\varepsilon(t) \tag{3}$$

And a complex module E_1* is expressed by this equation :

$$E_1^{*}=\frac{a+b(i\omega)^{\beta}}{1+c(i\omega)^{\beta}}\omega^{p}=\frac{a+b(\cos\frac{\pi}{2}\beta+i\sin\frac{\pi}{2}\beta)\omega^{\beta}}{1+c(\cos\frac{\pi}{2}\beta+i\sin\frac{\pi}{2}\beta)\omega^{\beta}}\omega^{p} \tag{4}$$

where the term ω^p is added here for correction [1]. In the present study the parameter identification for the master curve is conducted by using the parallel combination of N-set of the equation (4).

3.2. Classical spring-dashpot model

In the classical spring-dashpot model a spring element and a dashpot element are combined to represent the dynamic characteristics of a viscoelastic material. Figure 5 shows the standard combination model of a simple Maxwell-type model and a simple Voigt-type model, where k_i and c_i are a spring constant and a damping coefficient, respectively.

For the model a complex module E_2* is given by this equation :

$$\begin{aligned}E_2^{*}&=k_0+\frac{c_1k_1i\omega}{c_1i\omega+k_1}+\frac{c_2k_2i\omega}{c_2i\omega+k_2}\cdots\cdots\frac{c_Nk_Ni\omega}{c_Ni\omega+k_N}\\&=k_0+\left(\frac{k_1c_1^{\,2}\omega^2}{k_1^{\,2}+c_1^{\,2}\omega^2}+\frac{k_1^{\,2}c_1\omega}{k_1^{\,2}+c_1^{\,2}\omega^2}i\right)+\left(\frac{k_2c_2^{\,2}\omega^2}{k_2^{\,2}+c_2^{\,2}\omega^2}+\frac{k_2^{\,2}c_2\omega}{k_2^{\,2}+c_2^{\,2}\omega^2}i\right)\\&+\cdots\cdots\left(\frac{k_Nc_N^{\,2}\omega^2}{k_N^{\,2}+c_N^{\,2}\omega^2}+\frac{k_N^{\,2}c_N\omega}{k_N^{\,2}+c_N^{\,2}\omega^2}i\right)\end{aligned} \tag{5}$$

4. Parameter identification for complex module

In the present identification the master curve from 1 Hz to 10^5 Hz is picked up because the structural design and analysis of the material is considered in our research group.

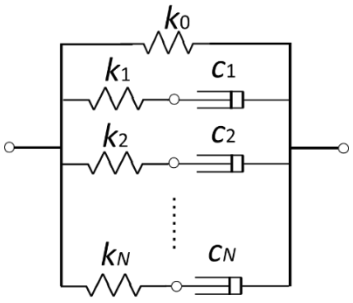

Figure 5. Standard spring-dashpot model

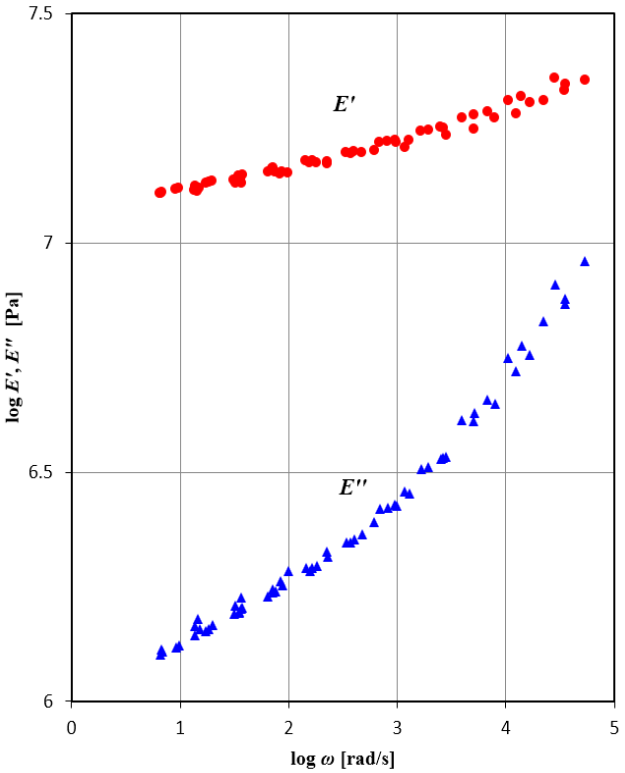

Figure 6. Master curve to be identified for the frequency of $10^0 \sim 10^5$Hz

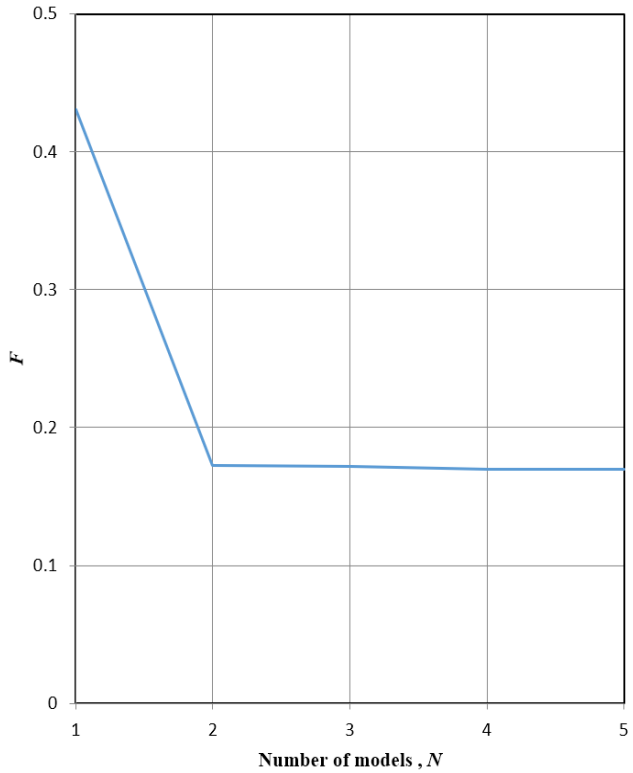

Figure 7. Evaluation function F with different set N of fractional derivative models

And the complex module is identified analytically by using not only fractional derivative models but also a standard spring-dashpot models. Figure 6 shows the master curve picked up from in Fig. 4.

In identification, the parameters of the two models are obtained numerically respectively by minimizing the evaluation function F :

$$F = \sum_i \frac{(E'_i - E'_{exp})^2}{(E'_{ave})^2} + \sum_i \frac{(E''_i - E''_{exp})^2}{(E''_{ave})^2} \qquad (6)$$

where E'_i and E''_i are estimated numerically from the equation (4) or (5), E'_{exp} and E''_{exp} are the experimental valued on the master curve and E'_{ave} and E''_{ave} are averaged values of experimental results, respectively, and the iteration calculations are carried out by using the Solver Procedure of the Microsoft EXCEL in the present study.

Figure 7 shows evaluation function F minimized by using the fractional derivative model with different N-set of models. As shown in the figure, the evaluation function can be converged by taking just 2 sets of models (N = 2). Figure 8 shows the function values by the standard spring-dashpot model with different N-set of models. In this case, more than 5-sets or 6-sets of models is required to the convergence of the estimation function, and the converged function value is also relatively higher than the one in Fig. 7. Tables 1 and 2 give the converged function values and identified parameters numerically in the fractional derivative model and the

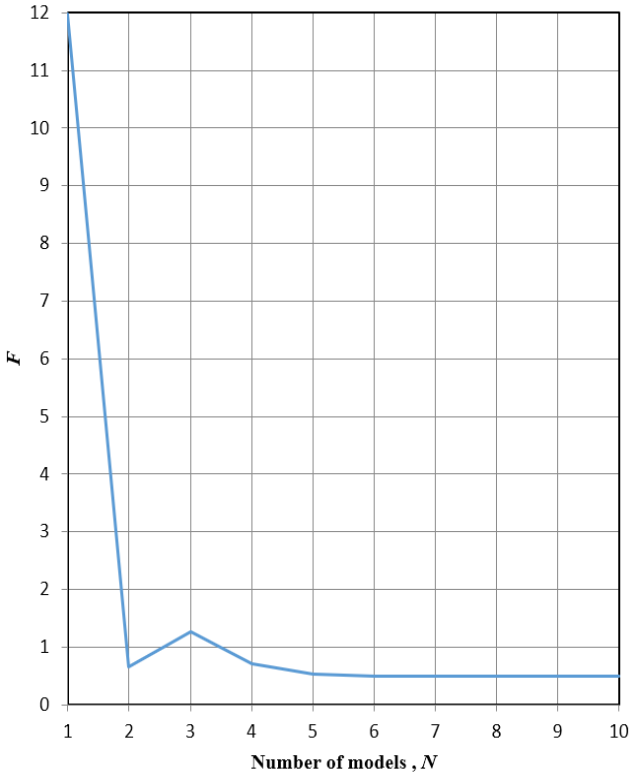

Figure 8. Evaluation function F with different set N of standard spring-dashpot models

Table 1. Identified parameters of fractional derivative models (N = 1～5)

N	F	i	a_i	b_i	c_i	β_i	p_i
1	0.43093	1	4.6811E-05	84316	-0.99253	0.00049106	-0.032311
2	0.17264	1	7910.9	26236	9.0599E-06	0.86224	-0.35332
		2	0.031970	7033726	-0.40147	0.035567	-0.015347
3	0.17220	1	1863523	39107	8.6148E-06	0.84426	-0.36249
		2	6636.0	1747.3	0.27436	0.24101	0.026965
		3	5.9905E-06	10341734	-0.036647	0.062576	-0.0050527
4	0.17012	1	10211817	82006	-0.066660	0.0026680	-0.038460
		2	-5658.2	37824	0.061469	0.62989	0.21621
		3	-3.1750E-05	2122739	0.61699	0.50741	0.063791
		4	4.1442E-05	197998	-2.1572E-06	0.82321	-0.47058
5	0.16970	1	5757191	99666	-0.44977	-0.018633	0.034067
		2	-9672.0	159221	-1.7362E-06	0.99886	-0.64038
		3	-3.1750E-05	514992	0.044898	0.10236	0.18080
		4	4.1442E-05	1419391	0.017474	0.53211	-0.48815
		5	4.1442E-05	934056	0.092329	0.57168	-7.0659

Table 2. Identified parameters of standard spring-dashpot models (N = 1～5)

N	F							
1	11.984	i	0	1				
		k	15266731	16162147				
		c	-	701.34				
2	0.65015	i	0	1	2			
		k	13232374	16662214	5353284			
		c	-	400.49	7436.9			
5	0.53291	i	0	1	2	3	4	5
		k	10135385	5.7948E+15	6702821	3826059	2462583	2740006
		c	-	140.84	417.54	2223.1	201770	17357
7	0.48970	i	0	1	2	3	4	5
		k	0	4.2803E+15	11275377	3133313	6191856	2392309
		c	-	133.91	20985159	860.09	310.25	3299.0
		i	6	7				
		k	1896709	1422234				
		c	15728	52545				
10	0.48970	i	0	1	2	3	4	5
		k	0	474175	474175	474175	474175	1422242
		c	-	3932.1	3932.1	3932.0	3932.0	52545
		i	6	7	8	9	10	
		k	11275385	1.3521E+16	2392307	6191855	3133308	
		c	20985067	133.91	3299.0	310.25	860.09	

standard spring-dashpot model, respectively.

Figure 9 shows the comparison of the complex modulus of E' and E'' identified numerically by assuming 1 set of the fractional derivative model (N = 1) (shown by solid lines) and the master curve data (shown by × mark). Figure 10, 11, 12 and 13 correspond to the comparison by assuming 2, 3, 4 and 5 set of the models, respectively. As shown in these figures, better agreement in the curve fitting can be observed as the number N of the model is increased from 1 to 5, and the curve fitting by taking more than N = 2 can be almost similarly. Therefore, the fractional model with N = 2 is enough to get better parameter identification.

Figure 14 shows the comparisons by assuming 1 set of the spring-dashpot model in contrast, and Figures 15, 16, 17 and

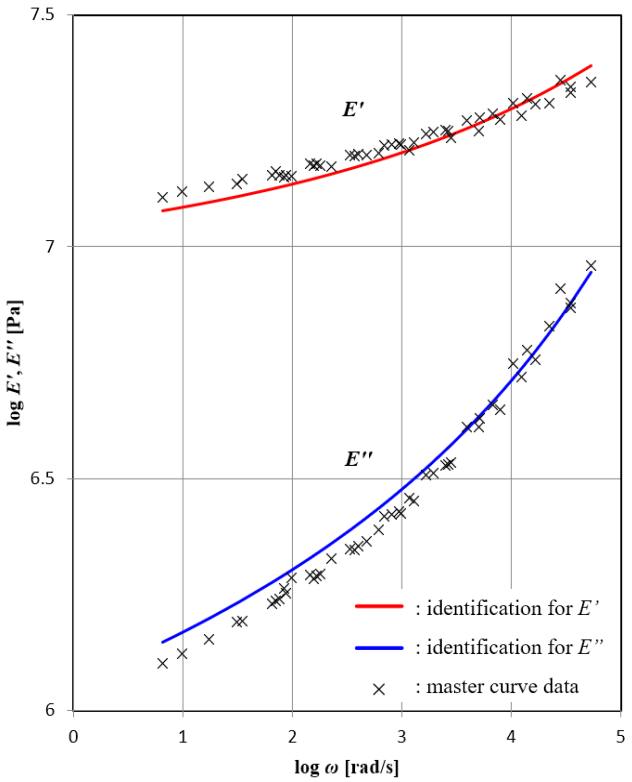

Figure 9. Curve fitting to master curve data by fractional derivative model (N = 1)

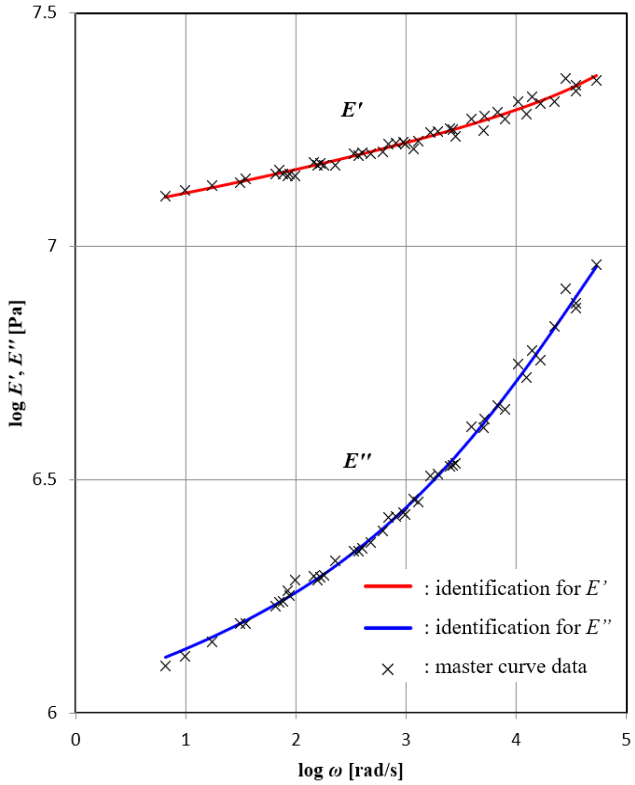

Figure 10. Curve fitting to master curve data by fractional derivative model (N = 2)

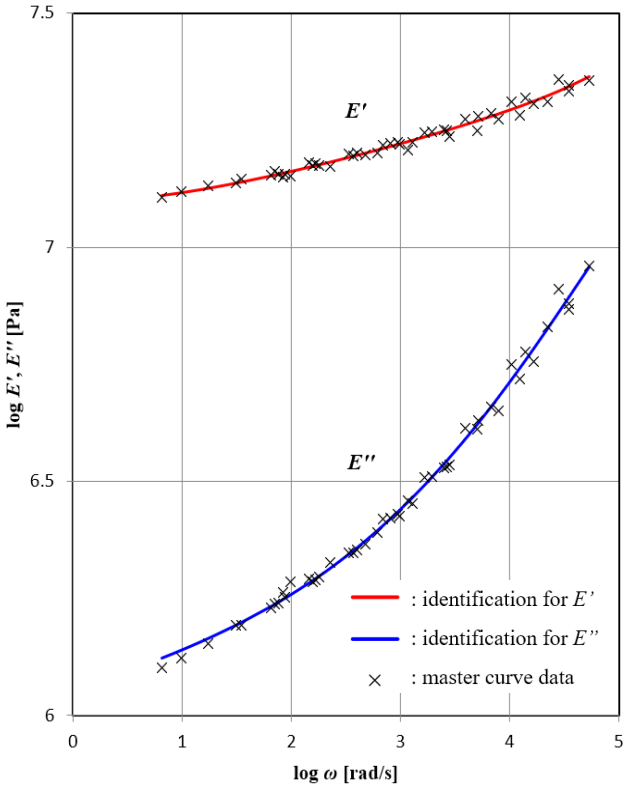

Figure 11. Curve fitting to master curve data by fractional derivative model ($N = 3$)

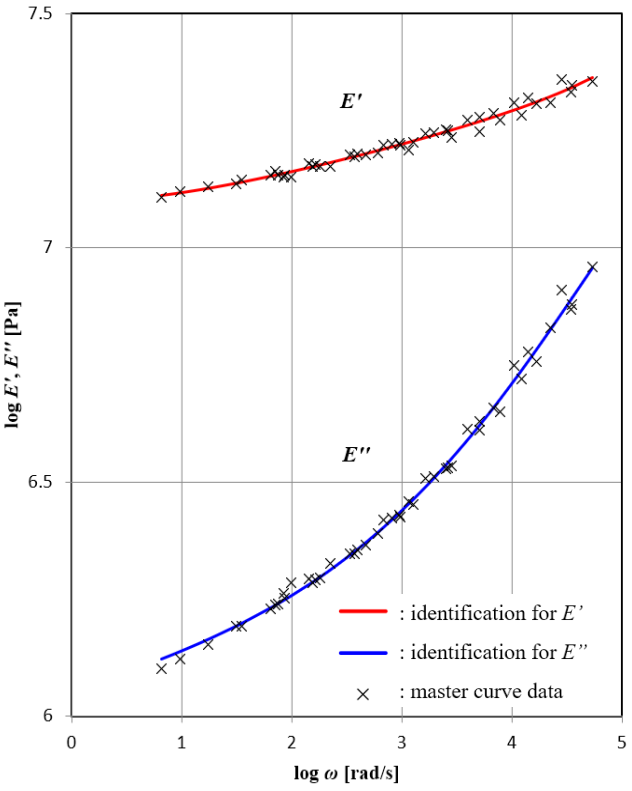

Figure 12. Curve fitting to master curve data by fractional derivative model ($N = 4$)

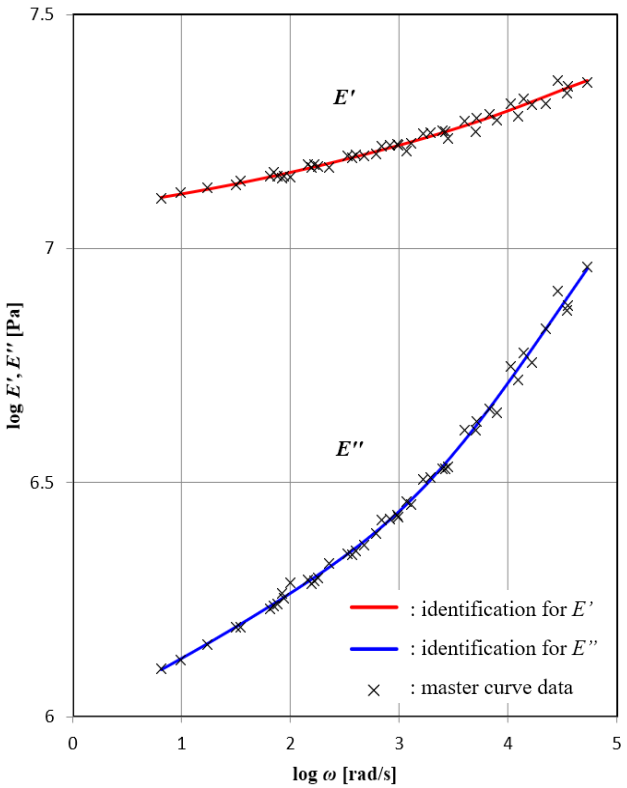

Figure 13. Curve fitting to master curve data by fractional derivative model ($N = 5$)

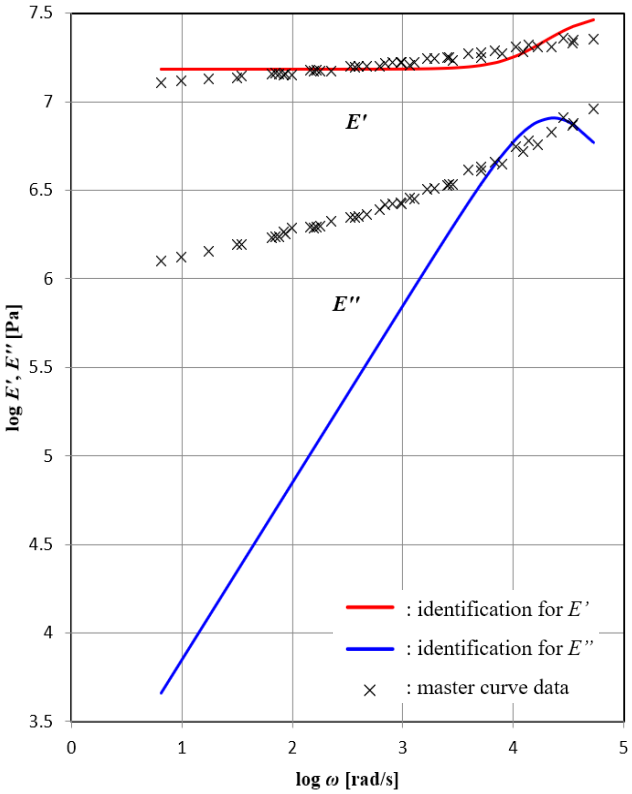

Figure 14. Curve fitting to master curve data by standard spring-dashpot model ($N = 1$)

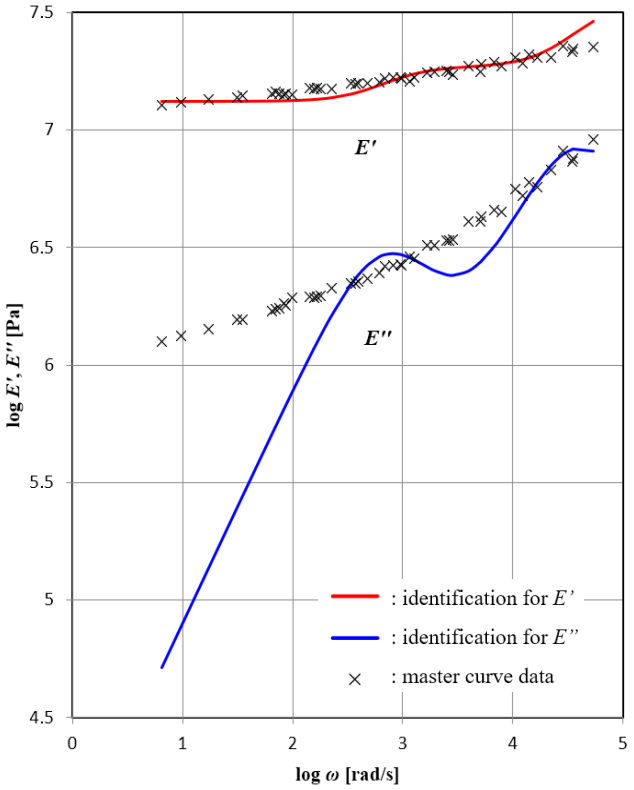

Figure 15. Curve fitting to master curve data by standard spring-dashpot model ($N = 2$)

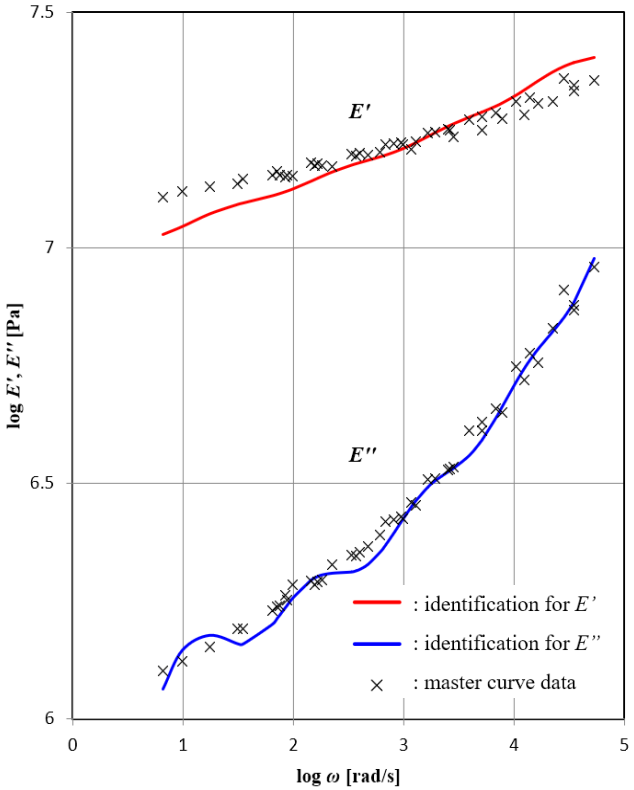

Figure 16. Curve fitting to master curve data by standard spring-dashpot model ($N = 5$)

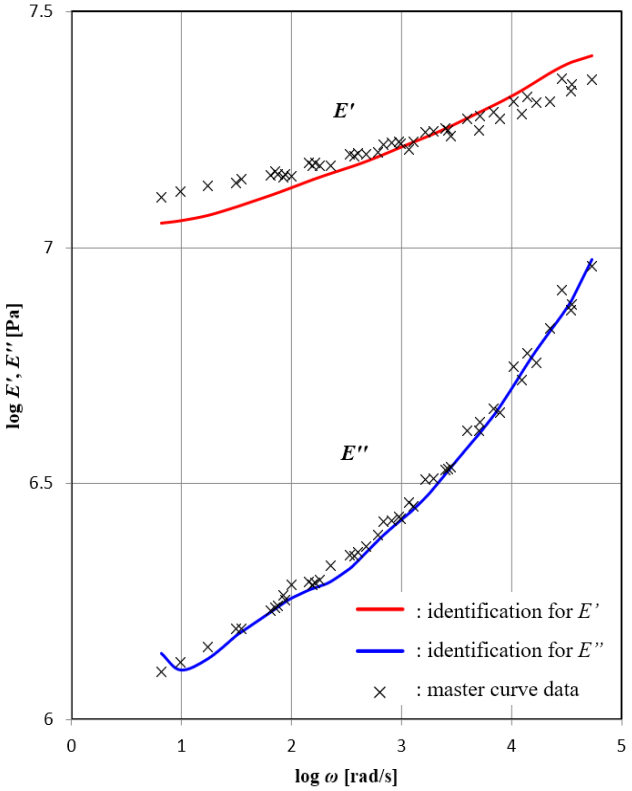

Figure 17. Curve fitting to master curve data by standard spring-dashpot model ($N = 7$)

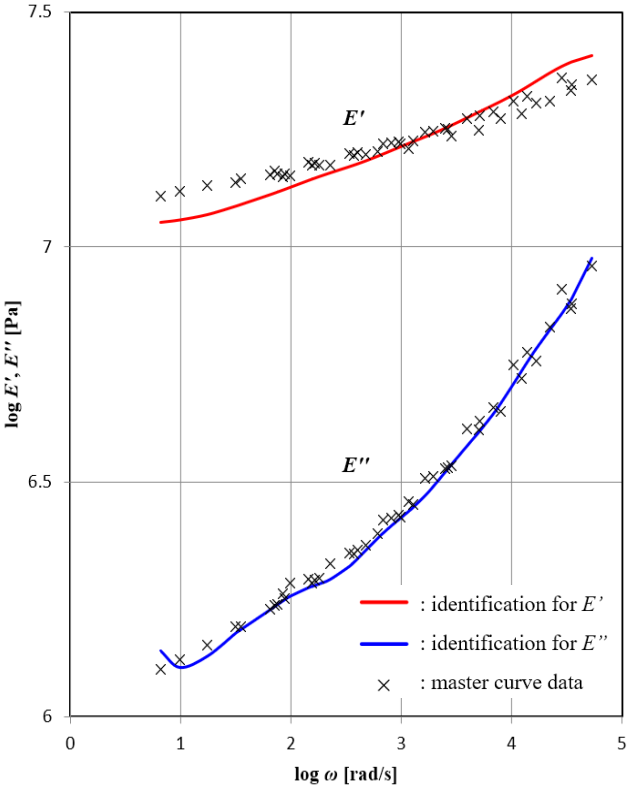

Figure 18. Curve fitting to master curve data by standard spring-dashpot model ($N = 10$)

18 correspond to the case of N = 2, 5, 7 and 10, respectively.

From these results even if by taking 10 set of the models the estimated curve cannot fit the experimental moduli well as the cases of the identifications by assuming the fractional derivative model N = 2. It can be observed from these results that the performance in identification of the spring-dashpot model is not good even if the number of set is increased more than N = 7.

5. Conclusions

In the present study, the vibration tests for a rubber material are carried out, and the master curve is obtained numerically by applying the W.L.F. equation. The fractional derivative model and the standard spring-dashpot model are assumed for the complex module of the material, and the parameters of the two models are identified numerically. Finally, the applicability of the fractional derivative models is discussed by comparing the numerical results by the spring-dashpot models, and thus it can be concluded that the fractional derivative model has a better performance in identification of the master curve of complex modulus of a rubber material rather than the spring-dashpot model.

References

[1] D. I. G. Jones, *Handbook of Viscoelastic Vibration Damping*. 2001.

[2] N. Shimizu, "Dynamic Characteristics of a Viscoelastic Oscillator," *Trans. JSME (Ser. C)*, vol. 61, no. 583, pp. 902–906, 1995. [in Japanese]

[3] N. Shimizu and M. Iijima, "Fractional Differential Model of Viscoelastic Material," *Trans. JSME (Ser. C)*, vol. 62, no. 604, pp. 4447–4451, 1996. [in Japanese]

[4] H. Nasuno, N. Shimizu, and T. Yasuno, "Geometrical Nonlinear Statical and Dynamical Models of Fractional Derivative Viscoelastic Body," *Trans. JSME (Ser. C)*, vol. 72, no. 716, pp. 1041–1048, 2006. [in Japanese]

[5] M. Fukunaga and N. Shimizu, "Nonlinear Fractional Derivative Models of Viscoelastic Impact Dynamics Based on Entropy Elasticity and Generalized Maxwell Law," *J. Comput. Nonlinear Dyn.*, p. 21005, 2011.

[6] D. Narita, M. Yoshida, Y. Ohta, and T. Yamagishi, "The Effect of Strain Amplitude on the Analytical Model for Stiffness of Viscoelastic Materials," in *Proceeding of Dynamics and Design Conference 2016 of JSME*, 2016.

EPI International Journal of Engineering
Volume 4, Number 1, February 2021, pp. 45-50
DOI: 10.25042/epi-ije.022021.07

*p*ISSN 2615-5109
*e*ISSN 2621-0541

Fluid Flow Through Serial Parallel Circular Cylinder Arranged in Tandem

Nur Ikhsani[a,*], Nasaruddin Salam[b], Luther Sule[c]

[a]Departmen of Mechanical Engineering, Hasanuddin University, Makassar, Indonesia. Email : mr.nikhsani24@gmail.com
[b]Departmen of Mechanical Engineering, Hasanuddin University, Makassar, Indonesia. Email : nassalam.unhas@yahoo.com
[c]Departmen of Mechanical Engineering, Hasanuddin University, Makassar, Indonesia. Email : luther.sule@yahoo.co.id

Abstract

The Fluid flow through circular cylinders in serial parallel positions arranged in tandem were analyzed computationally and experimentally at nine levels of Reynolds number, Re_D 34,229; 47,921; 61,612; 75,304; 88,996; 102,688; 116,379; 130.071 and 143,763 The variation in the ratio of the distance between the front and rear cylinders is determined as M/D = 0.3, M/D = 0.5, M/D = 0.7, M/D = 0.9, and M/D = 1.1. While the distance between cylinder number 2 and 3 we set constantly and determined as N/D = 5 cm. The results displayed are flow velocity with computational approach validated by flow visualization, computational pressure contour, and drag coefficient through experimental testing. The results showed that the smallest boundary layer thickness was obtained in the model with a distance ratio of M/D = 2.5, using both computational and experimental approaches. The characteristics of the minimum pressure contour and the lowest drag coefficient (C_D) = 0.7572 were also obtained at the ratio of the distance M/D = 0.25 and at upstream speed of 21 m/s.

Keywords: Drag coefficient; flow visualization; FLUENT 6.3.26; tandem serial-parallel circular cylinders; pressure coefficient

1. Introduction

Flow through vertical circular cylinders arranged in tandem is a form often used in structural and transportation engineering. Sharing of round cylindrical applications such as offshore structures, lighthouses, platform and port support structures as well as heat exchangers such as Shell and Tube heat exchangers [1]–[3]. Wind and water loads on a building are some of the main factors that must be considered in the design.

Previous research was conducted to determine the flow phenomenon across a tandem object and its effect on drag force [4]–[6] commonly used geometric bodies are cylindrical, often found inland transport vehicles such as trains and trailers as well as in marine transportation such as barges. The reduction of drag can be obtained by engineering the flow field by adding an object called the inlet fault body, which is placed in front of the main object.

It is known that the wind and water loads on a building in groups are different from single-building structures with the same shape, because the combined disturbance from the flow around the structure in groups shows interesting and unpredictable variations of phenomena [7]. Many researchers have made efforts to reduce friction forces. Some show how to reduce the drag force on a single cylinder or are arranged in tandem by a variety of methods. Research on the reduction of friction using a drag body has been widely applied. Based on Etminan et al. [8]. when the circular cylinder is arranged in tandem in front of the two cylinders are given a T-shaped resistance plate, with a head width of 5 mm and the distance to the cylinder is varied to get the optimal position results, the optimal results are obtained when the variation of cylinder distance with cylinder diameter is in L/D = 1.0 to 1.5.

Salam, et al [9]–[11], conducted a similar study regarding the effect of adding an Inlet Disturbance Body (IDB) in the form of a circular cylinder on the drag acting on a square cylinder in a tandem arrangement through a numerical simulation approach using computational fluid dynamics methods and experimental testing utilizing the subsonic wind tunnel facility. The Reynolds number used is in the range of 30.625 to 96.250. The ratio of IDB diameter and square cylinder diameter (d/D) is 0.08, 0.14, and 0.20, respectively, with the ratio of the distance between the IDB and the square cylinder (L/D) varying from 0.0 to 1.0. The results showed a decrease in the amount of drag coefficient (C_D) and pressure coefficient (C_P) along with the increase in L/D and d/D ratios. The decrease in the highest drag coefficient was 21.5962% and the decrease in pressure coefficient was 14.7059 at L/D = 0.43 and d/D = 0.14. Regards Salam, et al. Also investigated the flow separation that occurs in rectangular cylinders arranged in serial and parallel and found that the smallest flow separation for serial and parallel configurations is at M/D = 0.6.

*Corresponding author. Tel.: +62 813-4299-2098
Jalan Poros Malino km. 6 Bontomarannu
Gowa, Indonesia, 92171

Tsutsui and Igarashi [12] investigated the reduction of drag in circular cylinders through the application of a drag rod in front of the object. The results showed that the disturbance diameter and Reynolds number had an effect on the flow pattern. A 63% reduction in resistance was also found. For very blunt objects, such as a flat plate perpendicular to the flow, flow separation occurs at the edges of the plate regardless of the nature of the boundary layer flow [13]–[15].

2. Research Methods

The research begins with a numerical simulation using computational fluid dynamic fluent 6.3.26 software before being validated through experimental tests. For numerical simulation, the test model is designed using the Autodesk inventor device and assigned to the computational domain and then through the meshing process using the Gambit device 2.4.6. Numerical simulation is focused on analyzing flow phenomena in the form of velocity trajectories and pressure contours. Details of the model test and computational conditions are shown in Fig. 1 and Table 1.

The experimental test was conducted in a Sub-Sonic Wind Tunnel made by Plint & Partners LTD. Engineers England. The test section has made of transparent acrylic with a thickness of 2.5 cm for flow visualization. The test object was a tandem of circular cylinders as shown in Figure 1. Circular cylinders length, width, and height were equal referred to as square cylinders diameter (D) = 5 cm. The test object was made of acrylic with a thickness of 2 mm. The airflow velocity that entered the wind tunnel (U) was ranged from 5 to 21 m/s. The drag was measured by a *Load Cell* system with a measurement range of 0.00981 Newton to balance the left and right side. The result from the measurement of *Load Cell* toward the object was the drag force (F) of the test object.

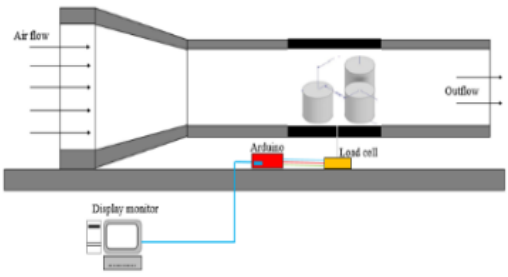

(a)

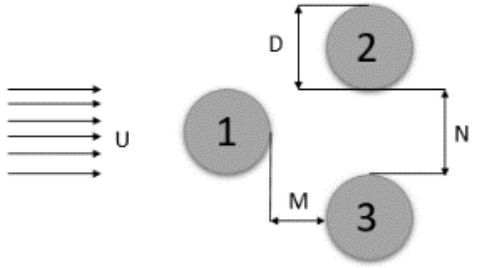

(b)

Figure 1. A parallel series tandem pattern on a circular cylinder body. (a) Position of specimen in the wind tunnel and (b) Computational arrangement condition

Figure 2. Sub-sonic wind tunnel

The circular cylinder size is 5 cm length and 5 cm height. The diameter of the cylinder is constantly 5 cm. Distance between front cylinder and rear cylinder (M) is changed with various distances. Comparison of distances between circular cylinders of the M/D series positions expanded from M/D = 0.3, M/D = 0.5, M/D = 0.7, M/D = 0.9, and M/D = 1.1 in centimeter (cm). Meanwhile, the distance of two vertical circular cylinders 1 and 2 in parallel position (N/D) is set constantly at 5 cm.

Subsequent research was carried out in the laboratory for experimental testing. For experimental testing, it is focused on collecting flow visualization data to validate the results of numerical and drag calculations using a subsonic wind tunnel which is equipped with a measuring instrument for the actual resistance force of the test object with the principle of force balance as shown in Figure 2. The resistance obtained is then written into dimensionless units through the application of equation:

$$C_D = \frac{FD}{\frac{1}{2}\rho U^2 A} \quad (1)$$

3. Results and Discussion

3.1. Flow field

The effect of changes in distance on the characteristics of flow patterns through numerical simulation approaches and visualization of flow of vertical circular cylinders arranged in tandem with M/D variations respectively at M/D = 0.3, M/D = 0.5, M/D = 0.7, M/D = 0.9, and M/D = 1.1, shown in Figure 3. In all comparisons, the M/D distance shows a significant increase in flow velocity when the fluid reaches the side of the specimen. This is due to a decrease in the intensity of the direct impact against the front side of the cylinder which minimizes the loss of flow momentum to move towards the boundary layer. The thicker the boundary layer that is formed, the greater its influence on the amount of drag that works. It can be seen that the model at M/D = 0.3 has a boundary layer that tends to be larger than the other models. Meanwhile, the smallest boundary layer thickness is obtained at M/D = 1.1.

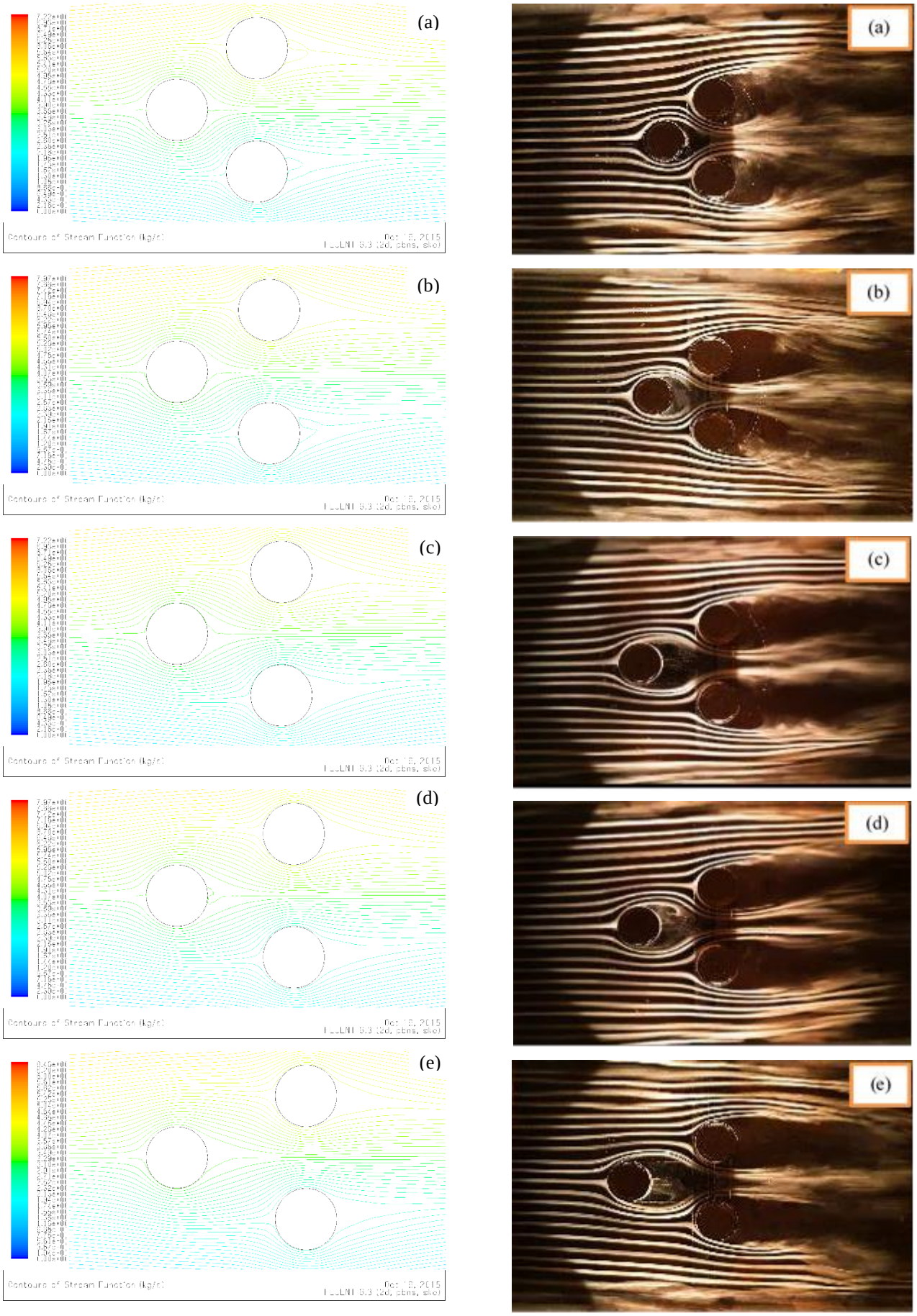

Figure 3. Computational and experimental streamlined comparison of (a) M/D = 0.3, (b) M/D = 0.5, (c) M/D = 0.7, (d) M/D = 0.9, and (e) M/D = 1.1 at U = 11m/s (Re_D = 75.304)

For M/D = 1.1 has the thickest boundary layer than four others. This was caused by the fact that vortex was not damped between serial-parallel circular cylinders and it pushed the flow apart from the cylinder that causes flow separation earlier in the upstream side of parallel cylinders. The almost same phenomenon occurred at M/D = 0.7, namely the vortex was not damped anymore and it rolls the flow apart from the cylinder so that separation of flow occurred earlier

3.2. Drag field

The drag coefficient is obtained through experimental testing at variations of each M/D = 0.3, M/D = 0.5, M/D = 0.7, M/D = 0.9, and M/D = 1.1 with variations in the upstream speed of 5 m/s, 7 m/s, 9 m/s, 11 m/s, 13 m/s, 15 m/s, 17 m/s, 19 m/s and 21 m/s is shown in Table 1. For the upstream speed of 5 m/s, the lowest drag coefficient comes at position M/D = 0,5 is 1.0783 and the highest drag coefficient is obtained at the distance ratio M/D = 0.3 of 1.0923. For the speed of 7 m/s, the lowest drag coefficient is obtained at M/D = 0.7 of 0.9612 and the highest is at M/D = 0.3 of 0.9755. For the speed of 9 m/s, the lowest drag coefficient is obtained at M/D = 0.5 with C_D = 0.8970 and the highest is obtained at M/D = 0.3 with C_D = 0.9083 and almost equal with M/D = 0.9 at C_D = 0.9018. For the highest upstream speed variation, namely 21 m/s, it was also found that the lowest drag coefficient was obtained at M/D = 0.5 at C_D = 0.7572 and the highest at M/D = 0.3 at C_D = 0.7647.

Table 1. Coefficient drag by CFD, M/D

U(m/s)	Re	M/D (cm)				
		0.3	0.5	0.7	0.9	1.1
5	34,229	1.0923	1.0783	1.0790	1.0816	1.0831
7	47,921	0.9755	0.9632	0.9612	0.9643	0.9650
9	61,612	0.9083	0.8970	0.8993	0.9018	0.8991
11	75,304	0.8638	0.8535	0.8523	0.8519	0.8516
13	88,996	0.8322	0.8223	0.8251	0.8261	0.8286
15	102,688	0.8091	0.8022	0.8017	0.8043	0.8061
17	116,379	0.7909	0.7824	0.7845	0.7870	0.7893
19	130,071	0.7768	0.7682	0.7711	0.7732	0.7748
21	143,763	0.7647	0.7572	0.7591	0.7618	07639

Table 2. Coefficient drag by experiment, M/D

U(m/s)	Re	M/D (cm)				
		0.3	0.5	0.7	0.9	1.1
5	34,229	1.0443	1.0498	1.0326	1.0306	1.0374
7	47,921	0.9360	0.9135	0.9237	0.9152	0.9215
9	61,612	0.8643	0.8528	0.8807	0.8673	0.8585
11	75,304	0.8423	0.8034	0.8259	0.8309	0.8288
13	88,996	0.8123	0.7888	0.8063	0.8016	0.7972
15	102,688	0.7870	0.7663	0.7808	0.7847	0.7790
17	116,379	0.7739	0.7435	0.7383	0.7662	0.7512
19	130,071	0.7574	0.7430	0.7509	0.7549	0.7519
21	143,763	0.7465	0.7318	0.7405	0.7408	0.7333

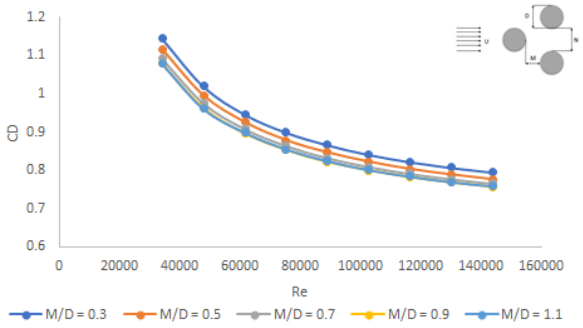

Figure 4. Comparison of the CFD drag coefficient against Reynolds number

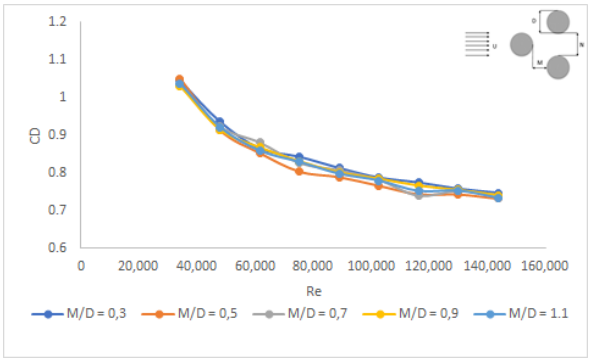

Figure 5. Comparison of the experimental drag coefficient against Reynolds number

Based on the graph in Fig. 5 we can summarize that the value of drag coefficient (C_D) is getting lower when the Reynolds number (Re) is getting more. It changed identically for every various distance (M/D) shows that the value is relevant each other. But although the trend for every M/D is almost the same, the value of drag coefficient at every distance (M/D) does not always change harmonically, as we can see on the table the lowest and the highest value did not settle at any specific distance (M/D) for every Reynolds number (Re). Based on this unique phenomenon explain how important to do and improve this tandem research with larger and more variables.

3.3. Pressure field

The effect of adding variation in distance with a ratio of M/D = 0.3, M/D = 0.5, M/D = 0.7, M/D = 0.9 and M/D = 1.1 for the pressure profile shown in Figure 4. The arrangement of serial parallel circular cylinder, the first specimen already reduces the direct collision between the fluid flow and rear side (second and third specimen) of the circular cylinder. It can be seen that the model with the distance ratio M/D = 1.1 has the lowest pressure contour when compared to other models.

Figure 4 also shows that the region of pressure different around the circular cylinders is the narrowest at M/D = 1.1. Consequently, the pressure difference does not strong enough to push the flow apart from the cylinder while the region of others M/D has pressure different around circular cylinders which getting larger and strong enough to push the flow apart from the cylinder so that the pressure drop is getting larger. This indicates that the smallest pressure coefficient at M/D = 1.1.

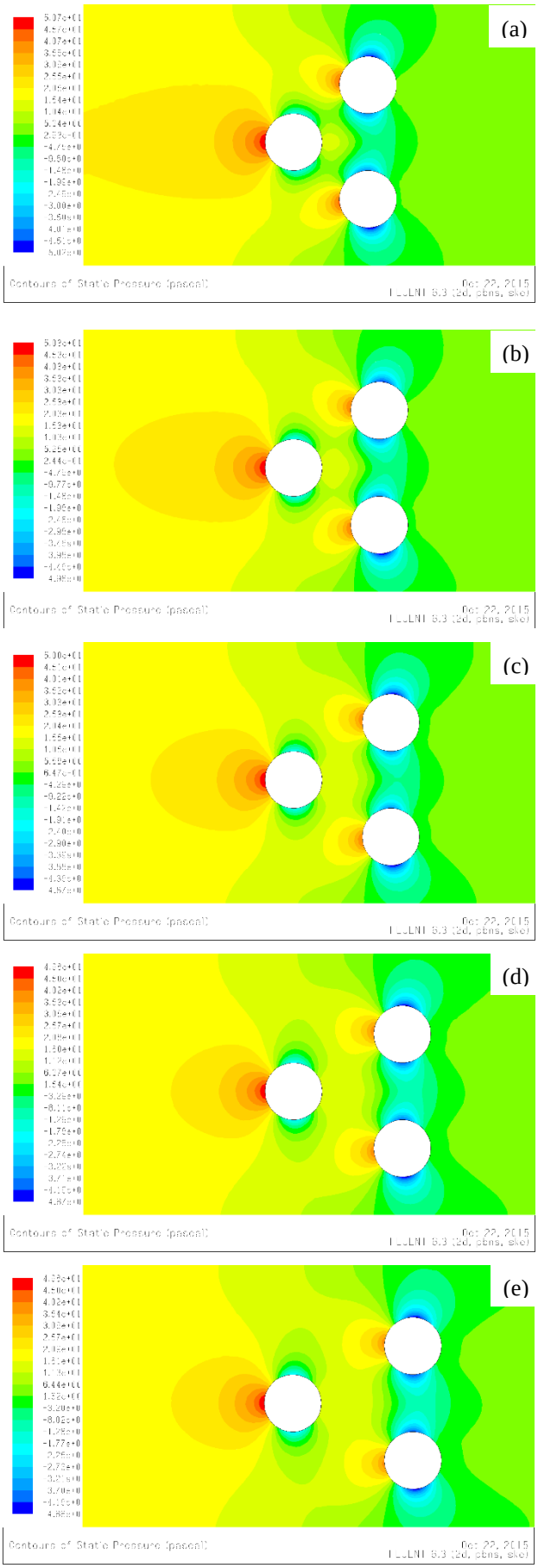

Figure 6. Contour profile on coefficient of flow pressure at U= 11 m/s (Re_D = 75.304). (a) M/D = 0.3; (b) M/D = 0.5; (c) M/D = 0.7; (d) M/D = 0.9 and (e) M/D = 1.1.

Numerical simulation result of pressure contour at various M/D with U = 11 m/s is shown in Figure 6. Figure 4 (a) shows that M/D = 0.3 the pressure changes over a wide region around the circular cylinder. The pressure difference between the upstream and the downstream is very large compared with other distances. Meanwhile, the smallest region of pressure is shown at M/D = 1.1 either in CFD method or experimental method. That is why we can see more blue color between the back tandem which shows a lower value of drag.

4. Conclusion

Experimental analysis and simulation of flow through a tandem of serial parallel circular cylinders has been done at 5 various M/D. The experimental data were validated with the flow visualization and flow simulation.

The smaller the distance between circular cylinders the stronger the vortex between the cylinders which tends to move toward the cylinders. This produces a thicker boundary layer that possibly induces a greater drag coefficient. Meanwhile, the smallest coefficient drag with U = 11 m/s is 0.8516 which occur at M/D = 1.1 and the biggest is 0.8638 at M/D = 0.5. The largest drag decreasing for all levels of Reynolds numbers, occurred when the tandem of serial parallel circular cylinders at M/D = 0.5 which is 0.7572 by CFD method and 0.7318 by experimental method with the comparison of percentage is 1.96% of difference.

Acknowledgements

We gratefully thanks the Head of the Fluid Mechanics Laboratory of Hasanuddin University who has facilitated the data collection process.

References

[1] A. Daloglu, “Pressure Drop in a Channel with Cylinder in Tandem Arrangement,” *Int. Commun. Heat Mass Transf.*, vol. 35, pp. 76–83, 2008.

[2] H. Hiroshi, W. Kenji, W. Yuki, and T. N. Takashi, “Experimental Study On The Flow Field Between Two Square Cylinders In Tandem Arrangement,” in *The Seventh Asia-Pacific Conference on Wind Engineering (APCWE-VII)*, 2009.

[3] A. Lankadasu and S. Vengadesan, “Interference Effect of Two Equal-Sized Square Cylinders in Tandem Arrangement: with Planar Shear Flow,” *Int. J. Numer. Methods Fluids*, 2007.

[4] K. S. Kumar and L. Kumaraswamidhas, “Numerical Study on Fluid Flow Characteristics Over the Side-By-Side Square Cylinders at Different Spacing Ratios,” *Int. Rev. Mech. Eng.*, vol. 8, no. 5, pp. 962–969, 2014.

[5] D. Sumner, S. J. Price, and M. P. Paidoussis, “Flow-pattern Identification for Two Staggered Circular Cylinders in Cross-Flow,” *J. Fluid Mech.*, vol. 411, pp. 263–303, 2000.

[6] M. B. S. Kumar and S. Vengadesan, “A Study On The Influence Of Gap Ratio On Turbulent Flow Past Two Equal Sized Square Cylinders Placed Side-By-Side,” in *The 37th National & 4th International Conference on Fluid Mechanics and Fluid Power December*, 2010, pp. 16–18.

[7] D. V. Patil and K. N. Lakshmisha, “Two-dimensional flow past circular cylinders using finite volume lattice Boltzmann formulation,” *Int. J. Numer. Methods Fluids Int. J. Numer. Meth. Fluids*, vol. 69, pp. 1149–1164, 2012.

[8] A. Etminan, M. Moosavi, and N. Ghaedsharafi, “Characteristics of Aerodynamics Forces Acting on Two Square Cylinders in the Streamwise Direction and its Wake Patterns,” *Adv. Control. Chem. Eng. Civ. Eng. Mech. Eng.*, pp. 209–217, 2010.

[9] N. Salam, R. Tarakka, Jalaluddin, and R. Bachmid, “The Effect of the Addition of Inlet Disturbance Body (IDB) of Flow Resistance Through the Square Cylinder Arranged in Tandem,” *Int. Rev.*

Mech. Eng., vol. 11, no. 3, 2017.

[10] N. Salam, R. Tarakka, Jalaluddin, and M. Ihsan, "Flow Separation Across Three Square Cylinders Arranged in Serial and Parallel Tandem Configuration," *Int. J. Eng. Appl.*, vol. 3, pp. 96–106, 2020.

[11] N. Salam, R. Tarakka, Jalaluddin, and R. Bachmid, "The Effect of the Addition of Inlet Disturbance Body (IDB) to flow Resistance Through the Square Cylinders Arranged in Tandem," *IREME*, vol. 11, no. 3, pp. 1970–8734, 2017.

[12] T. Tsutsui and T. Igarashi, "Drag Reduction of a Circular Cylinder in an Air-Stream," *J. Wind Eng. Ind. Aerodyn.*, vol. 90, pp. 527–541, 2002.

[13] Subagyo and Rachmat, "Experimental Study of External Flow Characteristics on Obtuse Quadrilaterals with Elliptical Edges," *J. Teknol. Technoscientia*, vol. 4, no. 2, p. 2012, 2012.

[14] N. Salam, R. Tarakka, Jalaluddin, M. Setiawan, and A. Mahfud, "Characteristics of the coefficient of Resistance to Flow Across Three Square Cylinders in Tandem Seriest and Parallel Configurations.," in *Prosiding Seminar Nasional Teknik Mesin Politeknik Negeri Jakarta*, 2019, pp. 1244–1251. [in Bahasa]

[15] M. M. Alam, H. Sakamoto, M. Moriya, and K. Takai, "Fluctuating Fluid Forceacting on Two Circular Cylinders in a Tandem Arrangement at a Subcritical Reynolds Number," *J. Wind Eng. Ind. Aerodyn.*, vol. 91, pp. 139–154, 2003.

EPI International Journal of Engineering
Volume 4, Number 1, February 2021, pp. 51-56
DOI: 10.25042/epi-ije.022021.08

*p*ISSN 2615-5109
*e*ISSN 2621-0541

Investigating the Local Stress of Car Deck Ro-Ro 5000 GT

Alamsyah[a,*], Ahmed Reza Falevi[b], Amalia Ika Wulandari[c], Muhammad Uswah Pawara[d], Wira Setiawan[e], Andi Mursyid Nugraha Arifuddin[f]

[a]Naval Architecture Program, Kalimantan Institut of Technology. Email: alamsyah@lecturer.itk.ac.id
[b]Naval Architecture Program, Kalimantan Institut of Technology. Email: Ahmedrezafalevi@yahoo.co.id
[c]Naval Architecture Program, Kalimantan Institut of Technology. Email: amaliaikaw@lecturer.itk.ac.id
[d]Naval Architecture Program, Kalimantan Institut of Technology. Email: uswah.pawara@lecturer.itk.ac.id
[e]Naval Architecture Program, Kalimantan Institut of Technology. Email: wira@lecturer.itk.ac.id
[f]Naval Architecture Program, Kalimantan Institut of Technology. Email: andi.mursid@lecturer.itk.ac.id

Abstract

A deck construction must be strong enough that it will not suffer structural damage if it works under a given load. In this case, the strain stress becomes very important from the strength of the deck, as the one that affects the strength of the deck construction, one of which is the stiffener distance. This study aims to analyze the maximum strain stress on the deck of the Ro-Ro Ferry. The method used is Finite Element Method (FEM) by varying the stiffener distance in the deck construction. The research results obtained, namely the variation of the stiffener distance of 600 mm. 285.5 N/mm^2 and the maximum strain is 1.76 x 10^{-3} mm, at a variation of 700 mm stiffener distance the maximum stress is 378,075 N/mm^2 and the maximum strain is 1.77 x 10^{-3} mm, at a stiffener distance variation 800 mm the maximum stress released is 383,737 N/mm^2 and the maximum strain released is 1.78 x $^{-3}$ mm, at 900 mm stiffener distance variations the maximum stress is 389,188 N/mm^2 and the maximum strain released is 1.79 x 10^{-3} mm, at variations in distance stiffener 1000 mm the maximum stress released is 425,388 N/mm^2 and the maximum strain released is 1.8 x 10 $^{-3}$ mm, The value of strain increasingly increases followed by the farther distance of the stiffener equal 0.6%, and the stress value is at a variation increasingly increases followed by the farther distance of the stiffener equal 12.24%.

Keywords: Car deck; stiffener; stress; strain

1. Introduction

Ro-Ro ferry is one of the means of transportation used for crossings in archipelagic countries such as Indonesia. This ship is used to transport people and their vehicles. On the deck, the ship receives a fairly large load. This requires that the ship is always in a safe condition, especially in terms of its strength of construction. The transverse strength of a ship is the ability of the transverse structure of the ship to maintain the cross-sectional shape of the ship against disturbances of loads acting on the ship such as deck loads, side loads, and bottom loads. So it is clear that the main components of the ship structure are the lower structure, side structures, and deck structures [1].

Factors that affect the strength of the construction include the distance between the tusks, the distance between the stiffeners, the unfolded length, the plate thickness, etc. The normal strength of a ship's steel structure has a minimum melting point of REH 235 N/mm^2 and a tensile strength of Rm 400 - 520 N/mm^2 (BKI, 2021). To meet the allowable stress (yield strength) in construction, it is customary to increase the construction modulus value by adding a thick insert plate or longitudinal carling [2].

Types of structural problems include stress analysis, frame analysis, buckling, and vibration analysis [3]. Loads that can affect the local structure and must be considered in the design of the transverse construction of the ship consists of two parts, namely: buoyancy and gravity. The upward pressure results from the distribution of hydrostatic pressure in the outer plane of the immersed hull. Gravity is the largest downward force on ships and their contents [4]. As a result of these loads, all parts of the ship's construction experience some type of stress. There are several factors that cause the actual stress distribution to be different from the ideal stress distribution. Due to the transverse shear stress, distortion occurs based on the length of the hull girder cross-section [5].

In problems involving complex geometries, such as problems applying to complex structures, it is generally difficult to solve them through mathematical analysis. This is because mathematical analysis requires a quantity or value that must be known at each point in the structure under study. Solving the analysis of complex geometrical differential equations, complex loading, is not easy to obtain. Nevertheless, the formulation of the finite element method can be used to solve these problems [3].

*Corresponding author. Tel.: +6285-242-800-578
Jl. Soekarno-Hatta KM. 15 Kampus ITK Karang Joang Balikpapan, Indonesia, 76127

The new method based on virtual displacement is the world's last solution. Applied mathematics problems and solutions are still being developed along with the development of computer science [6]. Finite element analysis is a numerical technique. In this method, By using this package, one can analyze several complex structures [7]. As a numerical method, it is used to solve technical and mathematical problems of a physical phenomenon. The types of physical and mathematical problems that can be solved by the method are structural and non-structural analysis. By using the method, all the complexity of the problem, such as various shapes, boundary conditions, and loads can be maintained but the solutions obtained are only approximate. This is due to its diversity and flexibility as an analytical tool. Rapid improvements in computer hardware technology and reduction in computer costs have driven this method because computers are a basic requirement for the application of this method. A number of popular brand element analysis packages are now commercially available to simplify complex structural analysis [8].

In this study, the strength of the deck construction of ro-ro ferry will be examined by modeling it in the FEM application. Modeling is done to determine the amount of stress and strain in construction. Stress is a static amount; it is a measure of the stress of structural materials. On the other hand, strain is total kinematic; it measures structural deformation. However, deformation depends on the loads acting on the structure. Therefore, stress and strain are not independent. The physical relationships that connect these numbers are called constitutive laws. It describes the structural behavior of the material under load. It depends on the material and can only be obtained with the help of experiments [9].

One of the assessments carried out to determine the strength of the construction is to estimate the stress ratio obtained by comparing the stress that occurs in the construction due to external loads working on the ship [10]. According to BKI 2021, a good stress ratio for working on ship construction is still smaller than 1 (<1) [11].

2. Methods

This research is a quantitative research that takes the sample ro-ro ferry. The object of research was the stiffener of the vehicle 01 deck on the Ro-Ro Ferry, namely KMP Legundi 5000GT as shown in Fig. 1.

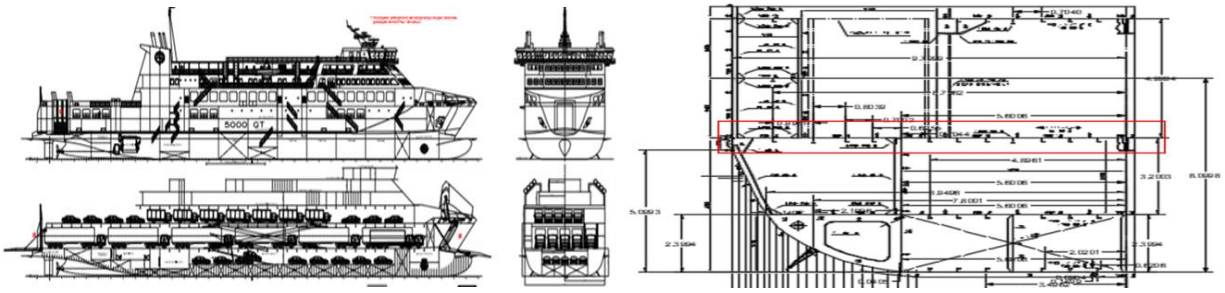

Figure 1. GA and midship construction of ferry ro-ro

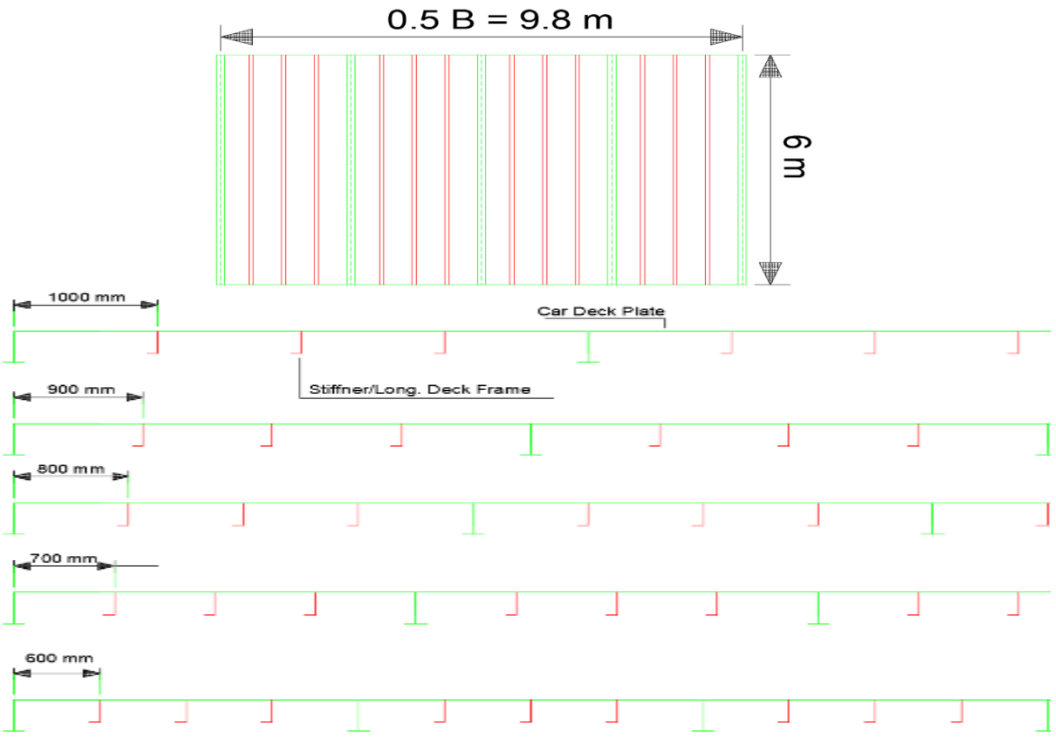

Figure 2. Plan view and transfer view of car deck

Figure 1 shows the red line marking on the vehicle deck which is the object of the study. The detailed illustration of the vehicle deck construction and the stiffener variation plan is shown in Fig. 2. Figure 2 is then converted to a 3D model using an FE-based application by taking the width of the ship on the ro-ro ferry car deck and the length of the deck model of 6 m then varying the stiffener distance shown in Fig. 3.

Furthermore, the meshing process is carried out on the 3D car deck model as one of the steps that are passed when using the FE analysis shown in Fig. 4. The mesh size used is 300 mm with the mesh type is hexahedron. As shown in Fig. 4. The next stage is to provide the boundary conditions on the 3D car deck model in the form of vehicle support and load shown in Fig. 5.

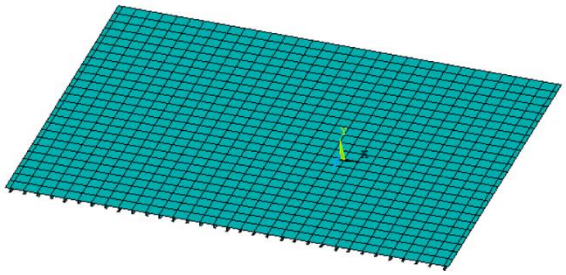

Figure 3. 3D modeling of car deck

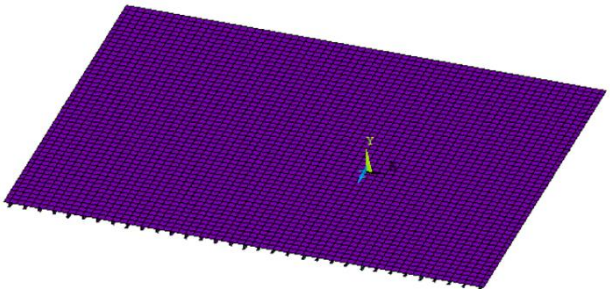

Figure 4. Meshing of 3D modeling car deck

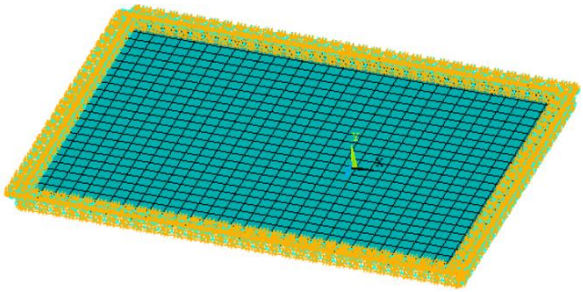

(a)

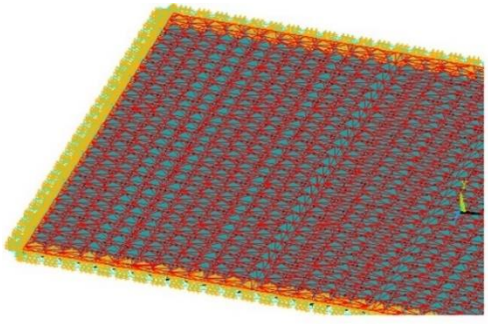

(b)

Figure 5. (a) input fixed support; (b) input pressure load

Figure 5a shows the pedestal input in the form of fixed support given around the 3D car deck model. Whereas Figure 5b shows the load input given in the form of the total load of the trailer truck according to the load case during operation [12] which is on the car deck of 1.18 x10^{-2} N/mm^2 which form of load pressure. The results of the running of the FEM application are NLFEA in the form of maximum stress values The output parameters used for each variation stiffener distance are the value of the maximum stress and strain against the maximum load acting on the car deck structure.

Stress is defined as the amount of force acting per unit area. There are two types of stress: normal stress and shear stress. Normal stress (σ) is a measure of the normal force or axial force per unit area [13]. Stress is the force of broad unity. When an object is subjected to a force, the stress is the ratio between the size of the force to the area to which the force is applied. If the force applied is perpendicular to the surface of the object (the area to be calculated), then the stress is normal stress. If the force applied to the object is tangential to the surface of the object, the stress is the shear stress [13].

$$\sigma = \frac{F}{A} \tag{1}$$

where σ = stress (Pa); F = force (N); A = cross-sectional area (mm^2). The strain (strain) is defined as the ratio between the increase in length or shortness of the stem and the size initially stated:

$$\varepsilon = \frac{\Delta L}{L} \tag{2}$$

where ε = strain (mm); ΔL = increase in length (mm); L = initial length (mm).

3. Results and Discussion

This research shows that the calculation of strength is obtained using an application based on the Finite Element Method (FEM) on the car deck of a ro-ro ferry. The simulation results at each variation of the stiffener distance can be seen in Fig. 6.

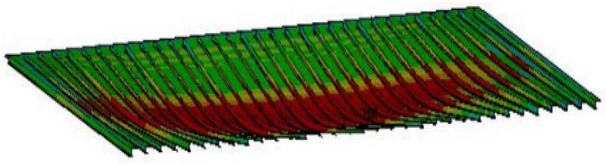

(a)

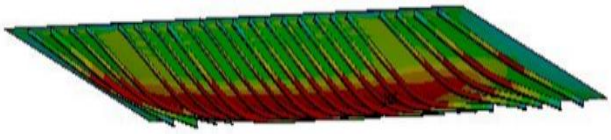

(b)

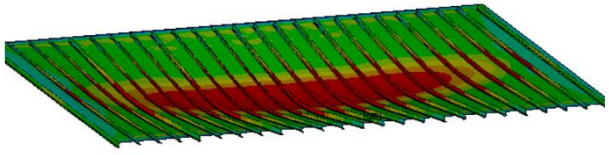

(c)

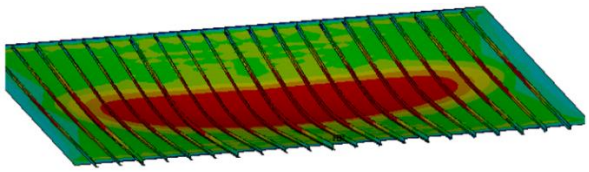

(d)

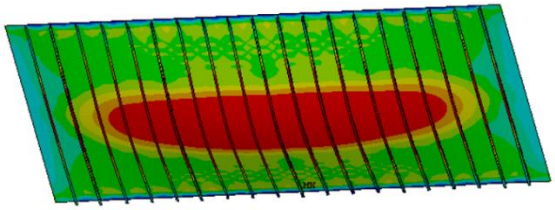

(e)

Figure 6. (a) 600 mm spacing; (b) 700 mm spacing; (c) 800 mm spacing; (d) 900 mm spacing; (e) 1000 mm spacing

Table 1 shows the value of von misses stress that occurs in the car deck model with variations in the stiffener distance starting from 600 ~ 1000 mm. Von misses stress and deformation values for each stiffener distance are summarized in Table 1.

Table 1 shows that the simulation results of the car deck stiffener distance variation of 600 mm, the maximum stress is 285.5 N/mm^2, and the maximum strain is 1.76 x 10^{-3} mm. For a stiffener distance of 700 mm, the maximum stress released is 378,075 N/mm^2, and the maximum strain released is 1.77 x 10^{-3} mm. For stiffener distance of 800 mm, the maximum stress released is 383,737 N/mm^2 and the maximum strain released is 1.78 x 10^{-3} mm. While the stiffener distance is 900 mm. The maximum stress released is 389,188 N/mm^2 and the maximum strain released is 1.79 x 10^{-3} mm and the maximum stress emitted is 425,388 N/mm^2 and the maximum strain released is 1.8 x 10^{-3} mm.

Based on the analysis, the results of the stress-strain acting on the car deck structure are obtained, by considering the boundary conditions, the stress-strain relationship curve for each stiffener distance variation is shown in Fig. 7.

Figure 7 shows the car deck with a stiffener distance variation of 600 mm with a stress value of 0 N/mm^2 to 221,798 N/mm^2, the car deck is still linear or within the proportionality limit and then when the car deck with a value of 223,095 N/mm^2 is already at the elasticity limit or the addition of the stress-strain value on the graph has reached non-linear and is in a plastic condition that will reach the ultimate stress.

Table 1. Von misses stress and deformation of car deck

Space of Stiffener (mm)	Von misses stress (N/mm^2)	Deformation (mm)
600	285.5	1.76 x 10^{-3}
700	378.075	1.77 x 10^{-3}
800	383.737	1.78 x 10^{-3}
900	389.188	1.79 x 10^{-3}
1000	425.388	1.8 x 10^{-3}

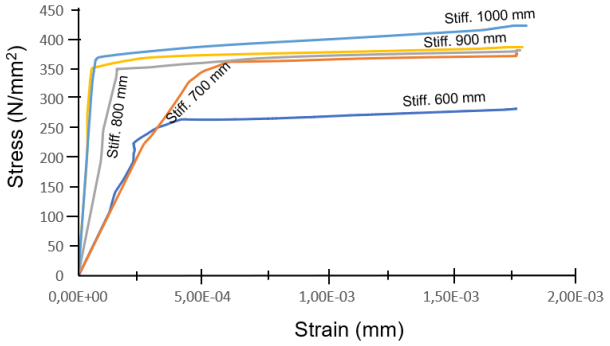

Figure 7. Stress-strain curve of car deck

The car deck with a stiffener distance variation of 700 mm with a stress value of 0 N/mm^2 to 313,414 N/mm^2 the car deck is still linear or still within the proportionality limit and then when the car deck ship with a stress value of 322,188 N/mm^2 is already at the elasticity limit or the addition of the stress-strain value on the graph has reached non-linear and is in a plastic condition that will reach the ultimate stress.

Car decks with stiffener distance variations of 800 mm with a stress value of 0 N/mm^2 to 340,605 N/mm^2 the car deck is still linear or within the proportionality limit and then when the ship car deck with a stress value of 345,746 N/mm^2 is already at the elasticity limit or the addition of the stress-strain value on the graph has reached non-linear and is in a plastic condition that will reach the ultimate stress.

Car decks with stiffener distance variations of 900 mm with a voltage value of 0 N/mm^2 to 345,832 N/mm^2 the car deck is still linear or still within the proportionality limit and then when the ship car deck with a stress value of 351,203 N/mm^2 is already at the elasticity limit or The added value of stress and strain on the graph has reached non-linear and is in a plastic condition that will reach the ultimate stress.

Car deck with stiffener distance variation of 1000 mm with a voltage value of 0 N/mm^2 to 362,864 N/mm^2 the car deck is still linear or still within the proportionality limit and then when the car deck ship with a stress value of 366,445 N/mm^2 is already at the elasticity limit or the addition of the stress-strain value on the graph has reached non-linear and is in a plastic condition that will reach the ultimate stress.

Based on the analysis, it is detected that the results of stress and strain acting on each of the elements in the car deck structure, by considering the variations in the stiffener distance that occur in each case, then a comparison of the stress values is obtained in Fig. 8.

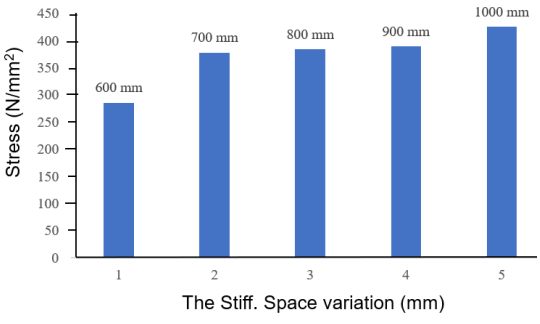

Figure 8. Stress influence of stiffener space

Figure 8 shows the stress value at the variation of the distance between 600 mm stiffener is 285.5 N/mm^2, the variation of the distance between 700 mm stiffener is 378,075 N/mm^2, the variation of the distance between 800 mm stiffener is 383,737 N/mm^2, at variations in the distance 900 mm stiffener is 389,188 N/mm^2 and the variation of the distance between 1000 mm stiffener is 425,388 N/mm^2. The highest stress value is in the variation of the distance between 1000 mm stiffener. There is an increase in the value of the stress as the distance between the stiffeners increases with an average percentage increase of 12.24%. This is in line with Amalia's 2019 research that the decrease in load is inversely proportional to the increase in frame distance, the farther the frame distance, the smaller the load required for the plate to buckle [14].

Based on the analysis, the results of the stress-strain acting on each of the elements in the car deck structure are obtained, by considering the variation in stiffener distance that occurs in each case, the comparison of the strain values is shown in Fig. 9.

Figure 9 shows the value of the strain at the variation of the distance between the stiffener 600 mm is 1.76 x 10^{-3} mm, the variation of the distance between the stiffener 700 mm is 1.77 x 10^{-3} mm, the variation of the distance between the stiffener 800 mm is 1.78 x 10^{-3} mm, The variation of the distance between 900 mm stiffeners is 1.79 x 10^{-3} mm, and the variation of the distance between 1000 mm stiffeners is 1.8 x 10^{-3} mm. There is an increase in the value of the strain as the distance between the stiffener increases with an average percentage increase of 0.6%. In line with Tumurang's 2016 research, the shear force of the beam with a stiffener that is installed close to the support area is getting smaller, while the shear force will increase if the stiffener is placed in the field area [15].

The results of the stress-strain acting on each element in the car deck structure are detected, taking into account the variations in the stiffener distance that occur in each case, namely the stiffener distance variations of 600 mm, 700 mm, 800 mm, 900 mm and 1000 mm, where the distance increases stiffener in the structure, the value of stress and strain continues to increase, this proves the decreasing of the strength level of the vehicle deck as the stiffener distance increases. Referring to the yield strength value of the car deck material 370 N/mm^2, the optimal stiffener distance can be determined where in this study the optimal distance of 600 mm is obtained when viewed from the resulting stress magnitude of 285.5 N/mm^2 which does not exceed the yield strength of the material.

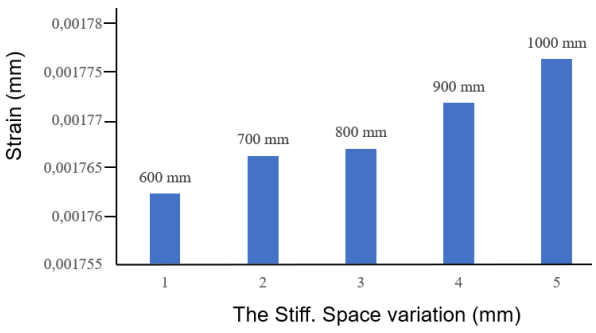

Figure 9. Strain influence of stiffener space

However, this value is not so accurate that further research is needed using a stiffener distance of 600 ~ 700 mm. This needs to be done because the simulation results are found with a stiff distance. 700 mm produces stress of 378,075 N/mm^2 which passes the yield strength of the material of 370 N/mm^2.

4. Conclusions

Stress-strain analysis on the car deck of the Ro-ro ferry ship which is influenced by variations in stiffener distance with a maximum evenly load condition of 1.18 x10^{-2} N/mm^2, it can be concluded that at the variation of the stiffener distance of 600 mm the maximum stress detected is 285.5 N/mm^2 and the maximum strain released is 1.76 x 10^{-3} mm. At the variation of the stiffener distance of 700 mm, the maximum stress released is 378,075 N/mm^2 and the maximum strain released is 1.77 x 10^{-3} mm. For variations in the stiffener distance of 800 mm, the maximum stress obtained is 383,737 N/mm^2 and the maximum strain released is 1.78 x 10^{-3} mm. For the stiffener distance variation of 900 mm, the maximum stress released is 389,188 N/mm^2 and the maximum strain released is 1.79 x 10^{-3} mm. At the variation of the stiffener distance of 1000 mm, the maximum stress released is 425,388 N/mm^2 and the maximum strain released is 1.8 x 10^{-3} mm. The increase in the average stress value generated by 12.24% in the car deck construction is influenced by the increase in the distance between the stiffeners. Likewise, the value of the strain detected was increasing by an average of 0.6% with increasing distance between the stiffeners.

Acknowledgements

Thanks to the Construction Drawing Design Laboratory and Ship Engineering Naval Architecture Program Kalimantan Institute of Technology for providing facilities in this research. Thanks also to the anonymous reviewer for his input and corrections so that this paper is worthy of publication.

References

[1] M. Shama, “Buckling of Ship Structures,” Alexandria University, 2013.
[2] A. M. Nugraha *et al.*, “Strength Behavior Analysis of Insert Plate for Placing Corner Fitting due to Container Load,” *IOP Conf. Ser. Mater. Sci. Eng.*, vol. 875, 2019.
[3] Y. Susatio, *Basics of Finite Element Method*. Yogyakarta: ANDI, 2004. [in Bahasa]
[4] D. M. Rasyid, *Strength of Ship Structure*. Jakarta: Pradnya Paramita, 2000. [in Bahasa]
[5] Hughes, F. Owen, and J. K. Paik, *Ship Construction Analysis and Design*. The Society of Naval Architecture and Marine Engineers, 2010.
[6] T. Lamb, *Ship Design and Construction*. New Jersey: SNAME, 2004.
[7] S. S. Bhavikatti, *Finite Element Analysis*. New Delhi: New age International Publisher, 2005.
[8] S. Moaveni, *Finite Elemen Analisis : Theory And Application With ANSYS*. United States of America: Pearson Prentice Hall, 2008.
[9] D. Gross, *Engineering Mechanics 2 “Mechanics of Materials.”* London: Springer, 2011.
[10] Rosmani *et al.*, “Study on Transverse Strength of the Deck-Container Ships Due to Laying All Containers on Deck,” *EPI Int. J. Eng.*, vol. 2, no. 2, pp. 178–184, 2019.
[11] BKI, *Rules For The Classification and Construction Seagoing Ship, Volume II*. Jakarta, 2021.

[12] A. H. Kalam, "Technical Study of Car Deck Strength on the Ro-Ro 500 GT Ferry Due to Changes in Load Using the Finite Element Method," *J. Tek. Perkapalan*, vol. 5, no. 1, pp. 174–185, 2017. [in Bahasa]

[13] S. N. and D. A. H. Patnaik, *Strength of Materials*. Amsterdam: Elsevier, 2004.

[14] A. I. Wulandari, Nurmawati, and A. Dianiswara, "Buckling Analysis Deck Plate of Ferry Ro-Ro," *J. Wave*, vol. 13, no. 1, pp. 1–6, 2019. [in Bahasa]

[15] O. M. Tumurang, "Analysis of Stiffener Layout Against Local Bending of Steel," *J. Sipil Statik*, vol. 4, no. 7, p. 407, 2016. [in Bahasa]

EPI International Journal of Engineering
Volume 4, Number 1, February 2021, pp. 57-64
DOI: 10.25042/epi-ije.022021.09

*p*ISSN 2615-5109
*e*ISSN 2621-0541

Comparison of the Strength of Midship Structures with and without Margin Plate

Rosmani[a,*], Andi Ardianti[b], Hariyono[c], Ganding Sitepu[d], Hamzah[e]

[a]Department of Naval Architecture, Engineering Faculty, Hasanuddin University, Gowa, Indonesia. Email: rosmanimunandar@ymail.com
[b]Department of Naval Architecture, Engineering Faculty, Hasanuddin University, Gowa, Indonesia. Email: aardianti@gmail.com
[c]Department of Naval Architecture, Engineering Faculty, Hasanuddin University, Gowa, Indonesia. Email: hariyono.ismail07@gmail.com
[d]Department of Naval Architecture, Engineering Faculty, Hasanuddin University, Gowa, Indonesia. Email: g.sitepu@unhas.ac.id
[e]Department of Naval Architecture, Engineering Faculty, Hasanuddin University, Gowa, Indonesia. Email: anca_naval99@yahoo.com

Abstract

Margin plate is a part of bottom construction that joint the floor and frame construction of the ship, so the inner bottom plate will be installed cut off on the margin plate. Lately, the bottom construction of the ship tends not to use the margin plate. The ship is currently built with an inner bottom plate continuously from the left side to the right side of the ship. This study aims to determine the transversal and longitudinal strength ratio of ships with and without margin plate. The analysis was carried out by using Finite Element Method so-called ANSYS™. The result shows if the load varied 0.2 x maximum load on the calculation of the transverse strength of the ship, the stress value on the ship model with a margin plate was 9.6242 (N/mm^2) and on the ship model without margin plate was 8.4739 (N/mm^2) under conditions 100%. The results of the comparison due to bottom load averaged 15.82%. The difference in stress due to the effect of deck loads was an average of 13.49% while the effect of side loads was on average 8.74%. The longitudinal strength of the ship was also varied of every increase of 0.2 x maximum moment with a review point of meeting between the bottom plate and bilge plate for the ship model without margin plates using the Multi-Point Constraint (MPC) method looking for results in sagging conditions of 12,443 (N/mm^2) and the hogging condition was -11.045 (N/mm^2) at 100% x maximum moment load conditions. So that the ship model with a margin plate sagging condition was 23,189 (N/mm^2) and hagging condition was -20,585 (N/mm^2). The results showed the stress that occurred in the ship model without using margin plate was better to withstand the transverse and longitudinal strength of the ship compared to the ship model with the margin plate.

Keywords: Load; margin plate; moment, stress; multi-point constraint (MPC)

1. Introduction

The strength of the ship construction is one of the technical aspects that also affects the level of ship safety in both calm and wavy sea conditions [1]. Recently, the ships building process with sophisticated technology can be completed quickly compared to the past. Thus the considerations in designing the ship construction are also very concerned, especially the strength of the ship, both transverse and longitudinal strength of the ship. One difference in the design of the current ship structure is the use of margin plates, now it is very rare to find ship construction using margin plate. If the construction of a ship is designed without margin plate, the inner bottom plate can be installed continuously from the left side to the right side of the ship [2] as shown in Fig. 1.

This research is related to the tendency of shipbuilding with a bottom structure without a margin plate which can affect the strength or affect the stress distribution in the construction components on the double bottom of the ship. Therefore, it is necessary to examine the stress distribution or the difference in the response of the vessel structure between a margin plate and without a margin plate. This study aims to determine the ratio of transverse and longitudinal strengths of ships with and without margin plates. The analysis was done using the finite element method with the help of software ANSYS™.

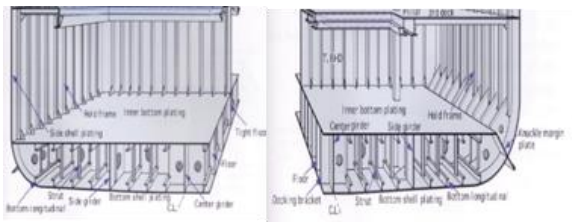

(a) (b)

Figure 1. Differences in Midship construction without using a margin plate (a) and construction using a margin plate (b)

*Corresponding author. Tel.: +62 813-4227-6450
Jalan Poros Malino km. 6 Bontomarannu
Gowa, Indonesia, 92171

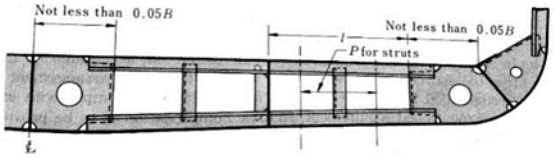

Figure 2. Open floor stipulates the distance of the plate margin from the supporting plate

The installation of double bottom can increase the safety of the ship as well as a ballast tank, if the ship collided with the reef and the outside of the bottom plate is torn, the watertight inner bottom plate will limit/protect the cargo from damage caused by water [3].

Based on Fig. 2, it can be seen that the bottom construction using a margin plate with the support plate distance to the edge of the edge plate is 0.05 B [4]. The inner bottom plate mounted on the top of the tank is continued to the side of the ship at a distance of not less than 1/10 of the height measured from the baseline to the inner bottom plate [5]. The edge plate construction works as a longitudinal beam, as support for bilge which is mounted perpendicular to the bilge plate and is welded to the bilge floor and knee. The width and thickness will be the same as the length of the ship where the thickness depends on the width of the vessel, but in practice the same thickness of the center support plate. Edge plates can also be cut by the knee or cut into each other [3].

There are two main types of framing systems; namely the transverse framing system and the longitudinal framing system. Of these two main systems, the combination/mixed framing system is also known [6]. Loads acting on the ship such as loads on the deck, loads on the sides, and loads on the plinth. So it is clear that the main components of the ship's structure are the bottom structure, the side structure, and the deck structure. These loads may affect the local structure and must be taken into account in the design including Fig. 3. These loads consist of two parts, namely: 1) upward compressive force, and 2) hydrostatic force on the outer plane of the submerged hull. Gravity is the greatest downward force on the entire ship and its contents [1].

Either of classifying loads on ships is according to the structural level acting as some loads affect the structure i.e. only one of four levels such as hull girders, hull modules, major construction components, and local components [7]. This moment is caused due to the load due to wave conditions such as hogging and sagging conditions. In hogging conditions, the ship gets a pull force at the bottom and a compressive force on the deck of the ship. On the other hand, the sagging condition [8] can be seen in Fig. 4.

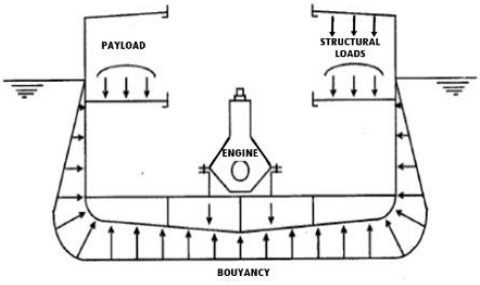

Figure 3. Load components on the hull

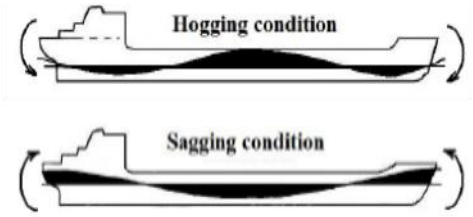

Figure 4. Hogging and sagging conditions

Finite Element Method is a numerical method used to solve technical problems and mathematical problems from a physical phenomenon. Types of technical and physical-mathematical problems that can be solved by the finite element method are structural and non-structural analysis. Types of structural analysis problems include stress, buckling and vibration analysis, while non-structure includes heat and mass transfer, fluid mechanics, and distribution of electric and magnetic potentials [9].

In a plane known to be a force, there will be two types of stresses that affect the plane. Generally, the three dimensions of stress elements are illustrated in Fig. 5. Three positive normal stress σ_x, σ_y dan σ_z, there are 6 positive shear stress, τ_{xy}, τ_{yx}, τ_{yz}, τ_{zy}, τ_{zx}, and τ_{xz}, displayed to ensure static balance, as equation (1) applies [10].

$$\tau_{xy} = \tau_{yx}, \qquad \tau_{yz} = \tau_{zy}, \qquad \tau_{zx} = \tau_{xz} \tag{1}$$

The normal stress equation for the three-dimensional plane is [10] :

$$\sigma_x = \frac{E}{(1+\nu)(1-2\nu)}\left[\varepsilon_x(1+\nu)+\nu(\varepsilon_y+\varepsilon_z)\right] \tag{2}$$

$$\sigma_y = \frac{E}{(1+\nu)(1-2\nu)}\left[\varepsilon_y(1+\nu)+\nu(\varepsilon_x+\varepsilon_z)\right] \tag{3}$$

$$\sigma_z = \frac{E}{(1+\nu)(1-2\nu)}\left[\varepsilon_z(1+\nu)+\nu(\varepsilon_x+\varepsilon_y)\right] \tag{4}$$

The strain is defined as the ratio between the increase in length or shortness of the rod with the initial size [11].

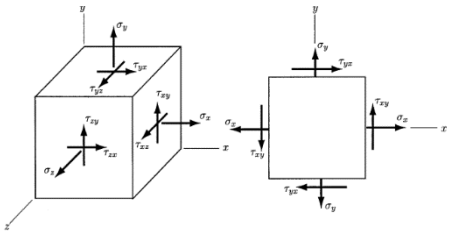

Figure 5. Stress acting on a plane

Description:

σ_x : normal stress acting on the x plane
σ_y : normal stress acting on the y plane
σ_z : normal stress acting on the z plane
τ_{xy} : shear stress acting on the x normal plane in the y direction
τ_{xz} : shear stress acting on the x normal plane in the z direction
τ_{yx} : shear stress acting on the y normal plane in the x direction
τ_{yz} : shear stress acting on the y normal plane in the z direction

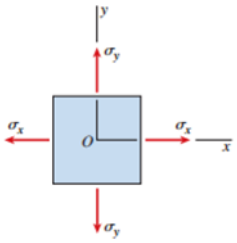

Figure 6. Biaxial tension system

The special case of biaxial stress (Fig. 6) occurs when in a structure axial loads act in two mutually perpendicular axes. We have $\tau_{xy} = 0$, so Hooke's law for plane stresses is simplified to [10]

$$\varepsilon_x = \frac{1}{E}\left(\sigma_x - \nu\sigma_y\right) \tag{5}$$

$$\varepsilon_y = \frac{1}{E}\left(\sigma_y - \nu\sigma_x\right) \tag{6}$$

$$\sigma_x = \frac{E}{1-\nu^2}\left(\varepsilon_x - \nu\varepsilon_y\right) \tag{7}$$

$$\sigma_y = \frac{E}{1-\nu^2}\left(\varepsilon_y - \nu\varepsilon_x\right) \tag{8}$$

Furthermore, the triaxial stress system occurs if the stress acts in the three directions of the coordinate axes. If the material follows Hooke's law, we can obtain the relationship between normal stress and normal strain as in Fig. 7 [10].

The strain generated by the stresses σ_x, σ_y, and σ_z acting independently to obtain the resulting strain. Thus, we easily arrive at the following equation for strain in triaxial stress [10].

$$\varepsilon_x = \frac{\sigma_x}{E} - \frac{\nu}{E}\left(\sigma_y + \sigma_z\right) \tag{9}$$

$$\varepsilon_y = \frac{\sigma_y}{E} - \frac{\nu}{E}\left(\sigma_z + \sigma_x\right) \tag{10}$$

$$\varepsilon_z = \frac{\sigma_z}{E} - \frac{\nu}{E}\left(\sigma_x + \sigma_y\right) \tag{11}$$

In this equation, the standard sign convention is used; that is, the tensile stress s and the extensional strain e are positive. The previous equation can be solved simultaneously for stress in terms of strain [10].

$$\sigma_x = \frac{E}{(1+\nu)(-2\nu)}\left[(1-\nu)\varepsilon_x + \nu\left(\varepsilon_y + \varepsilon_z\right)\right] \tag{12}$$

$$\sigma_y = \frac{E}{(1+\nu)(-2\nu)}\left[(1-\nu)\varepsilon_y + \nu\left(\varepsilon_z + \varepsilon_x\right)\right] \tag{13}$$

$$\sigma_z = \frac{E}{(1+\nu)(-2\nu)}\left[(1-\nu)\varepsilon_z + \nu\left(\varepsilon_x + \varepsilon_y\right)\right] \tag{14}$$

The equation for a simple supported beam that is uniformly loaded is as follows [10]:

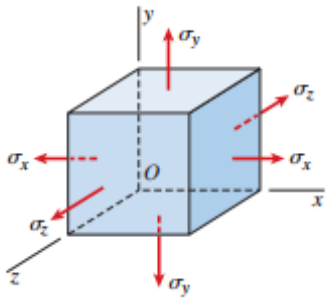

Figure 7. Biaxial tension system

maximum deflection

$$\Delta = \frac{SWL^4}{384}EI \tag{15}$$

deflection permit

$$\Delta_{permit} = \frac{SWL^4}{384} \text{ or}$$

$$\Delta_{permit} = \frac{5(360)SWL^4}{384EL} \tag{16}$$

where,
E : Modulus elastis (N/mm^2)
I : Momen inersia (m^4)
W : Load equivalent (N/mm)
L : Length deflection (m)

Deflection is a change in the shape of the beam in the y-direction due to the vertical loading applied to the beam or bar. Deformation in the beam can very easily be explained by the deflection of the beam from its position before experiencing loading. The deflection is measured from the initial neutral surface to the neutral position after deformation. The configuration assumed with the deformation of the neutral surface is known as the elastic curve of the beam [12].

The strain on the horizontal axis and stress on the vertical axis. The graph of the relationship between stress and strain is shown schematically (not scaled) for a steel specimen in Fig. 8 [13].

The load is evenly distributed with the point load, both of which have different deflection curves. In a uniformly distributed load, the slope that occurs at the closest part of the rod is greater than the slope of the point. This is because as long as the rod experiences a point load, it only occurs at a certain point [14].

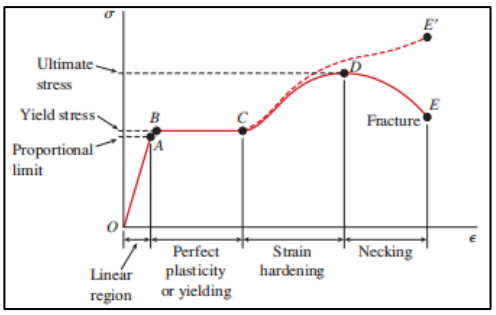

Figure 8. Stress-strain relationship diagram

2. Research Method

The research was conducted by using a numerical method, by using General Cargo ships as the models. The ship original is equipped with two cargo hold, with *inner bottom plate* construction continuous from the left side to the starboard side without margin plate, As for the drawing of margin plates according to the 1984 rules of Nippon Kaiji Kyokai (NK) "*Rules and Regulations For the Construction and Classification Of Ships*" [4]. The bottom construction of the models was then modified by adding the margin plate to analyze the effect of the margin plate on the strength of the ship's construction. Modeling was carried out on ANSYS^{TM} software from the engine room divider to the cargo hold bulkhead (one load room) with a load room length of 30.1 meters.

3. Result and Discussion

3.1. Calculations ship transverse strength

The load that used in the Ansys^{TM} model is based on the calculation of deck load, side load, and bottom load obtained from the BKI Rules for Volume 1, 2016 Edition [15]. Then the point of review on both models must be the same, namely the meeting between the bilge plate and side plate. The ship model without margin plate is abbreviated as TMP while the ship model with margin plate is abbreviated as DMP.

a) Analysis of transverse structure of the ship

- Displacement

Some parts of the structure being modeled will experience displacement when a load acts on them. The maximum displacement occurs in the deck plate. In the model without a margin plate (node 289189) there is a deflection with a maximum value of 3,3365 mm while in the ship model with a margin plate (node 198637) there is a deflection with a maximum value of 3.40964 mm which can be seen in Fig. 9.

- Stress

Based on the results of the comparative analysis of transverse strengths on ships with and without margin plates. The stress that occurs in the model without a margin plate at node 282746 is in 100% condition, namely 8.4739 N / mm^2, while the model with a margin plate at node 147724 is in 100% condition which is 9.6242 N / mm^2. Then carried out variations in the load including deck load, side load and bottom load to obtain the resulting stress ratio curve can be seen in Fig. 8 and Fig. 9.

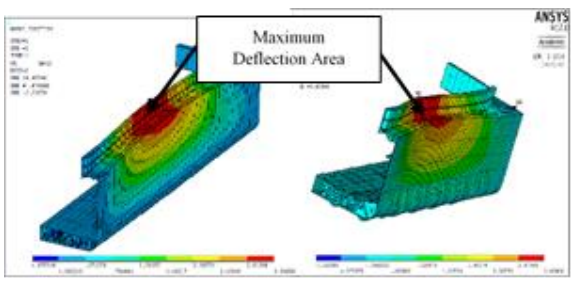

(a) (b)

Figure 9. Displacement in the x direction for the model without margin plate (a) and with margin plate (b)

3.2. Variations in the transverse force of the ship

Loading variations are carried out to get the tendency of the ship structure's response to each load change. In the variation of the load, the transverse strength of this ship includes deck load (P_D), side load (P_S), and bottom load (P_B), which are used as reference loads and assumed to be 100% load. By giving each load increase of 0.2 x the maximum load (100%) which is calculated using the BKI Rules. In the variation of deck load with constant side load and bottom load 100% the maximum load while the sideload variation with constant deck load and bottom load while in the variation of the bottom load with constant deck load and sideload are also varied as well as the deck, side, and bottom loads. The result of the relation between strees and variation of loads was shown in Fig. 10 to Fig. 15.

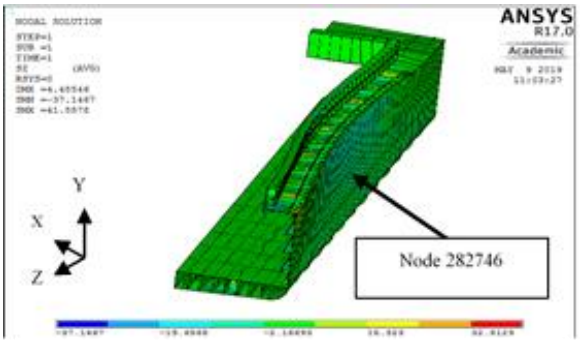

Figure 10. Viewpoints for Stress in Models without Margin Plate

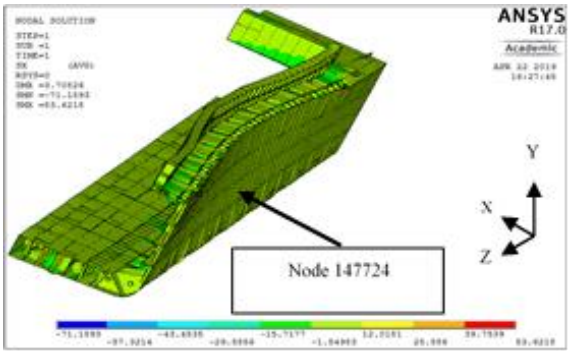

Figure 11. Viewpoints for Stress in Models with Margin Plate

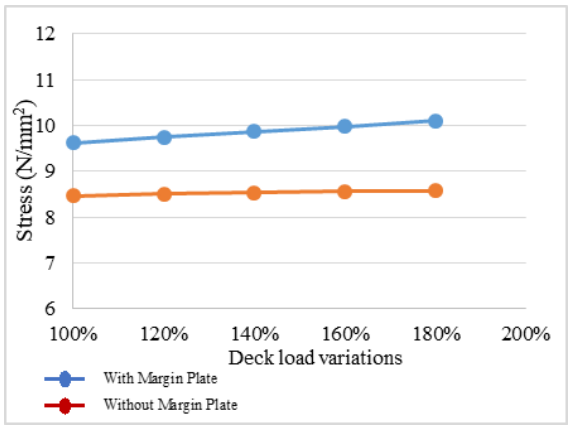

Figure 12. The relation between deck load variations and stress on models with and without margin plate

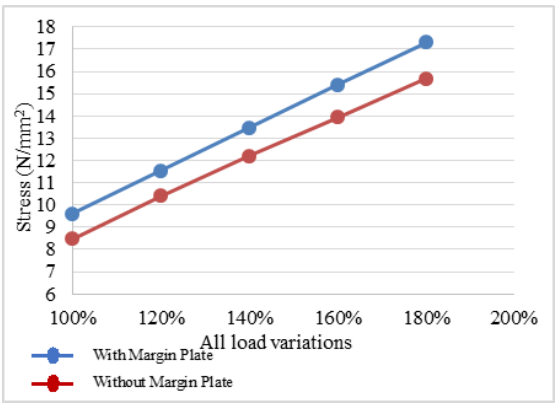

Figure 13. The relation between side load variations and stresses on models with and without margin plate

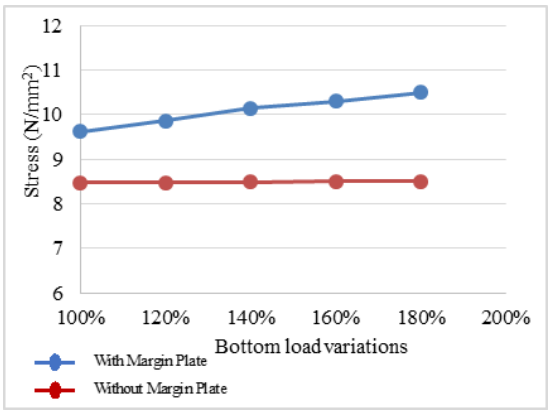

Figure 14. The relation between bottom load variations and stresses on models with and without margin plate

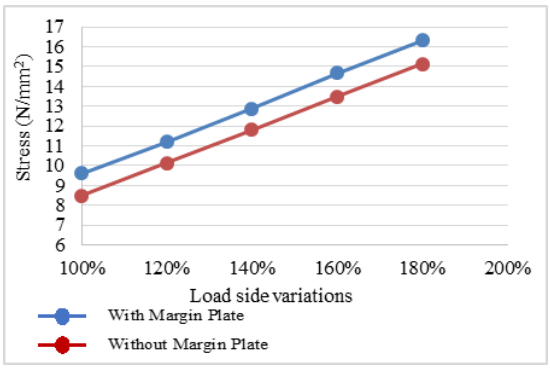

Figure 15. The relation between all load variations and stresses on models with and without margin plate

3.3. Calculations ship longitudinal strength

The ship loading installed in the Ansys model is based on the calculation of the external moment which is then defined in force (F). This style will later be installed on the Ansys model. Then for the longitudinal strength of the ship, the MPC (Multi-Point Constraint) method is used where one of the nodes at the and of the model is clamped and the other end node is given a moment.

a) Variation of the vertical bending moment the ship's longitudinal load

Based on the results of calculations on the BKI rules, the results of the variation of the vertical bending moment in the hogging conditions are 8.14 x 10^9 Nmm and the sagging conditions are -9.17 x 10^9 Nmm. Then vary every multiple of 0.2 x maximum vertical bending moment as shown in Table 1.

Based on the results of the analysis on Ansys software, the stress value is 100% x moment max. in the hogging condition it is 8.14 x10^9 Nmm and the sagging condition is -9.17 x 10^9 Nmm then it was varied as shown in Table 2 and Table 3. Then the point of review of the two models is in the bottom area (the meeting between the bottom plate and the bilge plate) and the deck (the meeting between the side plate and the deck plate).

Table 1. Variation of vertical bending moment

Load variations	**Vertical Bending Moment**	
	***Hogging* Conditions (Nmm)**	***Sagging* Conditions (Nmm)**
100% x Moment Max.	8.14 x 10^9	-9.17 x 10^9
120% x Moment Max .	9.77 x 10^9	-1.10 x 10^{10}
140% x Moment Max.	1.14 x 10^{10}	-1.28 x 10^{10}
160% x Moment Max.	1.30 x 10^{10}	-1.47 x 10^{10}
180% x Moment Max.	1.47 x 10^{10}	-1.65 x 10^{10}

Table 2. Variation of vertical bending moment in hogging conditions

Load Variation	***Hogging* Moment (Nmm)**	**With *Margin Plate***		**Without *Margin Plate***	
		Stress on Deck (N/mm²) node: 690200	**Stress on Bottom (N/mm²) node: 686946**	**Stress on Deck (N/mm²) node: 701345**	**Stress on Bottom (N/mm²) node: 661662**
100% x Moment Max.	8.14 x 10^9	11.38	-20.585	16.705	-11.045
120% x Moment Max.	9.77 x 10^9	13.659	-24.707	20.050	-13.257
140% x Moment Max.	1.14 x 10^{10}	15.538	-28.829	23.395	-15.469
160% x Moment Max.	1.30 x 10^{10}	18.175	-32.876	26.679	-17.640
180% x Moment Max.	1.47 x 10^{10}	20.551	-37.174	30.168	-19.947

Table 3. Variation of vertical bending moment in sagging conditions

Load Variation	***Hogging* Moment (Nmm)**	**With *Margin Plate***		**Without *Margin Plate***	
		Stress on Deck (N/mm²) node: 690200	**Stress on Bottom (N/mm²) node: 686946**	**Stress on Deck (N/mm²) node: 701345**	**Stress on Bottom (N/mm²) node: 661662**
100% x Moment Max.	-9.17 x 10^9	-12.82	23.189	-18.819	12.44
120% x Moment Max.	-1.10 x 10^{10}	-15.379	27.817	-22.574	14.93
140% x Moment Max.	-1.28 x 10^{10}	-17.895	32.369	-26.268	17.37
160% x Moment Max.	-1.47 x 10^{10}	-20.551	37.134	-30.168	19.92
180% x Moment Max.	-1.65 x 10^{10}	-23.068	41.726	-33.862	22.39

b) Displacement and Stress in Deck Plates and Bottom Plates on Ship Models with and without margin plate

- Sagging conditions

- Displacement

Some parts of the structure being modeled will experience a displacement when a load acts on them. and after analysis on ANSYS™ software, as shown in Fig. 16, the deflection of the ship model without plate margin on the deck plate at node 701345 is -2.4112 mm and on the bottom plate at node 661662 which is 1.9221 N/mm^2.

The deflection results on the ship model with the plate margin obtained on the deck plate at node 690200, namely -1.872 mm and on the bottom plate at node 686946 which is 2.6132 mm, as shown in Fig. 17.

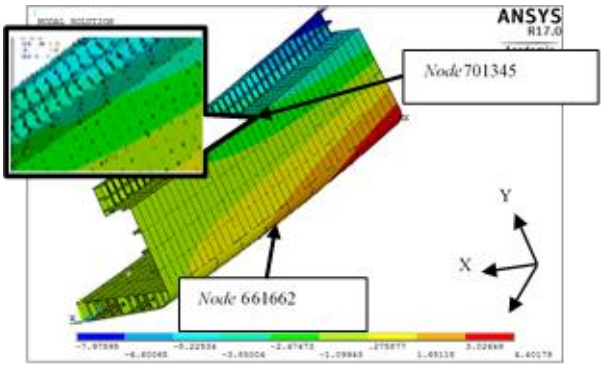

Figure 16. Respond and displacement z-direction in the sagging conditions on the ship model without margin plates on the deck plate and the bottom plate

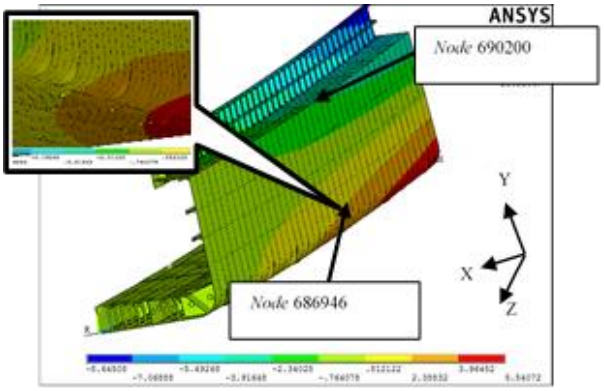

Figure 17. Respond and displacement in the z-axis direction of sagging conditions on the ship model with margin plates on the deck plate and the bottom plate

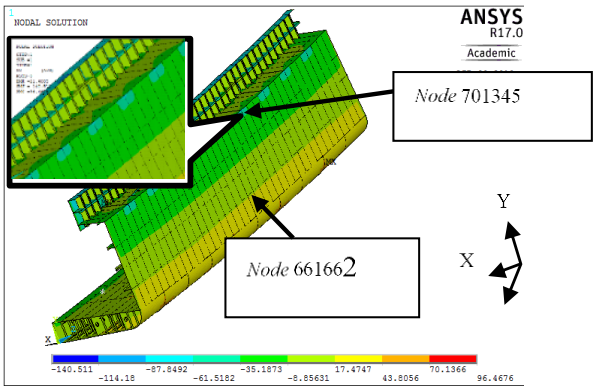

Figure 18. Respond and stress distribution in the z-axis direction of sagging conditions on a ship model without plate margins on the deck plate and bottom plate

- Stress

Some parts of the structure being modeled will experience stress when a load acts on them. The stress obtained on the ship model without a margin plate on the deck plate at node 701345 is -18.819 N/mm^2 and on the bottom plate at node 661662 which is 12.443 N/mm^2. as shown in Fig. 18.

The stress results on the ship model with the margin plate obtained on the deck plate at node 690200 is -12.82 N/mm^2 and on the bottom plate at node 686946 which is 23.189 N / mm^2, as shown in Fig. 19.

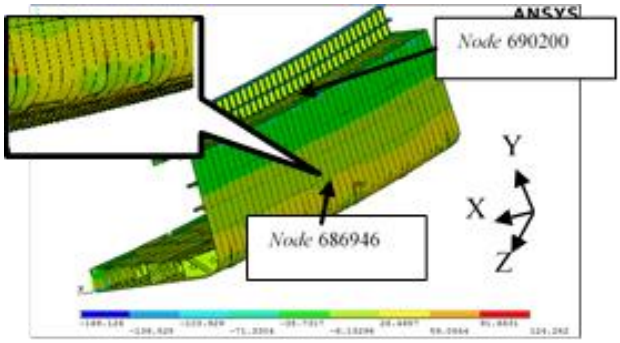

Figure 19. Respond and stress distribution in the z-axis direction of sagging conditions on a ship model with plate margins on the deck plate and bottom plate

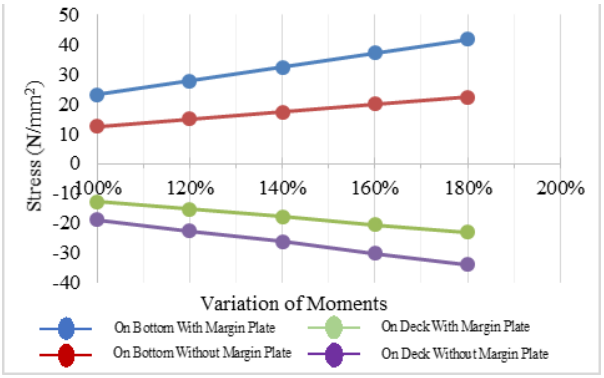

Figure 20. The relation between variation of bending moment and the stress in the sagging condition

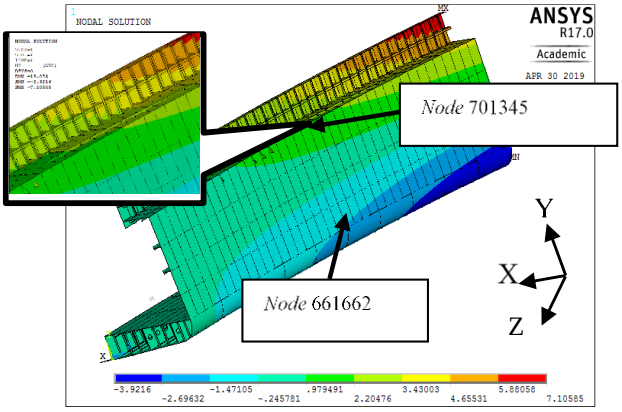

Figure 21. Respond and stress distribution in the z-axis direction of hogging conditions on a ship model without plate margins on the deck plate and bottom plate

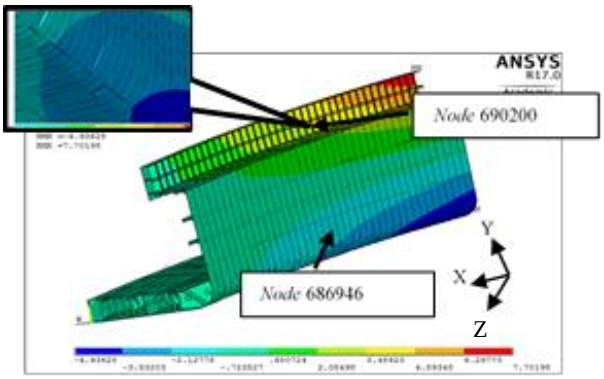

Figure 22. Respond and stress distribution in the z-axis direction of hogging conditions on a ship model with plate margins on the deck plate and bottom plate

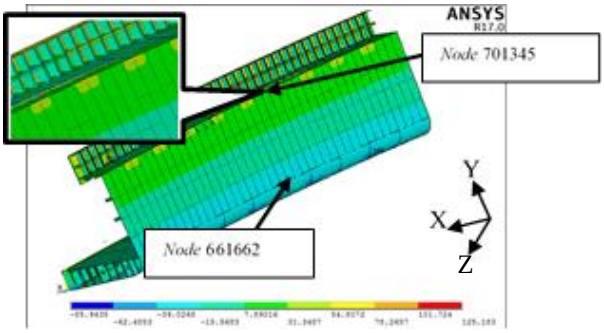

Figure 23. Respond and stress distribution in the z-axis direction of hogging conditions on a ship model without plate margins on the deck plate and bottom plate

- Hogging Conditions

- Displacement

Displacement in the ship model without plate margin on the deck plate at node 701345 is 2.1220 mm and on the bottom plate at node 661662 which is -1.7233 mm can be seen in Fig. 21 and Fig. 22.

The deflection results on the ship model with the margin plate obtained on the deck plate at node 690200 is 1.6224 mm and on the bottom plate at node 686946 which is -2.3421 mm.

- Stress

Some parts of the structure being modeled will experience stress (stress) when a load acts on them. The stress obtained on the ship model without a margin plate on the deck plate (the meeting between the deck plate and the side plate) at node 701345 is 16.705 N/mm^2 and on the bottom plate (the meeting between the bottom plate and the bilge plate) at node 661662 is -11.045 N/mm^2, as shown in Fig. 23.

The stress results on the ship model with margin plate obtained on the deck plate at node 690200 are 11.38 N/mm^2 and on the bottom plate at node 686946 which is -20.585 N/mm^2, as shown in Fig. 24.

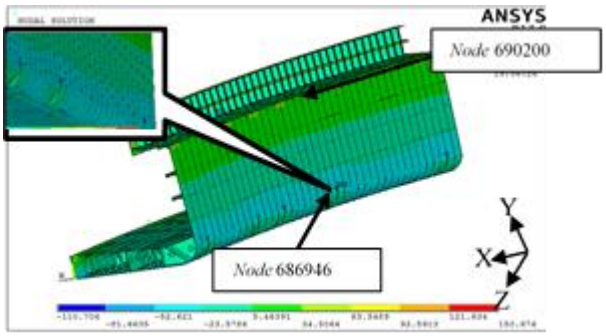

Figure 24. Respond and stress distribution in the z-axis direction of hogging conditions on a ship model with plate margins on the deck plate and bottom plate

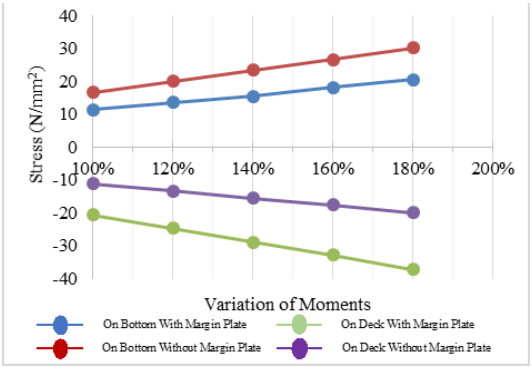

Figure 25. The relation between the increase in vertical bending moment and the working stress in hogging conditions

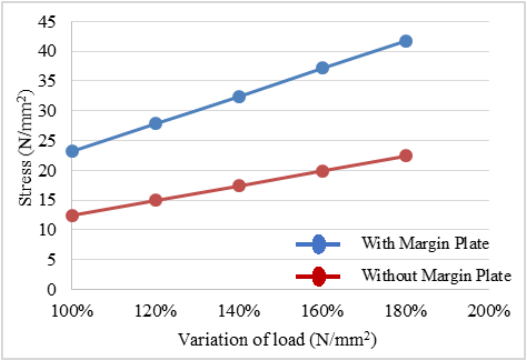

(a) Sagging condition

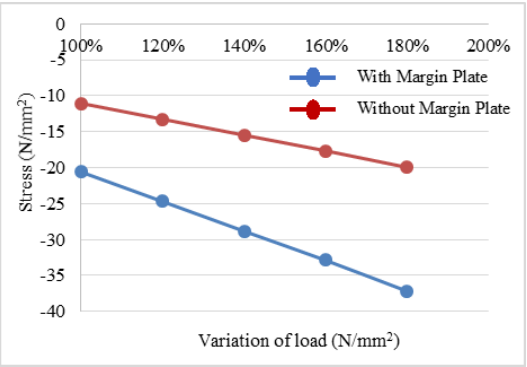

(b) Hogging condition

Figure 26. Relation between stress and variations of longitudinal loads at the meeting of the bottom plate with the bilge plate in sagging (a) and the hogging (b) conditions

4. Conclusions

The stress generated on a ship model without using a margin plate is better able to withstand transverse loads when compared to a ship model using a margin plate.

a) The amount of difference in high stress due to the influence of the load is an average of 15.82%. Then the difference in stress on the deck load is 13.49% on average, while the sideload is 8.74% on average.
b) The amount of stress difference generated at the vertical bending moment for the sagging and hogging conditions in the bottom area is 46.34%. The results of the stress on a ship model without using a margin plate are better able to withstand longitudinal loads when compared to a ship model using a margin plate.

References

[1] M. D. Rosyid and D. Setyawan, *Ship Structure Strength*. Jakarta: Pradya Paramita, 2000. [in Bahasa]
[2] E. Hirohiko, *Illustration Of Hull Structures*. Japan, 2007.
[3] Rosmani, *Ship Construction I Midship Section*. Makassar, 2000. [in Bahasa]
[4] Nippon Kaiji Kyokai, *Rules and Regulations for the Construction and Classification of Ships*. Japan, 1984.
[5] N. Barabanov, *Structural Design of Sea-Going Ships*. Moscow: Peace Publisher, 1960.
[6] I. K. Djaya, *Steel Ship Construction Engineering*. Book Center of the Ministry of National Education, 2008. [in Bahasa]
[7] Hughes, F. Owen, and J. K. Paik, *Ship Construction Analysis and Design*. New Jersey: The Society of Naval Architecture and Marine Engineers, 2010.
[8] M. Shama, "Buckling of Ship Structures," Alexandria University, 2013.
[9] Y. Susatio, *Finite Element Method*. Surabaya: ITS, 2004. [in Bahasa]
[10] D. B. Marghitu, *Mechanical Engineer's Handbook*. Academic Press, 2001.
[11] A. Setiawan, *Steel Structure Planning*. Jakarta: Erlangga, 2002. [in Bahasa]
[12] L. D. Schodek, *Structure*. Bandung: Rafika Aditama, 1998. [in Bahasa]
[13] J. M. Gere and B. J. Goodno, *Mechanics of Materials Seventh Edition*, 7th Ed. Cengage Learning, 2009.
[14] B. Hariandja, *Mekanika Teknik: Statics in Analysis of Frame Structure*. Jakarta: Erlangga, 1996. [in Bahasa]
[15] Biro Klasifikasi Indonesia, *Domestic Hull Guidelines Volume 1*. Jakarta, 2016.

EPI International Journal of Engineering
Volume 4, Number 1, February 2021, pp. 65-74
DOI: 10.25042/epi-ije.022021.10

*p*ISSN 2615-5109
*e*ISSN 2621-0541

Integration of Natural and Artificial Light on Energy Efficiency of Mega Bank Makassar Tower Building

Isty Cahyani[a,*], Ramli Rahim[b], Baharuddin Hamzah[c]

[a]Department of Architecture, Faculty of Engineering, Hasanuddin University, Makassar. Indonesia. Email: istythecat@mail.com
[b]Department of Architecture, Faculty of Engineering, Hasanuddin University, Makassar. Indonesia. Email: yb8bri@yahoo.com
[c]Department of Architecture, Faculty of Engineering, Hasanuddin University, Makassar. Indonesia. Email: baharsyah@unhas.ac.id

Abstract

One of the largest energy consumers in the world is buildings. The energy consumed generally comes from the air conditioning and lighting systems. Lighting systems account for 25% of the total energy consumption in buildings. The strategy used in building design is to reduce energy consumption while maintaining the best comfort in a building. The application of energy-saving concepts from the building sector is optimizing the lighting system by integrating natural and artificial lighting systems. This study aims to determine the light intensity in the integrated lighting system of natural and artificial manually and also to find out how much energy can be saved with the integrated lighting system manually. The research location is at the Mega Bank Makassar Tower Building. The research sample was selected by purposive sampling and the sixth floor was chosen as the research location. In this study, simulations were carried out using the DIAlux 4.13 program to integrate natural and artificial light and to calculate the amount of energy efficiency in the workspace. To obtain optimal light intensity and energy savings, a simulation was carried out by turning off half the light points in the workspace, especially the light points around the building openings. The simulation results show that the average integrated lighting quality meets the minimum lighting requirements and can save energy usage by up to 50%.

Keywords: Energy efficiency; integration lighting; workspace

1. Introduction

Buildings are one of the largest energy consumers, the World Green Building Council states that the construction sector absorbs 30-40% of the world's total energy. The average energy use of office buildings in Indonesia is 250 KWh/m^2/year. This figure exceeds the standard for energy use in office buildings, which is 180 KWh/m^2/year. It can be concluded that many office buildings in Indonesia are still energy-wasteful [1]. In a typical high-rise office building, the proportion of energy use generally includes 55% for air conditioning systems, 25% for lighting systems and the remaining 20% for other equipment (elevators, pumps, electronic equipment, etc.) [2]. Although the use of energy for artificial lighting is smaller than air conditioning, but by minimizing the use of energy for lighting, it means that energy consumption in the building can be reduced so that the lighting system must be a special concern at the early stages of planning to create energy-efficient buildings that meet the requirements of visual comfort of the space [3].

*Corresponding author. Tel.: +6281241741002
Perumahan Bukit Garaganti Graha Blok D/3
Gowa, South Sulawesi
Indonesia 92118

The office as a work area requires a comfortable level of natural lighting so that users in it can carry out activities smoothly and have good work productivity. Good lighting levels can be achieved by utilizing natural and artificial lighting. In some buildings, artificial lighting is needed in space zones that are far from natural light sources. By integrating natural and artificial lighting systems, it is easy to achieve the required light intensity in each space zone. For efficient use of energy, it is necessary to have a system that is used to control the lighting requirements so that lighting can be optimized and the demands of visual comfort can be achieved.

The Mega Bank Tower Building is one of the multi-story office buildings in Makassar City. Based on the initial survey in this building through direct observation, measurement of light intensity in the workspace and interviews with building users, it can be concluded that the distribution of lighting into the workspace is uneven. There are several workspaces that only use natural lighting because the intensity of natural light entering the space is high enough that it does not require artificial lighting. However, there are also workspaces that must use artificial

lighting because the work zone is far from natural light sources.

Based on some of the things mentioned above, the authors thought to analyze the lighting system, as well as effective design in energy use efficiency by properly integrating natural and artificial lighting in the workspace at the Menara Bank Mega Makassar Building to optimize the lighting system and increase work productivity his employee.

2. Literature Review

2.1. Lighting

Light is a form of energy that is radiated or emitted from a source in the form of waves and is part of the whole group of electromagnetic waves, which are converted into visible light [4]. Light is an important element in illumination and vision. The presence of light in the environment aims to illuminate the various forms of elements that exist in the building so that the space becomes clearly observed as if you feel the visual atmosphere (visual sense).

There are two types of light sources that can be used for lighting in the room, namely natural light from the sky dome and artificial light from electric lighting. Natural lighting plays an important role in sustainable development because it can be utilized without the need for energy and does not cause pollution, thereby reducing pollutants [5].

Based on Darmasetiawan and Puspakesuma [6], 5 (five) criteria to consider to get good lighting, are:

a. Lighting level
b. Luminance distribution
c. Luminance of glare
d. Light directionally and shadows
e. Light colours dan colours rendering

2.2. Natural lighting

Natural lighting is lighting produced by a natural light source, namely the sun with its strong light but varies according to hours, seasons, and places. Natural lighting in a building will reduce the use of artificial light, thus saving energy consumption and reducing pollution levels. According to Kroelinger in Thojib [7] that natural light is distributed into the room through openings on the side (side lighting), openings above (top lighting), or a combination of both.

2.3. Artificial lighting

Artificial lighting is lighting produced by light sources other than natural light. Artificial lighting is very necessary when the position of the room is difficult to achieve by natural lighting or when natural lighting is insufficient [8]. According to the National Standardization Agency No.03-6575-2001, artificial lighting systems can be grouped into three, namely: evenly distributed lighting systems, local lighting systems and uniform and local combined lighting system [9].

Table 1. Recommended average lighting level

Space Function	Lighting Level (lux)
Office complex	
Director's room	350
Workspace	350
Computer room	350
Meeting room	300
Drawing space	750
Archives	150
Educational institutions	
Class room	250
Library	300
Laboratory	500
Drawing room	750
Canteen	200

2.4. Visual comfort

Visual comfort is the need for a good level of lighting in a room. Good lighting is lighting that can meet the needs of its users, related to the types of activities carried out in the space [10].

Visual comfort has a very strong relationship with lighting. Visual comfort in a building is influenced by the lighting design in the building. Visual comfort is fulfilled if space users can form a comfortable spatial impression. Lighting design does not only function to show visual objects that can be seen, but also serves to generate visual comfort which psychologically affects its performance so that work productivity can increase [11]. For eye comfort, the recommended lighting level by SNI 03-6575-2001 is shown in Table 1.

2.5. Energy efficiency

Energy saving (energy efficiency) in architecture is to minimize energy use without limiting or changing the function of the building, the comfort, or productivity of its occupants. Energy saving is done by optimizing energy use according to the level of need. One way is through building design that can save electricity usage, both for cooling/cooling the air in the room and for lighting [12].

The problem of lighting both natural and artificial cannot be separated from the use of energy in a building, because lighting is one of the things that has a big influence on energy consumption besides the air conditioning system [13].

Energy Consumption Index (Energy Use Intensity) or IKE (EUI) based on the calculation formula in DKI Jakarta Governor Regulation No. 38 of 2012 is the amount of energy used by a building to expand its conditioned area in one month or one year. IKE is used as a reference to see how much energy conservation the building is doing. This Energy Consumption Intensity is the ratio between the total energy consumption during a certain period (1 year) and the building area. The IKE unit is kWh/m^2 per year [14].

According to the results of research conducted by ASEAN-USAID in 1987 whose report was only issued in 1992, the target size of the Energy Consumption Intensity (IKE) of electricity for Indonesia is as follows: IKE for offices (commercial) is 240 kWh/m^2 per year, shopping centers 330 kWh/m^2 per year, hotel/apartment: 300 kWh/m^2 per year and for hospitals: 380 kWh/m^2 per year. If the IKE value is lower than the lower limit, then the building is said to be energy efficient. If the IKE value is between the lower limit and the reference, then the building is said to be rather frugal. If it is between the reference and the upper limit, then the building is said to be a bit extravagant so it needs to make some changes. If it is above the upper limit, it is necessary to do retrofitting or replacement.

2.6. Energy efficiency

The office is a hall (building, house, room) where one takes care of a job (company and so on) or a place to work [15]. The office itself has several functions which include receiving information, recording information, managing information, providing information and protecting assets and assets.

3. Research Methods

This type of research is research with descriptive and correlational quantitative methods. This method was chosen in connection with the idea of research that seeks to combine the results of observations (observations made in the form of illumination measurements with a luxmeter) with simulations of natural and artificial integration lighting contours using the DIAlux 4.13 software simulation. In this study, calculations and optimization of electrical power consumption were also carried out in order to energy efficiency.

3.1. Research location

The research location is in the capital city of South Sulawesi Province, namely the city of Makassar. The Mega Bank Makassar Tower Building is located in Tamalate District, Maccini Sombala Village, which is precisely on Jl. H.M. Patompo in the Trans Studio area. The Bank Mega Makassar Tower has a land area of 9,600 m² and a building area of 6,000 m² consisting of 12 floors and 1 basement.

3.2. Population and sample

In this study, the subject population is all employees who are active in the workspace in the Mega Bank Makassar tower building who will be the respondents in this study. The sampling technique used was the purposive sampling method. The sample selection of the workspace was taken one floor from the total number of 12-story buildings. The workspace selected is the workspace on the 6th floor.

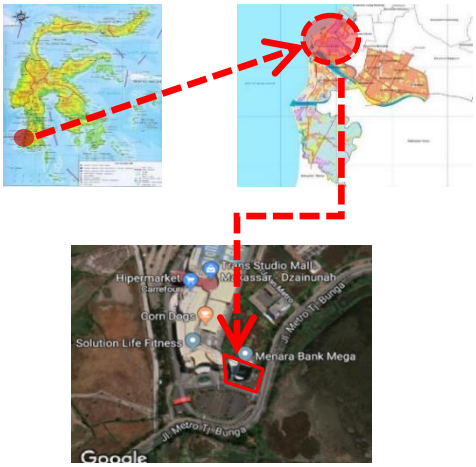

Figure 1. (a) Map of South Sulawesi; (b) Map of Tamalate district; (c) Map of Mega Bank Makassar Tower Building location

Figure 2. Mega Bank Makassar Tower Building

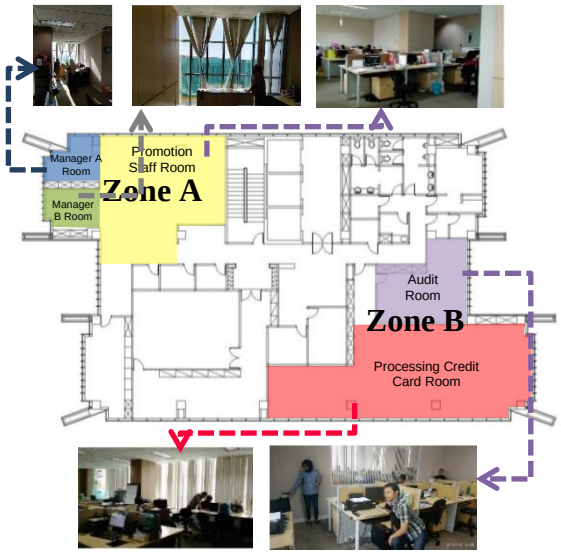

Figure 3. Division zone light intensity measurement

3.3. Data collection

The data obtained are sourced from primary data and secondary data. Primary data was obtained during observations and measurements in the workspace in the form of data from space measurements, the number of occupants in the room, dimensions and positions of openings, light intensity, and activities. While secondary data were obtained from relevant works of literature and through searching on the internet regarding the data related to this study.

Data collection techniques used in this research are literature study, observation, interviews and questionnaires, measurement of light intensity, simulation and calculation of electrical power in lighting.

3.4. Data analysis

The analysis of this research is quantitative with descriptive statistics. The descriptive statistic analysis technique used in this study is the presentation of data in a visual form such as histograms, polygons, and diagrams. Analysis of simulation with DIAlux program to integrate natural and artificial light and to calculate the amount of energy efficiency in the workspace.

4. Discussion

4.1. Lighting quality integration of natural and artificial (Manual)

In the existing condition, the research object still utilizes natural lighting from openings in the walls (windows) and also the use of lamps as lighting (combined lighting systems). The average natural lighting on the research object has met the standardization of lighting in the workspace, but there are still some areas where the lighting level is still below the standard so that artificial lighting is used to increase the level of illumination of the area which is still below standard. This causes the area that has been fulfilled by natural lighting to still receive artificial lighting so that the area's illumination level is far above the standard of 350 lux. This results in ineffective use of lamps and a waste of energy. For this reason, a simulation was carried out using the DIALux 4.13 program to obtain an even level of lighting according to standardization.

The simulation is done by turning off several light points in areas that have received sufficient natural lighting. This simulation is carried out with the sky conditions that are already in the simulation program, namely clear sky. Simulation time is morning, afternoon and evening at 09.00, 12.00 and 15.00. Location data that is input into the DIAlux program is Makassar City with a position of Longitude 119.40° and Latitude -5.10°. The workplane is placed at a height of 0.75 cm from the floor level.

a. Promotional Room Combination Lighting Quality (Manager A Room, Manager B Room and Promotion Staff Room)

The results of the manual combination lighting simulation shown in Fig. 4 consist of 16 light points with the type of lamp used is PHILIPS TCS260 2xTL5-28W HFP M6_827 with a distance between lamps of 2.4 meters. In this simulation, there are 8 light points that are extinguished close to the opening (window).

In Fig. 4 it can be seen that in the morning the promotional staff room gets more natural light from the opening on the Northeast side. So that the work area on that side is very bright. Likewise with Manager Room A because there is an opening on the Northeast side. Meanwhile, Manager B Room only gets a little natural light from outside because the opening is only on the Northwest side. At Daytime, the light intensity is almost evenly distributed in Manager Room A, Manager Room B and Promotion Staff Room. In the afternoon, a lot of natural light enters through the opening on the Northwest side. So Manager Room A and B are very bright in the afternoon.

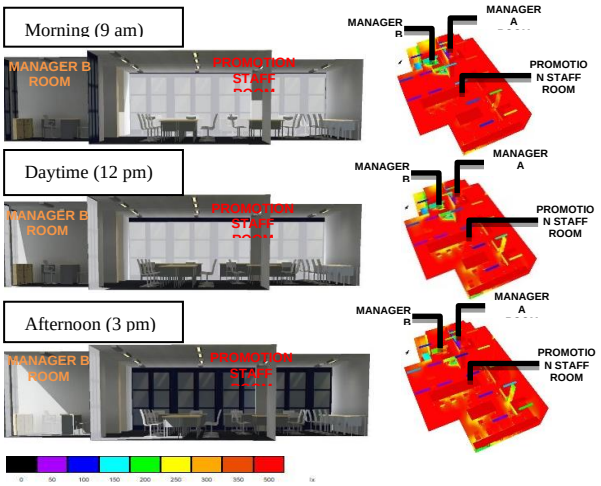

Figure 4. Zone A manual combination lighting (Manager Room A, Manager Room B and promotion staff room)

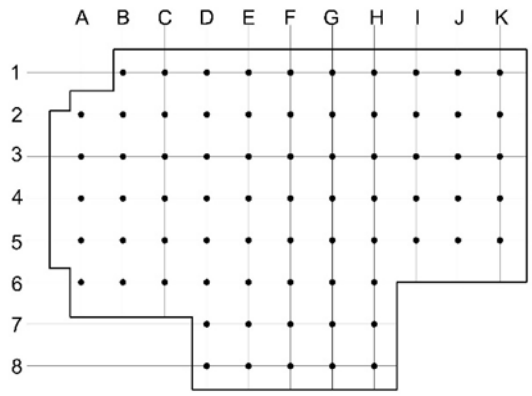

Figure 5. Measuring point of Zone A

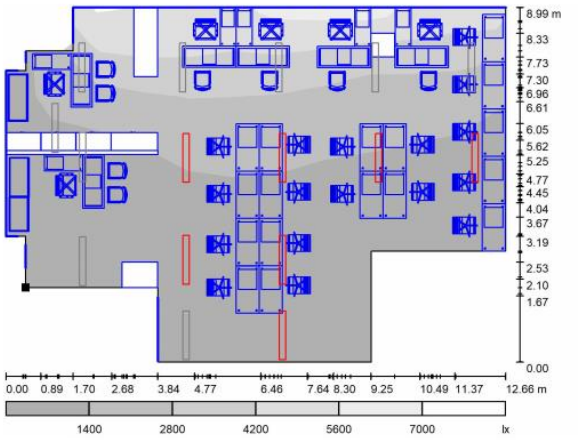

Figure 6. Simulation results of combination lighting Zone A in the morning

From Table 2, the simulation results show that the level of manual combination lighting in Zone A with clear sky conditions in the morning far exceeds the standard. This is because the average illumination is 1258 lux, which means it exceeds the standard workspace illumination of 350 lux.

In the Fig. 7, it can be seen at points B1, C1, D1, E1, F1, G1, H1, I1, J1 and K1 that the light intensity is above 3000 lux, far exceeding the standard. This is because this measuring point is at an opening facing the Northeast so that in the morning the light intensity in this area is very high.

From Table 3, the simulation results show that the level of manual combination lighting in Zone A with clear sky conditions during the day far exceeds the standard. This is because the average illumination is 1001 lux, which means it has exceeded the standard workspace illumination of 350 lux. However, the intensity of the light has decreased from the morning.

Table 2. Simulation results of combination lighting Zone A in the morning

	A	B	C	D	E	F	G	H	I	J	K	Average
1		5862	5228	5679	5133	4871	5124	4797	4798	4527	3968	4999
2	1184	2550	2503	3266	3276	3165	3124	2522	1905	2573	1895	2542
3	1380	1685	2055	2082	2038	1965	1880	1604	1598	1528	1269	1735
4	903	448	392	1336	1486	1476	1374	1274	1301	1130	1048	1106
5	1066	529	492	1065	1125	1193	1092	905	938	724	760	899
6	724	544	596	947	994	1041	1009	747				825
7				959	829	963	919	619				858
8				1106	790	883	865	559				841
Average												**1258**

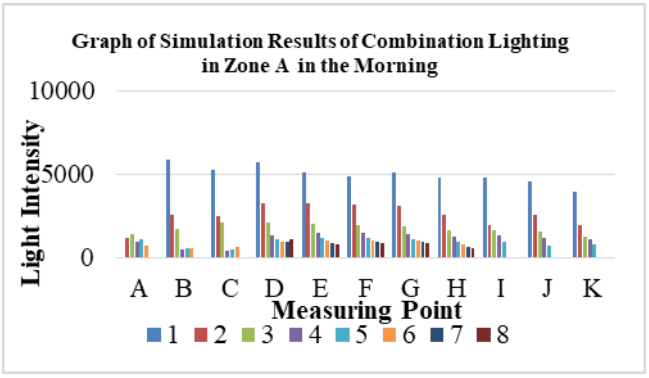

Figure 7. Simulation results of combination lighting in Zone B in the morning

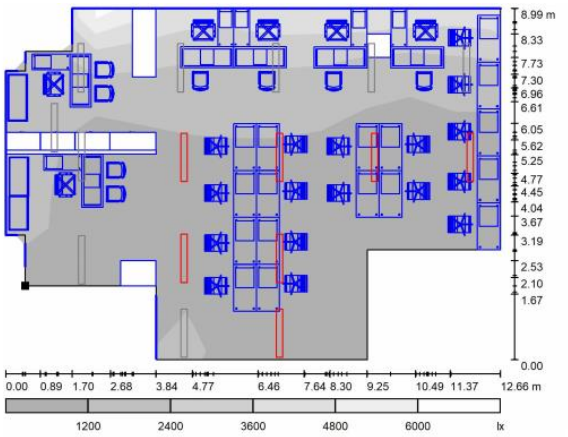

Figure 8. Simulation results of combination lighting Zone A in the daytime

Table 3. Simulation results of combination lighting Zone A in the daytime

	A	B	C	D	E	F	G	H	I	J	K	Average
1		5363	4264	3443	3440	3384	3485	3371	3215	3168	3160	3629
2	1716	1473	1741	1611	1785	1782	1779	1584	1069	1413	1427	1580
3	1752	1007	1331	1239	1228	1232	1216	1134	1059	1006	997	1200
4	1561	590	434	912	1043	1067	1030	944	975	881	888	939
5	1816	717	518	783	817	890	845	667	693	542	623	810
6	1162	703	541	775	794	865	833	567				780
7				964	738	844	800	498				769
				1802	839	793	752	473				932
Average												**1001**

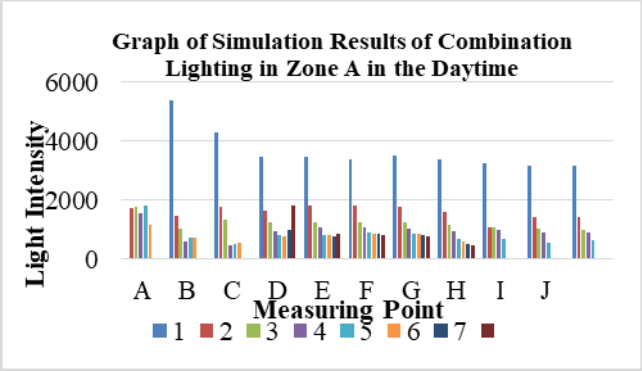

Figure 9. Simulation results of combination lighting in Zone A in the daytime

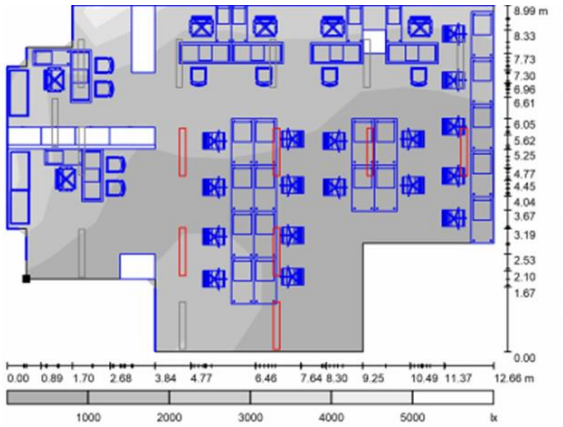

Figure 10. Simulation results of combination lighting Zone A in the afternoon

Table 4. Simulation results of combination lighting Zone A in the afternoon

	A	B	C	D	E	F	G	H	I	J	K	Average
1		4039	3528	2022	2074	2023	2130	2065	1904	1900	2004	2369
2	2718	1785	1538	1241	1318	1310	1305	1162	884	988	1070	1393
3	2164	1079	1222	199	1066	1050	1039	965	918	856	854	1037
4	2801	1389	791	966	1026	1011	971	874	903	809	812	1123
5	2703	1372	837	867	824	898	843	637	643	510	579	974
6	1909	1085	720	860	872	970	906	580				988
7				1487	1056	1037	914	537				1006
8				2553	1236	923	821	508				1208
						Average						**1104**

In Fig. 9, it can be seen that points B1, C1, D1, E1, F1, G1, H1, I1, J1 and K1 which are near the opening have high light intensity, which is above 3000 lux. However, it has decreased slightly compared to the morning.

From Table 4, the simulation results show that the level of manual combination lighting in Zone A with clear sky conditions in the afternoon exceeds the standard. This is because the average illumination is 1104 lux, which means it exceeds the standard workspace illumination of 350 lux.

In Fig. 11, it can be seen that at points B1, C1, D1, E1, F1, G1, H1, I1, J1 and K1 decreased from morning to evening. This is because in the afternoon the light entering through the opening in the Northeast direction has decreased. On the other hand, the points in the opening leading to the Southwest have increased, namely at points D8, E8, F8, G8 and H8.

b. Lighting Quality Combination of Credit Card Processing Promotion Room and Audit Room

The results of the manual combination lighting simulation in Zone B can be seen in Fig.10 consisting of 22 light points with the type of lamp used is PHILIPS TCS260 2xTL5-28W HFP M6_827 with a distance between lamps of 2.4 meters. In this simulation, 11 light points that were extinguished near the opening (window), can be seen in Fig. 12.

In Fig. 12, it can be seen that in the morning natural light enters the building from the opening on the southeast side so that the light intensity in this area is quite high. While the area on the Northwest side is a bit dark. During the day, the light entering the building is almost evenly distributed because light enters the building through openings to the Southeast and Southwest. In the afternoon, the area on the northwest side of the Credit Card Processing Room is very bright. While in the Audit Room it is not bright, because in this room there is only an opening on the southeast side.

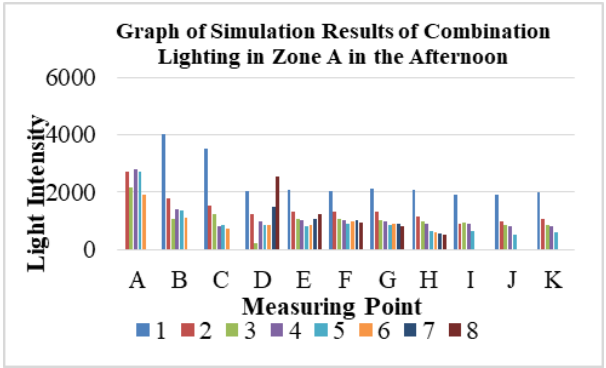

Figure 11. Simulation results of combination lighting in Zone A in the afternoon

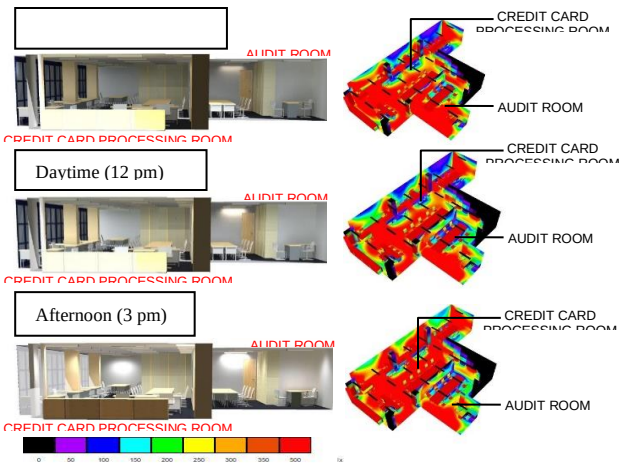

Figure 12. Simulation results of combination lighting Zone B in the morning, daytime and afternoon

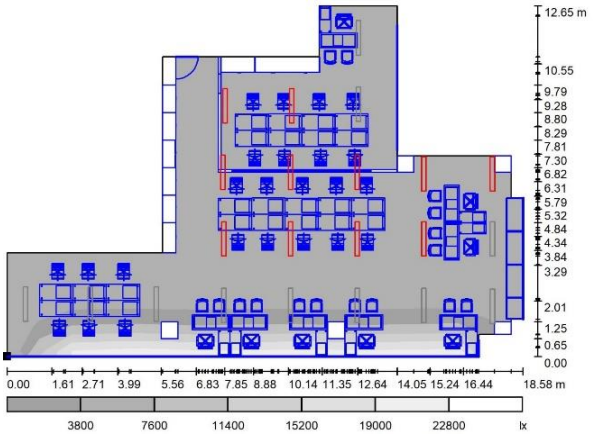

Figure 14. Simulation results of combination lighting B Zone in the morning

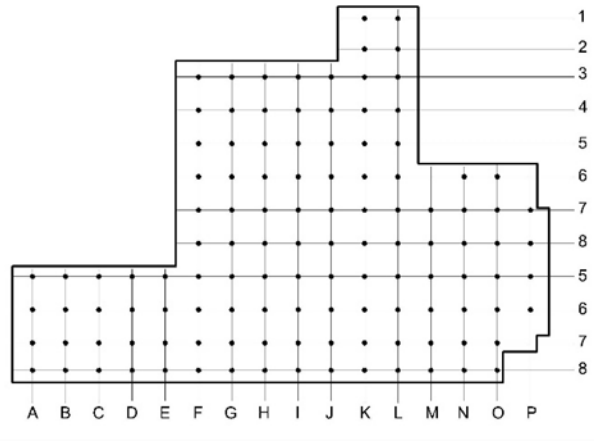

Figure 13. Measuring point of Zone B

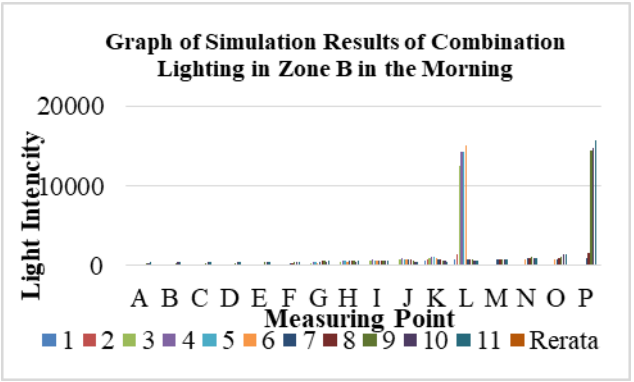

Figure 15. Simulation results of combination lighting in Zone B in the afternoon

Table 5. Simulation results of combination lighting Zone B in the morning

	A	B	C	D	E	F	G	H	I	J	K	L	M	N	O	P	Average
1											568	718					643
2											812	1430					1121
3						61	340	494	583	776	954	12447					535
4						56	497	671	765	886	1074	14193					658
5						92	445	581	664	805	1072	14227					610
6						184	337	431	576	801	1028	14972		819	815		560
7						311	529	597	680	741	831	719	837	900	859	1028	730
8						376	610	657	710	760	774	773	857	987	1024	1590	829
9	375	351	361	367	465	435	607	623	693	676	710	751	857	1060	1092	14442	1492
10	381	414	423	422	432	456	510	551	573	554	580	640	788	1024	1397	14757	1494
11	479	521	533	516	421	482	565	580	612	553	495	663	820	1027	1392	15639	1581
12	877	911	918	937	1042	917	952	828	947	818	1012	905	1158	1273	1397		993
									Average								**932**

Table 5 shows that the level of manual combination lighting in Zone B with clear sky conditions in the morning exceeds the standard. This is because the average illumination is 932 lux, which means it exceeds the standard workspace illumination of 350 lux.

Figure 15 shows the light intensity in the L and M measuring point areas is very high, this is because these points are close to the opening facing the Northeast. So in the morning, the light intensity is very high. While in the area of measuring points A12 to O12 even though they are also close to the opening, the light intensity is low compared to the area of measuring points L and M. This is because the area of measuring points A12 to B12 is in the southwest so that in the morning the incoming natural light is quite low compared to the measuring point area in the Northeast.

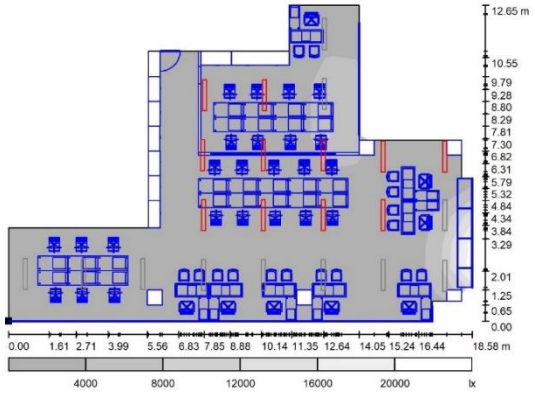

Figure 16. Simulation results of combination lighting Zone B in the daytime

From Table 6, it can be seen that the level of manual combination lighting in Zone B with clear sky conditions during the day exceeds the standard. This is because the average illumination is 662 lux, which means it exceeds the standard workspace illumination of 350 lux. The intensity of the light has decreased from the morning.

Figure 17 shows the measuring point area A12 to O12 has a very high light intensity because this area is close to building openings. So that during the day a lot of natural light enters the room. Table 7 shows that the level of manual combination lighting in Zone B with clear sky conditions in the afternoon exceeds the standard. This is because the average illumination is 718 lux, which means it exceeds the standard workspace illumination of 350 lux. The intensity of the light has increased from noon.

Table 6. Simulation results of combination lighting Zone B in the daytime

	A	B	C	D	E	F	G	H	I	J	K	L	M	N	O	P	Average
1											320	486					403
2											419	801					610
3						48	282	388	403	456	494	869					682
4						50	347	556	588	581	533	876					705
5						85	293	490	527	543	551	787					669
6						191	245	392	493	594	641	614		660	660		644
7						284	465	533	564	578	605	602	703	712	637	811	678
8						340	560	589	617	633	640	656	716	752	686	1037	748
9	374	342	369	379	460	419	580	599	628	614	634	652	690	730	588	1116	735
10	400	426	449	442	432	454	514	552	554	532	519	557	624	669	703	1100	695
11	529	580	605	579	455	518	619	638	650	583	454	613	710	753	761	993	714
12	1129	1221	1233	1249	1328	1202	1251	1119	1249	1102	1305	1123	1329	1370	1395		1304
								Average									**662**

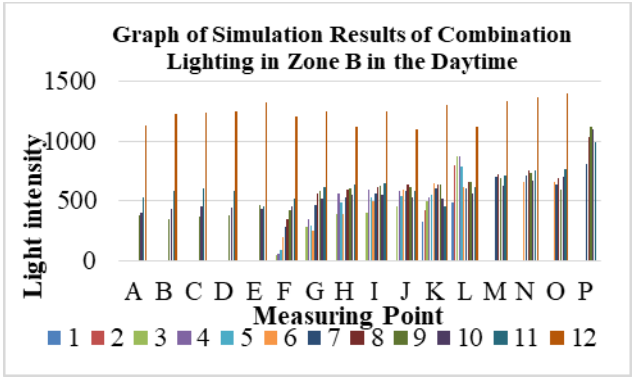

Figure 17. Simulation results of combination lighting in Zone B in the afternoon

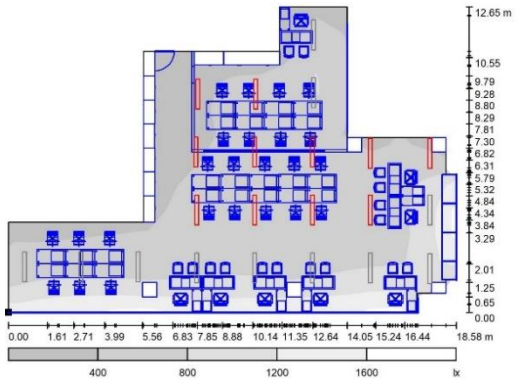

Figure 18. Simulation results of combination lighting Zone B in the afternoon

Table 7. Simulation results of combination lighting Zone B in the afternoon

	A	B	C	D	E	F	G	H	I	J	K	L	M	N	O	P	Average
1											281	407					344
2											353	597					475
3						64	299	413	397	463	425	621					523
4						63	410	581	610	591	473	625					549
5						113	367	523	561	569	530	627					579
6						206	326	434	540	627	651	575		785	789		700
7						368	582	646	691	699	720	742	854	837	749	881	797
8						447	713	759	774	795	805	826	854	887	783	989	857
9	590	566	637	640	856	686	857	864	903	901	893	906	916	971	760	1066	919
10	606	743	848	915	905	827	902	990	1003	969	899	894	990	1057	999	1116	993
11	787	1039	1177	1224	1162	942	1228	1310	1339	1291	899	1058	1296	1363	1278	1082	1163
12	1749	15080	15167	15421	16141	15354	15281	15023	15298	15129	17185	14989	15316	15359	15805		15731
								Average									**718**

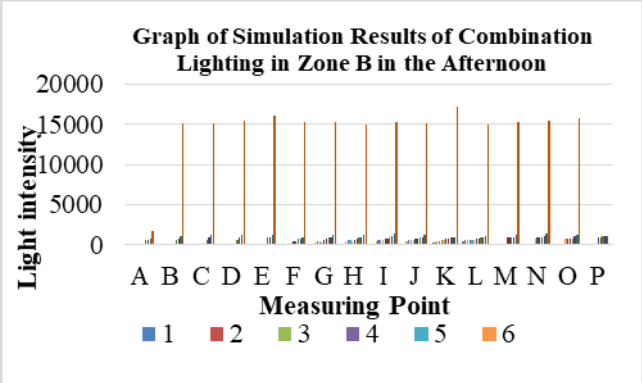

Figure 19. Simulation results of combination lighting in Zone B in the afternoon

Figure 19 shows that the light intensity in the measuring point area B12 to O12 experienced a very high increase, namely above 10,000 lux on average. This is because the area is close to the opening facing the Southwest so that in the afternoon there is a lot of natural light that enters the room. Meanwhile, the area of measuring points L and M which are also near the opening has decreased because the area is in the Northeast. So that in the afternoon the natural light that enters the area is quite a bit compared to the area in the Southwest.

4.2. Analysis of Natural and Artificial Lighting Energy Calculation

To determine the amount of energy consumption in the existing artificial lighting system on the research object, the researchers conducted a lighting simulation using the DIAlux 4.13 program on the artificial lighting system on objects with the same conditions as conditions in the field.

Table 8. Result of calculation of energy consumption of existing artificial lighting research object

No	Lighting Zone	Energy Lighting Evaluation (kWh/a)	Area	Total Energyper m² (kWh/(a.m²)
1	Zone A	1405.44	94.12	14.93
2	Zone B	1855.62	148.17	12.52
	Total	3261.06	242.29	13.46

Table 9. Result of calculation of energy consumption of existing artificial lighting research object

No	Lighting Zone	Energy Lighting Evaluation (kWh/a)	Energy Lighting Combination (kWh/a)	Area m²	Total Energy per m² (kWh/(a.m²))
1	Zone A	1405.44	702.72	94.12	7.47
2	Zone B	1855.62	927.81	148.17	6.26
	Total	3261.06	1630.53	242.29	6.73

From Table 8, it can be seen that the total amount of lighting energy in the research object is 3261.06 kWh/a. This amount is a calculation of lighting energy consumption per year, which is obtained from simulations of lighting energy consumption. To find out the amount of energy used in the manual combination lighting system, namely a lighting system that utilizes natural light that enters the building and also uses artificial lighting by turning on light points in areas that are less exposed to natural light and turning off light points in areas that have sufficient light intensity. so that energy use can be more efficient, can be seen in the following table.

From Table 9, the combined lighting energy is obtained from the amount of lighting energy used for a year multiplied by 50% (the number of light points that are lit half of the total number of light points). While the total energy per m² is obtained from the total lighting energy divided by the total area. From this description, it can be concluded that the amount of lighting energy per year used on the research object when all lights are on is 3261.06 (kWh/a). While the amount of manual combined lighting energy per year used is 1630.53 (kWh/a). So that the use of electricity with a combination lighting system can reduce half of the lighting energy consumption on the object.

5. Conclusion

An effective lighting system can be obtained from a lighting system that utilizes natural and artificial lighting optimally so that it can save energy and users feel comfortable occupying the space. The quality of lighting in the Menara Bank Mega building using a combination of natural and artificial lighting systems manually results in exceeding standardization. This system is carried out by turning off several light points in areas that have received sufficient natural lighting and continuing to turn on the lights in areas that still lack the level of illumination so that the lighting level can be evenly distributed but the result, the light intensity exceeds the minimum standardization for the workspace. But with this system can save energy use.

From the simulation results of the combination of natural and artificial lighting systems that have been done manually, this lighting system can save energy use by up to 50%, which is 1630.53 kWh/a. So, it can be concluded that the combination of natural and artificial lighting systems manually is a lighting system that can save energy use. Based on the results of the research discussed in the previous chapter regarding the Quality of Natural and Artificial Lighting and Manual Combination Lighting. So, it is recommended to the users of the Menara Bank Mega Building not to turn on the lights if the natural light illumination meets the minimum standardization for the workspace so that energy is not wasted. The building manager should also review the control grouping of the light points, the light points that are close to the openings should be grouped in one control so that the light points that are far from the opening can be turned on without turning on the light points that are close to the opening.

Acknowledgements

Thanks to the employees of Mega Bank Tower Building for their cooperation during this research.

References

[1] P. F. Erahman, A. M. Nugroho, and N. Sujudwijono, "Rent Office with Natural Lighting Approach in Malang City," *J. Mhs. Jur. Arsit. Univ. Brawijaya*, vol. 3, no. 4, 2015. [in Bahasa]

[2] O. R. Gw and B. S. Kusumo, "Evaluation Study of Natural Lighting in Joint Lecture Building III, University of Muhammadiyah Malang," *J. Media Tek. Sipil*, vol. 9, no. 1, pp. 50–60, 2011. [in Bahasa]

[3] N. Jamala, "Lighting Analysis of Energy Efficient Buildings (Case Study: Wisma Kalla Building in Makassar)," *J. Penelit. dan Karya Ilm. Arsit. Usakti*, 2018. [in Bahasa]

[4] R. R. Janis, W. K. Y. Tao, and P. E. Affiliate, *Mechanical and Electrical Systems in Buildings Sixth Edition*, Sixth Ed. New York: Pearson Education, Inc., 2005.

[5] B. Evans, *Daylight in Architecture*. New York: Architectural Record Book McGraw-Hill Book Company, 1981.

[6] L. Darmasetiawan, Christian, and Puspakesuma, *Lighting Techniques and Lamp Layout, Vol. 1*. Jakarta: Gramedia, 1991. [in Bahasa]

[7] J. M. S. A. Thojib, "Visual Comfort Through Natural Lighting In The Office," *J. RUAS*, vol. 11, no. 2, 2013. [in Bahasa]

[8] N. Amin, "Optimization of the Lighting System by Utilizing Natural Light (Case Study of the Lab. Electronics and Microprocessor Untad)," *J. Ilm. Foristek*, vol. 1, no. 1, pp. 43–50, 2011. [in Bahasa]

[9] I. Badan Standarisasi Nasional, "Procedures for Designing Natural Lighting Systems in Buildings," 2001. [in Bahasa]

[10] Soegijanto, *Buildings in Indonesia with a Humid Tropical Climate in Terms of Building Physics*. Jakarta: Direktorat Jenderal Pendidikan Tinggi, 1999. [in Bahasa]

[11] N. Jamala and R. Rahim, *Visual Comfort Theory and Applications*. Makassar: Badan Penerbit Universitas Negeri Makassar, 2017. [in Bahasa]

[12] T. Handayani, "Energy Efficiency in Building Design," *Spektrum Sipil*, vol. 1, no. 2, pp. 102–108, 2010. [in Bahasa]

[13] A. R. Riandito, "Energy Efficiency in the Library Room of the Faculty of Civil Engineering and Planning, Islamic University of Indonesia through Optimization of Natural and Artificial Lighting," Universitas Atma Jaya Yogyakarta, 2012. [in Bahasa]

[14] Pemerintah DKI Jakarta, "DKI Jakarta Government Regulation No. 38 of 2012 concerning Green Buildings." Jakarta, 2012. [in Bahasa]

[15] Pusat Bahasa Indonesia, *Indonesia Dictionary*, 3rd ed. Jakarta: Pusat Bahasa, Departemen Pendidikan Nasional, 2001. [in Bahasa]

EPI International Journal of Engineering
Volume 4, Number 1, February 2021, pp. 75-80
DOI: 10.25042/epi-ije.022021.11

*p*ISSN 2615-5109
*e*ISSN 2621-0541

Air Quality of a Parking Building in Makassar (A Case Study of Bosowa Tower Parking Building)

Nasrul[a,*], Baharuddin Hamzah[b], Rosady Mulyadi[c]

[a]Department of Architecture, Faculty of Engineering, Hasanuddin University. Email: nasrul9891@gmail.com
[b]Department of Architecture, Faculty of Engineering, Hasanuddin University. Email: baharsyah@unhas.ac.id
[c]Department of Architecture, Faculty of Engineering, Hasanuddin University. Email: rosady@unhas.ac.id

Abstract

This study aims to determine the level of air quality in the parking building based on the pollution content in it (CO, CO_2, HCHO and, VOC), to analyze the effect of the weather, intensity of motorized vehicle traffic, and surface elevation to the air quality. The dependent variable is the level of air pollution. The research sample is the Makassar Bosowa Tower Parking Building, data collection was carried out by direct measurement and observation in 12 days from November 24, 2020 till December 17, 2020. The research was done using the comparative method, The data was processed using the Mann-Whitney difference test, and the Spearman correlation test using the SPSS application. The results showed that the average CO levels had exceeded the limit of good air quality, the average of CO_2 levels was still within the limits for good air quality, and the average of HCHO and VOC levels were mostly within the limits for good indoor air quality, according to The Indonesia Minister of Health Regulation Number 1077 in 2011. The result of measurements and tests shows that the changes in the weather do not have a significant effect on the air quality. The amount and the intensity of motorized vehicle traffic affect the air quality, especially during rainy weather.

Keywords: Air quality; motorized vehicle; parking building; pollution; weather

1. Introduction

Indonesia is a tropical country that only has two seasons, namely the rainy season and the dry season [1], Makassar City is still being chosen by various countries to invest in [2], which make Makassar City is one of the cities with rapid development conditions in Indonesia [3].

The major contributor to increasing air pollution in Indonesia is motorized vehicles, considering that from the year 2004 - 2014, there has been a very rapid surge in the number of motorized vehicles, and approximately 70% are distributed in urban areas [4]. Meteorological parameters are also affected pollutant levels in the air, air temperature and humidity are part of meteorological parameters that can affect pollutant levels in the air [5].

Urban areas often have temperatures 1-6 degrees Celsius higher than the surrounding areas (rural areas), this phenomenon is known as an "Urban Heat Island" (UHI) [6]. Part of the building that could be a source of pollution is the parking area, since the parking area is a place for motorized vehicles to pass which is the main cause of pollution in urban areas, from the description above the objective of this study is:

- To determine the level of air quality in the parking building based on the pollution content in it.
- To analyze the effect of the weather on the air quality.
- To analyze the changes in the air quality based on the intensity of motorized vehicle traffic and surface elevation.

2. Study Literature

Good air quality is the air that has a low pollution content, and the levels of air pollution that are important to review in this study are Carbon Monoxide (CO), Carbon Dioxide (CO_2), Formaldehyde (HCHO), and Volatile Organic Compound (VOC).

The main cause of the emergence of Carbon Monoxide (CO) in cars is when the element of oxygen (air), complete combustion does not occur so that the carbon in the fuel does not burn completely. This is due to the imperfect mixing of fuel and air, causing the mixture to be difficult to burn completely or the combustion time is too fast [7].

Causes of increasing of the Carbon Dioxide (CO_2) to levels that can be dangerous, is smoking in the house, numbers of the occupant in the room are very high, and using the fuels material such as charcoal, wood, petroleum, and coal [8]. Formaldehyde (HCHO) is produced by burning carbon-containing materials, in the atmosphere, HCHO is produced from the reaction of sunlight and oxygen to methane and other hydrocarbons in the atmosphere. Formaldehyde can be used to eradicate most bacteria, so it is often used as a disinfectant and also as a preservative [9].

*Corresponding author. Tel.: +62811 989 124
Hasyim Street No. 2 Tamalatea, Jeneponto Regency, Makassar, Indonesia, 92351

Volatile Organic Compound (VOC) is a compound containing carbon, that evaporates at a certain pressure and temperature, or has a high vapor pressure at room temperature, the most commonly known VOCs are solvents, other types of VOCs such as monomers and fragrances, If VOC reacts with Nitrogen Oxide (NOx) and is exposed to sunlight to form ground-level ozone or fog, at certain concentrations in the air, ozone can affect health and the environment [10]. The limit of pollution levels to maintain indoor air quality is shown in Table 1.

Table 1. Chemical requirements for indoor air quality [8]

No	Parameter Type	Unit	Required Rate	Information
1	CO	Ppm	9	8 Hour
2	CO_2	Ppm	1000	8 Hour
3	HCHO	Ppm	0.1	30 Minute
4	VOC	Ppm	3	8 Hour

Indirectly, air temperature also plays a role in the formation of secondary pollutants because solar radiation and air temperature have an interrelated correlation, air temperature can affect the increase in chemical reactions in the atmosphere and result in the formation of fine particulates naturally [11]. Humid air will help the process of deposition of pollutants because, with the humid condition in the air, some pollutants in the form of particles will bind to the water in the air and form larger particles so that they easily settle to the earth's surface by the earth's gravity [12].

3. Research Methods

This research using quantitative method, and process in the quantitative research to find information uses data in form of numbers, to analyze the information about what you want to know [13], and the type of this research is comparative quantitative, where the comparative quantitative is a type of research that intended to find the differences in the studied variables [14].

The object of this study is the Makassar Bosowa Tower Parking Building, because Makassar City is one of the main growth centers in Indonesia, and also because the Bosowa Makassar Tower is the building with the largest office function in Makassar City, so the number of building users is very large according to the work hour, and consistently every week.

The Makassar Bosowa Tower parking building consists of six floors, each floor is divided into two (split floors), where each floor is an area for parking for four-wheeled vehicles/cars and is located separately from the main building of the Makassar Bosowa Tower. The placement of the measuring point is in the center of each floor in the measurement area, it is expected to be able to take the average value of air quality over the entire floor area, by determining the measuring point in the Split Floor Upper-Level area. The minimum height of the measuring instrument is at a height of 0.5 meters from the floor surface [15], and the measuring instrument is placed at that height.

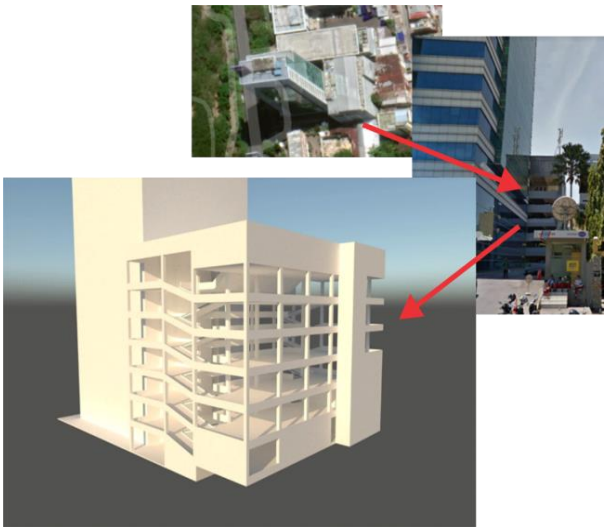

Figure 1. Makassar Bosowa Tower Parking building

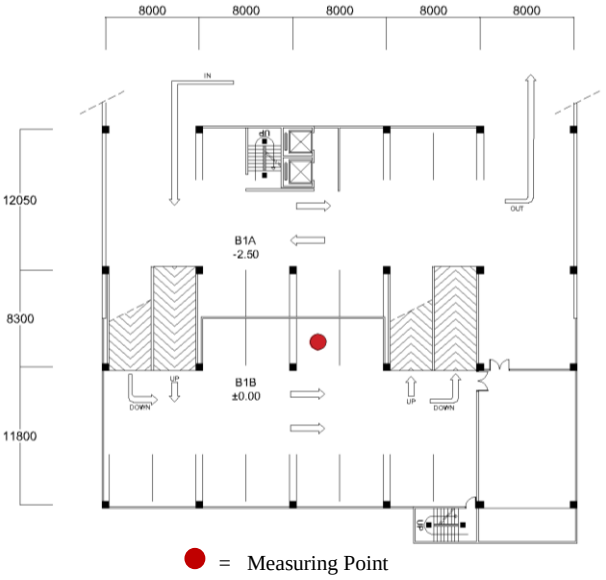

Figure 2. Makassar Bosowa Tower Parking building

Data was collected by direct measurement and observation in 12 days from November 24, 2020 till December 17, 2020 in two different types of weather which six-day when the sunny day and also six-day when the rainy day, and to measure the level of air pollution an "Air Quality Detector" is used, and to measure the air temperature and humidity a "Thermo Hygrometer HTC-1" is used.

a b

Figure 3. (a) Air quality detector; (b) Thermo Hygrometer HTC-1

Table 2. Research variables and indicators

Variable	Definition	Indicator
Air Quality (Y)	Air quality is determined based on the content of pollution levels, where the better the air quality, contain less pollution.	1. Carbon Monoxide (CO) levels shouldn't pass 9 PPM (particles per meter) in 8 hours 2. Carbon Dioxide (CO_2) shouldn't pass 1000 PPM to achieve a comfortable indoor state 3. Formaldehyde (HCHO) shouldn't pass 0.1 PPM for 30 minutes 4. Volatile Organic Compound (VOC) shouldn't pass 3 PPM for 8 hours
Weather Changes (X)	Analyze changes in air pollution levels based on changes in the weather under review, namely sunny weather and rainy weather	1. Changes in air pollution levels during sunny weather (air temperature increases and air humidity decreases) 2. Changes in air pollution levels During rainy weather (air temperature decreases and air humidity increases)
Number of Vehicles (Z1)	Analyze changes in air pollution levels based on the number of vehicles in the parking area and the intensity of passing vehicles	1. Changes in air pollution levels based on the number of vehicles parked 2. Changes in air pollution levels based on the intensity of passing vehicles
Surface Altitude (Z2)	Analyze changes in air quality based on differences in surface elevation (height ±0.00 Meters is the ground floor of the building)	Changes in air pollution levels at each different surface height of the parking area (Altitude ±0.00, +5.00, +10.00, +15.00, +20.00, +25.00 Meters)

The dependent variable (Y) in this study is the concentration of CO, CO_2, HCHO, and VOC, to determine the air quality, the independent variable (X) in this study is the weather changes from a sunny day, to a rainy day, Intervening variable (Z) in this study is the effect of motorized vehicles and surface height, explanation about the variable indicator can be seen at Table 2.

4. Result and Discussion

4.1. Measurement results

Measurements of air pollutant levels, namely Carbon Monoxide (CO), Carbon Dioxide (CO_2), Formaldehyde (HCHO), and Volatile Organic Compound (VOC), were carried out on each floor at an altitude of ±0.00, +5.00, +10.00, +15.00, +20.00 and +25.00 Meters based on the building level, and carried out when the weather is sunny and rainy with each measurement result can be seen in Fig. 4.

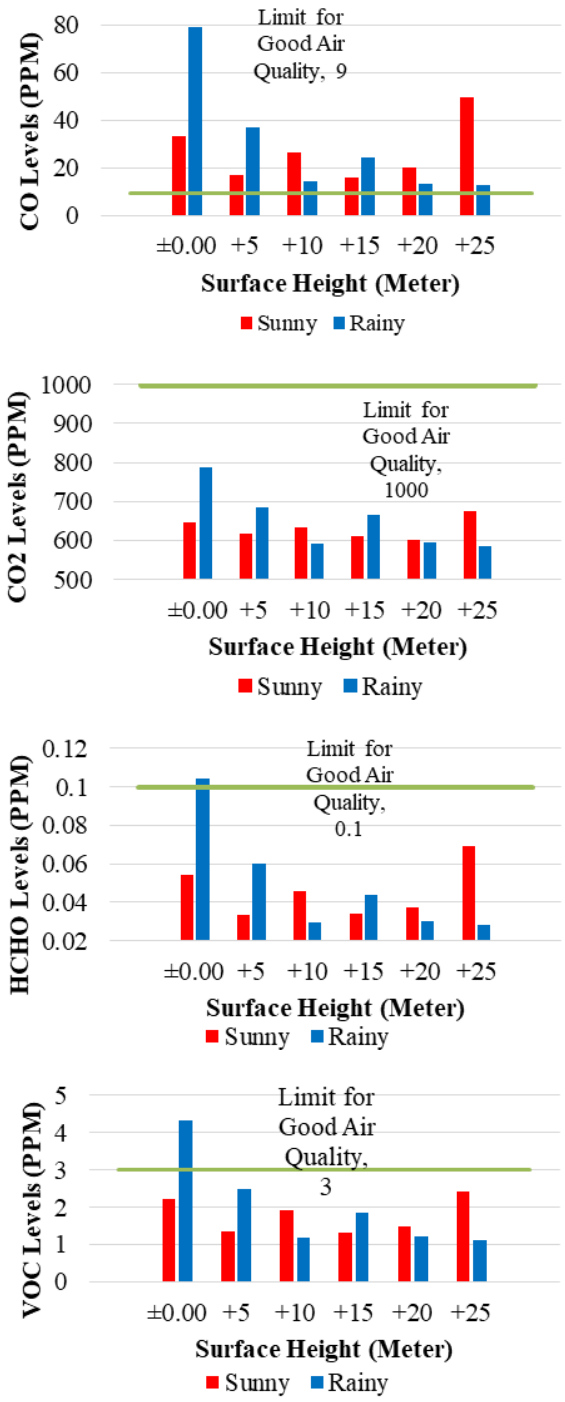

Figure 4. Average pollution levels in the Makassar Bosowa Tower Parking Building

Measurements of air temperature and humidity were carried out on each floor, were carried out on each floor at an altitude of ±0.00, +5.00, +10.00, +15.00, +20.00, and +25.00 Meters based on building level, and were carried out during sunny and rainy weather with each measurement result can be seen in Fig. 5.

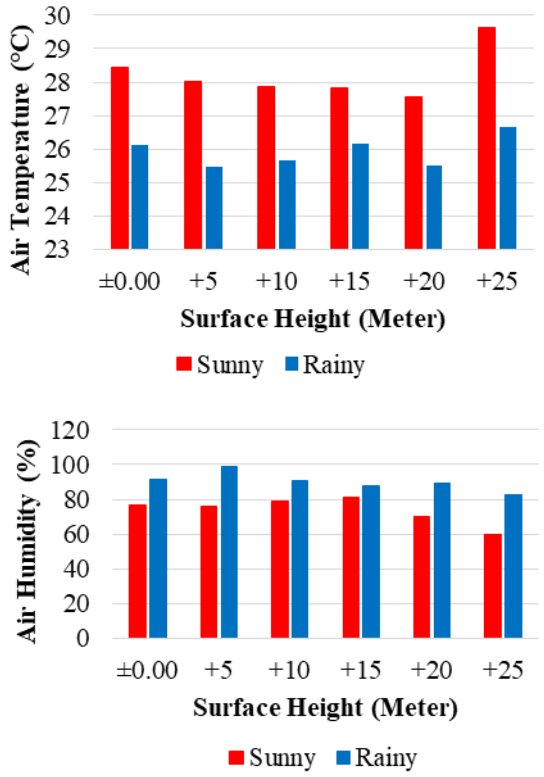

Figure 5. Air temperature and humidity measurement at the Makassar Bosowa Tower Parking Building

Figure 6. HVAC exhaust pipe in Makassar Bosowa Tower Parking building

The measurement shows that when the weather is sunny, the highest air pollution level is at an altitude of +25.00 meter, because at that altitude is an area close to the HVAC exhaust pipe from the Makassar Bosowa Tower, which operates optimally when the weather is sunny, The average level of air pollution that exceeds the limit for good air quality is only found in Carbon Monoxide (CO), this happens because the parking building is a place for motorized vehicles to pass which is the main source of CO.

Dangerous pollution such as Carbon Monoxide, Carbon Dioxide, Volatile Organic Compound, can be created from daily human activities, some building materials, and household products is a major source of indoor pollution, such as Formaldehyde, Benzene, Ethyl Benzene, Toluene, Xylene, and Styrene [16], these substances are pollutants that released from the exhaust fan, to maintain air quality inside the main building of Makassar Bosowa Tower.

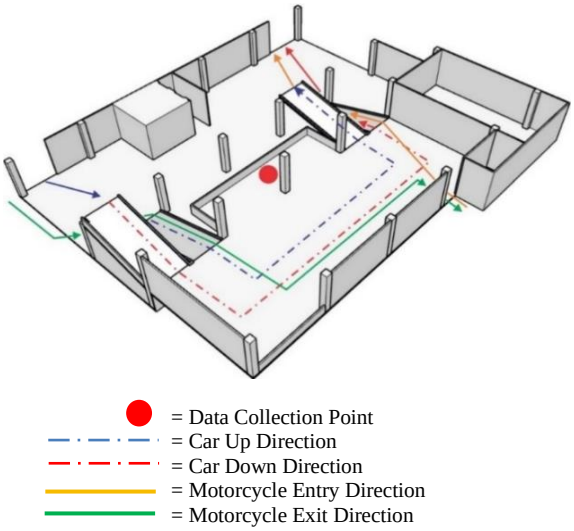

Figure 7. Vehicle flow at an altitude ±0.00 at the Makassar Bosowa Tower Parking building

During rainy weather, the highest air pollution level is at an altitude of ±0.00 meters (CO=78.98 PPM, CO_2=788.25 PPM, HCHO=0.1 PPM, VOC=3.98 PPM), because at that altitude is an area with a high intensity of vehicular traffic, because it is not only traversed by four-wheeled vehicles, but also by two-wheeled vehicles, and during the rainy weather air humidity increases (>80%), where air humidity can precipitate air pollution, resulting in average levels of HCHO and VOC at an altitude of ±0.00, exceeding the limit for good air quality.

4.2. Effect of weather changes on the air quality

In this research, data were collected in different weather conditions, which is sunny and rainy, to find out if there was a change in air pollution levels in two different weather conditions, the "Mann Whitney" test was carried out, with the "Mann Whitney" equation and the results obtained are as follows.

$$U_1 + U_2 = R_1 - \frac{n_1(n_1+1)}{2} + R_2 - \frac{n_2(n_2+1)}{2} \quad (1)$$

Based on the test results, it shows that the significance value of each level of air pollution based on weather changes, all of them show values above 0.05 (sig. > 0.05), where the significance value of Carbon Monoxide (CO) is 0.753, Carbon Dioxide (CO2) is 0.139, Formaldehyde (HCHO) is 0.859, and Volatile Organic Compound (VOC) is 0.890, so generally the weather changes does not affect the air quality, therefore, a more in-depth study of changes from the air temperature and humidity to the air pollution.

Table 3. Mann Whitney test result of the effect of weather changes on the air pollution

	Test Statistics*			
	CO	CO_2	HCHO	VOC
Mann-Whitney U	42575	40171	42853	42933
Wilcoxon W	85940	83536	86218	86298
Z	-.315	-1.479	-.177	-.139
Asymp. Sig. (2-tailed)	.753	.139	.859	.890

*Grouping variable: Weather

Weather changes will affect the temperature and humidity, because when the sunny weather, the air temperature will increase and the humidity will decrease, and vice versa, to determine the correlation between levels of air pollutants (CO, CO_2, HCHO, and TVOC) with temperature and air humidity, a test was carried out, called "Spearman" correlation test, where the "Spearman" correlation test equation and the results obtained are as follows.

$$r_s = \rho_{rgX,rgY} = \frac{\mathrm{cov}(rgX, rgY)}{\sigma rgX \, \sigma rgY} \quad (2)$$

The correlation value according to Young [17] is categorized as follows:

- < 0.2, is either positive or negative, the correlation is negligible or very weak
- 0.2 – 0.4, either positive or negative, low or weak correlation
- 0.4 – 0.7, both positive and negative, a strong correlation
- 0.7 – 0.99, both positive and negative, high correlation, very strong
- 1, both positive and negative, perfect correlation

Based on the test results, it shows that air temperature does not affect air pollution levels (CO, CO_2, HCHO, and VOC), air humidity levels almost have no effect on all of the air pollution levels except for CO_2 levels, where CO_2 levels have a very weak and even negligible correlation, which is 0.132 and has a positive correlation, which means that if the air humidity increases, the CO_2 level will also increase.

4.3. Effect of motorized vehicle and surface height on the air quality

Details about vehicle capacity, vehicle units that making reservations, and vehicle traffic in each parking area at different surface heights, on the Makassar Bosowa Tower Parking Building can be seen in Table 5.

Table 4. Spearman correlation test results of correlation between air temperature and humidity with air pollution levels

	CO	CO_2	HCHO	VOC
Air Temperature	0.049	-0.007	0.045	0.045
Air Humidity	0.016	0.132**	0.031	0.03

**Correlation is significant at the 0.01 level (2-tailed).

Table 5. Number, average occupancy, and intensity of motorized vehicle traffic

Surface Height	Vehicle Capacity (Unit)	Reservation (Unit)	Average Occupancy	Average Trafic Intensity
±0.00	15	15	Full	Very High
±5.00	24	8	Full	High
±10.00	26	10	Full	High
±15.00	28		3/4 Filled	High
±20.00	28		1/2 Filled	Low
±25.00	28		1/4 Filled	Very low

Table 6. Spearman correlation test results of surface altitude to air pollution levels in different weather

	CO	CO_2	HCHO	TVOC
Sunny	-0.019	-0.07	-0.01	-0.013
Rainy	-0.253**	-0.329**	-0.238**	-0.24**

**Correlation is significant at the 0.01 level (2-tailed)

The table above shows that the higher the surface height at a parking area, the number of vehicles and the intensity of vehicle traffic will decrease, this is following the results of measurements of the Carbon Monoxide (CO), where the higher the surface elevation, the CO levels will decreases, except on sunny days at an altitude of +25.00 meters, where CO levels are very high, due to the operation of the HVAC exhaust system from the Makassar Bosowa Tower.

Surface altitude will affect air quality because it is influenced by the number and intensity of motorized vehicle traffic, therefore the correlation between surface height and air pollution levels is tested using the "Spearman" correlation test, with results that can be seen in Table 6.

Based on Table 6, it can be seen that when the day is sunny, the surface elevation does not correlate with the level of air pollution, this condition occurs because the HVAC operating system in the building reduces the effect of differences in surface height on air quality. During the rainy day, surface elevation correlates with all levels of air pollution, although the correlation is weak (0.2 – 0.4), and the correlation is negative, which mean that if the surface elevation increase, the air pollution levels will decrease.

5. Conclusion

The air quality in the Makassar Bosowa Tower Parking Building when viewed from the pollutant Carbon Monoxide (CO), as a whole has been exceeded the limit of good air quality for humans (> 9 PPM). Overall levels of Carbon Dioxide (CO_2) are still within the limits for good and safe air quality for human habitation because they are still below 1000 PPM. The levels of Formaldehyde (HCHO) and Volatile Organic Compound (VOC), most showed that the average level was already at a safe level, except at an altitude of ±0.00 Meters which had passed the safe level (>0.1 PPM for HCHO and >3 PPM for VOC). There is no effect from weather changes on the air quality, in terms of changes in air pollution (CO, CO_2, HCHO, and TVOC). The results from the test on changes in air temperature and humidity, to the air pollution levels, only found a very weak positive correlation, between Air Humidity and CO_2 levels.

Results from the observations during rainy weather show that the higher the parking area, the number and intensity of vehicle traffic will decrease, according to the analysis results which show that the higher the building surface, the pollution content from the vehicle decreases. When the weather is sunny, the HVAC exhaust pipe operates optimally, so that increasing the level of air pollution, especially at an altitude of +25.00 meters in the Makassar Bosowa Tower Parking Building, even though the vehicle traffic is very low in the parking area.

References

[1] N. D. Rahayu, B. Sasmito, and N. Bashit, "Analysis of the Effect of the Indian Ocean Dipole (IOD)Phenomenon on the Java Island Rainfall.," *Geod. Undip J.*, vol. 7, no. 1, 2018. [in Bahasa]

[2] Ronalyw, "Canadian Investors are Interested in Makassar," 2019. [Online]. Available: https://beritakotamakassar.fajar.co.id/berita/2019/08/28/investorkanada-lirik-makassar. [Accessed: 11-Jul-2020]. [in Bahasa]

[3] H. Suyanto, "Urban Air Quality Management," *Gema Teknol.*, vol. 16, no. 2, 2011. [in Bahasa]

[4] Ismiyati, D. Marlita, and D. Saidah, "Air Pollution Due to Motor Vehicle Exhaust Emission," *Manaj. Transp. Logistik J.*, vol. 1, no. 3, 2014. [in Bahasa]

[5] D. B. Istantinova, M. Hadiwidodo, and D. S. Handayani, "Effect of Wind Speed, Humidity and Air Temperature on Concentration of Sulfur Dioxide (SO2) Pollutant Gas in Ambient Air around PT. Inti General Yaja Steel Semarang," *Manaj. Transp. Logistik J.*, vol. 1, no. 3, 2013. [in Bahasa]

[6] H. A. Belgaman, S. Lestari, and H. Lestari, "Urban Heat Island Study and Its Relation to Changes in Climate Temperature Parameters and Rainfall Using Landsat TM Satellite Imagery Case Study of DKI Jakarta and Surrounding Areas.," *Sains Teknol. Modif. Cuaca J.*, vol. 13, no. 1, 2012. [in Bahasa]

[7] A. R. Mohamed, T. L. Keat, and I. Dahlan, *Introduction to the Air Pollution*. Malaysia: University Sains Malaysia, 2015. [in Melayu]

[8] Indonesia Minister of Health, "Regulation No. 1077 Concerning Guidelines for Indoor Air Sanitation," 2011. [in Bahasa]

[9] R. R. Tangdiongga, L. C. Mandey, and F. Lumoindong, "Chemical Analysis of Formaldehyde in Melamine Tableware by Visible Light Spectrophotometry," *Ilmu dan Teknol. Pangan J.*, vol. 3, no. 1, 2015. [in Bahasa]

[10] Ismail, "Volatile Organic Compound," 2011. [Online]. Available: www.healthsafetyprotection.com. [Accessed: 01-Mar-2021]. [in Bahasa]

[11] A. D. R. Marhaeni, "Effect of Meteorological Factors on Fluctuations in PM10 and O3 Concentrations in DKI Jakarta.," Bogor Agricultural University, 2018. [in Bahasa]

[12] K. Prabowo and M. Burhan, *Healthy Air*. Indonesia, 2018.

[13] M. Kasiram, *Research Methodology: Reflection on the Development of Understanding and Mastery of Research Methodology*. Malang: UIN Malang Press, 2008. [in Bahasa]

[14] S. Awwaabiin, "Quantitative Research: Definition, Purpose, Types and Steps to Do It.," 2021. [Online]. Available: www.penerbitdeeppublish.com. [Accessed: 17-May-2021]. [in Bahasa]

[15] J. Waeytens and S. Sadr, "Computer-aided Placement of air quality using adjoint framework and sensor features to localize indoor source emission," *Build. Environ.*, vol. 144, 2018.

[16] A. Abdullah, "Monitoring of Air Ducting Using Mechanical Robot for Indoor Air Quality (IAQ) Improvement," Universiti Tun Hussein Onn Malaysia, 2013.

[17] C. Trihendradi, *Step by Step SPSS 16 Statistical Data Analysis*. Yogyakarta: Andi Offset, 2009. [in Bahasa]

EPI International Journal of Engineering
Volume 4, Number 1, February 2021, pp. 81-92
DOI: 10.25042/epi-ije.022021.12

*p*ISSN 2615-5109
*e*ISSN 2621-0541

The Artificial Lighting Analysis of Study Rooms in Dormitories and Classrooms Islamic Boarding School of Lil Banat Parepare

Ni'mah Natsir[a,*], Nurul Jamala[b], Asniawaty Kusno[c]

[a]Department of Architecture, Faculty of Engineering, Hasanuddin University, Makassar. Indonesia. Email: nimahna15@gmail.com
[b]Department of Architecture, Faculty of Engineering, Hasanuddin University, Makassar, Indonesia. Email: nuruljalama@yahoo.com
[c]Department of Architecture, Faculty of Engineering, Hasanuddin University, Makassar, Indonesia. Email: kusno_asniawaty@yahoo.com

Abstract

This study aims to determine the light intensity in the study room of the DDI Lil Banat Islamic boarding school in Parepare. Measurements were taken in classrooms and dormitories. The type of research used is quantitative with the simulation method. The dependent variable with the measurement of exposure is light intensity. While the independent variables are the arrangement of lighting points and the layout of the study room. Measurements were carried out for three days using a digital lux meter. The measurement results show that the light intensity in the dormitory has not met the Indonesian National Standard for study rooms both day and night. During the day the classroom meets the Indonesian National Standard but not at night. Although students as room users feel comfortable with the light intensity conditions in the study room and can study according to these conditions, students still feel some complaints in the form of sore eyes, eye strain and difficulty focusing. Therefore, researchers make recommendations for study room designs that can make students more comfortable studying in dormitories and classrooms so that they can reduce complaints while studying. Lighting design recommendations are made in several alternatives by increasing the number of lamps and changing lamp types using Dialux simulation. The simulation results of the study room lighting design recommendations have met the usage standards so that they can be applied to dormitories and classes at the DDI Lil Banat Islamic Boarding School in Parepare.

Keywords: Artificial lighting design; light intensity; study room

1. Introduction

Lighting has a very important role in architecture, both in supporting the function of space and the activities of the space, create aesthetic visual images, and creating comfort and security for space users [1]. In planning a building, lighting design is a very important thing to note, because the activities of space users affect the distribution of light in space. Light distribution not only serves to make a visual object clearly visible, but also serves to evoke visual comfort that psychically affects the resilience of space users in maintaining their performance [2]. Basically in designing space lighting, an architect will refer to the standard recommendations of illumination [3].

Lighting that is too bright will make the space user feel awake and very active. While the dim lighting creates a sense of relaxation may even be sleepy. This is a psychological effect in the physical form of lighting. The atmosphere of space can be created from the color and intensity of its light [4].

In the learning process that requires thoroughness in the absence of adequate lighting, the impact will be very pronounced on eye fatigue, the occurrence of eye muscle fatigue and eye nerve fatigue as a result of continuous stress on the eyes, although it does not cause damage to the eyes permanently, but the impact can increase workload, accelerate fatigue, loss of work time, interfere with concentration and decrease work productivity.

Learning is an activity that in the process supports high concentration. A comfortable place and learning environment make it easy for students to concentrate. By preparing the right environment, students will get better results and can enjoy the learning process carried out [5]. The Islamic boarding school environment, both schools, dormitories and mosques, must be designed as well as possible to facilitate students in the implementation of teaching and learning.

The current trend of building schools that implement a residential or boarding system, Islamic boarding school or tahfidz schools that require comfortable facilities, especially classes and dormitories as places for various activities, guiding the role of researchers to examine classrooms and dormitories in terms of lighting in order to maximize the function of space as a place to rest at once a place to learn.

*Corresponding author. Tel.: +62812 4506 4415
Pemuda Street No.16, Makassar, Sulawesi Selatan Indonesia

Islamic boarding school of DDI Lil Banat is one of the boarding school in the city of Parepare which has a dormitory. After conducting initial research through interviews of several students and measuring the lighting in the dormitory, the results indicated that there was discomfort in the learning activities of the students in the dormitory due to the unfavorable conditions of the hostel. Some things that result in less conducive conditions include poor lighting and ventilation. This is evidenced by making initial measurements using the Light Meter application, the average lighting in the dormitory is 168 lx. One example of a dormitory with only 2 lights in a room measuring 8.5m x 7.5m.

Based on this, the researcher intends to conduct research on the lighting of the study room, in this case, the class and dormitory at the Islamic Boarding School of DDI Lil Banat to find out whether the dormitory lighting system meets the Indonesian National Standard (SNI) and whether the effect of learning room lighting on students' learning activities. This research is expected to contribute to future researchers who will raise a similar theme and can be input for the parties involved in this research.

2. Literature Review

2.1. Lighting

Lighting is one of the factors to get a safe and comfortable environment and is closely related to human productivity. Good lighting allows people to see the objects they are working on clearly and quickly. Good lighting affects the quantity and quality of vision. Adequate lighting gives the impression of better scenery and refreshing environmental conditions [6]. Inadequate lighting creates additional physical or psychological burdens for space users. This can cause eye fatigue with symptoms such as decreased eye acuity, double/blurred vision, pain around the eyes and errors in work or work accidents [7]. According to the source, lighting can be divided into:

a. Natural Lighting

Natural lighting is a source of lighting that comes from sunlight. Natural rays have many advantages, besides saving electrical energy, they can also kill germs. To get natural lighting in a room, large windows or glass walls are required at least 1/6 of the floor area.

b. Artificial Lighting

Artificial lighting is lighting produced by light sources other than natural light. Artificial lighting is needed when the position of the room is difficult to reach by natural lighting or when natural lighting is insufficient. Artificial lighting or also known as artificial lighting is the second-largest energy consumer after air conditioning [8]. Electrical lighting in a building must be able to create ambient, accent space and objects, support the performance of certain work according to the function of space and expose decorative features [9]. The standard lighting level for educational institutions issued by SNI03-6575-2001 is 250 lx for classrooms, 120-250 lx for bedrooms, 300 lx for libraries, 350 lx for computer and workrooms, 500 lx for laboratories, and 750 lx for drawing space (using additional local lighting on the drawing table).

c. The Effect of Lighting on the Study Room

Light is an important element for seeing, therefore the amount of light received by the eye must be sufficient, neither less nor excess. Excess or lack of light can affect a person psychologically and physiologically. Poor quality of classroom lighting can cause drowsiness, lack of enthusiasm, and difficulty focusing on subjects [10]. In some conditions, it was found that the study room was not in accordance with the lighting standard, but the room users still felt comfortable in learning. Several studies on lighting show that the lighting design of the library reading room is not in accordance with the illumination standard recommended by SNI 03-6575-2001, namely 250 lx, but visitors can still do their activities properly [11].

2.2. Study room

In receiving and digesting lessons students need an environment atmosphere and conducive learning conditions. The atmosphere of the learning environment is neatly organized so that it supports students to receive and digest the subject matter taught by the teacher. Conducive learning room conditions must meet the criteria: good lighting, fresh air exchange, blinding wall coloring, good and neat condition of facilities and infrastructure, cleanliness of the study room [12].

a. Classroom

The classroom as a study room is a room that is bounded by walls, or bulkheads, and used as a place to learn to teach. There are several principles that need to be considered by teachers in organizing the physical environment of the class, namely: Visibility (Flexibility of Views), Accessibility (easy to achieve), Flexibility (Flexibility), comfort and beauty [13].

b. Dormitory

Dormitory is a type of housing that is permanent and has distinctive characters. Usually, a dormitory is always in contact with educational institutions. The activities in the dormitories are learning, sleeping and socializing.

2.3. Islamic boarding school

Pondok pesantren is a series of words consisting of pondok and pesantren. The word Pondok (room, hut, small house) is used in Indonesian, emphasizing its simplicity. Pondok comes from Arabic funduuq (فندوق) which means inn. a simple dormitory or guesthouse, because the cottage is indeed a simple shelter for students/santri who are far from their place of origin [14]. In terminology, Islamic boarding school is an Islamic education institution with a

boarding or boarding system where the chaplain is the central figure, the mosque is the center of the activity that animates it, and the teaching of Islam under the guidance of chaplain is followed by students as its main activity [15].

3. Research Methods

3.1. Research sites

The research are located in one of the cities in South Sulawesi shown in Figs. 1, namely the city of Parepare, which has an area of 99.33 km² and a population of ± 140,000 people. The city of Parepare is located on a bay overlooking the Makassar Strait. In the north it is bordered by Pinrang Regency, in the east, it is bordered by Sidenreng Rappang Regency and in the south, it is bordered by Barru Regency [16].

The research location is in Soreang District, precisely in Ujung Lare Village, Abubakar Lambogo street Number 53 shown in Fig. 2. Islamic boarding school of DDI Lil Banat Kota Parepare has a land area of 35,000 m² and a building area of 6,000 m². The status of the building itself belongs to the foundation consisting of school buildings, offices, halls, libraries, laboratories, dormitories, teacher housing, canteen, mosque and poskestren (pos boarding school health) [17].

3.2. Types of research

The used in this research is quantitative, using simulation methods. This research also uses the Positivism paradigm, the existing reality will be studied to test the hypothesis so that the results will be certain. This type of research is based on data collected during the study which is analyzed and then described or described based on standards or theories and related literature.

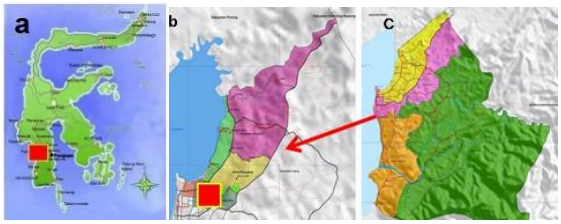

Figure 1. (a) Map of Sulawesi (b) Map of Soreang District (c) Map of Parepare City

Figure 2. Map of research locations, dormitory complex

a. Population and sampling techniques

The population in this study were all classes and dormitories with simple conditions used by the students while in the boarding school area. The sampling technique in this determination uses a non-probability sampling technique. For sampling using a purposive sampling method. The samples were chosen were dormitory Fatimah 1, Aisyah 1, Khadijah 2, Aminah 1, Hafsah 1, Maemunah 1, class XI IPS and VIII B.

b. Data collection technique

To have this research more focused, and based on the problem formulation that has been described, the data collection techniques used namely: observation, study of literature, documentation, measurement of light intensity in the study room, questionnaires and simulation.

3.3. Data analysis technique

This research is a quantitative analysis with descriptive statistics. The descriptive static analysis technique used in this research is the presentation of data in a visual form such as histograms, polygons, bar charts, pie charts and pastel diagrams (pie charts).

4. Discussion

4.1. Measurement results of the intensity of tubes lighting classrooms in Islamic Boarding School of DDI Lil Banat

Measurement of light intensity is divided into 8 classrooms are boarding Fatimah 1, dorm Aisyah 1, dorm Khadijah 2, dorm Aminah 1, dorm Hafsah 1, dorm Maemunah 1, classroom XI and clasroom VIII B.

Measurements using the Lux Meter are carried out in 4 times to represent the time of morning, afternoon, evening and night for 3 consecutive days, namely 15-17 September 2019. Morning 09.00 - 11.00 GMT +8, noon 12.00-14.00 GMT +8, afternoon 16.00-18.00 GMT +8 and night at 20.00-22.00 GMT +8. The following are the results of measuring the intensity of lighting in the learning room Islamic boarding school of the DDI Lil Banat Parepare

a. Fatimah 1 Dormitory

Fatimah 1 has a room size of 8 meters long and 7 meters wide inhabited by 20 students, has front (north) and rear (south) ventilation so that cross ventilation can occur in the room this, while there are only 2 lamps. This room has 12 measuring points, consisting of measuring points near the opening and under the lamp. Measuring points that are close to the openings towards the north are points A3, B3, C3 and D3, measuring points that are close to the south opening, namely points A1, B1, C1 and D1, while the measuring points that are close to the lights are point A2, B2, C2 and D2.

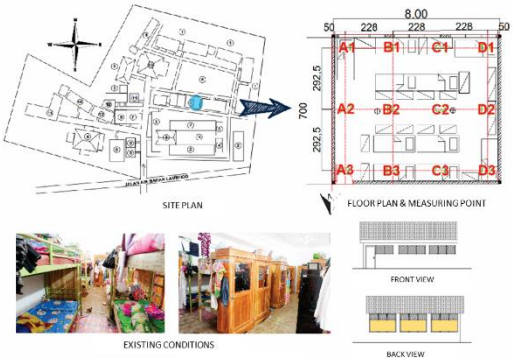

Figure 3. General overview of Fatimah 1 dormitory

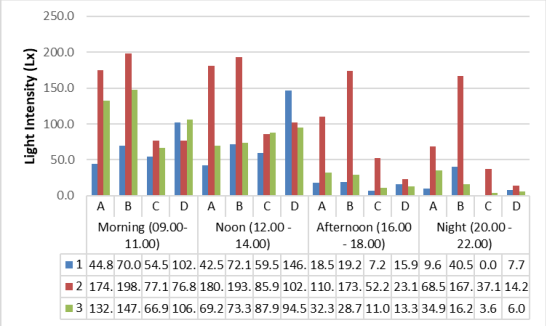

	A	B	C	D	A	B	C	D	A	B	C	D	A	B	C	D
	Morning (09.00-11.00)				Noon (12.00 - 14.00)				Afternoon (16.00 - 18.00)				Night (20.00 - 22.00)			
1	44.8	70.0	54.5	102.	42.5	72.1	59.5	146.	18.5	19.2	7.2	15.9	9.6	40.5	0.0	7.7
2	174.	198.	77.1	76.8	180.	193.	85.9	102.	110.	173.	52.2	23.1	68.5	167.	37.1	14.2
3	132.	147.	66.9	106.	69.2	73.3	87.9	94.5	32.3	28.7	11.0	13.3	34.9	16.2	3.6	6.0

Figure 4. Measurement results of Fatimah 1 dormitory

The results of measuring the light intensity of the Fatimah 1 dormitory for 3 days at 4 different times from 09.00 - 22.00 GMT +8 can be seen in Fig. 4 of the measurement results of the Fatimah 1.

The highest light intensity at point B2 is good in the morning, day, evening, or night, this is because point B2 is close to the lights, so the intensity is higher than the other points. While the lowest point is point C1 because the point is far from lights and openings so that it gets less light from both lights and sunlight from outside the room.

The results of the above measurements then made the average light intensity at Fatimah's dormitory for 3 days at 4 different times.

The highest average measurement result at point 2 (which is in the middle of the room) during the day is 140.4 lx when compared to the Indonesian national standard, namely 250 lx, it is concluded that the lighting of Fatimah 1 dormitory for the study room has not met standard.

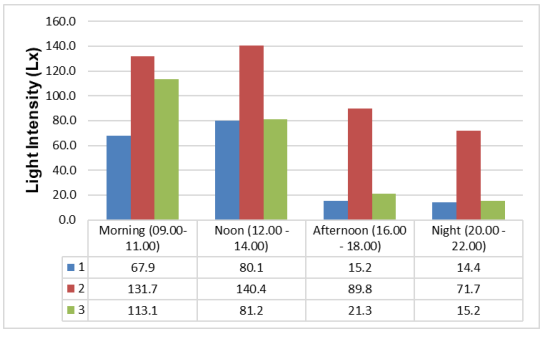

	Morning (09.00-11.00)	Noon (12.00 - 14.00)	Afternoon (16.00 - 18.00)	Night (20.00 - 22.00)
1	67.9	80.1	15.2	14.4
2	131.7	140.4	89.8	71.7
3	113.1	81.2	21.3	15.2

Figure 5. Average measurement of Fatimah 1 dormitory

Figure 6. General overview of Aisyah 1 dormitory

b. Aisyah 1 Dormitory

Aisyah 1 Dormitory has a room size of 8 meters long and 7 meters wide inhabited by 18 students. has front (north) and rear (south) ventilation so that cross ventilation can occur in the room, while there are only 2 lamps. This room has 12 measuring points, consisting of measuring points near the opening and under the lamp. Measuring points that are close to openings towards the north or in front of the building, namely points A3, B3, C3 and D3, measuring points that are close to the openings towards the south or behind the building, namely points A1, B1, C1 and D1, while the measuring points are near with lamps namely points A2, B2, C2 and D2.

The results of measuring the light intensity of aisyah 1 dormitory for 3 days in 4 different times from 09.00 - 22.00 GMT +8 as shown in Fig. 7 the graph of the measurement results of Aisyah's dormitory 1 figure. The highest light intensity is at point B2 in the morning, day, evening, or night, this is because point B2 is close to the lights, so the intensity is higher than the other points. While the lowest point is point D1 because the point is far from the lamp, even though it is close to the opening, there is a barrier in the form of a cupboard so that it gets less light from both lights and sunlight from outside the room.

The results of the above measurements are then made the average light intensity at Aisyah 1's dormitory for 3 days at 4 different times in the graph in Fig. 8.

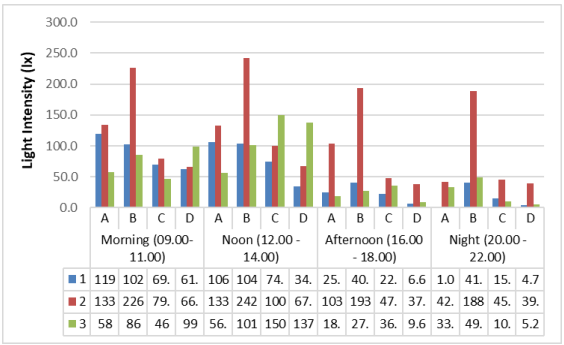

	A	B	C	D	A	B	C	D	A	B	C	D	A	B	C	D
	Morning (09.00-11.00)				Noon (12.00 - 14.00)				Afternoon (16.00 - 18.00)				Night (20.00 - 22.00)			
1	119	102	69.	61.	106	104	74.	34.	25.	40.	22.	6.6	1.0	41.	15.	4.7
2	133	226	79.	66.	133	242	100	67.	103	193	47.	37.	42.	188	45.	39.
3	58	86	46	99	56.	101	150	137	18.	27.	36.	9.6	33.	49.	10.	5.2

Figure 7. Measurement results of Aisyah 1 dormitory

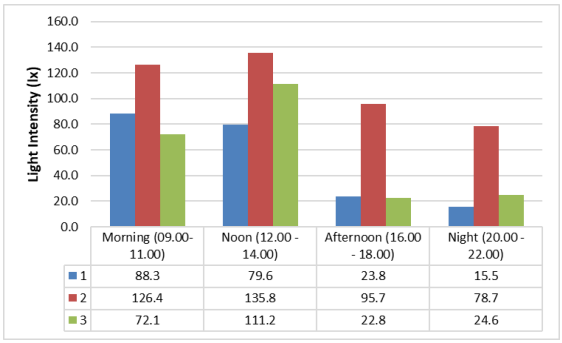

Figure 8. Average measurement results for aisyah 1 dormitory

Average of the highest measurement results during the day at point 2 (in the middle of the room) 135.8 lx, but if it is compared to the Indonesian national standard of 250 lx, it is concluded that the lighting of the Aisyah 1 dormitory for the study room does not meet the standard.

c. Khadijah 2 Dormitory

Khadijah 2 has a length of 13 meters and a width of 10.7 meters inhabited by 22 students. has 2 window openings (west direction) and rear ventilation (east direction), so cross ventilation cannot occurs in this room, while the number of lights there are only 2 lights. This room has 16 measuring points, consisting of measuring points near the openings and those under the lights. The measuring points that are close to the opening to the west are A4 and D3 points, while the measuring points that are close to the lights are B2, B3, C2 and C3.

The results of measuring the light intensity of Khadijah 2 Dormitory for 3 days in 4 different times from 09.00 - 22.00 GMT +8 as shown in Fig. 10 of the measurement results of the Khadijah 2. The highest light intensity is at point B2 and B3 both in the morning, afternoon, evening, or night, this is because points B3 and B2 are close to lights, so their intensity is higher than other points. While the lowest point is point D3 because the point is far from lights and openings so that it gets less light from both lights and sunlight from outside the room.

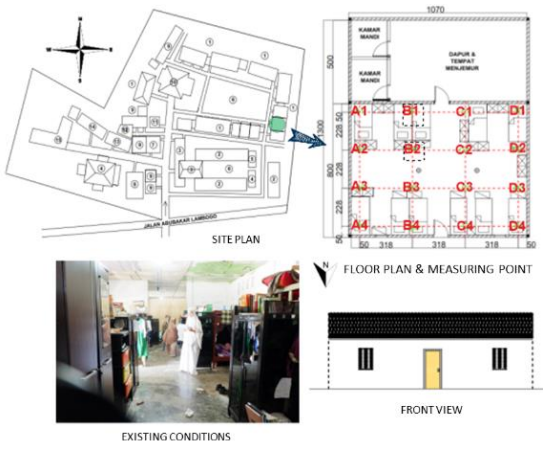

Figure 9. General overview of Khadijah 2 dormitory

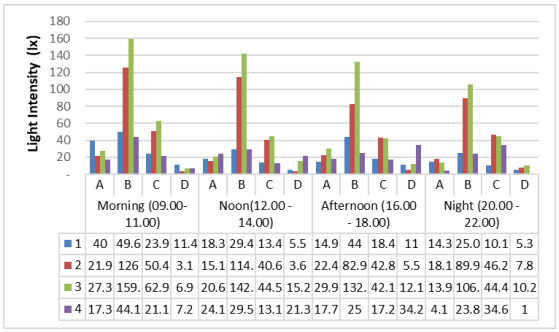

Figure 10. Measurement results of khadijah 2 dormitory

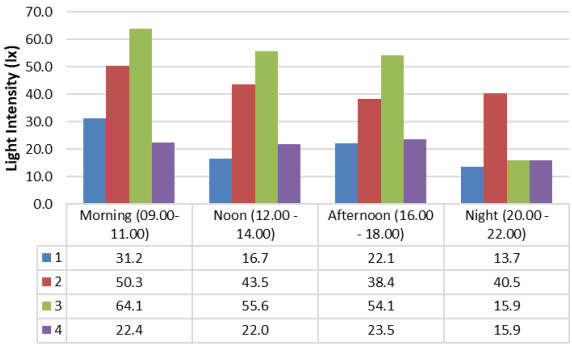

Figure 11. The average measurement of Khadijah 2 dormitory

The results of the above measurements then made the average light intensity at the khadijah 2 hostel for 3 days at 4 different times in the graph in Fig. 11. The average measurement result of the highest at point 3 (which is in the middle of the room) in the morning is 64.1 lx, but when compared to the Indonesian national standard of 250 lx, it is concluded that the lighting of the khadijah dormitory for the study room has not met the standards.

d. Aminah 1 Dormitory

Aminah dormitory has a room size of 6.7 meters long and 7.35 meters wide inhabited by 19 students, has window openings (west direction) and rear ventilation (east direction) in the kitchen, so cross ventilation cannot occurs in this room, while the number of lights are only 2 lights.

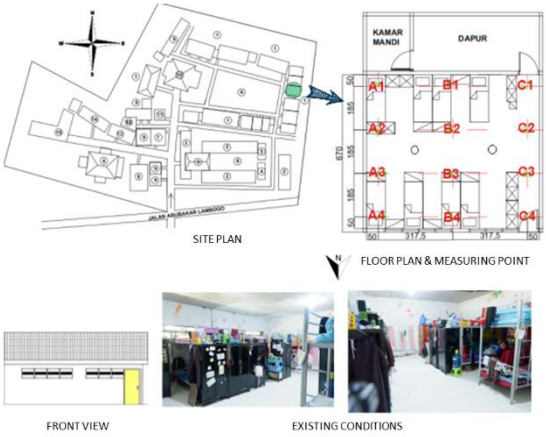

Figure 12. General overview of *Aminah 1* dormitory

This room has 12 measuring points, consisting of measuring points near the opening and under the lamp. The measuring points that are close to the opening to the west are points A4, B4 and C4, while the measuring points that are close to the lights are points B2 and C2.

The results of measuring the light intensity of the aminah dormitory for 3 days in 4 different times from 09.00 - 22.00 GMT +8 as shown in Fig. 13 on the graph of the measurement results of the aminah dormitory 1 figure.

The highest light intensity is at point B2 both in the morning and afternoon, evening, or night, this is because point B2 is close to the lights, so the intensity is higher than the other points. While the lowest point is point C1 because the point is far from lights and openings and there is a barrier in the form of a cupboard so that it gets less light from both lights and sunlight from outside the room.

The results of the above measurements then made the average light intensity at the Aminah 1 dormitory for 3 days at 4 different times in Fig. 14. The average measurement result of the highest at point 3 in the afternoon of 50.3 lx, However, if it is compared with the Indonesian national standard, which is 250 lx, it can be concluded that the lighting of the Aminah 1 dormitory for the study room has not met the standard.

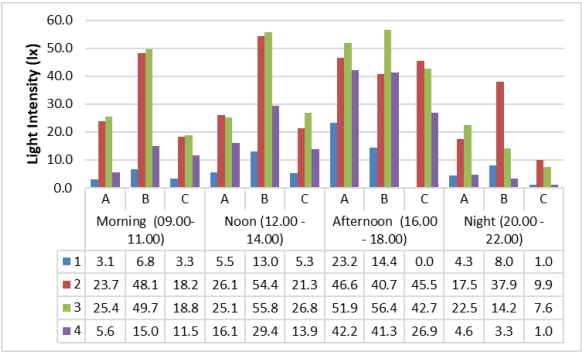

	A	B	C	A	B	C	A	B	C	A	B	C
	Morning (09.00-11.00)			Noon (12.00 - 14.00)			Afternoon (16.00 - 18.00)			Night (20.00 - 22.00)		
1	3.1	6.8	3.3	5.5	13.0	5.3	23.2	14.4	0.0	4.3	8.0	1.0
2	23.7	48.1	18.2	26.1	54.4	21.3	46.6	40.7	45.5	17.5	37.9	9.9
3	25.4	49.7	18.8	25.1	55.8	26.8	51.9	56.4	42.7	22.5	14.2	7.6
4	5.6	15.0	11.5	16.1	29.4	13.9	42.2	41.3	26.9	4.6	3.3	1.0

Figure 13. Measurement results for the Aminah 1 dormitory

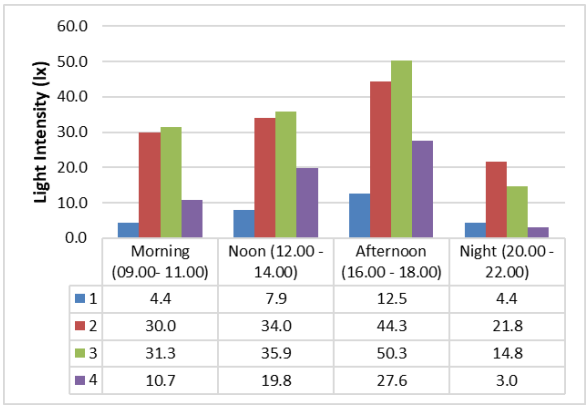

	Morning (09.00- 11.00)	Noon (12.00 - 14.00)	Afternoon (16.00 - 18.00)	Night (20.00 - 22.00)
1	4.4	7.9	12.5	4.4
2	30.0	34.0	44.3	21.8
3	31.3	35.9	50.3	14.8
4	10.7	19.8	27.6	3.0

Figure 14. The average measurement results of the Aminah 1 dormitory

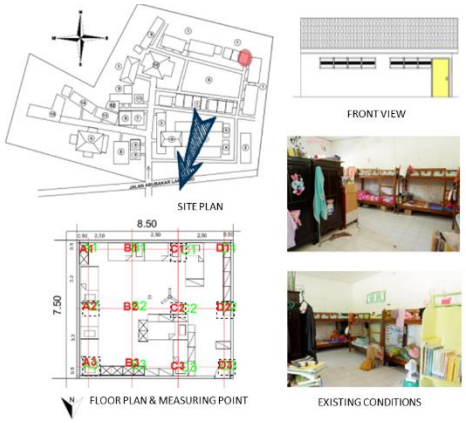

Figure 15. General overview of *Hafsah 1* dormitory

e. Hafsah 1 Dormitory

Hafsah dormitory has a room size of 8.5 meters long and 7.5 meters wide inhabited by 20 students, has front (south) and rear (north) ventilation but is small so that cross ventilation can occur in the room this, while the number of lights there is only 1 lamp in the middle of the room. This room has 12 measuring points, consisting of measuring points near the opening and under the lamp. The measuring points that are close to the southern opening are points A3, B3, C3 and D3, the measuring points that are close to the southern vent are points A1, B1, C1 and D1, while the measuring points that are close to the lights are points A2, B2 , C2 and D2.

The results of measuring the light intensity of the hafsah 1 dormitory for 3 days in 4 different times from 09.00 - 22.00 GMT +8 as shown in Fig. 16 of the measurement results of the Hafsah 1 dormitory figure. The highest light intensity at point C2 and B2 both in the morning, afternoon, evening, or night, this is because points B2 and C2 are close to lights, so their intensity is higher than other points. While the lowest points are points D1 and D3 because these points are far from the lights and close to the openings, but there are obstacles so that there is less light from both lights and sunlight from outside the room.

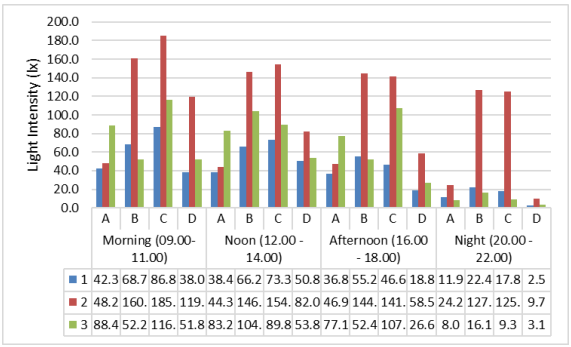

	A	B	C	D	A	B	C	D	A	B	C	D	A	B	C	D
	Morning (09.00-11.00)				Noon (12.00 - 14.00)				Afternoon (16.00 - 18.00)				Night (20.00 - 22.00)			
1	42.3	68.7	86.8	38.0	38.4	66.2	73.3	50.8	36.8	55.2	46.6	18.8	11.9	22.4	17.8	2.5
2	48.2	160.	185.	119.	44.3	146.	154.	82.0	46.9	144.	141.	58.5	24.2	127.	125.	9.7
3	88.4	52.2	116.	51.8	83.2	104.	89.8	53.8	77.1	52.4	107.	26.6	8.0	16.1	9.3	3.1

Figure 16. Measurement results for the Hafsah 1 dormitory

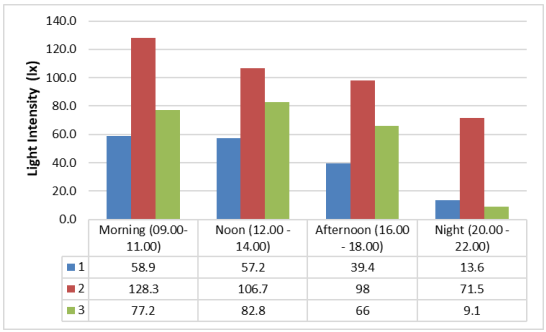

Figure 17. The average measurement results of the Hafsah 1 dormitory

The results of the above measurements then made the average light intensity at hafsah 1 dormitory for 3 days at 4 different times. Average measurement results at point 2 in the morning is 128.3 lx when compared to the Indonesian national standard, namely 250 lx, it is concluded that the lighting of hafsah 1 dormitory for the study room has not met the standard.

f. Maemunah 1 Dormitory

Maemunah 1 dormitory has a room size of 8.5 meters long and 8.5 meters wide inhabited by 22 students, has 2 openings in front (south direction) and rear (north direction) but small so cross ventilation can occur in this room, while there are only 2 lights in the middle of the room. This room has 16 measuring points, consisting of measuring points near the openings and those under the lights. The measuring points that are close to the southern opening are points C4 and B4, measuring points that are close to the southern ventilation, namely points A1, B1, C1 and D1, while the measuring points that are close to the lights are points B2, B3, C2 and C3 .

The results of measuring the light intensity of the maemunah 1 dormitory for 3 days in 4 different times from 09.00 - 22.00 GMT +8 as shown in Fig. 19 of the measurement results of the maemunah 1 dormitory.

Figure 18. General overview of *Maemunah1* dormitory

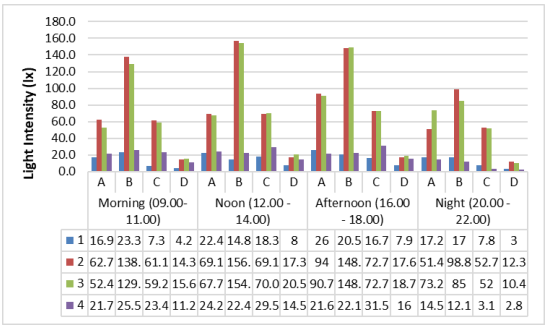

Figure 19. Measurement results of Maemunah 1 dormitory

The highest light intensity is at point B2 and B3 whether in the morning, afternoon, evening or night, this is because point B2 is close to the lights, so the intensity is higher than the other points. While the lowest point is point D1 because the point is far from lights and openings so that it gets less light from both lights and sunlight from outside the room.

The results of the above measurements then made the average light intensity at maemunah 1 dormitory for 3 days at 4 different times. The average measurement result at point 2 in the afternoon is 83.1 lx when compared to the Indonesian national standard, namely 250 lx, it is concluded that the lighting of maemunah 1 dormitory for the study room has not met the standard.

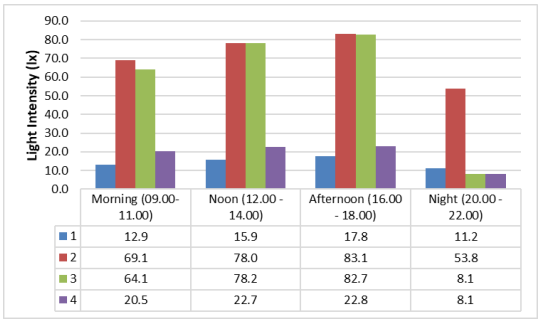

Figure 20. The average measurement results of the Maemunah 1 dormitory

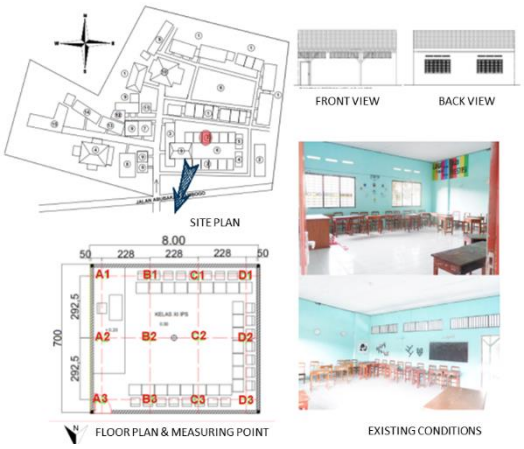

Figure 21. General overview of classroom *XI IPS*

g. Classroom XI IPS

Classroom XI IPS with a south-north orientation has a room size of 8 meters long and 7 meters wide, has front (south) and rear (north direction) vents, so cross ventilation can occur in this room, while there is only 1 lamp in the middle of the room. This room has 12 measuring points, consisting of measuring points near the opening and those under the lamp. Measuring points near the south opening are points A3, B3, C3 and D3, the measuring points that are close to the northern direction of the vent are A1, B1, C1 and D1, while the measuring points that are close to the lights are points B2 and C2.

The results of measuring the light intensity of classroom, XI IPS for 3 days in 4 times which is different from 09.00 - 22.00 GMT +8 as shown in Fig. 22 on the graph of measurement results for classroom XI IPS. The highest light intensity in classroom XI IPS is at point B1 both in the morning, afternoon, evening, and B2 at night, this is because B1 is directly near the window and point B2 is close to the light, so the intensity is higher than the other points. While the lowest points are points C2 and D3 in the morning, afternoon and evening, points A1 and D1 at night because these points are far from the lights so that they get less light from both lights and sunlight from outside the room.

The results of the above measurements then made the average light intensity in class XI IPS for 3 days at 4 different times.

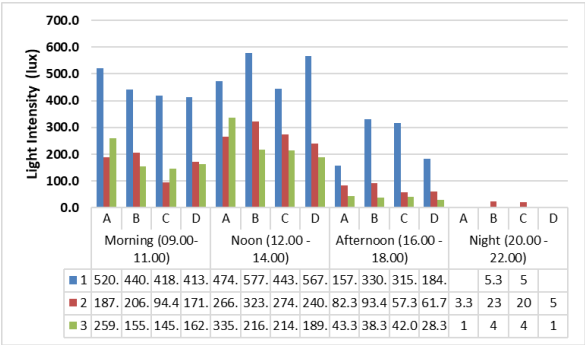

Figure 22. Measurement results of classroom XI IPS

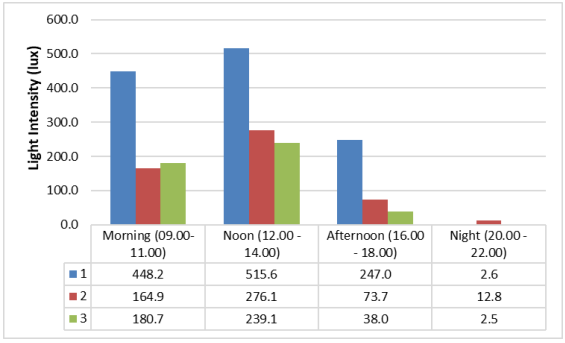

Figure 23. The average measurement results of classroom XI IPS

The average of the highest measurement results is at point 1, which is on the north side of the wall where there are openings during the day of 515.6 lx when compared to the Indonesian national standard, which is 250 lx, it is concluded that the lighting for class XI IPS during the day for the study room has met or exceeds the standard. It's just that at night it is impossible to use it for studying.

h. Classroom VIII B

Classroom VIII B with a south-north orientation has a room size of 8 meters long and 7 meters wide, has front (south) and rear (north) vents so that cross ventilation can occur in this room, while the number of lights there is only 1 lamp in the middle of the room. This room has 12 measuring points, consisting of measuring points near the opening and under the lamp. Measuring points that are close to the southern opening are points A3, B3, C3 and D3, measuring points that are close to the northern ventilation, namely points A1, B1, C1 and D1, while the measuring points that are close to the lights are points B2 and C2.

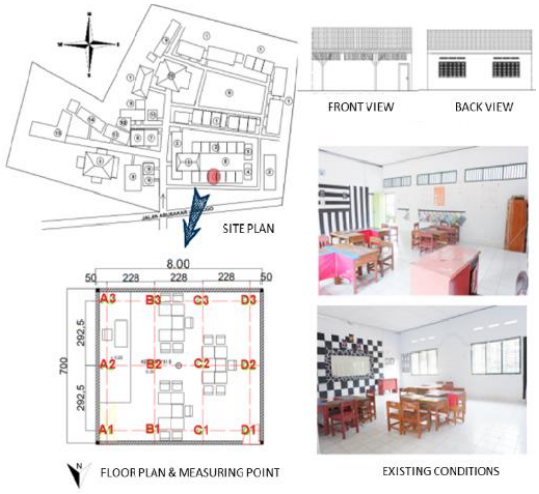

Figure 24. General overview of classroom *VIII B*

The results of measurement of classroom VIII B light intensity for 3 days in 4 different times from 09.00 - 22.00 GMT +8 as shown in Fig. 25 of the classroom VIII B measurement graph. The highest light intensity is at point C3 both in the morning, noon, as well as the afternoon compared to other points. this is because point C3 is close to the opening and without obstructions, so that its intensity is higher than the other points. points A3 and B3 and those near the lower opening because they are blocked by the road surface behind the building which is higher than the opening, point D3 is closer to the wall so that the light intensity is lower. While the lowest point is point A1 because the point is far away from the opening so that it gets less light from sunlight from outside the room.

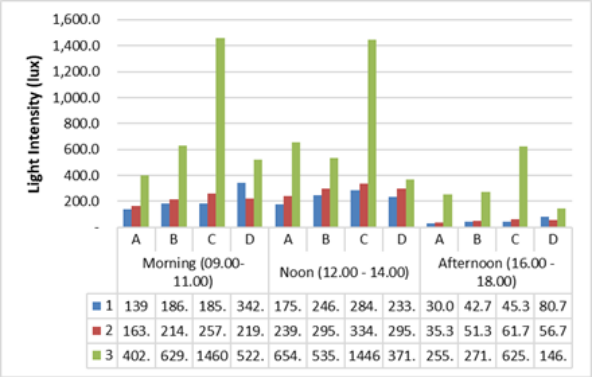

Figure 27. measurement results for clasrooms VIII B

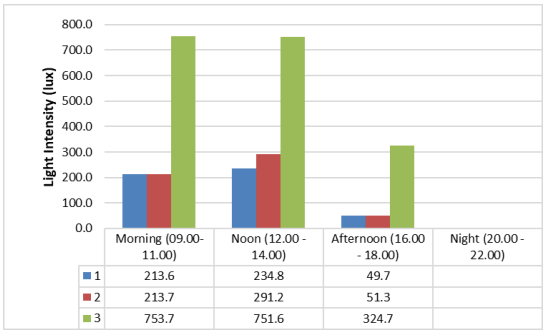

Figure 28. Average measurement results for classroom VIII B

The results of the above measurements then made the average light intensity in class VIII B for 3 days in 4 different times. The average of the highest measurement results at point 3 in the morning is 753.7 lx, during the day is 751.6 lx and in the afternoon is 324.7 lx when compared to the Indonesian national standard, which is 250 lx, it can be concluded that classroom VIII B lighting in the morning, afternoon and evening for the study room has met or exceeds the standard so that it allows glare, especially in areas close to openings. It's just that at night it can't be used for studying.

4.2. Artificial lighting design recommendations

After collecting data with measurements using a Lux Meter it is concluded that the lighting of the study room in the dormitory does not meet the standards used for learning in terms of lighting both during the day and at night, while the classroom as a place of study used during the day has met the standards lighting the study room, but at night the lighting in the classroom has not met the standard. Therefore, the researchers made recommendations for classrooms at night and dormitories that are in accordance with the lighting standards for the study room so that students can study in class at night and in dormitories.

a. Islamic Boarding School Of DDI Lil Banat Classroom Lighting Design at night

Classroom lighting design recommendations as shown in the picture above use an even lighting system with 4 lamps, the type of lamp used is the PHILIPS RC341B PSU

Figure 25. Recommended classroom lighting

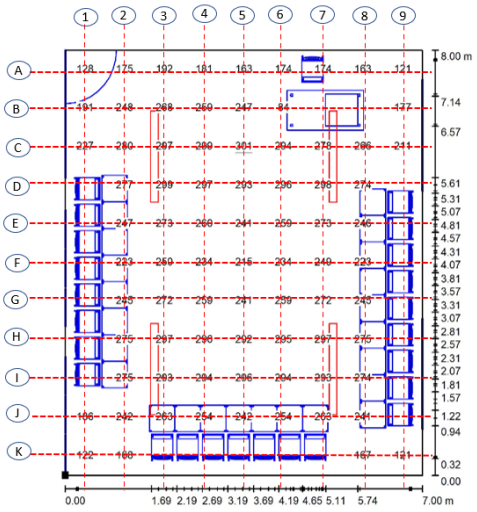

Figure 26. Simulation result of classroom

W15L180 1 xLED42S / 830 4200 lm and 31 watts. The distance between the lights is 3.5 meters and 2.28 meters. From Fig. 28 it can be seen that the workplane area of 76 cm from the floor surface has a value of approximately 250 lx. The highest light intensity value is 301 lx, while the lowest light intensity is 39 lx with an average light intensity of 226 lx. The average light intensity on the table or study area is 255 lx, while the standard of lighting for the study room is 250 lx, so the classroom meets the standard and can be used by students to study at night.

b. Lighting Design of Islamic Boarding School of DDI Lil Banat Dormitory at night

Recommendations for placing lights in order to meet the light intensity in the dormitory according to the Indonesian National Standard and for user convenience there are two options for 2 different dorm plans. The first is for the dormitory plan where the bed placement is linear, so that the study area is in the middle of the room which is more like a corridor. The second is for dormitory plans where the bed is laid out in a U-shape so that the study area is in the middle and wider, according to the layout in the field.

Figure 29. Dormitory lighting recommendations at night

The first recommendation is a linear plan with the simulation results such as Fig. 29. Recommendations as shown in Fig. 29 use an even lighting system with 16 lamps, the type of lamp used is PHILIPS DN570B PSE-E 1xLED12S / 930 F SG-FRC 900 lm and 11.6 Watt. The distance between the lights is 2.1 meters.

The simulation results of the dormitory at the Islamic boarding school of DDI Lil Banat showed unfavorable results, therefore a recommendation was made for good lighting design to be used for all activities in the dormitory, especially studying and sleeping. Design recommendations that have been made based on SNI standards for lighting while studying are 250 lx and 120-250 lx during sleep. Below are the results of the simulation of the dormitory lighting system recommendations.

From Fig. 30 it can be seen that the area that is often used for learning, namely in the middle of the workplane room 80 cm from the floor surface, has a value of approximately 250 lx. The highest light intensity value is 256 lx, while the lowest light intensity is 51 lx with an average light intensity of 170 lx. The average light intensity in the study area is 244.5 lx, while the standard of lighting for the study room is 250 lx, with a difference of 5.5 lx, the dormitory can be used by students to study at night. While the area for sleep from the simulation results, the value of the light intensity ranges from 120-250 lx so it is good to use for sleeping.

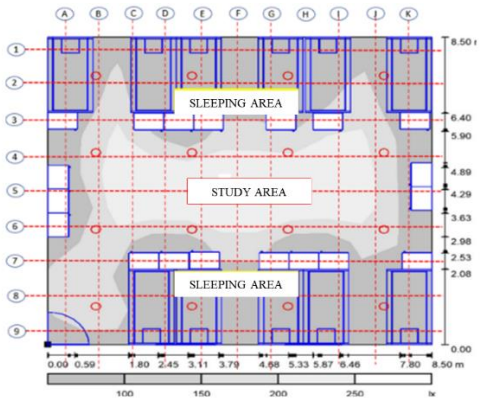

Figure 30. The distribution of light from the simulation results of dormitory lighting recommendations.

Figure 31. Alternative dormitory lighting recommendations 1

The second recommendation, namely a U-shaped dormitory plan. The simulation is carried out as many as 2 alternatives, the first alternative is a lamp for sleeping, the light intensity is as standard, ranging from 120-250 lx and the second alternative is the lamp used during study time and extinguished when it is bedtime.

The results of the first alternative simulation for the U layout type are as shown in Fig. 31. Dormitory lighting design recommendations for alternative U-type layouts are shown in Fig. 31 using a combined evenly and localized lighting system with 14 light points located in Fig. 31. edge close to the wall, the type of lamp used is PHILIPS DN571B PSE-E 1xLED12S / 930 F SG-FRC 1050 lm and 11.8 Watt. The distance between the lights is 2.1 meters which is turned on when you want to sleep.

The simulation results of the dormitory at the Islamic boarding school of DDI Lil Banat show unfavorable results for studying because it is dark and glare for sleeping, therefore a recommendation is made for lighting design that is good for sleeping. Design recommendations that have been made based on SNI standards for lighting during sleep are 120 - 250 lx. Below are the results of the simulation of alternative dormitory lighting system recommendations 1.

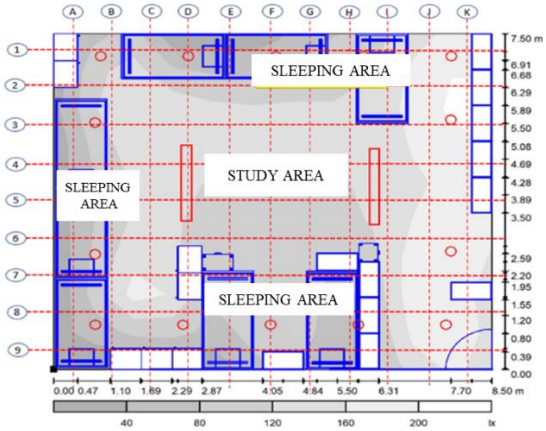

Figure 32. The light distribution from the simulation results. Alternative Dormitory Lighting Recommendations 1

Figure 33. Results of recommendations 2 for alternative dormitory lighting

From Fig. 32 it can be seen that the bed area, which is the edge of the room, has a value of approximately 200 lx or ranges from 40 - 200 lx, meaning that the room can be used for sleeping because it has reached the bedroom lighting standard. ie 120-250 lx.

The simulation results of the two alternative lights are used for learning, as shown in Fig. 33. Recommendations for dormitory lighting design for alternative U type layout 2 as shown in the picture above using a combined lighting system having 2 light points in the middle of the room, the type of lamp used is PHILIPS RC341B PSU W15L180 1 xLED42S / 830 4200 lm and 31 watts. The distance between lamps is 3.65 meters distance between lamps and 2.5 meters distance from the walls.

The simulation results of the dormitory at the Islamic boarding school of DDI Lil Banat showed unfavorable results for studying because it was dark and glare for sleeping, therefore recommendations for lighting design were made that were good for learning. Design recommendations that have been made based on SNI standards for lighting when studying are 250 lx. Figure 34 are the results of the simulation of an alternative dormitory lighting system recommendation.

Figure 34 shows that the study area, which is in the middle of the room, has a light intensity value between 180 - 290 lx. The highest light intensity value is 290 lx and the lowest light intensity is 14 lx with an average light intensity of 130 lx. The standard of lighting for the study room is 250 lx, so the dormitory with lighting like in session 2 can be used by students to study.

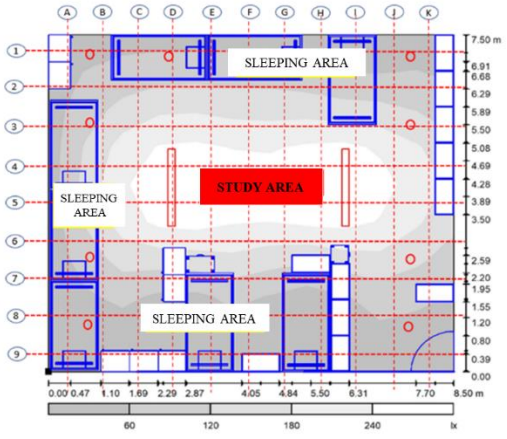

Figure 34. The light distribution simulation results for alternative dormitory lighting recommendations 2 When the study lights are turned on and the sleep lights are turned off

5. Conclusions and Suggestion

5.1. Conclusions

The results of measuring light intensity in the study room at the Islamic boarding school of DDI Lil Banat show that none of the light intensity in the dormitory meets the Indonesian National Standard for study rooms both at night and during the day. During the day the classrooms meet Indonesian National Standards but not at night. Even though students as room users feel comfortable with the light intensity conditions in the study room and can study according to these conditions, the students still feel some complaints in the form of sore eyes, eye tension and difficulty focusing. So, the researchers made recommendations for study room designs that could make students more comfortable studying in dormitories and classes so that they could reduce complaints while studying. Lighting design recommendations are made in several alternatives by increasing the number of lamps and changing the lamp type using Dialux simulation. The simulation results of the study room lighting design recommendations have met the standards for use so that they can be applied to dormitories and classes at the Islamic boarding school of DDI Lil Banat Parepare.

5.2. Suggestions

Based on the above conclusions, the authors provide suggestions to further researchers who wish to conduct research with a similar theme in order to provide information about the quality of lighting in dormitories according to SNI and its effect on activities in dormitories other than studying and sleeping. Suggestions for practitioners with this research are expected to be a reference in dormitory design and consideration in terms of dormitory lighting design so that it can support students' learning activities.

References

[1] Manurung, *Natural Lighting in Architecture*. Yogyakarta: ANDI, 2012. [in Bahasa]

[2] N. Jamala and Rahim, *Visual Comfort Theory and Applications.* Makassar: Badan Penerbit UNM, 2017. [in Bahasa]

[3] N. Jamala, N. Soewarno, J. A. Suryabrata, and A. Kusumawanto, "Visual Comfort of Office Workspace," *Forum Tek.*, vol. 35, no. 1, 2013. [in Bahasa]

[4] H. Indrani and I. P. Santosa, *Hospital Lighting Design Upscale Hospital. Darmo and St. Vincentius A. Paulo Surabaya*. Surabaya, 2009. [in Bahasa]

[5] Mahmuddin, "Learn and Share," 2010. [Online]. Available: www.mahmuddin.wordpress.com. [Accessed: 04-Sep-2017]. [in Bahasa]

[6] M. Soeripto, "Higiene Industri," Universitas Indonesia, 2008. [in Bahasa]

[7] E. Widowati, "Effect of Local Lighting Intensity," *J. Kesehat. Masy. Uns. Kesmas*, vol. 5, no. 1, 2010. [in Bahasa]

[8] Kwong and Ali, "A Review of Energy Efficiency Potentials in Tropicsl Buildings-Perspective of Enclosed Common Areas," *Renew. Sustain. Energi Rev.*, 2011.

[9] R. Prihatmanti and M. Y. Susan, "Lighting Performance in Classrooms in Historic Buildings," *Aksen*, vol. 46, 2016. [in Bahasa]
[10] S. Samani, "The Impact of Indoor Lighting on Students' Learning Performance in Learning Environments," *Int. J. Bus. Soc. Sci.*, vol. 3, no. 24, 2012.
[11] Nurul, "Study of Natural Lighting in Central Library Building of UNHAS," *J. Enj.*, 2001. [in Bahasa]
[12] U. Awak, "Conducive Study Room Physical Conditions," 2015. [Online]. Available: https://www.matrapendidikan.com/2015/04/kondisi-ruang-belajarkondusif.html%0A. [Accessed: 01-Apr-2015]. [in Bahasa]
[13] W. Udin S, *Teaching and Learning Strategy*. Jakarta, 2003. [in Bahasa]
[14] Z. Dhofier, *The Tradition of Islamic Boarding Schools Studying Kyai's View of Life and His Vision on Indonesia's Future*. Jakarta Barat: LP3ES, 2011. [in Bahasa]
[15] H. F. Zarkasyi, *Liberalization of Islamic Thought (Joint Movement of Missionaries, Orientalists, and Colonialists)*. Ponorogo: CIOS, 2008. [in Bahasa]
[16] Pareparekota, "Parepare City Statistics," 2016. [in Bahasa]
[17] Janah, "DDI Lil Banat Islamic Boarding School Parepare," 2013. [Online]. Available: https://pareparekota.go.id/index.php/profil/geografis/. [Accessed: 25-Jul-2021]. [in Bahasa]

EPI International Journal of Engineering
Volume 4, Number 1, February 2021, pp. 93-100
DOI: 10.25042/epi-ije.022021.13

*p*ISSN 2615-5109
*e*ISSN 2621-0541

The influence of Transit Area in Public Open Space of Losari Beach Makassar Pavilion on the Activities of Group Visitors

Miftahuljannah[a,*], Triyatni Martosenjoyo[b], Rosady Mulyadi[c]

[a]Architecture Department, Engineering Faculty, Hasanuddin University, Makassar Indonesia. Email: miftahuljannah117zb@gmail.com
[b]Architecture Department, Engineering Faculty, Hasanuddin University, Makassar Indonesia. Email: triyatni@gmail.com
[c]Architecture Department, Engineering Faculty, Hasanuddin University, Makassar Indonesia. Email: rosady@unhas.ac.id

Abstract

Urban communities are social beings who have a high level of activity. One of the activities to unwind is a refreshing type of activity. A developing city like Makassar needs open space for the public as a container for community activities, including refreshing activities. The Losari Beach Pavilion is present as a public open space that is visited by the majority of visitors in groups to carry out refreshing activities. This public open space has a space configuration with the design of providing a stopover for activities in several parts of the space. This part of the space looks like overlapping activities so that there is space utilization at the stopover point and part of it becomes unoccupied space. Therefore, this study was conducted to explain the effect that occurs on the stopover space and unoccupied space in this case the unused space based on its function. This study used the descriptive qualitative method. The data collection technique used the behavior mapping method by recording activities and sketches to get an image of the activity pattern carried out by group visitors and then presented in the form of tables, pictures and descriptions. The results of the study found that the transit space as a place of stoping point because of the influence of spatial area, visibility, historical area, iconic elements, social interaction, while the shelter space was not functionally visited due to the influence of minimizing visibility, social interaction, and arrangement of attribute elements.

Keywords: Activities patterns; group visitors; public open space; transit space

1. Introduction

Public open space at this writing is an open space that is able to accommodate the need for meeting places and joint activities in the open air. This space allows a meeting between humans to interact with each other [1]. They carry out various activities in a visit including sightseeing, meetings, transit, taking pictures, deliberation, public open space occurs because of the need for a city space so that it can accommodate all visitor activities on a visit to enjoy Makassar City facilities. The Losari beach pavilion is a public open space that has been known as a city icon, attracting the attention of visitors that come from within and outside the city. The type of group visitor emphasizes the activities that occur so that events can be seen at each stopover.

In the design of this public open space, especially in the space configuration, parts of the space have been designed functionally as a space for visitors to stop by. The space that has been provided as a shelter space is not all used by visitors in its function, even some shelters accommodate overlapping activities so as to create unoccupied space in the sense that space is not functional in this case by Carr [1] argues that public open space is a public area where people doing ritual activities and functional activities that overlap should be avoided. Thus the importance of minimizing these incidents is also for social equality for visitors to the space configuration that has been planned functionally.

Project for Public open spaces (PPS) stated in a handbook for creating successful public open spaces that they find four key qualities of a successful public open space from its 1000 studies on public open space, one of which is "uses and activities". Activities or space allotment are the basis of a place to have something to do and give people a reason to come and come back to this place again. When there is no activity, space will be empty and generally, this means that something is wrong and wrong [2] and "Sociability" This is a quality that is difficult for any place to achieve but once it is successful it will become a clear feature. When people see colleagues meet and greet each other and feel comfortable interacting with others, they will tend to feel the enthusiasm of one space to gather with their

*Corresponding author. Tel.: +62811 413 6880
BTN Tabaria, Makassar, Sulawesi Selatan Indonesia

group so that it becomes a place that fosters types of social activities [2].

Some of the conditions described and opinions according to experts related to the issues raised became the focus of research. The purpose of this problem is to find and reveal what effects there are on the transit space to stop by and the occurrence of unoccupied space on group visitor activities, the meaning in this case, is not used as a spatial function so that it is useful for the consideration of the developer of the Losari Beach Pavilion in Makassar City and hopes that it can be the basis for the design consideration of space configuration in public open spaces.

2. Literature Review

The systematic variables of this study reviewed several studies namely public open spaces and the activities/behavior of visiting people

2.1. Public open space

Carr invites us to see people's need for public open space as a means of interaction and the public open space that is most interested in society, in general, is the circulation route because it has dynamic values so that it is not boring [3].

Public open space is also articulated by Hanna Arendt into two dimensions, that is the space of appearance and the world together The apparition space is a public open space that humans use to show who they are in front of others. The shared world space is a life that is shared among other human beings like a table among those who sit around it [4]. The public sphere can collapse under conditions such as radical isolation and mass hysteria Radical isolation where everyone no longer gives mutual consent and private desire to opt for public open space. The mass hysteria of everyone suddenly acting as if they are part of a family, they duplicate the values or perspectives of members of the family [5].

Belief in the point of view of the main value of the public open space, that is that there are three things that are responsive, democratic, and meaningful. Responsive in the sense of public open space is a space that can be used for various activities and broad interests that have environmental functions. Democratic means that public open space can be used by the general public from various social, economic and cultural backgrounds as well as access to various human physical conditions. Meanwhile, it means that public open space must have a link between humans, space, and the world at large and the social context. In other words, there is a system of meaning in the public open space [3].

According to Hantono, there are two forms of public open space, that is Elongated (the street), which is a space that has a longer dimension on both sides than the other. Space shaped like this has a tends to form a linear, one-way, parallel circulation pattern. In general, public open spaces that have this form are roads, rivers, corridors, and others. The square, which is a space that has almost the same dimensions on all sides, has a tends to form circulation patterns in all directions, random, organic. In general, public open spaces like this take the form of fields, parks, and so on [6].

Characteristically, both have the same geometric shape, but what distinguishes them is the function and circulation patterns. And these two basic forms interpret public open spaces, both closed and open, especially in the public open space of the Losari beach pavilion, including in the elongated basic form, therefore it tends to have a pattern of visiting activities that occur.

2.2. The activities of group visitors

a. Activities

The meaning of activity in a space can be divided into three kinds of activities, according to Zhang and Lawson [7], that is:

- Necessary activities, namely routine activities carried out because of an obligation to fulfill a certain need. A good environment is an environment that can accommodate and accommodate all types of activities needed.
- Optional activities, namely activities carried out when there is an opportunity or the right time. Usually, these activities are carried out in a pleasant environment and there are no other more pressing activities.
- Social activities, namely activities that involve interaction with other parties around them. These are because of the planned main activities and optional activities because there are main activities and optional activities.

Passive involvement and active involvement in public open space utilization activities occur as a result of this interaction process (Necessary, Optional and Social), where users of public open space can interact in different ways. Space as a place must be able to provide a conducive environment for the fulfillment of interaction requirements, namely opportunities for social contact and communication. Social interaction can occur in the form of passive activities such as sitting enjoying the atmosphere or situation and can also occur actively by talking with other people discussing a topic or even doing activities together according to Carmona [8].

Figure 1. Entertainment can increase the vitality of space to visitor activities

Gehl [9] revealed that visitor activities attract other people and as a public open space it can attract other people as well because of something that is done in it if there is something to be done people want to spend time in public.

b. Group behavior

Humans are the center of the environment as well as being part of the environment. An individual interacting with space is influenced by the atmosphere of the space and affects the atmosphere of that space. Behavior can be defined as part of the interaction process between human personality and the environment. The environment contains stimuli (stimuli) which are then 'rewarded' with responses by the personality, one of which is behavior [10]. The reciprocal relationship between atmosphere and behavior is also influenced by design factors and the dominant characteristics of the humans who interact in it. The quality of the environment is formed because the spatial atmosphere sensed by humans becomes a perception that is reflected in human behavior, on the other hand, human activities or behavior itself can affect the atmosphere of space, [9].

The word behavior shows humans in their actions, relating to all human activities physically in the form of human interactions with each other or with their physical environment. On the other hand, architectural design will produce a physical form that can be seen and can be held. Therefore, the results of architectural design can be one of the facilitators of behavior, but can also be a barrier to behavior [11]. Meanwhile, Whyte said that the behavior of urban public open space users in America can be influenced by several factors using open space, including seating, sunlight, wind, vegetation, water, food, direct physical and visual access to the main road [12].

The behavior of the people who interact and hang out forms a group as well as the behavior of visitors at the Losari Beach Pavilion, directly or indirectly related to elements of "sociology", "psychological" and "environmental psychology". Because of that, there is a reciprocal relationship between public open space and visitor behavior by seeing it in an interrelated state and not standing alone. In terms of the relationship between the use of facilities that have been designed with behavior that tends to be created in the public open space.

Human behavior is shown in the nature of a person and how that person adapts to the environment around him. The adaptation that humans make to architecture creates a meaning or more that can be seen by everyone to cover the needs of human life. Human behavior is identified by observing human behavior based on the meaning of someone doing these activities.

3. Research Methods

This type of research is qualitative. This type of research is inductive [13]. This is inductive because at the beginning of the observation it collects field data and concludes the statements of the results of the observations in a statement that is more general and characterized by empirical sciences.

This research method uses the behavior mapping method because with this method you can get detailed activities in the form of a behavior map in each group of visitors. One of the mapping based on the actor (person-centered mapping) this technique emphasizes the movement of humans over a certain period of time [14]. This technique is concerned with not just one place but several places. The researcher deals with a person or group that is specifically observed. The step taken is to follow the activities carried out by group visitors by recording, sketching, and making notes on the base map.

The data analysis carried out in this study approached an empirical study. Empirical is also research whose nature is exploring (explorer), describing (descriptive) and also explaining (explaining) [15].

The object of research is group visitor activity in the public open space of the Losari Beach Makassar Pavilion, starting from the beginning of arrival to the end of the visit and leaving the research location, this results in the overall results of the activity to be able to see what influences are in each room and activity. Presentation of the analysis results in the form of a table matrix, activity map images and description explanations. This presentation produces answers to the problems that occur.

The public open space that is the object of research is in South Sulawesi Province, Makassar City, Penghibur Street, right in front of Datuk Museng Street and Maipa Street. This pavilion faces westward so many visitors come to see the sunset.

Sources of research data are taken from two sources:

a. Primary sources are observations, interview results, sketch results and video recordings of visitor activities. Observations were made on two platforms located between the entrance and exit doors, namely the Makassar Bugis Pavilion and the Losari Beach Pavilion. Interviews were conducted with 30 groups of visitors and activity sketches and video recordings were carried out on 20 groups of visitors at busy times, namely 16.30 WIB - 22.00 WIB on Fridays and Saturdays.
b. Secondary sources are research supporting data from related agencies such as regional planning offices, books related to research titles, and publications that support research.

Figure 2. Losari beach pavilion location

In connection with the research method used is behavior mapping by means of sketching, describing, recording, recording the activities of the actors of the research object, research instruments, namely:

a. Research team
b. Base map image
c. Stationery
d. Smartphone
e. Interview module

The validity technique used in this research is the credibility test by means of the triangulation of the technique of reanalyzing the results of the interview and then matching them with the results of observations and documentation so that the results of the triangulation of this technique obtain the same or valid data. The next test tests the reference material that the reference shows the results of interviews, recorded data sources, field photos and documentation tools so that it can be stated to support the credibility of the data and testing of increased persistence is done by checking all data collection techniques from initial to final observations so that the data found to provide accurate and systematic descriptions thereby increasing the credibility of the data.

4. Results and Discussion

4.1. Research results

a. Makassar Bugis Pavilion and Losari Beach Pavilion

The Losari Beach Pavilion is a beach located west of Makassar City, right in the heart of Makassar City on Jalan Penghibur, where various activities take place there. Losari Beach is a public area for the community and is one of the icons of Makassar City. Geographically, Losari Beach, Makassar City is limited by the coordinates 119 ° 22'42 "- 119 ° 24'38" East Longitude and 05 ° 07'36 "- 05 ° 08'54" LS. Administratively, Losari Beach is bordered by Jl. Somba Opu and Makassar Golden Hotel (North side), Jl. Entertainers, commercial buildings, residential areas and Stella Maris Hospital (East Side), Tanjung Bunga Metro Area (South Side) and Makassar Strait (West Side). The public open space of the Losari Beach Pavilion consists of 3 courts, namely the Makassar Bugis Pavilion, the Losari Beach Pavilion, the Toraja Mandar Pavilion with a length of more than 800 m^2.

Figure 3. Losari beach area, (www.google.earth.com)

Figure 4. Research location limitation (www.google.earth.com)

From the observations of the activity observations on the three platforms, there are only two platforms that have the potential for group visitor activity patterns, including the Makassar Bugis Pavilion and the Losari Beach Pavilion which are supported by their existence between the entrance and exit distance, while the Mandar Toraja Pavilion has become a traditional culinary area and There is no potential for a pattern of activity in public open space visits so that only two platforms were chosen for the boundaries of the research location.

b. Group visitor activity pattern

The Losari Beach public open space is one of the city's icons that is attractive to be visited by both local people and migrants. Since the first construction of this element, the letter statue with the inscription "Pantai Losari" has been recognized by people both inside and outside Makassar City. Visitors who come are not a few from out of town. The visitor category is also the majority of group visitors to enliven this public open space. The condition of visitors is not experiencing density every day where this study looks for the dense time of visits so that it can provide real results from Monday to Sunday, only weekends experience visitor density, namely on Friday, Saturday and Sunday. Friday and Saturday between 16-30 and 22-00.

Of the total group visitors, 20 groups were taken to become participants with a different number of group personnel, of the 20 groups totaling 153 visitors and the categories of visits were divided based on the number of visitors.

- Friday at 6:00 p.m. local time, there were 3 groups (6,5,5) people, the rooms that were visited were the Makassar Plaza (1), the stage (3), the Bugis Plaza (2), in front of the Bugis Plaza, the seats (7a), (7c) and Losari Beach Plaza (6).
- Friday at 19.00 WITA there were 5 groups (8,9,8,9,10) people, the rooms that were visited were the Makassar Plaza (1), seats (4a), (4b), and Losari Beach Plaza (6).

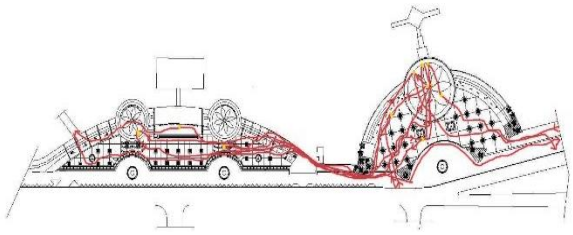

Figure 5. Finding the travel patterns of group visitors based on (day and time) Friday at 18.00 WITA

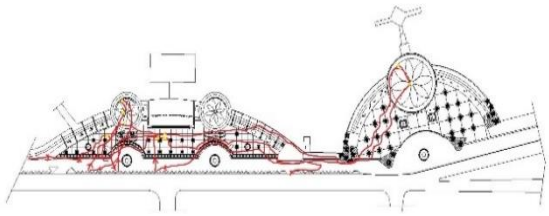

Figure 6. Finding the travel patterns of group visitors based on (day and time) Friday at 19.00 WITA

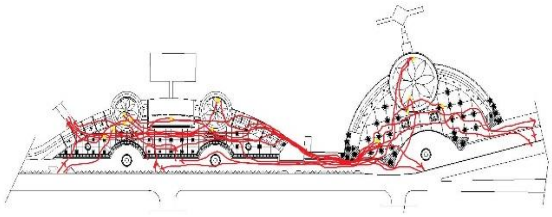

Figure 7. Finding the travel patterns of group visitors based on (day and time) Saturday at 18.00 WITA

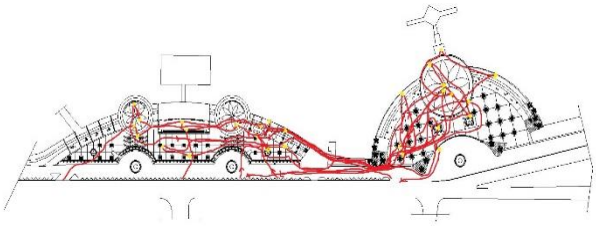

Figure 8. Finding the travel patterns of group visitors based on (day and time) Saturday at 1.00 WITA

- On Saturday at 18.00 WITA, there were 6 groups (5,5,7,7,10,4) people, the rooms that were visited were the Makassar Plaza (1), the Bugis Plaza (2), the stage (3), the seats (4a), and Losari Beach Plaza (6), seats (7a), (7b).

- Saturday at 19.00 WITA there were 6 groups (8,11,11,13,5) people, the rooms that were visited were the Makassar Plaza (1), the Bugis Plaza (2), the stage (3), the seats (4b), (4c), (7a), (7c), (7d), the statue area (5), the Losari beach plaza (6), and the Adipura monument (8).

Table 1. Activity type coding

No.	Type of activity	Coding	The meaning of activity
1	Sit back		optional activities
2	Tell stories, talk		necessary activities, social activities
3	Played		optional activities
4	Photo with public art and elements		necessary activities dan social activities
5	Group photo		necessary activities dan optional activities dan social activities
6	Waiting		necessary activities
7	Stand relaxed		optional activities dan social activities

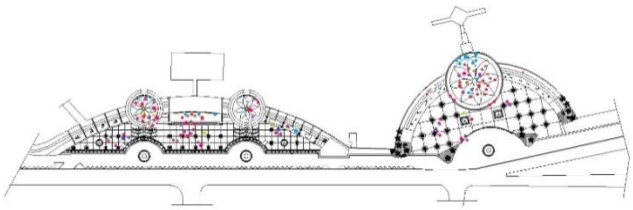

Figure 9. Mapping activity types

Description:

: 29 activities : 17 activities : 20 activities
: 38 activities : 11 activities
: 6 activities : 12 activities

From the analysis of the activity patterns of group visitors who carry out visiting activities from the entrance to the exit, there are 6 types of activities that occur in the convex space, from coding activities, it can be seen that an assessment of what types of activities occur the most.

The meaning of activities in a transit space, there are three categories of activities, namely necessary activities, which are the main activities such as waiting for stories, talking, group photos, photos with public art and elements, optional activities, which are optional activities such as playing, sitting and standing, and social activities which are activities such as chatting, talking casually, taking pictures with public art or with groups and standing up to casually having a look. Analysis. In the activities that occur at each stopover, there are 7 types of activities carried out in groups [7].

4.2. Research discussion

a. Analysis of the Parts of Space

Both of these pavilions have spaces that become transit points where this is used by visitors to an interesting spot or space to stop by and this pavilion also has an arrangement of elements. The transit points are shown in Fig. 10.

- Makassar Plaza Roundabout (Fig. 11)

This space has dimensions of 21.4 m in diameter plus a trap width of 1.7 m and 2 m with a total diameter of 25 m. The area that is owned gives the impression that it is free to make visitors stop just to stand back and sit down to rest for some time.

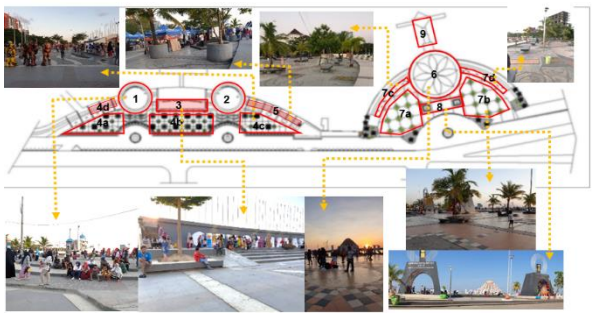

Figure 10. Division of transit Space

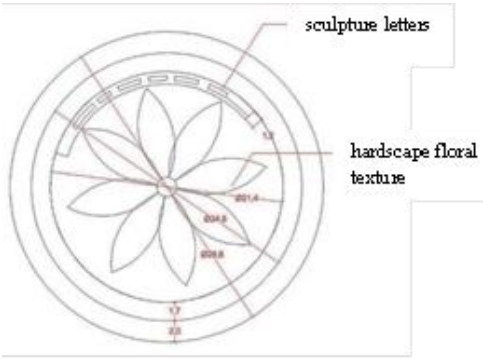

Figure 11. Transit space specifications (1)

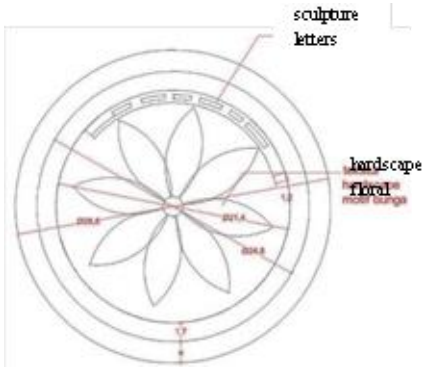

Figure 12. Transit space specifications (2)

This space is equipped with the property elements of a letter statue with the words "Makassar". Each letter is about 30 cm - 70 cm high, 2 m high red letters with sea views up to the planning area of the Center Point Of Indonesia. The hardscape is patterned with flowers with the material used in the form of natural stone for outdoor so that from its durability it can face rainy and dry seasons.

- Plaza Bugis Roundabout (Fig. 12)

This plaza has dimensions and hardscape and the same shape as the Makassar roundabout plaza. (1) The only difference is that the letter statues that read “Bugis” are sculptures of Makassar and Bugis letters.

a) Stage (Fig. 13)

This space is a platform like a stage for City event activities with dimensions of 40 m long and 7.7 m wide. The blocked stairs are planned for the development of the next stage, just like the roundabout plaza.

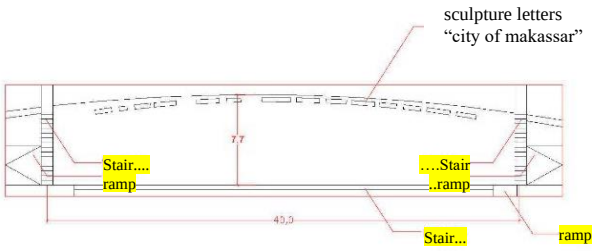

Figure 13. Transit space specifications (3)

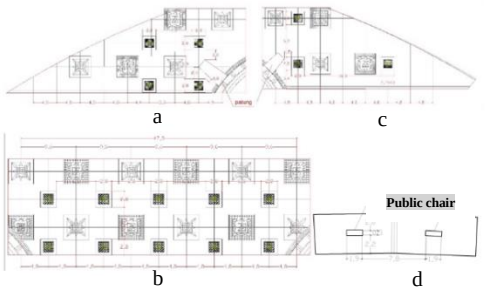

Figure 14. Transit space specifications (4a, 4b, 4c, 4d)

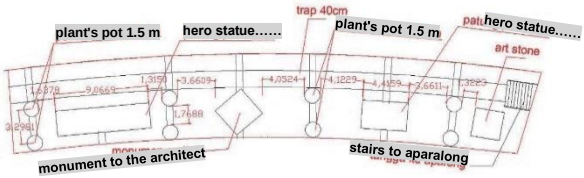

Figure 15. Transit space specifications (5)

It also has a letter statue with the words 'city of Makassar' 2 meters high, 30-60 cm in white, visitors use this space to stop taking photos with the object of a letter statue with white color making elements It gets dirty quickly and reduces the aesthetic value of the existing public art area as well as choosing this place as a stopping point for offering photo property services.

b) Seating area (a, b, c, d) (Fig. 14)

Visitors to this seating area are not as busy as visitors who stop in areas (1), (2), and (3). All permanent concrete seats are in a rectangular shape measuring 2.8mx 2.8m with a plant arrangement in the middle measuring 1.8mx 1.8m, the distance between the seats is 5m - 16m and other forms of seating are rectangular with a size of 1.9mx 0.5m and a material floor natural stone combination tiles. The capacity of people to sit in rectangular seats per one unit is 27 people, this capacity is enough to accommodate 2-3 groups per one seat and the rectangular seating capacity for 4-5 people accommodates 1 group while the number of rectangular seats is 17 units and a 2 unit rectangle.

c) Sculpture Area (Fig. 15)

The area of the statue is a space that is located in the position of the connecting access between the two platforms, this area is often crowded with visitors because of the narrow connecting route and becomes a stopover point. Group visitors who pass through this area feel uncomfortable with the traps up and down the surface level of the space for movement or the hallway between the statue properties.

d) Losari Beach Plaza (Fig. 16)

This room is the room that has the highest level of visits from the first 20 groups of roundabout plazas built in this area. A letter statue is also available in this plaza with a display of "Pantai Losari", a letter height of 2 m, the distance between letters 30-40 cm in white.

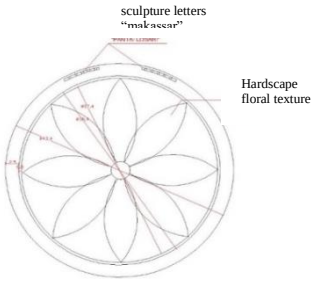

Figure 16. Transit space specifications (6)

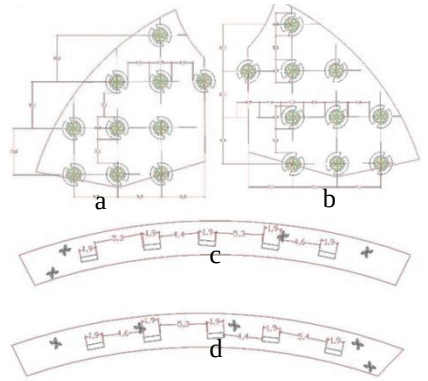

Figure 17. Transit space specifications (7)

This letter statue is what is known by the immigrant visitors. Not a few visitors come with the aim of taking photos as a backdrop of this element. The plaza with a diameter of 37.4 m plus a trap dimension of 0.5 m and 2.5 m made of natural stone with floral motif tiles.

e) Seating area (a, b, c, d) (Fig. 17)

This space is designed as a place to sit, rest, relax. This seating area is available in 4 areas, but out of the 20 groups who visited, only 1-4 visitors stopped to use this space. Seats in a circular shape measuring 5m in diameter and in the middle are provided a plant pot with a diameter of 2.5m, the capacity of people to sit per one unit is 24 people, accommodating 1-2 groups, while the long rectangular seat measuring 1.9mx 0.5m has a capacity of 5 people per one unit. 1 group. The number of circular seats is 20 units in areas 7a and 7b, while areas 7c and 7d are elongated as many as 10 seats in the area where vegetation is available as protection, but the condition of small vegetation does not protect all seats.

f) Adipura monument (Fig. 18)

This room is the area of the Adipura trophy monument. The first monument is the Adipura monument in the small town category, which was won during the leadership of Malik B Masri in 1997.

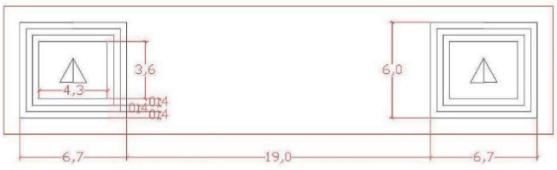

Figure 18. Transit space specifications (8)

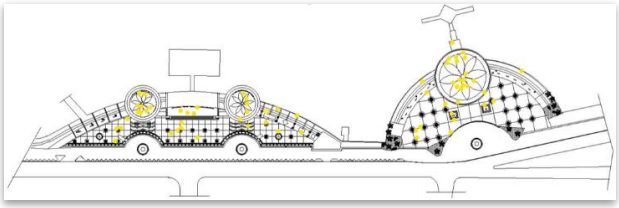

Figure 19. Stop point for group visitors

The second monument is the Adipura Cup in the metropolitan city category which was won under the leadership of Ilham Arief Sirajuddin in 2013. Then these two pillars were put together at the Losari Beach Pavilion placed in front of the Bundara plaza These two monuments are designed in the form of a tunnel that functions as a shelter for visitors who want to take shelter under it during the day and are equipped with spotlights in the tunnel from the lower corner at night as well as abstract motifs on the walls to add to the beauty of the photos. The distance between the two monuments is about 19m and a height of about 10m attracts visitors to capture the moment of their visit and stop in this area.

The image of the display of transit points in group activities of 20 visitors in the transit space is shown in Fig. 19. The Losari Beach Pavilion Plaza gets the largest number of visitors to stop by for a moment, supported by the good spots this space has in terms of visualizing sea views, size, location and more elements. wider and larger dimensions than other plazas, the plaza is located in the center of 3 pavilions coupled with the availability of the property of the "Pantai Losari" letter statue that has become an icon of public open space in this city which attracts visitors.

Table 2. Transit space for group visitors

Space	Total transit	Type of activity
Makassar Plaza Roundabout	8	Stands, take a picture, talks
Plaza Bugis Roundabout	5	Stand up, take a picture, talk, sit down
stage	4	Sit down, talk
Seating area 4a MB	4	Sit down, talk
Seating area 4b MB	5	Sit down, talk
Seating area 4c MB	2	Sit down, talk
Seating area 4d MB	0	-
Sculpture area	4	take a picture
Losari Beach Plaza roundabout	17	Stands, take a picture, talks,
Floating plaza	1	Stand up
Seating area 7a PL	4	Sit down, talk
Seating area 7b PL	1	Sit down, talk
Seating area 7c PL	1	Sit down, talk
Seating area 7d PL	0	-
Adipura monument	2	take a picture

Note :
MB : Makassar Bugis Pavilion
PL : Losari Beach Pavilion

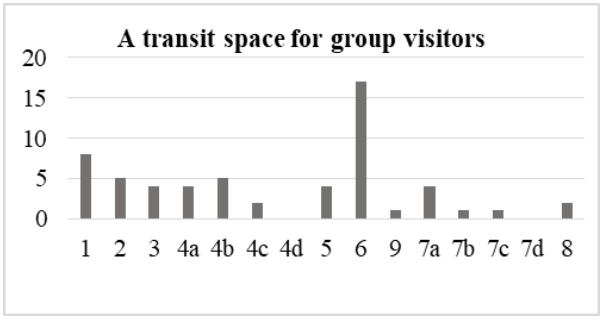

Figure 20. A diagram of the size of the transit point in the transit space

In some spaces that are always a place for visitors to stop by, they are equipped with elements as a property for completing photos, in this case, it is clear to get a good spot as one of the goals of visitors besides just taking a walk is to take a moment by taking pictures.

5. Conclusions and Recommendation

5.1. Conclusions

The conclusion of this study is based on the results and discussion of research showing and finding the effect of shelter space on group visitors who are escorted by several theories for the process of this research. These influences are as follows:

a. Influence on transit space which causes activities to overlap
   1) Spatial area is a space that has an area without any buildings above it so that in terms of taste, it is able to give the impression of being plong when stopping to carry out various activities.
   2) Visibility is a situation that is owned by the space that attracts visitors to stop by to enjoy the view while doing various activities
   3) Historical area is an impression of historical traces that have settled in a space and can be felt by visitors.
   4) Iconic elements, an arrangement of attributes, which the property offers to capture the moment of visit.
   5) This social interaction is an activity that is quite influential for visitors to stop by and increases the vitalization of space.
b. The influence of space that has been designed to be a shelter does not appear to be functioning in its function, it is influenced by the minimization of visibility, internal space, social interaction, attribute and building elements such as seating do not affect visitors because they stop by to sit, rest, tell stories. carried out anywhere that makes visitors fit to stop by to do these activities including spaces that have been discussed from the research results.
c. The effects that are obtained make visitors do activities simultaneously and all visitors want to feel it so that there is overlapping activity.

5.2. Recommendation

From the conclusion statement, there are several recommendations which are:

a. Maintain the influence that has been obtained and then developed and that influence is implemented in the that occurs, the unoccupied space that is meant is the space where there is minimal visiting activity.
b. By cultivating the effects that the existing overlapping activities can spread and minimize the occurrence of unoccupied space.

References

[1] S. Carr, M. Prancis, G. Rivlin, L, and M. Stone, A, *Enviroment and Behavior Series Public Space*. America: Cambrige university press, 1992.
[2] Project for Public Spaces, *How To Turn A Place Around, A Handbook For Creating Successful Publik Spaces*. New York, United States Of America, 2008.
[3] M. P. D'Entreves, *Filsafat Hannah Arendt*. Yogyakarta, 2003. [in Bahasa]
[4] D. Hantono, "Pattern of Public Open Space Activities in Fatahillah Park Area," *J. Arsit. Komposisi*, vol. 1, no. 1, 2017. [in Bahasa]
[5] D. Hantono, Y. F. D. Sidabutar, and U. I. M. Hanafia, "City Public Space Study Between Activities and Limitations," *Langkau Betang J. Arsit.*, vol. 5, no. 2, pp. 80–86, 2018. [in Bahasa]
[6] D. Hantono, "Behavioral Studies in Public Open Space," *NALARs*, vol. 18, no. 1, pp. 45–56, 2019. [in Bahasa]
[7] Zhang and Lawson, "Activities in Publik Outdoor Spaces Outside Highdensity," *urban Resid. communities. Urban Des. Int.*, 2009.
[8] M. Carmona, T. Healt, T. Oc, and S. Tiesdell, *Publik Place-Urban Space:The Dimention of Urban Design*. Tokyo: Architectural Press, 2003.
[9] J. Gehl, *Life between Buildings: Using Publik Space*. Washington DC: Island Press, 2011.
[10] T. Hidjaz, *Interior Design and Visitor Behavior in the Kelapa Gading Mall Public Space Case*. Bandung: National Institute of Technology. [in Bahasa]
[11] J. M. Laurens, *Architecture and Human Behavior*. Jakarta: PT. Grasindo, 2005. [in Bahasa]
[12] H. W. Whyte, *The Social Life of Small Urban Spaces*. New York, 1980.
[13] Sugiyono, *Research Methods Combined (Mixed Methods)*. Bandung: Penerbit Alfabeta, 2017. [in Bahasa]
[14] H. R. Agustapraja, "Pedestrian Behavioral Mapping Study on Pedestrians in Lamongan City Square," Islamic University, 2018. [in Bahasa]
[15] H. Hadikusuma, *Methods of Making Working Papers or Legal Thesis*. Bandung: Mandar Maju, 1995. [in Bahasa]

EPI International Journal of Engineering
Volume 4, Number 1, February 2021, pp. 101-108
DOI: 10.25042/epi-ije.022021.14

*p*ISSN 2615-5109
*e*ISSN 2621-0541

Accessibility Based on User Perception of Rehabilitation Center for People with Physical Disabilities (BRSPDF) Wirajaya Makassar

Mutmainna Mansyur[a,*], Triyatni Martosenjoyo[b], Edward Syarif[c]

[a]Architecture Department, Engineering Faculty, Hasanuddin University. Email:mutmainnamansyur@yahoo.co.id
[b]Architecture Department, Engineering Faculty, Hasanuddin University. Email:triyatni@gmail.com
[c]Architecture Department, Engineering Faculty, Hasanuddin University. Email:edosyarif@yahoo.com

Abstract

In planning a building and environment, not only design that needs to be considered but also accessibility. Accessibility that can be accessed by everyone for the creation of equal opportunities. In designing, the perception of the environment is important, The Social Rehabilitation Center for People with Physical Disabilities (BRSPDF) Wirajaya is a rehabilitation center for people with physical disabilities to acquire skills so that they can work independently. So accessibility is very important in supporting activities in Rehabilitation Center. Based on this, this study aims to analyze the level of conformity of accessibility elements to the principle of facilities and accessibility. In this research the method used is the survey method and use the questionnaire as a research instrument, a type of quantitative descriptive research.. The results showed that the level of conformity of accessibility elements to safety is 74.1%, convenience 79.5%, usability 71.8%, and independence 64.1%.

Keywords: Accessibility; people with disabilities; perception; universal design

1. Introduction

In planning a building and environment, not only the design that needs to be considered but one of them is accessibility Accessibility is not only intended for normal people, but also for people with disabilities so that there is no architectural discrimination for the creation of equal rights and opportunities. Equal opportunity is a situation that provides opportunities and/or provides access to people with Disabilities to channel potential in all aspects of state and community organizing [1] and facilitated for people with disabilities in providing accessibility.

Accessibility is the convenience provided for people with disabilities to realize equal opportunities [1]. The law also explains the similarity of opportunities where people with disabilities are given opportunities in providing access in all aspects to channel their potential.

The phenomenon that occurs today, people with disabilities still do not fully get equal rights and equality in terms of facilities and accessibility, especially in public spaces. Along with the rapid development of the city of Makassar, it is still not fully implemented the concept of universal design where public spaces should be accessible from children, adults, seniors and people with disabilities so that there is no discrimination in public spaces.

The similarity of opportunities is not only in the social aspect, but also in the economic aspect. The government has opened up employment opportunities for people with disabilities, both in government and non-governmental environments such as jobs that require skills. One of the government's efforts in creating equal opportunities in terms of skills is by providing a place of social rehabilitation. Through the ministry of social affairs, the government has provided halls such as the Wirajaya Makassar Social Rehabilitation Center for People with Physical Disabilities (BRSPDF) to accommodate the skills of people with physical disabilities.

For the creation of rehabilitation patterns in BRSPDF Wirajaya Makassar, it is considered necessary to pay attention to the supporting factors of activities contained in it. One of the supporting factors of the activity is accessibility that can be accessed by people with disabilities. Accessibility rights are clearly regulated in Law No. 8 of 2016, where it is mentioned that accessibility rights for persons with disabilities include obtaining accessibility to utilize public facilities and obtaining decent accommodation as a form of accessibility for individuals.

The existing conditions in BRSPDF Wirajaya apply some accessibility including signs and markers, ramps, guide lanes, pedestrian paths but have not reached the

*Corresponding author. Tel.: +6285-241-843-494
Poros Malino Street Km.6, Gowa
Sulawesi Selatan, Indonesia 92171

entire hall area. Although BRSPDF Wirajaya is specialized for people with physical disabilities, but regional planning must apply the concept of universal design, where the design of the place is not only for people with physical disabilities who can access but also other people with disabilities. The principle of universal design is very likely to be applied to create facilities for people with disabilities because the segmentation of this design is not limited to age, gender, normal or disability etc. [2].

From some of these conditions, it is considered necessary to conduct research on existing accessibility in order to provide recommendations for effective and accessible accessibility design directives both for the hall and for similar buildings.

2. Literature Review

2.1. Accessibility

Accessibility is the convenience that is provided for everyone to realize equal opportunities in all aspects of their lives and livelihoods. Accessibility is a part of people's lives, so accessibility is essential for people with disabilities [3].

From the above definitions, it can be concluded that accessibility is an ease that is provided to be accessible to all people including people with disabilities without discrimination so as to realize equal opportunities in various aspects of life. Accessibility includes the following principles [4].

a. Safety, i.e. everyone can reach all places or buildings that are general in an environment.
b. Uses, namely everyone should be able to use a place or building that is general in an environment.
c. Safety, every building that is general in a waking environment, must pay attention to safety for everyone.
d. Independence, everyone must be able to reach in and use all places or buildings that are general in an environment without the need for the help of others.

2.2. People with disabilities

According to The Great Dictionary of Indonesian, people with disabilities are defined as people who bear (suffer) something. While disability is an Indonesian word derived from the English word disability (plural: disabilities) which means disabled or inability [5]. Disability is generally defined as a condition in which a person experiences physical, mental, intellectual and sensory deficiencies or imperfections [6]. Disability is generally interpreted as a condition in which a person experiencing deficiencies or imperfections in terms of physical, mental, intellectual and sensory [7].

People with disabilities are any person who has long-term physical, intellectual, mental and/or sensory disabilities who in interacting with the environment may experience obstacles and difficulties in participating fully and effectively with other citizens based on equal rights [8]. From several definitions of persons with disabilities, it can be concluded that people with disabilities are people who have limitations both physically and mentally and have difficulty in some aspects of life.

2.3. Universal design

Universal Design is a design concept intended for everyone regardless of difference [9]. According to Makassar City Regional Regulation No. 6 of 2013 universal design is a product design, environment, programs and services that can be used by everyone to the maximum extent possible, without the need for an adaptation or special design including aids for certain groups of people with disabilities at the time of need [10]. Any public space required to provide an inclusif design in order to accommodate a variety of different needs because everyone have the same human rights [7].

Universal Design aims to facilitate everyone's life through product creation, built environment and communication to be used as much as possible and provide added value for everyone of all ages and abilities [8].

From some of the above definitions, it can be concluded that universal design is a design that can be used by everyone ranging from children, the elderly and people with disabilities. The main principles of Universal Design, according to Folente Story in the Universal Design Handbook [11].

a. Can be used by anyone (Equitable Use).
b. Flexibility in Use
c. Simple and Intuitive Use
d. Perceptible Information
e. Tolerance for Error
f. Low Physical Effort
g. Size and Space for Approach and Use

2.4. Perception

Etymologically, perception comes from the Latin percipere, which means to receive or take. Perception is a process within a human being that allows it to have the ability to select, organize, and interpret stimuli from the surrounding environment, and that process affects individual behavior [12]. Humans have different characteristics and perceptions based on age children, adolescents and adults [13]. Therefore, perception is a person's response in receiving something from the environment.

There are several theories about perception. In general, some experts agree that perception is influenced by factors such as experience, knowledge background, physical background, social and cultural [14].

a. Environmental Perception
   Environmental perception is the interpretation of an individual's setting, based on the individual's cultural background, reason and experience [15].
b. Perceived Environment
   Perceived Environment is a product or form of environmental perception of a person or group of people [15].

3. Research Methods

3.1. Research type

This type of research is descriptive quantitative. The research was conducted by describing the conditions in BRSPDF Wirajaya Makassar. The method in this study uses survey method. The research started from observation in the field and measurement, then adjusted to Permen

PUPR No. 14/PRT/M/2017. In addition, the distribution of questionnaires intended for individu, in this case the individual in question is the beneficiary in BRSPDF Wirajaya Makassar. The population in this study was 39 people, 31 men and 8 women. In this study using sampling techniques, namely saturated sampling for the distribution of questionnaires because people with physical disabilities who are in BRSPDF Wirajaya Makassar are few in number. As for the interview, use incidental sampling, which represents one of the types of disabilities encountered at the time.

3.2. Research data source

The data sources in this study are primary and secondary data:

a. Primary Data
   Primary data in the form of data collected by researchers, directly from the first source or place of research object is conducted through observation method and interview / interview. The data collected is in the form of documentation of accessibility conditions at BRSPDF Wirajaya Makassar, the results of questionnaires that have been shared and the results of interviews in person.
b. Secondary data
   Secondary data in the form of publications of journals, books or other relevant reading sources.

3.3. Research instruments

In connection with the research method used, it takes several research instruments to support this research. Research instruments are tools used by researchers in retrieving data and as a means of supporting the research process, research instruments in this research include:

a. Camera
   Camera used to document the condition of accessibility elements in BRSPDF Wirajaya Makassar.
b. Quetionnaire
   The questionnaire contains several questions related to user convenience.
c. Meters
   Meters are used in measuring accessibility elements such as ramps, guide paths, pedestrian paths, as well as the dimensions of signs and markers.
d. SPSS software
   SPSS software is used to process questionnaire data to measure the validity of data. SPSS software used is SPSS 16.0

3.4. Location

Research location of Social Rehabilitation Center for People with Physical Disabilities (BRSPDF) Wirajaya Makassar located at Jalan A.P Pettarani Km.4 Subdistrict Tamanuang Panakkukang Makassar Province South Sulawesi. The research was conducted in the part of the hall that is often used by beneficiaries, namely in the dormitories, skill buildings, sports halls, halls, mosques, and workshops. The area is an area often used by beneficiaries so that researchers can meet directly for interviews and questionnaires. As for the location of the research can be seen in Fig. 1.

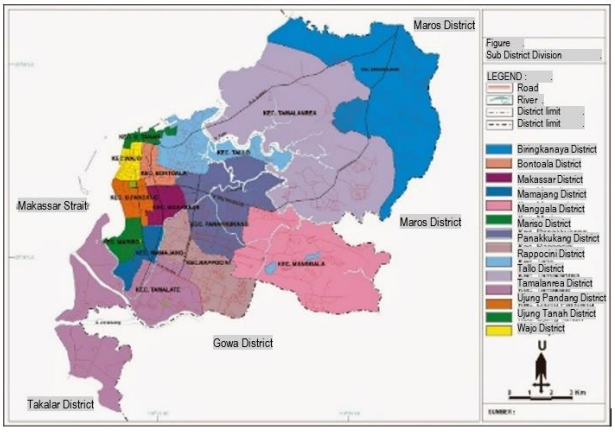

(a)

(b)

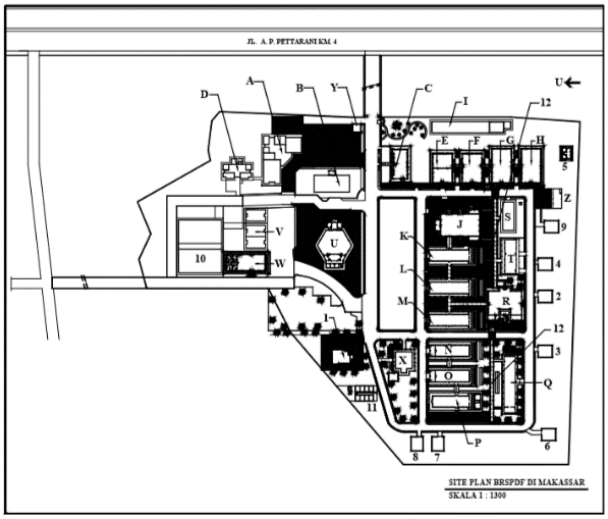

(c)

Figure 1. Research location (a) Makassar City Map, (b) BRSPDF Wirajaya Makassar location map, (c) BRSPDF Wirajaya Makassar floor plan

3.5. Research variables

The variables in this study were distinguished into two namely free variables and bound variables. In this study the bound variables were accessibility and user perception. free variables are signs and markers, ramps, guide paths, pedestrian paths, safety, convenience, usefulness, and independence.

4. Validity and Reliability Test

In quantitative research, to obtain valid, reliabel and objective data, the research was conducted using valid and reliabel instruments, conducted on samples close to population numbers and data collection and analysis was carried out in the right way [3]. Analysis of user perception of accessibility is measured by using SPSS which is a test of validity and reliability.

4.1. Validity

To perform a validity test using the likert scale, all questions answered from respondents were weighted, strongly agreed = 4, agreed = 3, disagreed = 2 and strongly disagreed = 1.

Number of questions 12, number of respondents 39 people. All questions are said to be valid because r count is greater than r table. Where for the number of respondents n = 39, the value r table is 0.3.

4.2. Reliability

In this study also used reliability test to find out the reliability of questions in the questionnaire. This test is done by comparing cronbach alpha with cronbach alpha provision of at least 0.6. Based on the results of the questionnaire data processing in this study, the value of cronbach alpha obtained was 0.912 greater than cronbach alpha at least 0.6, so it can be concluded that the questionnaire in this study is reliabel.

5. Results and Discussion

5.1. Sign and markings

Standard:

a. Embossed or Braille signs that can be read by the blind and other people with disabilities;
b. Signs in the form of images and symbols should be embossed, so that their meaning is easy and fast to interpret;
c. Signs in the form of international signs and symbols;
d. Signs that apply special methods (eg soil pavement differentiation, contrasting colors, etc.);
e. The character and background of the sign must be made of a non-glare material. Characters and symbols must contrast with the background, whether the characters are light over dark, or vice versa;
f. The proportions of letters or characters on a sign must have a width-to-height ratio between 3:5 and 1:1, and a letter thickness between 1:5 and 1:10;
g. The height of the letters and numbers on the sign must be measured according to the visibility from where the sign is read.

Field Data:

From the results of observations at BRSPDF Wirajaya Makassar, there are several signs and markings located at several points. Signs in the form of symbols for the blind, wheelchair users, crossing symbols and in the form of writing. The available writing signs are not embossed or braille.

Figure 2. Signs in the form of symbols for the blind and wheelchair users

Figure 3. Sign in the form of a crossing symbol

Figure 4. Sign in writing

Figure 5. sign in the form of a picture

Design Instructions:
For people with physical disabilities, signs and markings have met the needs, but for universal design building standards they should be accessible for all people with disabilities without exception. There are no braille signage that can be accessed by persons with sensory disabilities (disabled blind).

5.2. Ramp

Standard:
a. The slope of a ramp inside the building must not exceed 7° while the slope of a ramp outside the building is a maximum of 6°.
b. The minimum width of the ramp is 95 cm without guard edges, and 120 cm with guard edges.
c. Flat face/bordes at the beginning or end of a ramp with a minimum size of 160 cm.
d. The width of the ramp/kanstin/low curb safety edge is
e. 10 cm.
f. The vines should be easy to hold with a height of 65 - 80 cm.

Field Data:
a. 6° . ramp incline
b. The width of the ramp is 100cm. Dimensions of ramp 300cm x 230cm and 250cm x 200cm.
c. Border 180cm.
d. Canteen width 20cm.
e. Vines handle height 80cm.

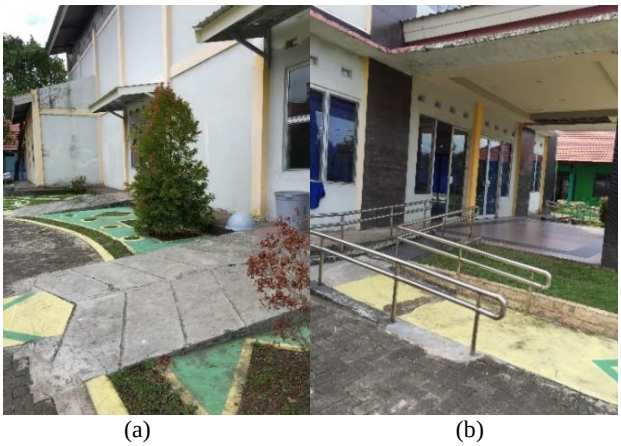

(a) (b)

Figure 6. (a) Ramp next to the gym, (b) Ramp in front of the gym

Figure 7. Ramp beside hostel

Design Instructions:
Some of the ramps have met the standard, but there are some rams that do not use safety edges/kanstin and handles like the ram located next to the gym. Therefore, the available ramps need to be equipped with handles and safety edges so that wheelchair users can easily access them.

5.3. Guide path

Standard:
a. Striped guiding block
b. Round pattern warning tile
c. Size 30x30cm

Field Data:
a. Striped guide tiles and round patterned warning tiles. There are tiles with a yellow contrast color.

Design Instructions:
Tiles are only found in certain sections. tiles are not found in all pedestrian paths and corridors. It is recommended that the tiled guide path covers the whole.

5.4. Pedestrian path

Standard:
a. The minimum width of the pedestrian path is 120 cm for one-way lanes and 160 cm for two directions.
b. The minimum safety edge height is 10 cm and a width of 15 cm along the pedestrian path.

Figure 8. Striped and round pattern tiles

Figure 9. Tiles with contrasting colors

Figure 10. Pedestrian path equipped with seating/resting facilities

Field Data:

a. The width of the pedestrian path is appropriate.
b. The size of the safety edge is high 20 cm and wide 20 cm.

Design Instructions:

The width of the pedestrian path is in accordance with the standard but not all pedestrian paths are equipped with safety edges for wheelchair users. Completing the pedestrian path by adding a minimum safety edge of 10 cm and a width of 15 cm along the pedestrian path.

5.5. Safety

Safety variables to measure the user's perception of the height, lighting and texture of accessibility elements.

Based on the Table 1, the accessibility safety principles include height, lighting, textures for signs and markers, ramps, guide paths and pedestrian paths.

a. Signs and markers
   For the height of signs and markers are appropriate, respondents answered agreed with a percentage of 66.7%, for lighting signs and markers as much as 48.7%, and the texture of signs and markers 38.5%.
b. Ramp
   For ramp height is appropriate, respondents answered agreed with a percentage of 74.4%, for ramp lighting as much as 41.0%, and ramp texture of 66.7%.
c. Guide Path
   For the appropriate tile height, respondents agreed with a percentage of 56.4%, for guide path lighting as much as 66.7%, and guide path texture of 74.4%.
d. Pedestrian Path
   For the height of the rambat handle is appropriate, respondents answered agreed with a percentage of 74.4%, for pedestrian lane lighting as much as 71.8%, and pedestrian lane texture of 61.5%.

5.6. Facilities

Variable ease to measure user perception of the location, achievement and understanding of beneficiaries in accessing accessibility elements.

Based on Table 1, the principles of accessibility include location, achievement, easy to understand for signs and markers, ramps, guide and pedestrian paths.

Table 1. Accessibility safety results and percentages

Questions	Respondent's Answer	Frequency	Percentage
Height of signs and markers	SS	7	17.9
	S	26	66.7
	TS	5	12.8
	STS	1	2.6
Lighting signs and markers	SS	3	7.7
	S	19	48.7
	TS	14	35.9
	STS	3	7.7
Texture of signs and markers	SS	4	10.3
	S	15	38.5
	TS	12	30.8
	STS	8	20.5
Ramp height	SS	8	20.5
	S	29	74.4
	TS	2	5.1
	STS	-	-
Ramp lighting	SS	11	28.2
	S	16	41.0
	TS	9	23.1
	STS	3	7.7
Ramp texture	SS	7	17.9
	S	26	66.7
	TS	5	12.8
	STS	1	2.6
Tile height	SS	11	28.2
	S	22	56.4
	TS	6	15.4
	STS	-	-
Guide path lighting	SS	12	30.8
	S	26	66.7
	TS	1	2.6
	STS	-	-
Guide Path Texture	SS	8	20.5
	S	29	74.4
	TS	2	5.1
	STS	-	-
Height of propagate handle	SS	8	20.5
	S	29	74.4
	TS	2	5.1
	STS	-	-
Pedestrian path lighting	SS	9	23.1
	S	28	71.8
	TS	2	5.1
	STS	-	-
Texture of pedestrian paths	SS	7	17.9
	S	24	61.5
	TS	8	20.5
	STS	-	-

a. Sign and markers
   For the location of signs and markers respondents answered agreed with a percentage of 61.5%, for the achievement of signs and markers as much as 79.5%, and signs and markers easy to understand 48.7%.
b. Ramp
   For the ramp location respondents answered agreed with a percentage of 79.5%, for the achievement of ramps as much as 56.4%, and easy-to-understand ramps of 69.2%.

Table 2. Accessibility facilities results and percentages

Questions	Respondent's Answer	Frequency	Percentage
Location of signs and markers	SS	14	35.9
	S	24	61.5
	TS	1	2.6
	STS	-	-
Signs and markers are easy to find	SS	6	15.4
	S	31	79.5
	TS	1	2.6
	STS	1	2.6
Signs and markers are easy to understand	SS	18	46.2
	S	19	48.7
	TS	2	5.1
	STS	-	-
Ramp location	SS	6	15.4
	S	31	79.5
	TS	1	2.6
	STS	1	2.6
Ramp is easy to reach	SS	8	20.5
	S	22	56.4
	TS	9	23.1
	STS	-	-
Ramp is easy to understand	SS	10	25.6
	S	27	69.2
	TS	1	2.6
	STS	1	2.6
Guide Path Location	SS	9	23.1
	S	24	61.5
	TS	6	15.4
	STS	-	-
Guide path is easy to reach	SS	6	15.4
	S	26	66.7
	TS	7	17.9
	STS	-	-
Easy-to-understand guide path	SS	17	43.6
	S	16	41.0
	TS	6	15.4
	STS	-	-
Pedestrian Line Location	SS	9	23.1
	S	28	71.8
	TS	2	5.1
	STS	-	-
Pedestrian paths are easy to reach	SS	6	15.4
	S	26	66.7
	TS	7	17.9
	STS	-	-
Easy-to-understand pedestrian path	SS	5	12.8
	S	19	48.7
	TS	13	33.3
	STS	2	5.1

c. Guide Path
   For the location of the guide path respondents answered agreed with a percentage of 61.5%, for the achievement of the guide path as much as 66.7%, and the guide path is easy to understand 41.0%.
d. Pedestrian path
   For the location of pedestrian lanes respondents answered agreed with a percentage of 71.8%, for the achievement of pedestrian lanes as much as 66.7%, and easy-to-understand pedestrian lanes 48.7%.

5.7. Uses

Usability variable to measure user perception of accessibility element functionality.

Based on Table 3, the principles of accessibility use include the function of signs and markers, ramp function, guide path function and pedestrian path function. For sign and marker function reseponden answered 56.4%, ramp function 48.7%, guide path function 71.8%, and pedestrian path function 48.7%.

Tabel 3. Accessibility uses results and percentages

Questions	Respondent's Answer	Frequency	Percentage
Signs and markers functions	SS	7	17.9
	S	22	56.4
	TS	9	23.1
	STS	1	2.6
Ramp functions	SS	5	12.8
	S	19	48.7
	TS	14	35.9
	STS	1	2.6
Guide path functions	SS	4	10.3
	S	28	71.8
	TS	6	15.4
	STS	1	2.6
Pedestrian path functions	SS	5	12.8
	S	19	48.7
	TS	14	35.9
	STS	1	2.6

Table 4. Results and percentages of independence

Questions	Respondent's Answer	Frequency	Percentage
Confidence Level	SS	16	41.0
	S	19	48.7
	TS	3	7.7
	STS	1	2.6
Discipline	SS	11	28.2
	S	21	53.8
	TS	7	17.9
	STS	-	-
Responsibility	SS	12	30.8
	S	25	64.1
	TS	2	5.1
	STS	-	-

5.8. Independence

Independence variables to measure a user's perseption against a degree of confidence. user discipline and responsibility.

Based on Table 4, the principles of accessibility independence include self-reliance, discipline and responsibility. For the independence of respondents answered 48.7%, discipline came on time in each activity 53.8%, responsibility can complete each task given 64.1%.

6. Conclusions and Suggestions

6.1. Conclusions

a. The availability of overall accessibility elements in BRSPDF Wirajaya Makassar has met the needs of people with physical disabilities but does not yet include the overall principles of universal design. BRSPDF Wirajaya provides facilities in accordance with the type of disability received, namely people with physical disabilities.
b. The level of conformity based on the principles of facilities and accessibility include safety, convenience, usefulness and independence as follows.
   - For safety variables, the highest percentage of respondents answered agreed 74.4% for ramp height, guide path texture and propagate handle height.
   - For ease variables, the highest percentage of respondents answered agreed 79.5% for the achievement of signs and markers and ramp location.
   - For usability variables, the highest percentage of respondents answered agreed 71.8% for the guide path function.
   - For variable of independence, the highest percentage of respondents answered agreed 64.1% is the responsibility in completing the task

6.2. Suggestions

a. Universal design should be a reference in designing accessibility, so that accessibility can be accessed not only for people with physical disabilities but for all people with disabilities.
b. The guide path that already exists but does not cover the entire building, it is considered necessary to pay attention to the existing guide path so that it is accessible for all people with disabilities.
c. The existing guide path but does not cover the entire building, it is considered necessary to pay attention to the existing guide path so that it can be accessed for all persons with disabilities.
d. Further research is needed on the specific accessibility of indoor space at BRSPDF Wiraya Makassar.
e. The government in providing a hall such as BRSPDF Wirajaya pays attention to accessibility, and one of the references can be used the results of this research

References

[1] S. Hanrahan, “Persons with Disabilities,” 2016.
[2] M. F. K. Thezar, “Accessibility of Disabilities in Karebosi Field as a Public Space of Makassar City,” 2016.
[3] L. Nuraviva, “Accessibility of Persons with Disabilities to Public Facilities In Surakarta City.”
[4] N. Dewang and Leonardo, “Accessibility of public open space for certain community groups study public facilities for people with disabilities in the area of suropati menteng park - central Jakarta,” *PLANESA J.*, vol. 1, no. 1, 2010.
[5] *Great Dictionary of Indonesia*. 2018.
[6] E. Chandra *et al.*, “Accessibility of People with Physical Disabilities to Work in Cipaisan Subdistrict Of Purwakarta Purwakarta Regency,” *Sci. J. Policy Soc. Work Serv.*, vol. 2, no. 1, 2020.
[7] R. M. Harahap *et al.*, “The Influence of Universal Design and Usability in Public Facilities in Universities for Persons with Disabilities,” *J. Eng. Comput. Sci.*, vol. 3, no. 2, 2019.
[8] Ministry of Public Works and Public Housing, “Permen PUPR No. 14/PRT/M/2017,” 2017.
[9] I. Pujiyanti, “Implementation of Universal Design in Higher Education Facilities,” *J. Archit. Plan.*, vol. 1, no. 2, pp. 223–239, 2018.
[10] Ministry of Law and Justice, “the Fulfillment of The Rights of Persons with Disabilities,” 2013.
[11] M. F. Story, “The Universal Design File: Designing for People of All Ages and Abilities,” North Carolina State University, 1998.
[12] D. Mulyada, *Communication Science An Introduction*. Bandung: Teenager Rosdakarya, 2010.
[13] Suharto, S. Deby, and L. Kristanto, “Evaluation of Visitor Perception Against Architectural Elements at the Ten November Struggle Museum,” *eDIMENSI Archit. J.*, vol. 7, no. 1, pp. 369–376, 2019.
[14] A. Harisah and Z. Masiming, “Human Perception of Signs, Symbols, and Spatial,” *SMARTek J.*, vol. 6, no. 1, pp. 29–43, 2008.
[15] Haryadi and B. Setiawan, *Environmental and Behavioral Architecture. Yogyakarta: Project developer of The Center for Environmental Studies*. Directorate General of Higher Education Ministry of Education and Culture of the Republic of Indonesia, 1995.